POLITECNICO DI MILANO
DEPARTMENT OF ENERGY
DOCTORAL PROGRAM IN ELECTRICAL ENGINEERING

BATTERY ENERGY STORAGE SYSTEMS: MODELLING, APPLICATIONS AND DESIGN CRITERIA

Doctoral Dissertation of:
Claudio Brivio

Supervisor:
Prof. Marco Merlo

External advisor:
Dr. Vincenzo Musolino

Tutor:
Prof. Alberto Berizzi

The Chair of the Doctoral Program:
Prof. Gabriele D'Antona

2017 – XXX Cycle

A mia madre e mio padre

Abstract

Nowadays, the specific costs of battery energy storage systems (BESSs) are decreasing exponentially and at the same time their installations are increasing exponentially. BESS are in fact becoming pivotal in the development of several heterogeneous industrial sectors like energy, automotive, electronics, telecom etc. However, BESS performances (energy density, power density, efficiency, lifetime) cannot be assumed expandable from one application to another and from one technology to another. Therefore, methods and models have to be developed to end up with a proper design criteria for the selected application.

The General objective of the thesis is to contribute in expanding the knowledge about BESSs by focusing on appropriate methodologies capable of linking the technological studies with the economic analyses required in real life applications. The dissertation is centred on electrochemical batteries, considering power electronics well-established with respect to both industrial applications and mathematical modelling. Specific objectives of the thesis are: the development of a reference framework related to technologies, performances and modelling of BESS; the proposal of innovative BESS models representing dynamic and aging phenomena; the development of proper methodologies to analyse the techno-economic performances of BESS when deployed in stationary applications.

The work is theoretical, numerical and experimental. A theoretical framework serves to identify and formulate the correct BESS models. The experimental activities are fundamental in developing and tuning the models. The numerical analyses, based on field data, are needed to test and validate the models on real applications. These themes are specifically developed for lithium-ion battery technology and stationary applications.

The first part of the thesis offers the reference framework about BESS and is based on literature analyses together with experimental activities. Chapter 2 gives an overview on electrochemical storage options (expected performances, market share, costs) with special attention to Li-ion technology. Chapter 3 presents experimental measurements on three different Li-ion chemistries. Energy density, power density and efficiency are used to discuss BESS performances in real applications. Chapter 4 proposes a literature review on battery modelling which are categorized into four general different approaches: electrochemical, analytical (empirical), electrical and stochastic. Two main tasks are identified for battery models: the estimation of operating conditions (i.e. SoC estimation), the estimation of the lifetime (i.e. SoH estimation).

The second part of the thesis offers the modelling framework about BESS. Chapter 5 provides the main theoretical pillars necessary for a proper electrical modelling process. Chapter 6 represents the main element of originality. A novel electrical model for Li-ion technology is developed that reproduce the dynamic response of battery cells as a nonlinear function of the Soc. The model is composed of impedance blocks which have clear links with the underlying electrochemical phenomena. The model parameters are determined by a specific testing procedure based on EIS and OCV measurements which are applied to a commercial lithium-ion cell. The model is validated in the time domain and shows excellent capability in estimating the voltage at the device terminals, efficiency, power and energy density under different operating rates and SoC. Chapter 7 investigates lifetime modelling of BESS. Aging tests are carried out on Li-ion technology and used to discuss the main degradation effects. Three lifetime modelling approaches

are proposed which are linked to experimental measurements and characterized by a different degree of complexity.

The third part of the thesis offers the design framework about BESS by bridging the modelling phase with stationary applications. Chapter 8 deals with a grid-tied application that is the Primary Control Reserve. A proper methodology is proposed which includes: a specific control mechanism; an unconventional droop-control law and proper BESS models derived from the previous chapters. The procedure has been applied to the Italian context. Simulations show that different BESS models highly affect the reliability evaluation. Differently from simplified models (i.e. empirical models), the adopted electrical model can evaluate the impact of the high stressful rates of the application. The carried techno-economic analyses show that this fact can bring to a 20% variation in the BESS optimal design, which can highly impact on investment decisions. The analyses are based on real measurements taken at the Politecnico di Milano within the framework of the IoT-StorageLab. The methodology is proposed in the form of a computational tool in MATLAB®Simulink® named BESS4PCR. Chapter 9 deals with the design of off-grid power systems for rural electrification in Developing Countries. A novel sizing methodology is proposed which is composed of separated blocks addressing the different sizing phases: data elaboration, load and source profiles formulation, modelling of the main components (e.g. BESS) and their simulation, heuristic optimization method to formulate the robust design from a technoeconomic perspective. The procedure has been applied to design a PV+BESS microgrid system in supplying power to a rural village of Tanzania. Also in this case, simulations show that different BESS models can bring to different sizing results, especially if very simplified empirical models (based on literature/manufacturers data) are adopted. However, given the less stressful application, proper empirical models (i.e. based on laboratory test) can bring to a similar conclusion with respect to more complex electrical models. This fact provides a great opportunity in energy planning analyses like the one proposed because it can reduce the simulation time by more than ten times. The analyses are based on real data gathered within the framework of the Energy4growing project. The methodology is proposed in the form of a computational tool in MATLAB® named Poli.NRG (POLItecnico di Milano –Network Robust design).

Estratto in Lingua Italiana

Oggigiorno le installazioni di Sistemi di Accumulo a batteria (SdA) sono in aumento esponenziale, mentre i loro costi specifici diminuiscono in egual misura. Gli SdA stanno infatti assumendo un ruolo sempre più cruciale nello sviluppo di svariati ed eterogenei settori industriali come il settore energetico, il settore automobilitstico, l'elettronica, le telecomunicazioni, ecc.. Tuttavia, le prestazioni stimate degli SdA (densità di energia, densità di potenza, efficienza, vita utile) non possono essere assunte constanti e trasferibili da un'applicazione all'altra o da una tecnologia all'altra. Pertanto, è necessario utilizzare metodi e modelli corretti per definire criteri di progettazione adeguati per l'applicazione selezionata.

L'obiettivo generale della tesi è quello di contribuire ad ampliare la letteratura di riferimento sui SdA con particolare attenzione allo sviluppo di metodi e modelli appropriati che possano fare da ponte fra studi prettamente tecnologici e le analisi tecno-economiche richieste nelle applicazioni reali. La tesi è focalizzata sulle batterie elettrochimiche, considerando l'elettronica di potenza ormai matura sia dal punto di vista tecnologico sia della modellazione matematica. Gli obiettivi specifici sono: lo sviluppo di un background di riferimento sulle tecnologie, le prestazioni e la modellazione degli SdA; la formulazione di modelli innovativi di SdA per rappresentare i fenomeni dinamici e d'invecchiamento; lo sviluppo di metodologie adeguate per analizzare le prestazioni tecno-economiche dei SdA quando impiegati in applicazioni stazionarie.

Il lavoro si basa su attività teoriche, numeriche e sperimentali. Le attività sperimentali sono state fondamentali per sviluppare e affinare i modelli. Le analisi numeriche, basate su dati reali raccolti sul campo, sono state necessarie per testare e validare i modelli in applicazioni reali. Questi temi sono sviluppati specificamente per la tecnologia delle batterie agli ioni di litio e per applicazioni stazionarie.

La prima parte della tesi offre un quadro di riferimento sugli SdA e si basa sull' analisi della letteratura insieme ad attività sperimentali preliminari. Il capitolo 2 offre una panoramica sulle opzioni di accumulo elettrochimico (prestazioni, quote di mercato, costi) con particolare attenzione alla tecnologia agli ioni di litio. Il capitolo 3 approfondisce le performance dei SdA grazie a misurazioni sperimentali su celle agli ioni di litio. Densità energetica, densità di potenza ed efficienza sono utilizzati come indicatori chiave per discutere delle prestazioni degli SdA in applicazioni reali. Il capitolo 4 propone una revisione bibliografica circa la modellazione degli SdA che si articola in quattro approcci: elettrochimici, analitici (empirici), elettrici e stocastici. Sono identificati due compiti principali ai quali i modelli di batterie devono assolvere: la stima delle condizioni operative (cioè la stima dello stato di carica, SoC), la stima della vita utile (cioè la stima del SoH).

La seconda parte offre un quadro di riferimento per quanto concerne la modellazione dei sistemi di accumulo. Nel capitolo 5 vengono esposti i principali elementi teorici necessari per sviluppare modelli con approccio elettrico. Il capitolo 6 raccoglie il principale elemento di originalità della tesi: un nuovo modello elettrico per le celle agli ioni di litio capace di riprodurne la risposta dinamica come funzione non lineare dello SoC. Il modello è composto da impedenze equivalenti, caratterizzate da un chiaro nesso con i relativi fenomeni elettrochimici che intendono rappresentare. I parametri del modello sono determinati da una procedura specifica basata su misurazioni di spettroscopia di impedenza e di scarica a vuoto. Il modello è validato nel dominio del

tempo e dimostra una grande accuratezza nello stimare la tensione ai terminali del dispositivo, l'efficienza, la densità di potenza e la densità energetica a diverse correnti e SoC. Il capitolo 7 approfondisce la modellazione della vita utile dei SdA. Risultati da prove sperimentali sono presentati e utilizzati per discutere i principali effetti di degradazione. Tre approcci di modellazione della vita utile sono quindi proposti, caratterizzati da un diverso grado di complessità.

La terza parte della tesi ha l'obiettivo di creare un ponte fra le attività di modellazione e le applicazioni stazionarie. Il capitolo 8 approfondisce un'applicazione stazionaria connessa alla rete: la regolazione primaria di frequenza (RPF). Viene proposta una metodologia di studio appropriata che include: un controllore specifico, una legge di statismo non convenzionale e modelli di SdA adeguatamente sviluppati sulla base dei risultati dei precedenti capitoli. La procedura è stata applicata al contesto italiano. Le simulazioni mostrano che l'uso di modelli diversi di SdA influenza la valutazione dell'affidabilita. A differenza dei modelli semplificati (i.e. modelli empirici), il modello elettrico sviluppato riesce a valutare l'impatto delle condizioni operative molto "stressanti" determinate dalla particolare applicazione. Le analisi tecno-economiche mostrano che questo aspetto impatta su una variazione del 20% del dimensionamento ottimale, fatto che può drasticamente impattare sulle valutazioni di investimento. Le analisi sono basate su misurazioni reali effettuate presso il Politecnico di Milano nell'ambito dello IoT-StorageLab. La metodologia è proposta in forma di strumento computazionale in MATLAB®Simulink® denominato BESS4PCR. Il capitolo 9 riguarda invece l'analisi di sistemi off-grid per l'elettrificazione rurale nei Paesi in via di sviluppo. Si propone una nuova metodologia composta da blocchi distinti che affrontano separatamente le diverse fasi del dimensionamento: l'elaborazione dei dati provenienti dal contesto; la formulazione di appropriati profili di carico e di produzione; la modellazione dei componenti principali dell'impianto (SdA e PV) e loro simulazione, l'uso di un metodo di ottimizzazione euristico per formulare il dimensionamento "robusto" sulla base delle prestazioni tecno-economiche ottenute; La metodologia proposta è quindi applicata per dimensionare una microrete composta da PV+SdA per fornire alimentazione elettrica a un villaggio rurale della Tanzania. Anche in questo caso risulta evidente come diversi modelli di SdA influenzino il dimensionamento finale, in particolar modo quando sono utilizzai modelli empirici semplificati (i.e. basati su dati di letteratura o datasheet). Ciononostante, data l'applicazione meno "stressante", si mostra come un modello empirico opportunamente sviluppato (i.e. basato su dati di laboratorio) possa condurre a risultati finali molto simili a quelli ottenibili con un ben più complesso modello elettrico. Questo fatto rappresenta una notevole opportunità in analisi energetiche come quella proposta in quanto può ridurre i tempi di simulazione di più di dieci volte. Le analisi si basano su dati reali raccolti nell'ambito del progetto Energy4growing. La metodologia è proposta in forma di strumento computazionale in MATLAB® denominato Poli.NRG (POLItecnico di Milano - Network Robust desiGn).

Contents

Notation

Main acronyms used in the text

BES   Battery Energy Storage
BESS   Battery Energy Storage System
BMS   Battery Management System
CC   Constant Current
CV   Constant Voltage
DC   Direct Current
DCs   Developing Countries
DG   Distributed Generation
DoD   Depth of Discharge
EES   Electrical Energy Storage
EIS   Electrochemical Impedance Spectroscopy
EoL   End of Life
EPR   Energy to Power Ratio
EVs   Electric vehicles
GEIS   Galvanostatic EIS
HEV   Hybrid Electric Vehicle
IC   Interface Converter
IoT   Internet of Things
LCO   Lithium Cobalt Oxide
LCoE   Levelized Cost of Energy
LFP   Lithium Iron Phosphate
LL   Loss of Load
LLP   Loss of Load Probability
LMO   Lithium Manganese Oxide
LNCO   Lithium Nickel Cobalt Oxide
LoR   Loss of Regulation
LTO   Lithium Titanate Oxide
NCA   Nickel Cobalt Aluminium
NMC   Nickel Manganese Cobalt
NPC   Net Present Cost
NPV   Net Present Values
OCV   Open Circuit Voltage
PCR   Primary Control Reserve
PHEV   Plug-in Electric Vehicle
PV   Photovoltaic
RES   Renewable Energy Systems
RES-E   Renewable Energy Systems for Electricity
RETs   Renewable Energy Technologies
RoPCR   Revenue of PCR
SEI   Solid Electrolyte Interface
SoC   State of Charge
SoH   State of Health
TSO   Transmission System Operator

CHAPTER 1

Introduction and Motivations

This doctoral thesis copes with proper models and design criteria for battery energy storage systems (BESSs). This theme is specifically developed for lithium-ion battery technology and has been tested and validated in real life case studies.

The general objective is to contribute expanding the knowledge about BESSs with particular attention on appropriate methods and models which are necessary to link the technological studies with the necessary economic analyses required in real life applications. Specific objectives are: the development of a reference framework about technologies, performances and modelling of BESS; the proposal of innovative BESS models to represent dynamic and aging phenomena; the development of proper methodologies to analyse the techno-economic performances of BESS when deployed in stationary applications.

The work is theoretical, numerical and experimental. A theoretical framework is needed to identify and formulate the correct BESS models according to the different available technologies. The experimental activities are fundamental to develop and tune the models. The numerical analyses, based on field data is needed to test and validate the models on real applications.

1.1 Background

The thesis theme refers to the field of research in "Battery Energy Storage Systems (BESSs)". Though the topics might appear more related to the disciplines of chemistry, science of material, physics and the related engineering fields, nowadays experts from energy, electrical, electronics and transports sectors are asked to play an important role to bridge the gap between the technology and the final use. While the technological development is connected to the discoveries of new materials and chemistries, the investment evaluation and system design must be linked to the final application or service the BESS is asked to provide

For this reason, there is an increasing demand of a more "systemic approach" to the topic of energy storage. The different know-hows should merge to create an effective multidisciplinary layer of analysis that ranges from electrochemical studies to final system design. For instance, electrochemical cells' producers might be asked to provide more information about the performance of their products, being also open to the diffusion of databases and international standards that simplify the work of engineers.
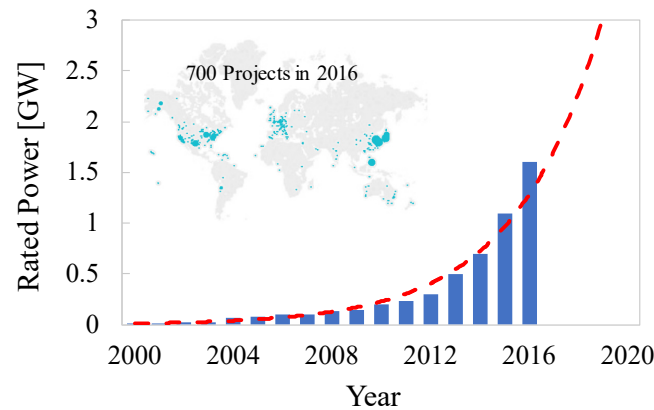
Figure 1.1 BESS stationary project installations over time [21]

Similarly, the same engineers are asked to abandon simplified approaches of analysis that clearly do not match with the technology's features. Only in this way, it might be possible to perform the right techno-economic assessments and to develop the right business models able to conform to the specific final application.

This is even more true when observing that BESS are becoming pivotal in the development of several and heterogeneous industrial sectors like energy, automotive, electronics, telecom etc. By looking at the rise in the global battery manufacturing capacity in the near future, projections say that lithium-ion cells' production is set to be of about 280 GWh in 2021, i.e. to double the installed capacity in only five years (100 GWh in 2016) [1]. This huge increase in battery demand can be explained by the fact that some of the aforementioned industrial sectors are the market response to some of the most intriguing challenges of our today's society [2], [3]:

- *The transition towards a Renewable Energy Systems (RESs) based energy sector.*
  Recently, the Paris agreements set out the common goal to limit the global warming and identified the ways in which this can be achieved [4]. One issue is related to the further increase of RESs penetration in the electricity sector. In EU-28 the energy production from Renewable Energy Systems for Electricity (RES-E) has increased from 12% of total production in 1990 (mainly hydro power plant) to 28% of 2014 (with the addition of PV and wind power plants) and, globally, RES are expected to cover the 60% of the new installed capacity up to 2040 [5], [6]. This fact represents a tremendous challenge because it is commonly accepted that RESs in the form of scattered distributed generators are creating new challenges for grid operators [7]–[11]. Their integration into existing grids affects the optimum power flow computation and brings about problems of congestion, safety and reliability, events unpredictability, power quality, voltage and frequency control and system economics [12]–[16]. In this context, BESS could be a viable technical solution to maximize the local consumption of RES electricity and/or to provide ancillary services to the grid like primary and secondary control reserves, spinning reserve, voltage control, load levelling and peak shaving [17]–[20]. This is confirmed by the increase of stationary projects worldwide during the last few years. Figure 1.1 shows nearly an exponential increase of BESS installation over the last 10 years.

- *The rural electrification of Developing Countries (DCs):*
  Extending electricity supply in rural areas of DCs represents one of the issues to be faced in order to provide modern energy services to those 1.2 billion of people who until 2013 did not have access to electricity [22]. The features of these areas introduce
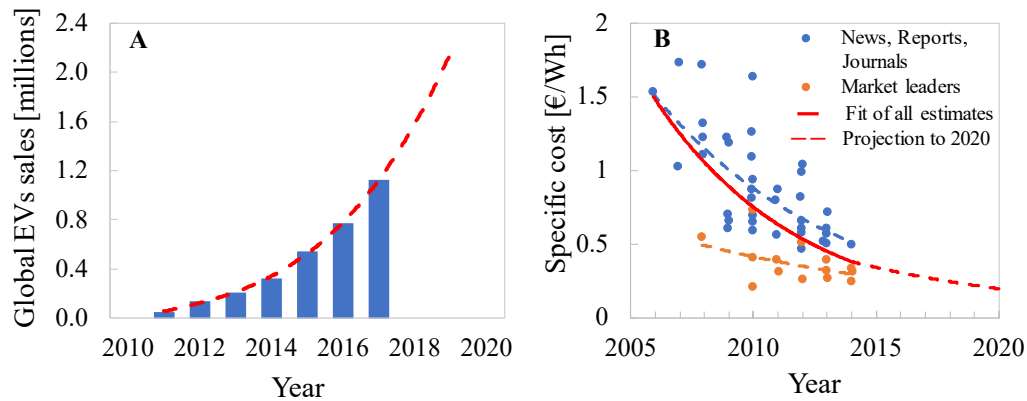
Figure 1.2 A: Global electric vehicles sales over time [27]; B: Cost of Li-ion battery packs in automotive sector [1]

economic and technical constraints to the implementation of traditional technologies based on the centralized electrification approach [23]. This means that the strategy for scaling up access to electricity mostly aims at integrating small-scale RES-based off-grid systems in local micro-grids ready to be connected once the national grid will be available. Even in this frame, BESS could be an effective technology to exploit the potential of RES [24]–[26]. Off-grid systems can benefit from the use of BESS to mitigate both short-term fluctuations (to ensure the instantaneous power balance) and intermediate-term energy deficiency which are typical consequences of unpredictability of RES.

- *The rise of electric vehicles:*
  Electrified road transport has been the first choice adopted for mobility purposes at the beginning of 20th century. It was then totally replaced by the petroleum-fuelled internal combustion engine (ICE) mainly for cost and technical reasons (vehicle autonomy mainly). Nowadays, several Countries are considering again electric vehicles (EVs) based on batteries. Governments have established goals for the diffusion of EVs, aiming at reducing CO2 emissions while strategically decreasing fossil fuel dependency. Several studies are therefore forecasting a huge increase of EVs sales (Figure 1.2-A) in the next few years that are projected to reach 20 million units in 2020 [28]. As a result, the automotive industry is the main driver of recent BESS technological developments. BESS on EVs is decisive for two main issues: (i) the driving range depends on the advancements in the cell performances, especially on the energy and power densities; (ii) the total cost of ownership (TCO) depends on the battery price to evaluate the CAPEX and on the lifetime of the battery pack to evaluate the OPEX (replacement cost mainly). While the first issue is mainly technological: new cell chemistries are needed to meet the performance requirements, the second one is mainly a problem of production costs. The increasing demand from the automotive sectors is answered by an increasing production of cells from manufacturers and this is causing a drop in the specific costs thanks to economy of scale. Figure 1.2-B shows the notable numbers of lithium-ion cells: Specific cost of leading technologies has more than halved in 5 years passing from 800 €/kWh of 2010 to 400 €/kwh of 2015. The same cost is projected to reach around 200 €/kWh in 2020 [1] thanks to a constant learning rate (-24%) that will influence also the other industrial sectors. Given the assumptions, IEA states that EVs are projected to be cheaper than regular ICE by 2026 when the TCO will be lower even in the case of a short investment period of 5 years (the typical period owners have a car).

Within this frame, this thesis deals with the definition of proper models and design criteria for BESS. This theme is specifically developed for lithium-ion battery technology and properly taking into account the implementation in real-life study cases. Two main observations can be recognized as general motivations of this research theme:

- BESS is pivotal to promote development in different industrial sectors. However, performances cannot be assumed expandable from one application to another. Energy/power densities, efficiencies, lifetime are application dependent and their right estimation affect the design criteria. Proper models are needed to evaluate the right BESS performances for the specific final use.

- The design process of BESS is not straightforward and there are several issues that can be investigated with a different degree of details. Therefore, specific methods and models can be used to tackle these issues. Specifically, the suggested models should be able to estimate SoC (State of Charge) and SoH (State of Health) indicators accepting a different level of precision according to the specific application the model is used for.

1.2 Motivational example and problems formulation

This thesis contributed to the research activities of the electric power system research group at the Energy Department of the Politecnico di Milano. Thanks to the group network with private sector, research centers, NGOs and other academia, it was possible to actively collaborate on several projects that highlight how the BESSs are becoming fundamental in the future energetic scenario. To cite the most important:

- *Energy4Growing*. This project, started in October 2013 and finished in October 2015, funded by the Polisocial Award. It aimed at studying, developing and deploying a hybrid Micro-Grid to supply power to a school in a rural area of Tanzania, completely detached from the national grid. The deployed BESS (lead-acid technology) played a pivotal role because it allowed to fulfil essential loads during nights like the security lights for resident schoolchildren, which were rarely guaranteed before the commissioning was made in the framework of *Energy4Growing* project. For more details about the project, we recommend the reader to refer to Appendix A

- *IoT-StorageLab*. This project, that started in 2016 partially funded by the Politecnico di Milano Research office, is devoted to the research on the Internet of Things(IoT) concept. The new laboratories facilities aim at creating a suitable environment for the research, design, development and test of IoT solutions, with specific reference to energy and power system applications. BESSs represent one of the most interesting topics studied in the project. The analyses of BESS behaviour during real-operation, the deployment of advanced control strategies to increase the effectiveness to the final application, the study about shared control mechanisms to integrate multiple BESS with one single managing logic are just some of the opportunities provided thanks to the project. For more details about the project, we recommend the reader to refer to Appendix B.

Moreover, a relevant part of the research activities has been devoted to experimental measurements and modelling of BESS with specific focus on Li-ion cells. This was possible in the framework of the collaboration between the Politecnico di Milano (DoE department) and CSEM-PV Center (Swiss Center for Electronics and Microtechnology). All the measurements have been taken with cutting edge machineries at the Energy Storage Research Center (ESReC) located in Nidau (CH). Specifically, two different periods abroad have been spent at CSEM facilities to carry on experimental measurements: (i) April-September 2016 – dynamic modelling of Li-ion cell; (ii)
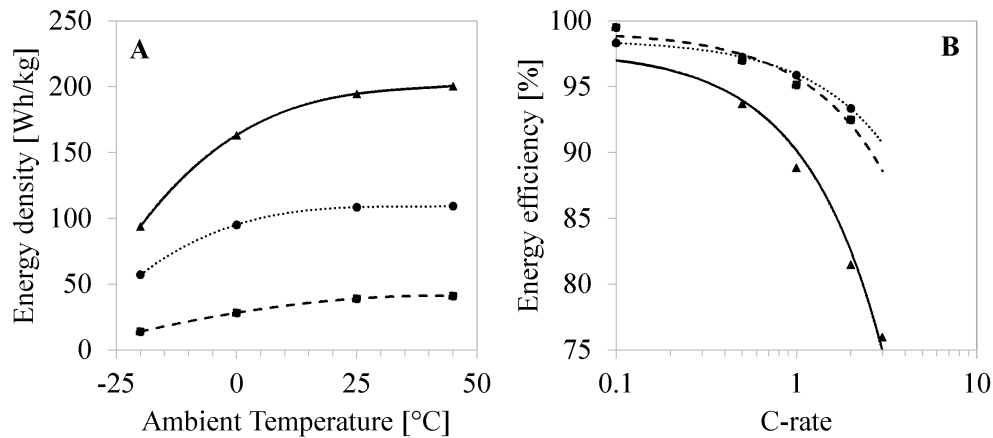
Figure 1.3 Measurements of Energy density (A) and Energy efficiency (B) trends on 3 different lithium-ion cell technologies (LNCO, LFP and LTO).

February 2017 (2 weeks) – set-up of aging tests on Li-ion cells.

Motivational example

By analysing the outcomes coming from the different projects/collaborations, some issues were raised. Significant question marks have emerged about the real BESS performances when deployed in real on-the-field applications. Measurements at ESReC lab highlight deviations in performances in between datasheet performances and "real-life" operations. If neglected, these variations could affect the reliability in the final application, jeopardising the investment.

As a flashy example (more analyses in the thesis's body), Figure 1.3 shows a comparison in the performances in between three different lithium-ion BESS that were measured in the framework of the collaboration between the Politecnico di Milano and CSEM-PV Center (details will be presented in chapter 3). By looking at the trends, one can easily conclude that BESS designers should not underestimate the differences in performances of the different available technologies. Each of them responds differently to changes in external conditions. The specific application that determines the severity of operations, together with the environmental conditions have to be taken into account in the design phase.

In general, energy density and power density are the most meaningful indicators used to compare the ability of different electrochemical devices in sustaining long periods of charge/discharge conditions or in providing to high currents peaks, given the same size of installation. Then, energy efficiency is used to understand the reliability of the technology in storing electricity. It is well accepted that new technology like lithium-ion BESS are standing at higher values of performances if compared to former technology like lead-acid BESS.

However, Figure 1.3-A shows the huge variability of the energy density of lithium-ion BESS with ambient temperature. All technologies underperform at very low temperatures and perform better at higher temperature. Figure 1.3-B shows an equally significant variation in the energy efficiency with the current rate. Even lithium-ion BESS can exhibit very low efficiencies. Losses can be more than 20% for some specific conditions.

This remarkable dependency from the operating conditions could have clearly a strong impact in the investment evaluation. Much attention is being paid to the capital

Table 1.1 Selected areas of analysis about BESS within the PhD work

1	Analysis of the different technology from a application perspective
2	Analysis of the theoretical framework that is required to identify the main working characteristics
3	Analysis of typical representative models both from electric and energetic perspectives
4	Transfer of knowledge into suitable models
5	Analysis of proper design strategies/tools that embraces a correct quantitative representation of BESS performances
6	Analysis of the impact of proper modelling on the design phase and model selection

costs (CAPEX) of BESS, in particular to the initial investment. However, the total cost of ownership of BESS includes other factors such as, in some cases, air conditioning to maintain the system in its operating temperature range, and in all cases by the cost of electricity lost over a charge/discharge cycles. Both are determined by the efficiency of the battery. BESS designers should then pay attention to the specific application for which the battery will be asked to work.

Energy density, power density and efficiency are strongly linked to the operating conditions. Similarly, lifetime of electrochemical devices is affected by many variables. It is well known that the available energy of a cell decreases with different cycling conditions. In some condition, the cell can last thousands of cycles while in other conditions only hundreds. This fact impacts decisively on the operational costs (OPEX) evaluation since it is based on the right evaluation of the expected lifetime to account for replacement costs.

Problems formulation

As emerged in the previous sections, several problems can be identified as main motivation of this thesis work. Table 1.1 summarizes the identified areas of analysis which are required to tackle the different issues:

1. Glaring differences in the performances are present among the different electrochemical technologies and, within the same technology, among the different chemistries. In general, different chemistries address different needs (e.g. energy vs. power). This should be considered when facing real applications because it will impact on the cost analysis and on the technical suitability. Consequently, a first area of study is the analysis of the different technology by differentiating them in terms of macro-area of performances (i.e. energy/power densities, efficiency, cost, durability) to acquire a picture of the overall technological situation.

2. Wide difference in performances requires the understanding of the main processes behind BESS operations. This means to identify the typical electrochemical processes (conduction processes, redox reactions, diffusion processes) that describe the overall response of an electrochemical device. Consequently, the second area of study is the analysis on the underlying theory of battery to capture the relationship between the real-time operation conditions and the overall BESS performances.

3. Substantial differences in the performances emerge in operations. The same device will perform differently if the operating and external conditions are changed. Factors like temperature, SoC variations, current rates affect how the same device perform and how long it will last. From an application perspective, this create lots of uncertainties as regards to the expected on-service reliability and expected lifetime. It is not plausible to measure and map all the performances of the selected device in all the possible conditions. Right models must play the role to represent the electrochemical device in its working characteristics. In this way, any kind of final

application can be simulated and the final design can be trusted. Consequently, a third area of analysis is the identification of the typical models used to represent BESS and to acquire the state of the art of the possible methodologies (energy analyses, electrical modelling, etc..).

4. BESS is not only a matter of electrochemical cells. Together with Battery Management Systems (BMS) and inverters, they normally constitute what is commonly called and sold as "battery systems". BMS play the role of controlling the different cells forming a battery module, while the inverter establishes the interface with the external world: loads, grids etc.. On the one hand, by including these elements in the modelling phase, the level of the analysis goes increasingly towards the final application perspective, on the other hand it increases the computational effort of the model. Consequently, a forth area of analysis rely on transferring the main findings into suitable models to be used for application evaluation. This means usually to find the right balance between a required level of accuracy and an acceptable time of elaboration.

5. Once a model is built, the next issue relies on the design analyses that allow to built reliable information about the BESS design for a specific application. In this case the context is of great importance because the complexity of the modelling should be linked to the level of details required to make a decision. For instance, planning analyses for off-grid systems that look at the right size of BESS from an energetic perspective are completely different from analysis of reliability for UPS services. The surrounding model might be the same but the level of details should be different. Consequently, the fifth area of study relies on the development of proper tools for the correct BESS design that embraces correct models.

6. Modelling of BESS highly influence the design analyses. Simplified models can give approximate evaluation in very fast time while a very complex model can give very precise information in a longer time. Consequently, the last area of analysis stands in the evaluation of the impact of a different modelling approach onto the design phase.

1.3 Methodology

As already highlighted, the issues which have just been introduced represent the typical topics which concern BESS modelling and design from a final application perspective. This thesis addresses the above issues by tackling them from three different methodology frameworks which aim at answering separately three main questions.

- *Framework of reference*: which theoretical framework and models should be considered to correctly describe BESS functioning?
- *Modelling framework:* How can BESS be properly modelled from an electrical perspective?
- *Design framework*: Which methodologies/tools can be developed to assess proper design of BESS in real application?

Figure 1.4 shows a schematic overview of the whole methodological frame. The introduced frameworks correspond to a different block of analysis:

The background analysis that is defined by:

- Analysing the different storage technologies available on market. This analysis serves to create a solid background about the main magnitudes that describes electrochemical storage systems. In the thesis, the focus is not general but tailored to the final application. The different technology are discussed and compared in terms of possible fields of application.
- Analysing experimentally the performances of different BESS technologies to

Framework 1: background analysis

Technology Overview

Performance analyses	Modelling approaches

Framework 2: Modelling analysis

Underlying physics

Cell modelling	Lifetime modelling

BMS modelling	Interface converter modeling

Framework 3: Design analysis

Stationary application		Automotive application	
Grid-tied	Off-grid	(P)HEV	BEV

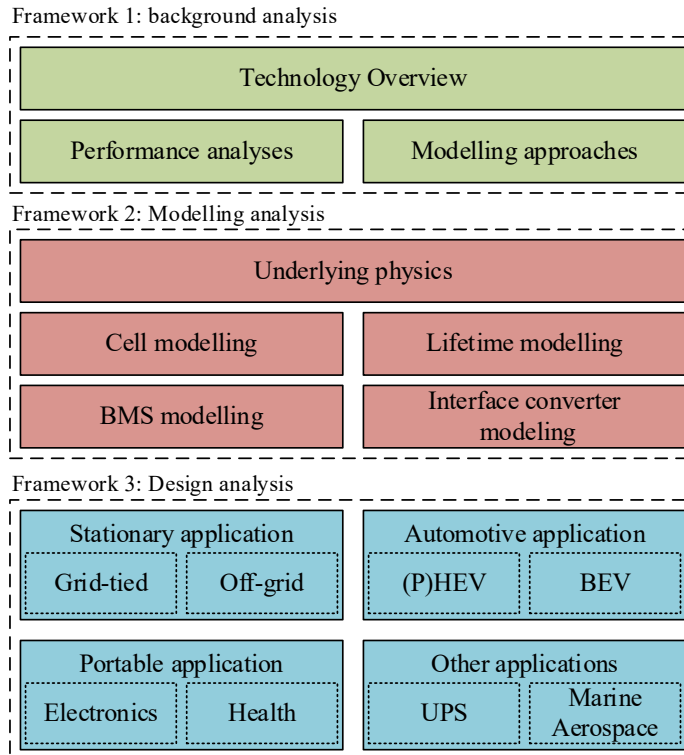| Portable application		Other applications	
Electronics	Health	UPS	Marine Aerospace

Figure 1.4 Schematic overview of the structure adopted to organize the typical topics concerning BESS correct modelling and design from final application perspective

effectively deepen the main characteristics and to define the parameters needed to properly measure BESS behaviours. These parameters formulation is an essential step for the approach adopted in the PhD thesis.

- Analysing the state of the art of the modelling approaches present in literature. This analysis is worthy and necessary in any research work since it creates the term of reference to which compare the proposed work. Moreover, it allows to describe the typical models features and make use of the most interesting one for the following phases of modelling and design development

2. The Modelling analysis which is divided by five macro-blocks which represent five tasks to be faced totally or partially depending on the degree of precision that is needed in the BESS modelling process:

- The study of the underlying *theoretical fundamentals* is needed to understand the different working conditions and to develop a proper modelling phase. The investigation is carried out starting from the basics of the electrochemical phenomena. This step is inevitable in order to build a significant model for the analyses of the next phases.

- The *cell modelling* focuses the attention on the founding element of any electrochemical device. With this assumption, we mean that the full representation of the dynamic response of the cell is assumed as pivotal for any further step of development. Then, the same model can be simplified to adapt to the specific analyses required for the final application.

- The *Battery Management System (BMS) modelling* is required to scale up from the purely cell model to the battery pack level. BMS is responsible for: (i) evaluating and monitoring the SoC and SoH of the battery pack; (ii) protecting

the battery from over-currents, over-pressures, faults and preventing it from operating outside safe values of voltages and temperatures; (iii) balancing and equalizing the charge levels of the different cells inside the battery pack which can behave differently due to variability in the manufacturing process of the cells.

- The *interface converter modelling* is required to move then from the battery pack to the integrated battery energy systems level. Several commercial BESS are sold as integrated systems which couples battery packs with inverters. Given the specific application, the role of the inverter is to determine the specific charge/discharge profile to be adsorbed or injected by the battery. Therefore, it has to communicate in a close way with the BMS.

- The *lifetime modelling*: once the battery modelling is ended in all its constituting elements, the lifetime modelling is also needed to properly evaluate the system degradation over time. This aspect is fundamental especially for design purposes because any investment evaluation closely depends on the accuracy in the lifetime estimation of BESS.

3. The <u>Design analysis</u> that can be assessed once the context of the final applications is defined. Different applications require different services from BESS, but different services bring to distinct charge/discharge profiles that impact on the performances and on the design phase. As highlighted at the beginning of this chapter, some major industrial sectors are interested by diffusion of BESS. In terms of the applications we can distinguish between:

- Stationary applications: that define those installations made for energy purposes. Two macro-areas can be further identified in terms of the different required approach in the design phase: (i) grid-tied BESS that are normally deployed for grid-support services on utility scale (from hundreds of kWh to tens of MWh) or for consumer use on domestic scale (maximum tens of kWh); (ii) off-grid BESS that are usually coupled with RES systems to provide electricity to remote areas of the world in the form of small stand-alone systems (maximum tens of kWh) to micro-grid (maximum hundreds of kWh).

- Automotive applications: that define all those applications made for mobility purposes. Taking EVs as a term of reference, three main categories can be distinguished (i): Hybrid electric vehicle (HEV) that uses small BESS (< 5 kWh) to recover braking energy leaving to ICE the main traction role; (ii) plug-in hybrid electric (PHEV) vehicle that couples BESS of medium size (5-20kWh) with ICE; (iii) battery electric vehicle (BEV) that use bigger BESS (20-100 kWh) being full electric. Given the different concepts, different design assumptions on BESS have to be made.

- Portable applications: that define applications of small size. Electronics devices represents the main market sector. Laptops, mobile phones, tablet are just some of the commercial products that contain an electrochemical cell to power the device. In this case, given the small size of the BESS (tens of Wh), the cost is not an issue while the performance in terms of charging time and SoC estimation are of relevant importance. For this reason, the approach to BESS design is completely different from stationary and automotive applications.

- Other applications: that comprehend all those applications that cannot be included in the above categories. For instance, Uninterruptible Power Supply (UPS) that constitutes a huge market especially for the secondary and tertiary sectors. Finally, also the marine and aerospace applications are interested in BESS development given their intrinsic off-grid nature coupled with other design requirements (e.g. weight in aerospace application).
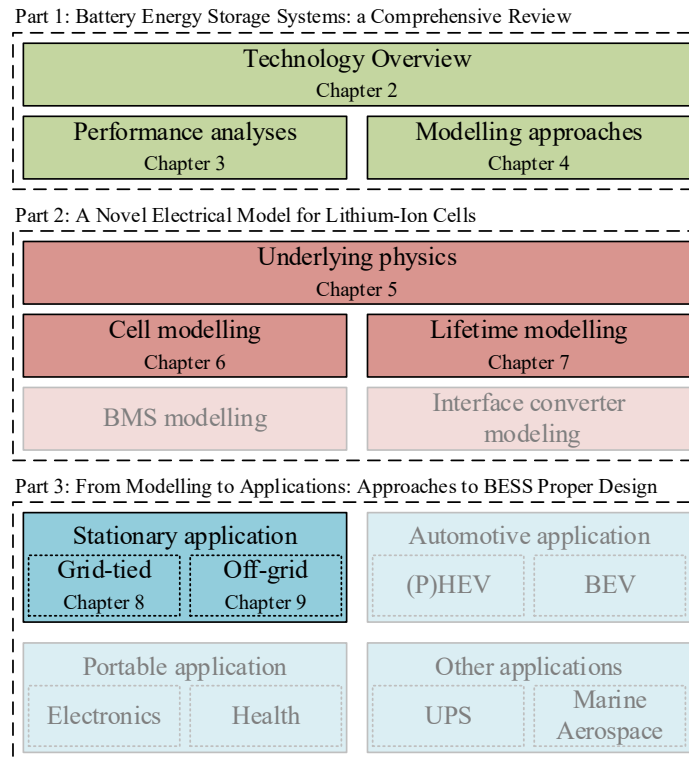
Figure 1.5 Summary of the thesis' contributions

1.4 Thesis Outline and Contributions

This thesis is a compilation of results published in scientific journals and conferences. It addresses some of the blocks of the three frameworks of analysis. With reference to the structure already proposed (Figure 1.4), the contributions are illustrated in Figure 1.5 and summarized in the following.

The thesis is divided into three parts:

- Part I: Battery Energy Storage Systems: a Comprehensive Review which addresses the topics constituting the Background analysis framework
- Part II: A Novel Electrical Model for Lithium-Ion Cells which address some of the topics constituting the Modelling analysis framework
- Part III: From Modelling to Applications: Approaches to BESS Proper Design which address some of the topics constituting the Design analysis framework

Part I is based on literature analyses combined with experimental activities which were necessary to synthetize and capitalize the main important aspects of BESS's behaviour that are needed for a proper BESS modelling and design phase.

Part II represents the main element of originality of the thesis. Starting from theoretical fundamentals, a novel electrical model for lithium-ion cells based on experimental measurements is presented, discussed and validated. Lifetime modelling elements are also proposed to create a wider background useful for application-oriented analyses, techno-economic analyses and investment evaluations.

Part III bridges the modelling phase with final applications, emphasizing BESS design criteria. Two different stationary applications are discussed that show how proper BESS model can influence the design conclusions. Specifically, the proposed novel model is

compared with traditional or well-established literature approaches. Therefore, each chapter of this part is structured according to: context analysis, the description of the BESS model, case study presentation, discussion. Overall, the analyses of part III are centred on electrochemical batteries, considering power electronics well-established with respect to both industrial applications and mathematical modelling. Nevertheless, power electronics could impact on electrochemical cells performances: this is one of the possible future development of the PhD work.

Chapter 2: Overview on Storage systems: from technologies to stationary applications

This chapter introduces the technology: BESS are among the most promising Electrical Energy storage technologies. The aim is to give a general overview about storage options, but with more focus on BESSs and Li-ion chemistries. The different available cathode, anode and electrolyte materials are presented. Expected performances, market share, producers and costs are used to compare the different BESS technologies. Finally, the whole discussion is contextualized for stationary uses: typical features of storage technologies are matched with the requirements of the final applications. This is to understand the feasibility of BESS in addressing the needs of the today's electric power system scenario in terms of expected performances and reliability.

Chapter 3: Performance evaluation of lithium-ion cells

This chapter deals in depth with BESS performances. Experimental measurements are presented about a technological comparison among three different Li-ion chemistries. Energy density, power density and efficiency are discussed in different testing conditions (temperature, SoC, operating rate). The analyses are carried out at cell level by following the IEC 62660-1 international standard in parallel with novel testing procedures. Finally, tests results about real application are presented and discussed. The final purposes are: (i) to understand the impact of the final applications on expected BESS performances and (ii) to create a reference of comparison for the analysis and development of a critical bibliographic review which aim at identifying the appropriate mathematical models capable of representing the dynamic behaviour and final performances measured in the laboratory.

The results have been capitalized in the following publications:

C. Brivio, V. Musolino, P.-J. Alet, M. Merlo, A. Hutter, C. Ballif, Analysis of lithium-ion cells performance, through novel test protocol for stationary applications, *6th International Conference on Clean Electrical Power, Santa Margherita Ligure,* (2017). 410-415.

C. Brivio, V. Musolino, P.-J. Alet, M. Merlo, A. Hutter, C. Ballif, Application-independent protocol for predicting the efficiency of lithium-ion battery cells in operations, *Journal of Energy Storage,* (Under-review)

C. Brivio, M. Delfanti, D. Falabretti, M. Merlo, M. Moncecchi, V. Musolino, I sistemi di accumulo elettrochimico: prospettive ed opportunità. *Libro bianco dei sistemi di accumulo elettrochimico ANIE-RSE 2017.*

Chapter 4: Review of approaches to battery modelling

This chapter reviews approaches to battery modelling. Literature review on battery modelling (mainly at cell level) is presented. The models have been grouped into four general different approaches: electrochemical models, analytical (empirical) models,

electrical models and stochastic models. Moreover, two main tasks are identified for battery models: the estimation of the operating conditions (i.e. SoC estimation), the estimation of the lifetime (i.e. SoH estimation). These two main aspects create the frameworks of discussion through which the modelling approaches are deepened and compared.

Chapter 5: Physics of battery for impedance based modelling

This chapter provides the main theoretical pillars which are necessary for a proper electrical modelling process. The underlying physics about electrochemical cells functioning is deepened. Main novelty is represented by the approach used to link electrochemical phenomena to electrical modelling building process. Equivalent impedance representation is proposed for each phenomenon, which must be characterized by clear links in between the characterizing equation and the derived circuital element in the electrical model.

Chapter 6: Novel electrical model for Lithium-ion cell

This chapter presents a novel electrical model for Li-ion technology. The model is developed in the frequency domain by means of EIS measurements and is based on the theoretical framework of the previous chapter. The presented model is composed of impedance blocks connected in series and it accounts for the dynamic response of lithium-ion cells as a nonlinear function of SoC. Each block is derived from a specific electrochemical equation linked to the battery operations. The Model's parameters are determined by a specific procedure that is presented and applied to a commercial lithium-ion cell (lithium nickel oxide). Finally, validation of the model has been carried out in the time domain to understand the capability of the model in estimating the voltage at the device's terminals, efficiency, power and energy density under different operating rates and SoCs.

The results have been capitalized in the following publications:

C. Brivio, V. Musolino, M. Merlo, C. Ballif, Novel impedance-based model for lithium-ion cells: bridging the gap between electrical and electrochemical approaches, *IEEE transactions on energy conversion,* (under-review)

Chapter 7: Elements on lifetime modelling

This chapter investigates about lifetime modelling of BESS. The objective is to extend the dynamic modelling analyses of previous chapters by including elements of lifetime modelling. This serves to create a wider background useful for application-oriented analyses, techno-economic analyses and investment evaluations. The proposed modelling approaches are directly linked to experimental measurements on Li-ion technology. First, the aging testing procedure developed expressly to test Li-ion cells at different cycling conditions is presented; then, the test results are presented and used to discuss about the main aging effects; finally, three lifetime modelling approaches with different degrees of complexity are detailed.

Chapter 8: BESS for grid-tied applications: PCR service

This chapter deals with a first promising grid-tied stationary application for BESS: the Primary Control Reserve ancillary service. The objective is to identify the presence of business cases for the discussed application. A proper methodology is proposed which includes: specific control mechanism to change BESS working conditions in agreement

with external signals; unconventional droop-control law that takes into account BESS specific features; proper BESS models derived from previous chapters. The procedure has been applied to the Italian context. Simulations are run to discuss about: the influence of different BESS models in the evaluation of reliability for PCR service; the correct BESS design from a techno-economic point of view; proper control mechanisms to increase BESS availability.

The analyses are based on real measurements taken at the Politecnico di Milano within the framework of the *IoT-StorageLab*. The methodology is proposed in form of a computational tool in MATLAB®Simulink® named BESS4PCR.

The results have been capitalized in the following publications:

C. Brivio, S. Mandelli, M. Merlo. Battery energy storage system for primary control reserve and energy arbitrage, *Sustainable Energy, Grids and Networks*; (2016). 6:152-165.

D. Falabretti, M. Moncecchi, C. Brivio, M. Delfanti, M. Merlo, V. Musolino, IoT-oriented management of distributed energy storage for the primary frequency control. *2017 IEEE International Conference on Environment and Electrical Engineering and 2017 IEEE Industrial and Commercial Power Systems Europe (EEEIC/I&CPS Europe),* (2017). 1-6.

Chapter 9: BESS for off-grid applications: PV-BESS systems for rural electrification

This chapter deals with a second stationary application for BESS. The focus is on off-grid power systems for rural electrification in Developing Countries (DCs). The aim is to address the robust design of off-grid systems by including the majority of available inputs of these contexts. A novel sizing methodology is proposed which is composed of four blocks which separately face the different design phases: (i) the data inputs gathering block provides a methodology to collect field data as regards to weather condition and load demand; (ii) the inputs processing block elaborates the inputs to obtain load and sources profiles over the entire lifetime of the plant; (iii) the system modelling and simulation block models the main components (i.e. BESS), simulates different off-grid system configurations and evaluates the related techno-economic performances; (iv) the output formulation block finds the most robust design for the targeted context through specific optimization methods. The procedure has been applied to size a PV+BESS microgrid system to supply power to a rural village of Tanzania. Simulations are run to discuss about: the impact of different BESS model on the system energy design; the evaluation of the correct system design by accounting for different scenarios of load evolution.

The analyses are based on real data gathered within the framework of the *Energy4growing* project. The methodology is proposed in the form of a computational tool in MATLAB® named Poli.NRG (POLItecnico di Milano –Network Robust design)

The results have been capitalized in the following publications:

C. Brivio, M. Moncecchi, S. Mandelli, M. Merlo, A novel software package for the robust design of off-grid power systems, *Journal of Cleaner Production*, (2017), 166 (2017) 668-679.

S. Mandelli, C. Brivio, M. Moncecchi, F. Riva, G. Bonamini, M. Merlo, Novel LoadProGen procedure for micro-grid design in emerging country scenarios: application to energy storage sizing. *Energy Procedia*. 135 (2017) 367-378.

S. Mandelli, C. Brivio, E. Colombo, M. Merlo, Effect of load profile uncertainty on the

optimum sizing of off-grid PV systems for rural electrification, *Sustainable Energy Technologies and Assessments*. 18 (2016) 34–47.

S. Mandelli, C. Brivio, E. Colombo, M. Merlo, A sizing methodology based on Levelized Cost of Supplied and Lost Energy for off-grid rural electrification systems, *Renewable Energy* 89 (2016) 475–488.

S. Mandelli, C. Brivio, M. Leonardi, E. Colombo, M. Molinas, E. Park, et al., The role of electrical energy storage in sub-Saharan Africa, *Journal of Energy Storage*. 8 (2016) 287–299.

M. S. Carmeli, P. Guidetti, S. Mandelli, M. Merlo, R. Perini, G. Marchegiani, D. Rosati, C. Brivio, R. Di Molfetta. Hybrid Micro-Grid experimental application in Tanzania. *5th International Conference on Clean Electrical Power, Taormina*, (2015). 534-541.

S. Nassuato, G. Magistrati, G. Marchegiani, C. Brivio, M. Delfanti, D. Falabretti, et al., Distributed Storage for the Provision of Ancillary Services to the Main Grid: Project PRESTO, *Energy Procedia*. 99 (2016) 182–193.

M. Mauri., M.S. Carmeli, M. Merlo, C. Brivio. M. Mbuya, Neural network based load forecasting and fuzzy logic EMS for Ngarenanyuki school microgrid. *IEEE International Symposium on Power Electronics, Electrical Drives, Automation and Motion (SPEEDAM)*, (2016) 321-326.

Barbieri J, Colombo E, Ndma Mungwe J, Riva F, Berizzi A, Bovo C, et al. Set4food guidelines on sustainable energy technologies for food utilization in humanitarian contexts and informal settlements. *Energy Department – Politecnico di Milano*. 2015. ISBN: 978-88-941226-0-2

Chapter 10: Conclusions

A summary of thesis contributions is given to the reader.

Part I: Battery Energy Storage Systems: a Comprehensive Review

Part I of the thesis offers the reference framework about BESS and is based on literature analyses combined with experimental activities which are necessary to synthetize and capitalize the main important aspects of BESS's behaviour, which are needed for a proper BESS modelling and design phase.

Chapter 2 gives a general overview about storage options with more focus on electrochemical systems and Li-ion chemistry. Expected performances, market share, costs are used to compare the different BESS technologies with specific attention on stationary applications.

Chapter 3 concentrate in depth on BESS performances thanks to experimental measurements on three different Li-ion chemistries (LNCO, LTO, LFP). Energy density, power density and efficiency are discussed. Tests results about real application (frequency regulation) are presented and discussed.

Chapter 4 proposes a literature review on battery modelling which are categorized into four general different approaches: electrochemical models, analytical (empirical) models, electrical models and stochastic models. Two main tasks are identified for battery models: the estimation of the operating conditions (i.e. SoC estimation), and the estimation of the lifetime (i.e. SoH estimation). These two main aspects create the frameworks of discussion through which the modelling approaches are detailed and compared.

Overview on Storage systems: from technologies to stationary applications

Electrical energy is the product of conversion from a primary energy resource. It has several advantages, it is: (i) easy to transport once the proper infrastructure is built (i.e. electrical grid) with high efficiency, (ii) clean in the place of final use, (iii) easy to convert into other forms of energy: chemical, mechanical, etc. For this reason, a close nexus exists between the electrical consumptions and the GDP of a Country [23].

In the past, the storage of electrical energy was not convenient because of lower system efficiency: it was better to consume electricity when produced. Today, the emerging of new needs and applications (see Section 1.1), are changing the framework making valuable the storage choice.

BESSs are just one of the possible storage options. They belong to the broader family of Electrical Energy Storage (EESs), which collect all those technologies that are used to store electrical energy. ESS technologies can be classified, according to literature [3], [29], [30], following different methods based on their function, response time and suitable storage duration. However, the most widely used method is based on the form of energy stored in the system (Table 2.1).

- Mechanical Energy storage (MES) to which belong flywheels (FES), pumped hydro plants (PHS) and compressed air systems (CAES);
- Chemical Energy storage (CES) that include batteries (BES), fuel cells storage systems (FC) and Flow-batteries (FB)
- Electric or Magnetic storage (EMES) that include supercapacitors (SCES), Super conducting magnetic coils (SMES);
- Thermal Energy storage (TES) to which belong hot-thermal (HTES) and cryogenic (CrES) energy storages.

This chapter is structured with a succession of specific insights: after a brief review of all the EES technologies (Section 2.1), the review will focus on BESS options (Section 2.2), with specific attention on Li-ion chemistries (Section 2.3). Finally, the most used technologies will be discussed from a final application perspective (Section 2.4).

Table 2.1 Electrical Energy Storage technologies classification

MECHANICAL	ELECTRO-MAGNETIC	CHEMICAL	THERMAL
Pumped Hydro	Capacitors	Batteries	High-Temperatures
Compressed Air	Super Capacitors	Fuel cells	Cryogenic
Flywheels	Super conducting magnetic coils	Flow-Batteries	

2.1   Electrical Energy Storage technologies

Mechanical Energy Storage Systems

Pumped hydro storage

PHS is the most widely used (99% of world-wide installed electrical storage capacity) among the EES technology and it boasts a high technical maturity. PHS, which uses gravity to store energy, contributes about 3% of global generation capacity [3], [31]. A typical pumped hydro storage system uses two water reservoirs at different higher levels to pump water during off-peak hours, from the lower to the higher reservoirs. PHS system has a long history, the first one was built in Italy and Switzerland in the 1890s [32]. The efficiency of PHS ranges from 70% to 85% and the power rating from 1 MW to 3 GW with more than 40 years of lifetime [33], [34]. One limitation of pumped hydro storage is the dependence on topographical conditions and on an adequate supply of water [30], [35].

Compressed air energy storage

Compressed air energy storage (CAES) is another EES technology that, in terms of bulk energy storage plant available today, is the second in order after PHS technology. CAES can provide power output of over 100 MW with a single unit [30], [35]. This system uses air, at high pressure, as a storage medium. Electricity is used to compress air and store it in a reservoir, as cavern aquifers, abandoned mines [36]. When electricity is needed, the stored air is used to run a gas-fired turbine-generator, the electricity produced is delivered back onto the grid. The first utility-scale CAES plant was installed in Germany in 1978 [37], [38]. CAES has an estimated efficiency of 70% with an expected lifetime of about 40 years [39]. If, from one side, CAES has the advantage of a large capacity, on the other side, the major disadvantage to implement large-scale CAES plants is the identification of geographical locations.

Flywheel energy storage

FES is a system that stores electrical energy in the form of rotational kinetic energy. It included five main components: a flywheel, a group of bearings, a reversible electrical motor/generator, a power electronic unit and a vacuum chamber (which helps to reduced self-discharge losses) [40]. The amount of energy stored is proportional to the angular velocity reached. FES operates in charging and discharging mode: during the charge mode, a motor is used to accelerate a big rotating mass (flywheel); during the discharge mode, the kinetic energy is extracted by a generator driven by the inertia of the flywheel, resulting in a deceleration of the rotating mass. FESs can be classified in low speed FESs which rotate below 6×10^3 rpm, and high speed FES which can run up to about 10^5 rpm by exploiting advanced component material [30]. The key features of FES are: limited maintenance cost, cycle stability, long life, high power density, wide operating temperature range and environmental compatibility. However, these systems have a very high rate of self-discharge due to air resistance and bearing loss. In about 5-10 hours up

to 50% of stored energy can be lost [41]. For this reason, flywheels perform well when used in applications which demand high power for short periods together with a high number of charging-discharging cycles.

Electro-Magnetic Storage Systems

Capacitors

CS allow a direct storage of electricity. They are composed of, at least, two electrical conductors separated by a thin layer of insulator (as ceramic, glass or plastic film) called dielectric. During the charge phase, energy is stored in an electrostatic field. The maximum operating voltage of a CS is dependent on the breakdown characteristics of the dielectric material. Capacitors show high power density and they can perform several thousand of charge/discharge cycles with a high efficiency and without material degradation [29]. Nevertheless, CS has limited capacity, low energy density and high-energy dissipation due to self-discharge. For these reasons, capacitors are used in power quality applications as high voltage power correction.

Supercapacitors

SCES, also known as double-layer capacitors (DLC) or ultracapacitors, are composed by two conductor electrodes, an electrolyte and a porous membrane separator. In SC, the energy is stored in form of static charge on the surface between the electrolyte and the two conductor electrodes. Compared to conventional capacitors, SC have higher energy storage capabilities by approximately two order of magnitude ($\sim$ 20 Wh/kg) [29]. The energy storage capacity of SCES is directly proportional to the square of its voltage:

$$E_{SCES} = \frac{1}{2} CV^2 \tag{2.1}$$

where C is the capacitance of the SCES. Supercapacitors have both characteristics of conventional CS and batteries. The main features of SC are: long cycling times (more than 10^5 cycles), very fast charging and discharging capability (due to low inner resistance, unlike traditional CS), high reliability, no maintenance, operation over a wide temperature range and high cycle efficiency (about 84%-97%) [3]. However, they have high self-discharge rate per day, about 5%-40%, and high capital cost, 6000 $/kWh [42]. Since the energy stored must be used quickly, SCES are suited for short-term storage applications, but not for large-scale and long-term energy storage.

Superconducting magnetic energy storage

SMES systems store energy in a magnetic field generated by the flow of a direct current (DC) in a superconducting coil, which is cryogenically cooled below its superconducting critical temperature. SMES are mainly composed by: a superconducting coil unit, a power conditioning subsystem and a cryogenically cooled refrigerator system [43]. The energy stored in SMES is represented by the following equation:

$$E_{SMES} = \frac{1}{2} LI^2 \tag{2.2}$$

where L and I are current and inductance of the wire. Among the superconducting materials the most commonly used is the Niobium-Titanium (NbTi) that operates at a very low temperature of about 9.2K [44]. Superconducting coil can be classified in two groups: low temperature superconducting (LTS) coils which work at 5 K and high

temperature superconducting (HTS) coils which work at 70K. The main features of SMES are: high power density, very quick response time (millisecond), very quick discharge time, high cycle efficiency (from 85% to 95%) and long lifetime (more than 30 years) [30]. Theoretically the energy in SEMS can be stored indefinitely (as long as the cooling system is operating), however this is limited by the energy demand of the refrigerator system. This storage system has a high capital cost (up to 10000 $/kWh) and highly day self-discharge (10%-15%) [45], [46].

Thermal Energy Storage Systems

Thermal Energy Storage System (TES) comprises a variety of technologies that store electric energy in the form of heat in insulated containments [47]. TES systems are currently under research and are usually composed of: a storage medium in a reservoir, a packaged chiller or built-in refrigeration system, piping, pumps and controls. TES, depending on the range of operating temperature, can be divided into cryogenic energy storage and high-temperature energy storage.

Cryogenic energy storage

CrES uses a cryogen to obtain the electrical and thermal energy conversion [48], [49]. CrES main feature are: high energy density (100-200 Wh/kg), low capital cost and a relative long storage period. Nevertheless, CrES has a low efficiency, about 40%-50% [29].

High-temperature

HTES convert electricity into high-temperature heat (about 500°C). An electrical heater generates the charging process. Heat is stored in a thermal storage (magnesium oxide bricks or molten salt). During discharge, the heat is extracted from the thermal storage to generate steam that drives a turbine to produce power [41].

Chemical Energy Storage Systems

CES include batteries (BES), fuel cells systems (FC) and Flow-batteries (FB). In this sub-section, a brief overview about all of them is presented. Afterwards, in section 2.2 and section 2.3, the attention will be moved to BES systems. The different available technologies will be deeply discussed and compared, with special focus on Lithium-ion chemistries.

Battery Energy Storage

If Alessandro Volta, Luigi Galvani, and Benjamin Franklin were alive today they probably would be mesmerized by the different types of battery and how much they have evolved from their original inventions and discoveries. Nowadays, BES, also known as rechargeable (secondary) batteries, are one of the most used EES technologies to the point that they have permeated industries and everyday life activities and devices. There are several existing types/technologies of BESS to choose from. The wide assortment of technologies is directly linked to the wide range of applications in which they can be used. For this reason, they have attracted huge attention from public and private sectors in the last decade, both for research and industrial development. Section 2.2 will detail the functioning, characteristics and opportunities of the main BESS technologies available on the market. Moreover, section 2.3 will go deeply into details of one specific technology that is the Lithium-ion chemistry. Given their high performance together with the huge decreasing costs, they are actually forecasted to play a relevant role in the future energetic panorama.

Flow Batteries

FBs store energy in one or more electroactive species, which are dissolved in liquid electrolytes. The electrolytes are contained in external tanks and they can be pumped through the electrochemical cell that converts chemical energy directly to electricity and vice versa. The system is based on the reduction-oxidation reactions of the electrolyte solutions. The power capability of the FB system is dependent on the size and design of the electrochemical cell, while the volume of electrolytes determines the energy capability. An important feature of FB systems is the low self-discharge thanks to the electrolytes stored in separated and sealed tanks. Moreover, FB can release energy continuously at a high rate of discharge for up to 10 hours [50]. The main drawback is the low gravimetric energy density due to the massive plant configuration needed. FB are differentiated based on the electrolytes and onto the electrochemical reactions. The ones knows mostly are:

- Vanadium Redox Flow Batteries (VRB), which store energy using vanadium redox couples (V^{2+}/V^{3+} in the negative half-cell and V^{4+}/V^{5+} in the positive half-cell). These are stored in mild sulphuric acid electrolytes. During the charge/discharge cycles, H^+ ions are exchanged through the ionic selective permeable polymer membrane. The cell voltage is about 1.4–1.6 V and the efficiency can be up to 85% [51]. Main features of VRB are the quick responses (faster than 1 ms) and the possibility of operating for 10000-16000 cycles [52]. However VRB presents low electrolytes stability and high operating costs [53].
- Zinc Bromine Flow Batteries (ZnBr) are based on zinc and bromine elements, which are the reactive component of aqueous electrolyte solutions stored in external tanks. The main characteristics of ZnBr batteries are: the relatively high volumetric energy density (30-60 Wh/l), the cell voltage (1.8 V), the estimated lifetime of about 10-20 years, the discharge duration up to 10h [54]. Nevertheless, ZnBr batteries present some disadvantages: material corrosion, dendrite formation, relatively low efficiency (65%-75%) and they operate in a narrow temperature range [55].

Fuel cells

The fuel cell is an electrochemical energy conversion device, not a storage mean. For this reason, it is often confused with the fuel-cell based storage system (FC) which is the storage solution composed by an electrolyser, a hydrogen storage tank and the fuel cell. The idea is to use "excess" electricity (from RES for instance) to produce hydrogen via electrolysis. Hydrogen is then stored under pressure in tanks for an unlimited time. When requested, hydrogen and oxygen flow into the FC where an electrochemical reaction takes place, resulting in heat releasing and electricity generation. Until now, no commercial fuel-cell based storage systems are present for electricity purposes. This is because cycle efficiency is tremendously low and cost is high.

2.2 Battery Energy Storage Systems

The main element of a BESS is the electrochemical cell. Number of cells are connected in series or in parallel to constitute a battery of the chosen capacity and voltage.
A typical electrochemical cell is composed of (Figure 2.1):

- The anode that gives electrons to the load and is oxidised during the electrochemical reaction.
- The cathode accepts electrons and is reduced during the reactions.
- The electrolyte (solid, liquid, or viscous) that provides the medium for transfer of ions between the two electrodes.
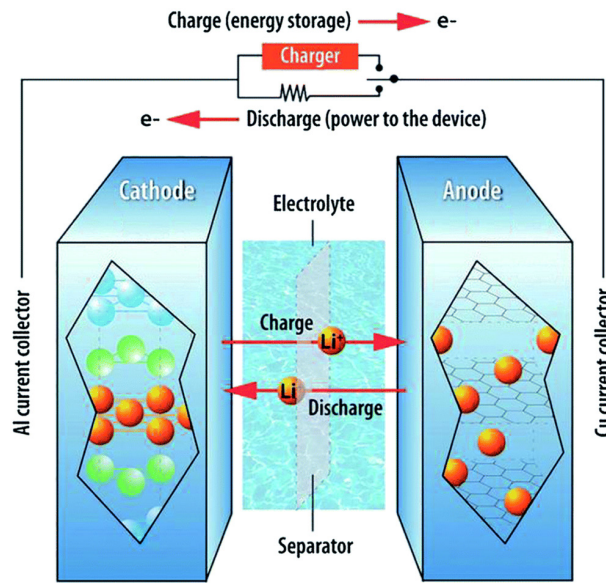
Figure 2.1 Schematic diagram of rechargeable batteries working principles [56].

- The separator between positive and negative electrodes for electrical insulation.

During the discharge phase, the electrochemical reaction provides the electrons (i.e. current) to sustain the loads and therefore the cathode is the "+" terminal while the anode is the "-" terminal. During the charge phase, the reverse reaction occurs by applying an external voltage source; therefore the cathode is the "-" terminal while the anode is the "+" terminal.

The several possible chemical reactions, which are listed in Table 2.2, differentiate the available technologies and result in a wide spectrum of available performances (energy density, power density, efficiency), lifetime and costs Table 2.3. Overall, BESS can be classified according to the main element involved in the chemical reaction. We can identify lead-based, lithium-based, Nickel-based and Sodium-based BESS.

Table 2.2 Chemical reactions and cell voltages of main BESS technologies

Type	Anode and Cathode reactions	Cell voltage
Lead-Acid	$Pb + SO_4^{2-} \leftrightarrow PbSO_4 + 2e^-$ $PbO_2 + SO_4^{2-} + 4H^+ + 2e^- \leftrightarrow PbSO_4 + 2H_2O$	2.0 V
Li-ion (graphite anode)	$LiXXO_2 \leftrightarrow Li_{1-n}XXO_2 + nLi^+ + ne^-$ $C + nLi^+ + ne^- \leftrightarrow Li_nC$	3.6 V
Nickel-metal-hydride (NiMH)	$Ni(OH)_2 + OH^- \leftrightarrow NiOOH + H_2O + e^-$ $H_2O + e^- \leftrightarrow 0.5H_2 + OH^-$	1.2 V
Nickel-cadmium (NiCd)	$Cd + 2OH^- \leftrightarrow Cd(OH)_2 + 2e^-$ $2NiOOH + 2H_2O + 2e^- \leftrightarrow Ni(OH)_2 + 2OH^-$	1.2 V
NaS	$2Na \leftrightarrow 2Na^+ + 2e^-$ $xS + 2e^- \leftrightarrow xS^{2-}$	2.0 V
NaNiCl$_2$	$2Na \leftrightarrow 2Na^+ + 2e^-$ $NiCl_2 + 2e^- \leftrightarrow Ni + 2Cl^-$	2.6 V
VRB (Flow battery)	$V^{4+} \leftrightarrow V^{5+} + e^-$ $V^{3+} + e^- \leftrightarrow V^{2+}$	1.4-1.6 V
ZnBr (Flow battery)	$2Br^- \leftrightarrow Br_2 + 2e^-$ $Zn^{2+} + 2e^- \leftrightarrow Zn$	1.8 V

Table 2.3 Characteristics of different BESS technologies. Costs refer to year 2015 [30], [57]

	Lead-Acid	Ni-Cd	NiMH	NaS	NaNiCl$_2$	Li-ion
Cell voltages [V]						
Nominal	2	1.2	1.2	2	2.6	2.4-3.8
(voltage limits)	(1.8-2.4)	(1-1.5)	(1-1.5)	(-)	(-)	(1.8-4.2
Energy density:						
Gravimetric [Wh/kg]	25-50	40-80	30-80	90-120	100-120	60-260
(Volumetric [Wh/l])	(60-70)	(50-150)	(140-300)	(345)	(160-190)	(130-600)
Power density:						
Gravimetric [W/kg]	60-180	150	250-1000	-	-	500-3000
(Volumetric [W/l])	(100)	(2110)	(400)	150-160	150	(1200-6500)
Cycle-life	300-2000	1000-2500	500-1500	2500-4000	2500-3000	700-7000
Operating temp. [°C]	-20/+60	-40/+60	-20/+60	300/400	300/400	-40/+60
Cost [€/kWh]	100-200	350-750	150-250	300	100-250	200-1900

Lead-acid

Lead-acid battery is the most mature, well known and widely used BESS type. Lead-acid batteries are used in all industrial applications, from telecommunications system to automotive but also in naval and submarine applications. The first rechargeable lead-acid battery was developed by Gaston Planté, who began experiments in 1859 towards development of a commercial storage battery. In the first decade of the 20th century, lead-acid batteries found use in the new-born automobile market as prime movers for electric vehicles; however, this application faded as gasoline ICE became the favoured prime movers for vehicles. The technology re-entered the automotive market in the 1920s for starting batteries. Lead-acid battery technology continues to dominate the rechargeable battery market to the present day.

There are different types of lead-acid batteries, each appropriate for specific applications. Although all types of lead-acid batteries follow the same basic chemical reaction, they can vary widely in terms of cost, method of manufacture and performance. The main components are: cathode made of PbO$_2$, anode made of Pb, electrolyte that is sulphuric acid. Lead-acid batteries have fast response times, small daily self-discharge rates (<0.3%), low capital costs and a service life which can reach up to 6-15 years [19], [46], [58]. However, they have a relatively low cycling times (1500 cycles at 80% of DoD), very low gravimetric and volumetric energy density (25-50 Wh/kg, 50-90 Wh/L) and very poor performance at a very low temperature [30].

There are two main categories of lead-acid batteries: flooded or vented types (VLA), in which the electrodes are immersed in reservoirs of excess liquid electrolyte; and sealed or valve-regulated types (VRLA), in which electrolyte is immobilized in an absorbent separator or in a gel. These two types are significantly different in terms of design, manufacturing, operating characteristics, life expectancy, and cost.

- VLA batteries are the traditional form of lead-acid batteries and continue to form the bulk of the market, due to their use in automotive sector and in most industrial applications. There are three general types of VLA: starting, lighting and ignition batteries, deep-cycle or traction batteries, and stationary batteries.
- VRLA batteries are constructed and operated quite differently from VLA, due to their starved electrolyte design. The electrolyte is contained within an absorbent separator or a gel to prevent migration out of the cell. VRLA batteries typically have shorter service life than conventional flooded lead-acid designs. These batteries have found application in portable electronics, power tools, and uninterrupted power supplies

(UPS), and in a few large applications such as forklift batteries. There are two types of VRLA batteries, depending on how the electrolyte is immobilized, the absorbed glass mat (AGM) VRLA and the gelled electrolyte VRLA (often known as gel cells).

In order to improve lead-acid battery performances, while maintaining their low systems cost, new innovating materials are under R&D. For instance, carbon-enhanced electrode is increasing the energy density up to 150 Wh/kg and the coupling with carbon supercapacitor is creating new advanced hybrid lead-acid batteries [59].

Nickel-based battery

The positive characteristics of nickel-electrode batteries have been recognized since Thomas Edison introduced the first commercial nickel-iron battery a century ago. Nickel-based batteries are composed by the association of nickel with different material, leading to the production of a variety of technologies, each with its own advantages and disadvantages.

There are five main battery technologies that use the nickel-electrode: nickel-iron (NiFe, the first designed to replace lead-acid battery), nickel-cadmium (NiCd, the most common), nickel-hydrogen (NiH$_2$, often used for aerospace applications), nickel-metal hydride (NiMH, the most promising option), and nickel-zinc (NiZn, the least mature of Nickel-based technologies). Among all Nickel-based battery options, NiCd and NiMH are the most used in today market.

Nickel-cadmium battery

Nickel-Cadmium (NiCd) batteries are the most common nickel-electrode batteries in the utility industry today [60]. NiCd battery uses nickel hydroxide and metallic cadmium as the two electrodes and an aqueous alkali solution as electrolyte. This technology presents two main weaknesses: the use of cadmium and nickel, which are toxic heavy metal, and the so-called "memory-effect". Production, use, and disposal of NiCd batteries are carefully monitored. The industry has made significant efforts to promote recycling, so that all cadmium from the battery industry is recovered. Concerning the "memory-effect", this means that the available capacity of the battery can be dramatically decreased if the battery is charged after being only partially discharged. This effect is correctable through a reconditioning process in which the battery is fully discharged and then recharged [61]–[63].

Nickel-metal Hydride battery

Nickel-metal Hydride (NiMH) battery is an outgrowth of NiH$_2$ technology. It is similar to NiCd battery, but with hydrogen as the negative electrode. In NiMH batteries, the hydrogen is absorbed in a metal alloy, which is usually a complex mix of elements. These batteries have good gravimetric and volumetric energy densities: around 70-100 Wh/kg and 170-420 Wh/l respectively, better that those of NiCd batteries [64], [65]. Moreover, they have a reduced "memory-effect" and are more environmental friendly (no cadmium). NiMH batteries have replaced NiCd in relatively low-current applications, including portable computers, cellular phones, and camcorders, but not in high-rate applications such as power tools. The production of large NiMH batteries has been limited, in part due to the difficulty of manufacturing the metal-hydride complex [66].

Molten-salt battery

Sodium-sulfur battery

Ford Motor Company is credited with initial recognition of the potential of the

sodium-sulfur battery based on a beta-alumina solid electrolyte in the 1960's.

The main features of NaS battery are the high volumetric energy density (150-300 Wh/l), almost zero daily self-discharge, long cycle capability (2500 cycle upon 90% DoD) and long discharge period (about 6 h) [36], [67]. NaS battery works in the temperature range of 300-350°C. During discharge, the sodium (negative electrode) is oxidized at the sodium/beta alumina interface, forming Na^+ ions. These ions move through the beta alumina solid electrolyte and combine with sulfur that is reduced at the positive electrode to form sodium pentasulfide (Na_2S_5), which is immiscible with the remaining sulfur thus forming a two-phase liquid mixture. After consuming all the free sulfur phase, the Na_2S_5 becomes converted into single-phase sodium polysulfides with progressively higher sulfur content (Na_2S_{5-x}).

NaS batteries are economic and with limited maintenance cost, thanks to the material of construction that is affordable and also recyclable. However, the main weaknesses of these batteries are high capital cost, high operational temperature requirement and high operational hazard due to use of metallic sodium, which is combustible if exposed to water. R&D is focused mainly on enhancing the cell performances and on decreasing the high temperature operating constrains.

The main application are in the electric utility distribution grid support, wind power integration, and grid services [36]. One of the largest single installations of NaS batteries is the 34 MW Rokkasho wind-stabilization project in Northern Japan which has been operational since 2008. Moreover, the capability to provide prompt and precise response makes NaS useful for applications in grid power quality regulation. For these reasons, just a few years ago, NaS batteries were considered as one of the most promising candidate for EES applications. Nowadays, the progress in Lithium-ion technology has reduced the interests in NaS technology.

Sodium Nickel Chloride (NaNiCl₂) battery

Sodium nickel chloride battery is also known as the ZEBRA battery, because it was invented in 1985 by the Zeolite Battery Research Africa Project (ZEBRA) group at the Council for Scientific and Industrial Research (CSIR) in Pretoria, South Africa.

During the charging phase, salt (NaCl) and nickel (Ni) are transformed into nickel-chloride ($NiCl_2$) and molten sodium (Na). The chemical reaction is reversed during discharge. The electrolyte is a fully dense ceramic material, similar to NaS battery, which provides fast transport of sodium ions and ensures the electrical insulation between anode and cathode. Cells are hermetically sealed and packaged into modules of about 20 kWh each.

ZEBRA batteries are high-temperature battery devices like NaS, they operate in a temperature range of 270°-350°C. They present moderate energy density and power density: 94-120 Wh/kg and 150-170 W/kg respectively [68]. The main advantages of sodium nickel chloride battery are good pulse power capability, cell maintenance, very little self-discharge and relatively high cycle life.

Lithium-based battery

Nowadays, Li-ion based BESS are dominating the market of portable devices and currently are a pivotal technology for the development of several industrial sectors (e.g. EVs and RES-E).

The history of Li-battery began with the use of Li-metal as anode. Li was found to be the most electropositive (–3.04 V versus standard hydrogen electrode) as well as the lightest metal. This eases the design of storage systems with high energy density. The first non-rechargeable Li-cells based on Li-metal was assembled in the 1970's [69]. The

key step for the first rechargeable Li-ion battery was the discovery of intercalation compounds which were found to react with alkali metals in a reversible way. In 1976, Whittingham, while working at Exxon, produced the first rechargeable Li-battery with cathode of layered TiS_2 (the best intercalation compound available at the time) and anode of Li-metal [70]. However, the commercialization of this battery failed due to problems of Li dendrite formation and short circuit upon extensive cycling and safety concern (explosion hazards) [69]. In the same period, Besenhard, Yazami, and Basu discovered that graphite, also with a layered structure, could be a good candidate to reversibly store Li by intercalation/deintercalation. Goodenough was then the first to propose the use of layered $LiCoO_2$ as high energy and high voltage cathode materials in 1981 and manganese spinel as a low-cost cathode material in 1983 [71]. In 1987, Yohsino et al. presented a patent on a prototype cell using carbonaceous anode and $LiCoO_2$ as a cathode [72]. However, the mass commercialization of these batteries started only in 1991 by Sony, who started to use Li-ion cells in personal electronic devices (e.g Walkman). The cells used by Sony had a maximum voltage of 4.1 V and an energy density of 80 Wh/kg [73]: considerably higher than Ni-Cd or NiMH cells, which were already commercialized for the same purposes. Other progresses were made from that time especially in the discoveries of new cathode and anode materials able to improve the performances (e.g. at the moment of the thesis writing energy density of lithium-ion cells can reach up to 300 Wh/kg), like the introduction of low-cost cathode of $LiFePO_4$ by Goodenough in 1996. Nowadays, R&D is still ongoing to improve Li-ion batteries available on the market and to introduce new disruptive innovations like Li-air or Li-Sulfur batteries.

Overall, lithium-ion BESS present better performances if compared to competing technologies as Ni-Cd, NiMH and lead-acid technologies. The main features of Li-ion cells are: high operating voltage (3.7 V on average), high gravimetric and volumetric energy density, no memory effect, low self-discharge rate (less than 20% per year) and operation in a wide range of temperature [73]. As well-known, the main drawback is represented by its high cost. However, as showed in Figure 1.2-B, a relevant cost reduction is ongoing, boosted by the automotive sector.

The following sections will firstly detail the functioning and main characteristics of lithium-ion technology. Secondly, it will detail the different available chemistries that are competing on the market from different perspectives: performances, costs, lifetime, safety and leading manufacturers. Finally, a brief overview about the future prospects will be presented.

2.3 Lithium-ion technology

There are four main types of lithium-ion cell form factors: cylindrical, prismatic, button, and pouch (or polymer) cells. Cylindrical and prismatic cells are commonly made of "laser-welded" aluminium cans and consist of liquid electrolyte. Pouch (or polymer) cells use a soft laminate casing. The pouch type cell has become the standard in many of the portable power applications such as smartphones and tablets due to their thin form factor [74]. The button cells are small and inexpensive to build; they reach high voltage because the cell is stacked into a tube. Button cells have no safety vents and can only be charged at a very low current rate. Nowadays, most of the button cells in use are not rechargeable and they are found only in devices like calculators, watches, car keys and memory backup.

Regardless of the form factor, a typical lithium-ion battery contains four main components: cathode, anode, separator and electrolyte. As regards to the electrodes, the cathode is an aluminium foil in many designs that is coated with the specific active cathode material, while the anode is a copper foil which is coated with a specific active

anode material. These two-coated foils are kept separate through the use of a separator material most often made of some type of polypropylene (PP) or polyethylene (PE) plastic. This forms the jellyroll, which is then inserted into the container or housing. This can be a metal can, a plastic enclosure, or a metal foil-type pouch. Finally, the electrolytic liquid is injected into the assembly which is then hermetically sealed.

Cathode Materials

The cathode materials are transition metal oxides having lithium. They represent the major source of Li-ions [76]. Ions must be able to diffuse freely through their crystal structure in order to classify them as cathode materials. The morphology of the crystal structure could be: one-, two-, or three-dimensional, and it determines the number of dimensions in which li ions are able to move. Cathode materials currently in use, can be divided in:

- Layered rock salt structure materials (two-dimensional crystal morphology). The most common example is lithium cobalt oxide ($LiCoO_2$), but also lithiated nickel as lithium nickel cobalt aluminium oxide ($LiNiCoAlO_2$) or lithium nickel manganese cobalt oxide ($LiNiMnCoO_2$). They are characterized by high structural stability; however, they are costly (due to their limited resources) and hard to synthetize.
- Spinel structure materials (three-dimensional crystal morphology). The main member of this category is lithium manganese oxide ($LiMn_2O_4$), which enables Li-ions to diffuse in all three dimensions. $LiMn_2O_4$ is one of the oldest compounds researched and still widely used. Spinels advantages are: lower cost and lower environmental impact than layered rock salt materials, but on the other side they provide lower energy density.
- Olivine structure materials (one-dimensional crystal morphology). The main compound of this category is lithium iron phosphate ($LiFePO_4$). They are non-toxic and they show lower capacity reduction during lifetime.

In 1995 when mass production of the lithium-ion battery had just started, $LiCoO_2$ was the dominant cathode material, with the spinel $LiMn_2O_4$ occupying only a small part of
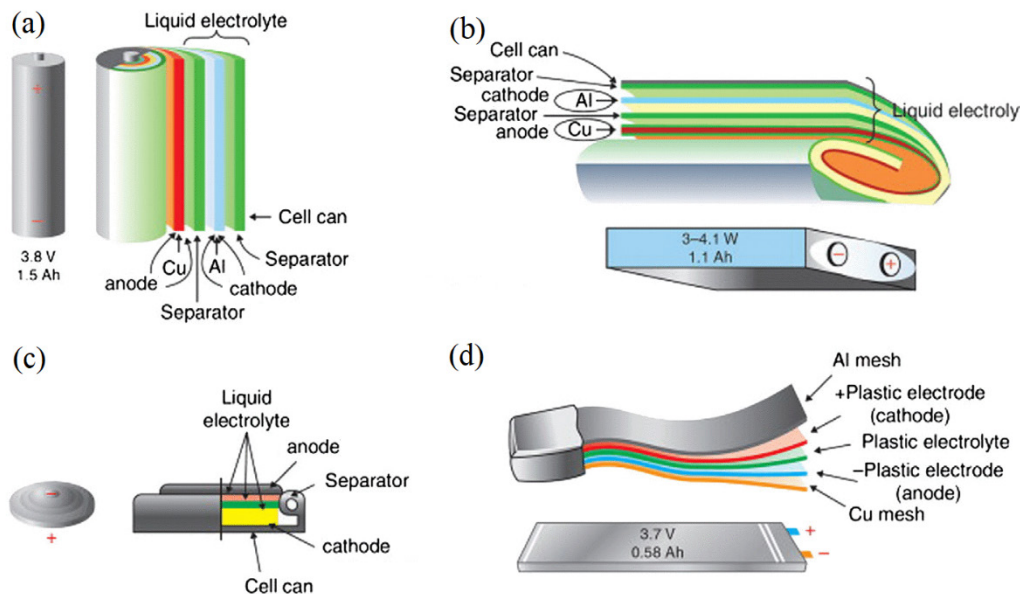

Figure 2.2 Four different form factors of commercially available lithium-ion cells: (a) cylindrical, (b) prismatic, (c) button, (d) pouch [75]
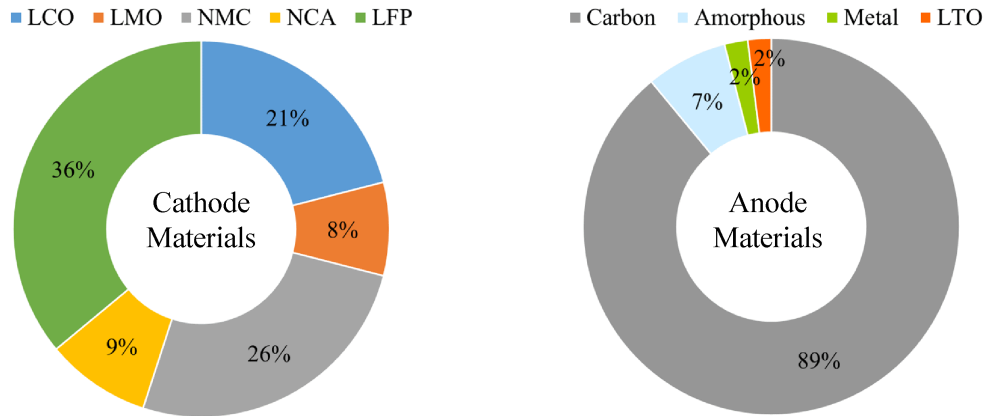
Figure 2.3 Cathode and anode active materials raw productions in 2016 by type [77]

the total market. $LiCoO_2$ predominance has been gradually declined due to considerations of cost and resource availability. By 2010, the market share for $LiCoO_2$ had declined to 40% while other materials like $LiNiMnCoO_2$ had increased considerably [73]. In 2016, $LiFePO_4$ and $LiNiMnCoO2$ occupied the 36% and 26% respectively, whereas $LiCoO2$ decreased to 21% (Figure 2.3).

Overall, cathode materials occupy 35% of the total cost of cells [57]. Therefore, the cost reduction of cathode materials is a pursued strategy by cell manufacturers to increase competitiveness. For this reason, manganese and iron-based cathode materials are replacing the widely used $LiCoO_2$: Mn and Fe are cheaper than Co due to their naturally abundant amounts [78].

Anode Materials

Currently, most anodes are carbon-based, however there are other types of anodes: lithium titanium oxide (which has been successfully commercialized) alloying-metal and amorphous. Current anode materials market share (i.e. raw production) are reported in Figure 2.3.

▪ Carbon-based anode. Carbon is still the anode material of choice; it allowed Li-ion battery to become commercially viable more than 20 years ago. Electrochemical activity in carbon comes from the intercalation of Li between the graphene planes, which offer good 2D mechanical stability, electrical conductivity, and Li-ion transport. Carbon has the joint properties of low cost, abundant availability, low potential vs Li, high Li diffusivity, high electrical conductivity, and low volume change during charge/discharge processes. Commercial carbon anodes can be divided into two types: graphitic carbons, which have large graphite grains, and hard carbons, which have small graphitic grains [79].

▪ Lithium titanium oxide ($Li_4Ti_5O_{12}$). Lithium titanate nanocrystals on the anode surface instead of carbon has been recently introduced into the market. Advantages are the high thermal stability (i.e. safety) and unequalled cycling capabilities. The main drawbacks are the high cost of titanium and the low voltage when coupled with any cathode materials [79].

▪ Alloying-metals. They are elements which electrochemically alloy and form compound phases with Li. They can have extremely high volumetric and gravimetric capacity, but they suffer from huge volume change which can cause serious damage (fracturing) and hazards [80]. Among the top studied Li-alloy anodes it is possible to mention: Li-Al (lithium aluminium) that suffer severe fracturing; Silicon which has

low potential vs Li, abundance, low cost, chemical stability, and non-toxicity; Selenium which has similar properties with Silicon except a lower gravimetric capacity; Germanium which does not suffer from fracturing even at larger particles sizes but it is too expensive for most practical application; Zinc, cadmium and lead which have good volumetric capacity but suffer from low gravimetric capacity.

- Amorphous: This type of anode uses oxides in which Li_2O are formed on the initial charging of the battery. The Li_2O acts as a 'glue' to keep particles of the alloying material (such as Silicon or Selenium) together [81]. Drawbacks of Li_2O is the low electrical conductivity and the large voltage hysteresis.

Electrolytes

The electrolyte is a mixture of organic solvents, additives and electrolytes salt compound which create a solution. Electrolyte acts as a conductor allowing the Li-ions to move between the anode and the cathode. The common solvents are a mixture of cyclic carbonate esters, such as ethylene carbonate and propylene carbonate, and linear carbonate esters, such as dimethyl carbonate and diethyl carbonate [73]. Functional additives are used to provide different functionality within the cell (e.g. flame-resistant solutions). Additives are specific and different from one manufacturer to another; forming one of the key areas of intellectual property of cell makers. Finally, two are the main choices for electrolyte salts: $LiPF_6$ (90%) and $LiBF_4$ (10%) [57].

Apart from liquid electrolyte, a new generation of bonded electrolyte have spread into the market. This is commonly linked to the so-called Li-ion polymer (LiPo) cells. LiPo cells cannot be considered a unique cell chemistry since they use identical cathodes (they can be built on many cathode/anode materials: LCO, NMC, LMO etc.) and anode material and contain a similar amount of electrolytes. The only difference with "traditional" lithium-ion cells is the use of a gelled-electrolyte [69]. Pouch cells are often identified as being LiPo cells.

Separators

The separator is a thin piece of material; usually made from PP or PE plastic, which separates the cathode and the anode while enabling ions to pass through. The separator material must be able to withstand the often-corrosive electrolytes environment while still maintaining the isolation of the two electrodes within the cell. If the two halves of the electrode come into contact, an internal short circuit will occur, causing a cell failure. Some manufacturers are beginning to integrate ceramic-layered separators in their cells as it enables higher temperatures and increases the safety. This also tends to improve the power rate capability of the cells by reducing the internal resistance [57]

Li-ion chemistries

Nowadays, many different chemistries that use different combinations of anode and cathode materials are competing in the market. Each of them has its own electrical and economical characteristics. Six are the principal Li-ion cell chemistries that are described below and summarised in table 2.4.

- <u>LCO</u> ($LiCoO_2$ -Graphite). The lithium cobalt oxide based battery is a mature battery technology characterized by high energy density. LCO is the most popular chemistry used in portable electronic devices due to its excellent charging/discharging rate and high energy density. A typical LCO cell has a nominal voltage of 3.7 V. Concerns with thermal stability and general safety make LCO not suitable for several applications like automotive [82].
Main manufacturers: Sony and Kokam.
- <u>LMO</u> ($LiMn_2O_4$-Graphite). The lithium manganese oxide based batteries have the

highest nominal voltage of 3.8 V. However, LMO cells have an energy density that is on average 20% less than the ones of LCO chemistry. Other key features of LMOs are high thermal stability, lower cost and improved safety. The drawbacks are lower energy and power densities, short cycle life and high capacity losses.
Main Manufacturers: Hitachi, Sanyo, GS Yuasa, LG Chem, Samsung, Toshiba, Altairnano.

- NCA (LiNiCoAlO$_2$-Graphite). The lithium nickel cobalt aluminium oxide based battery has a nominal voltage of 3.6 V and a better safety characteristic if compared with LCO-based battery. NCA chemistry present one of the highest performance in terms of power density and energy density.
  Main Manufacturers: SAFT, PEVE, AESC.
- NMC (LiNiMnCoO$_2$-Graphite). The lithium nickel manganese cobalt oxide based battery show a nominal voltage of 3.6 V. The cathode is composed of cobalt, nickel and manganese in different formula. The most commonly used NMC composition contains equal amount of all three metals (i.e. Ni$_{1/3}$ Mn$_{1/3}$ Co$_{1/3}$). NMCs have good energy density and lifetime.
  Main manufacturers: PEVE, EIG, Hitachi, Sanyo, LG Chem, Samsung, GS Yuasa, Boston Power, Kokam.
- LFP (LiFePo$_4$-Graphite). The lithium iron phosphate based battery has a voltage of 3.3 V, sensibly lower than the other chemistries mentioned above. However, LPF cells show a flat voltage profile that enhances the usage window. Moreover, this chemistry is the one with the lowest environmental impact among all the lithium-ion chemistries [83]. LFP is considered to be a leading chemistry of the future being suitable for stationary, automotive and back-up power applications because of their characteristics of high safety, good thermal stability and good lifetime.
  Main manufacturers: A123, BYD, GS Yuasa, SAFT, EIG, Lishen.
- LTO (Li$_4$Ti$_5$O$_{12}$-various). The lithium titanium oxide based battery is using a lithium titanate nanocrystals on the anode surface, instead of carbon. The cathode can be LMO or NMC. Using titanate instead of carbon at the anode represents an advantage since they can enhance the charge capabilities (i.e. sustaining higher currents) [87]. The main disadvantage are: (i) the very low voltage level that decrease sensibly the energy density if compared to other chemistries; (ii) the high specific cost that is

Table 2.4 Characteristics of different chemistries of lithium-ion batteries. Cost refers to cell price for utility-scale applications [84]–[86]

|	LCO	LMO	NMC	LFP	NCA	LTO
Cathode material	LiCoO$_2$	LiMn$_2$O$_4$	LiNiMnCoO$_2$	LiFePo$_4$	LiNiCoAlO$_2$	Various
Anode material	Graphite	Graphite	Graphite	Graphite	Graphite	Li$_4$Ti$_5$O$_{12}$
Cell voltages [V] Nominal (voltage limits)	3.7 (3-4.2)	3.8 (3-4.2)	3.6 (3-4.2)	3.3 (2.5-3.65)	3.6 (3-4.2)	2.4 (1.8-2.85)
Energy density: Gravimetric [Wh/kg] (Volumetric [Wh/l])	110-190 (250-450)	100-120 (250-265)	150-220 (325)	90-120 (220-250)	200-260 (210-600)	60-80 (130)
Power density: Gravimetric [W/kg] (Volumetric [W/l])	600 (1200-3000)	1000 (2000)	500-3000 (6500)	1400-2400 (4500)	1500-1900 (4000-5000)	750 (1400)
Cycle-life	500-1000	700-1000	2000-3000	>3000	>1000	3000-7000
Operating temp. [°C]	-20/+60	-20/+60	-20/+55	-20/+60	-20/+60	-40/+55
Cost [€/kWh]	200-400	300-850	450-850	350-1150	250-950	550-1900
Market launch [y]	1991	1996	2008	1996	1999	2008
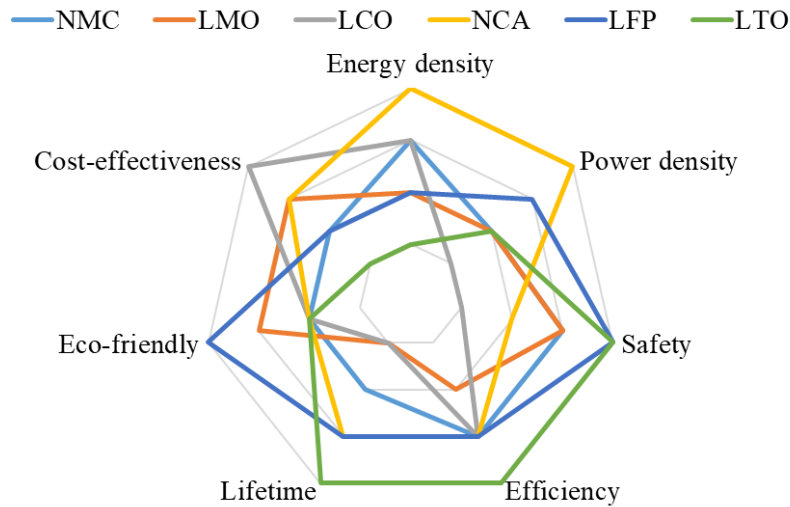
Figure 2.4 Comparison of Li-ion battery chemistries. Author's elaboration based on [84], [89]

limiting LTO diffusion, probably due to the current limited market share (Figure 2.3). The main advantages of LTO are: (i) the highest cycling performances; (ii) the high thermal stability in both charge and discharge state [88]; (iii) the tolerance of low temperatures. These characteristics make LTO a promising candidate for the future especially for applications that demand high power: automotive but also stationary applications.

Main manufacturers: Altairnano, Toshiba, EIG, Leclanché.

Radar plot of Figure 2.4 resumes the findings of previous sections by comparing the different available chemistries along six dimensions: energy density [Wh/kg], power density [W/kg], safety, efficiency, lifetime, cost and environmental impact. If we avoid focussing on the costs (a common issue among all lithium-ion chemistries), three chemistries seem to be the most promising for the near future: NCA, LFP and LTO. NCA appears to be the right choice when the requirements are on performances (energy density, power density and efficiency), LTO appears to be more suitable when long lifetime and safety are of main concern, while LFP seems to be preferable in term of overall environmental impact that consider damages to human-health, damages to ecosystems and recyclability [89].

In this frame, Chapter 3 will present a detailed analysis about Li-ion cells performances. A technological comparison is carried out through specific laboratory testing procedures. Three different chemistries: LFP, LTO and LNCO (very similar to NMC) are tested and compared as regards to their measured energy densities, power densities and efficiencies. Moreover, the same performances are evaluated also in case of real application (i.e. stationary application).

Future prospects of lithium-ion technology

In order to further advance in the science and technology of lithium batteries improvements in safety, environmental sustainability and energy content are needed. Apart from evolutions in the cathode and anode materials structures (Silicon for the anode and $LiNi_{0.5}Mn_{1.5}O_4$, $LiMO_2$ and Li_2MnO_3 for the cathode are expected to be the most promising materials for the near future [90]), new disruptive technologies are draining attentions and resources of many research centres around the globe.

A very promising option (at early stage of development) is the lithium-air, (Li_2O_2, Li-air) battery. This chemistry produces voltages of between 1.7-3.2 V and consists of a
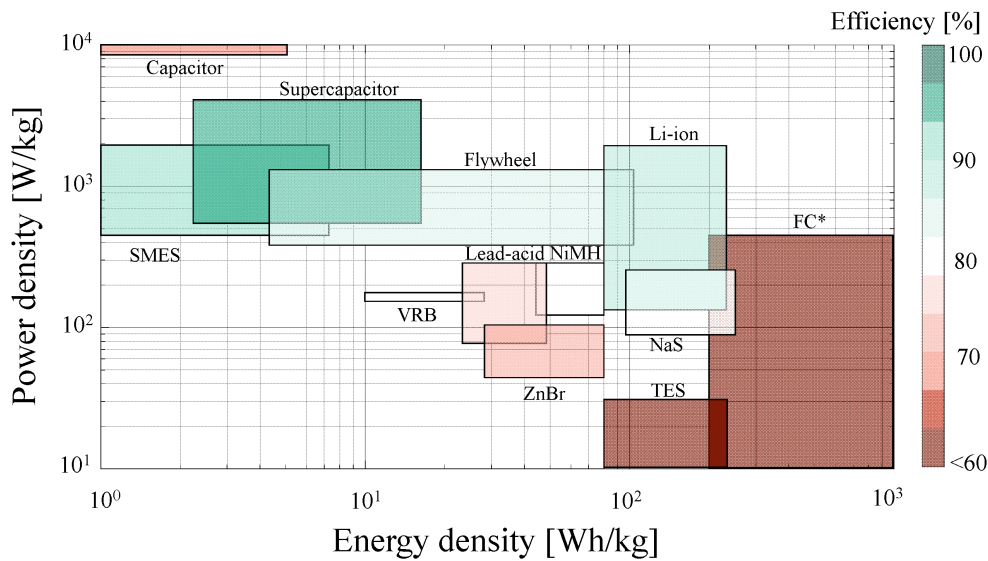
Figure 2.5 Comparison about energy density, power density and cycling efficiency for various EES technologies [11], [30], [93][1]

positive electrode of porous carbon and a negative electrode of lithium metal. By reacting lithium directly with oxygen from air, an incredibly high theoretical energy density (up to 13 kWh/kg) can be reached [91]. The main remaining challenges are: (i) the air quality, since the technology accept only very pure air that need to be filtered; (ii) the death syndrome that involves the formation of films producing barriers for the reactions; (iii) the very poor cycle life that currently reaches only 50 cycles [92].

Another promising candidate for high energy systems is the lithium-sulfur based battery (Li_2S, Li-S). Li-S has a cell voltage of 2.10 V and uses lithium metal as a negative electrode and sulphur as the positive electrode (instead of oxygen) in order to produce solid Li_2S (instead of solid Li_2O_2). Li-S is claimed to reach very high gravimetric and volumetric energy density of 2500Wh/kg and 2800Wh/l together with greater efficiency than the Li-air battery cells [69], [83]. Due to the low cost of sulfur, Li-S batteries have the potential to compete with the more established Li-ion chemistries. The main challenge is the limited cycle life of only 40–50 charges/discharges as sulphur is lost during cycling by reacting with the anode. Nevertheless, there already exist two manufacturers that claim to have solved the issue: Oxys Energy and Sion Power.

Finally, a fascinating evolution of the lithium battery is represented by the use of organic materials. Organic compounds are very attractive for positive electrodes because no expensive metal is used. The challenge is to exploit organic lithium battery electrode materials that can be synthesized by green chemistry from biomass, which is easily recyclable [83].

2.4   BESS performances for stationary applications

Previous sections have provided a full overview about the state-of-art of ESS technologies. However, this is not sufficient for system engineers since the main issue is to identify which technology is the most suitable for the different final application. In this

---

[1] As detailend in section 2.1, with FCs we intend fuel-cell based storage systems: the storage system composed by electrolyser, a hydrogen storage tank and the fuel cell. The overall efficiency is then the result of the efficiencies of each single component. FCs efficiency are always <40%.

section, an overview of this theme is proposed with focus on stationary applications.

In general, it is well accepted that no single EES technology can meet the requirements for all possible applications. Selection of ESS is based on the assessment of the characteristics of the different EES options against the requirements of the specific application.

Figure 2.5 compares ESS in terms of their typical energy densities, power densities and efficiencies. Energy densities and power densities are crucial when the size of ESS is of main concern. The higher the two indicators are the lighter and performant the BESS will be. Li-ion technology is the most positioned to the top-right of the graph: they have the best combination of energy/power performance available in the market to date. Good cycle efficiency is fundamental when the application is very stressful and prolonged in time. Efficiency has been continuously improved in time for all available technologies. As regards of BESS technologies, Li-ion batteries occupy the first position (η > 90% in standard conditions) followed by Nickel-based batteries (η > 85%), Molten-salt batteries (η > 80%) and lead-acid batteries (η > 75%).

In Table 2.6 and Figure 2.6 the focus is more on characteristics of BESS for industrial applications. Table 2.6 resumes the typical power rating, discharge time (i.e. typical capacity can be determined) and cycling factors of EES technologies. These three indices are more or less associated with the EES category. EMEST usually bring limited power (hundreds of kWs) and limited discharge time (secs) coupled with almost infinite cycling performances (> 10^5). MEST are good for very high power (hundreds of MWs) demand and long discharge time (hours) with high cycling capabilities (> 10^4). BESS can range widely in term of power (from ten of kWs to hundreds of MWs) and storage durations (from minutes to hours) being suitable for various applications, but they have considerably lower cycling capabilities if compared to other EES technologies (< 10^4).

Figure 2.6 resumes these statements by comparing the typical power and energy ratings in the same graph. The nominal discharge time at power rating is also shown within the range seconds-months. A mention deserves to be made about lithium-ion technology that is shown to occupy the wider area on the graph. This means a high suitability of Li-ion BESS for final applications. By merging the different areas in the figure, it is possible to derive a capability area for EES plants which should be matched
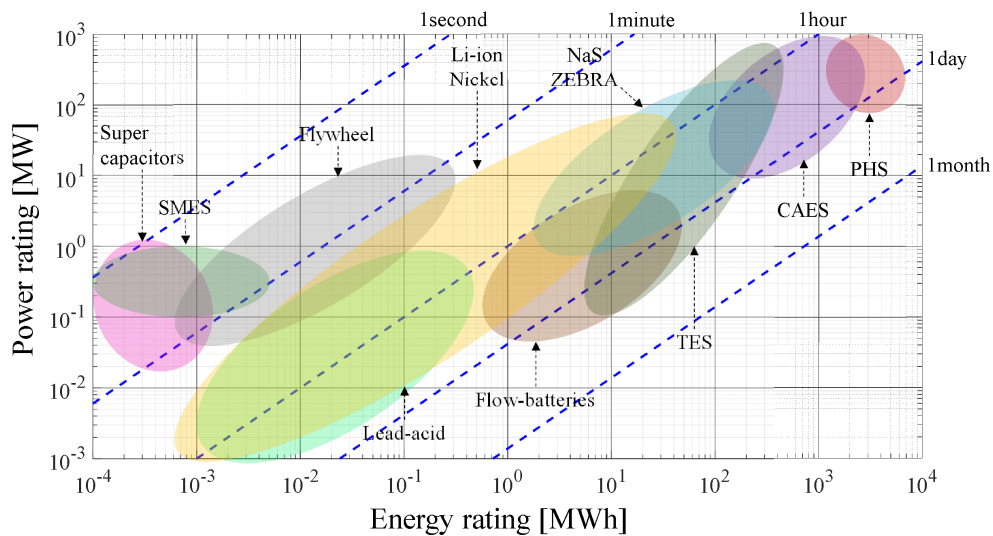

Figure 2.6 Comparison of Power/Energy ratings with discharge time at power rating for various EES technologies [2], [11], [30], [93]

45

Table 2.6 Typical key characteristics of EES technologies [30], [94], [95]

technology	Power Rating [MW]	Storage duration	Cycle-time	Calendar life [years]	Response time
Super capacitors	0.01-1	ms-mins	10^4-10^5	10-20	10-20 ms
SMES	0.1-1	ms-mins	$>10^5$	15-20	< 100 ms
PHS	100-1000	hours	$>10^4$	50-60	mins
CAES	10-1000	hours	$>10^4$	20-40	secs-mins
Flywheels	0.001-10	secs-mins	10^4-10^5	15-20	secs
NaS	1-100	mins-hours	2500-4000	10-15	10-20 ms
NaNiCl$_2$	1-10	hours	2500-3000	15	10-20 ms
Lead-acid	0.01-1	mins-hours	500-2000	5-15	10-20 ms
Li-ion	0.01-100	mins-hours	1000-7000	5-15	10-20 ms
Ni-Cd	0.01-10	mins-hours	2000-2500	10-20	10-20 ms
Flow Battery	0.1-100	hours	10^4	10-20	10-20 ms

with the areas belonging to stationary applications.

By considering the entire value chain of electrical systems, EES can be classified in terms of their discharge duration [93]. If seconds to minutes, they are used for achieving power quality, if minutes to hours for bridging power, if several hours for energy management. Within these categories, it is possible to highlight some key stationary applications (Table 2.5) that represent actual opportunities for EES [17], [30], [35]:

- *Renewable integration*: to minimize intermittency of RES by time-shifting production and dispatching. The storage is used to optimize the RES production in terms of supply quality and value. The typical size of application can be from hundreds of kW (distribution networks) to tens of MW (Transmission level). The discharge duration can be in the range of some minutes to some hours.
- *Load levelling*: to balance the large fluctuations associated with electricity demand and to smooth intermittent generation. The energy is stored during off-peak periods and used for the application. The capacity is typical at the MW level and it requires high energy efficiency since the charge/discharge periods can last several hours.
- *Spinning reserve*: to reduce requirements on idle generators that are dedicated to take over of any sudden failure of major generator. Reserve capacity used to keep the system balanced. The installations are usually in the range of MW. The chosen technology must respond immediately (few seconds) and have the ability of

Table 2.5 Typical Key characteristics of various stationary applications [2], [11], [30]

| Application	Size	Discharge duration	Cycles/day	Response time
Renewable integration	MW level	Mins - hours	0.5-2	Secs to minutes
Load levelling	MW level	Hours	-	Mins
Spinning reserve	Hundreds of MW	Mins – hours	0.5-2	Few seconds
Customer-side Peak-shaving	kW level	Mins - hours	1-20	Mins
Primary Control Reserve	MW level	Mins	5-25	< 1min
Voltage support	Tens of MW	Secs – Mins	10-100	ms to secs
Energy arbitrage	Tens of MW	Hours	0.25-1	> 1 hour
Off-grid	kW to MW	Hours - days	0.75-1	< 1 hour
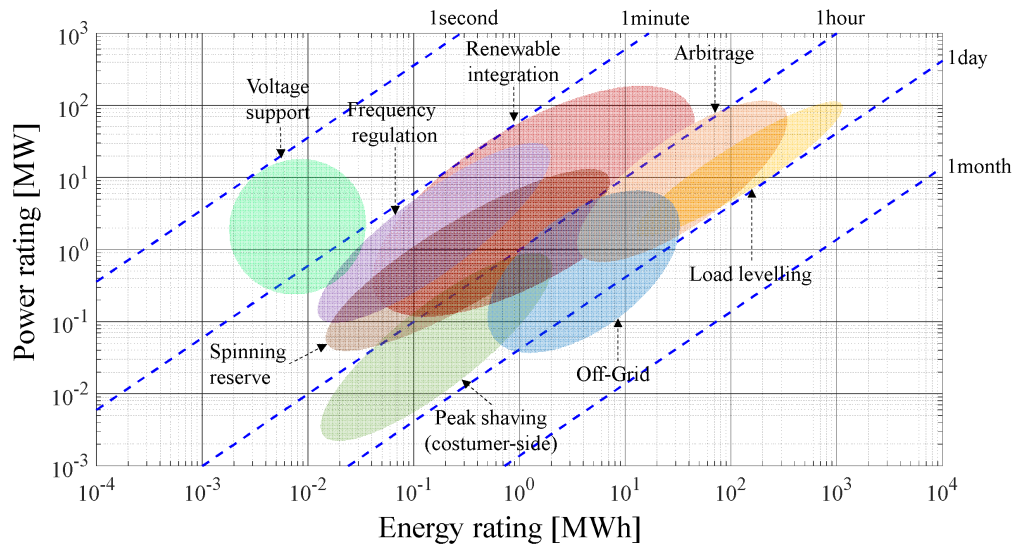
Figure 2.7 Typical Power/Energy ratings requested to EES technologies by various stationary applications [30], [94]

maintaining the outputs for up to few hours.

- *Customer-side peak shaving:* to reduce the customer maximum (peak) energy demand level by exploiting EES at local level. Energy demand can be also shifted in order to assist the integration of local RES. This application is very similar to load levelling but at the customer level. The only difference is the typical size that can vary from kW to hundreds of kW.
- *Primary Control Reserve (frequency regulation)*: to support the balancing of continuously shifting supply and demand (frequency regulation). In this case the requirements are the ability to react in some seconds and to maintain the service for several minutes. Typical size of application goes from hundreds of kW to tens of MW.
- *Voltage support*: to inject or adsorb reactive power to maintain voltage levels in the transmission and distribution systems under normal conditions. Discharge duration is very short (seconds) and the energy/power ratio of the installations can be very low.
- *Arbitrage/storage trade*. This involves storing low-priced energy during period of low demand and subsequently selling it during high-priced periods within the same market. This application requires EESs that have high round-trip efficiency and can achieve long storage duration (hours to days).
- *Off-grid:* storage is deployed in conjunction with local generation (mostly RES) to ensure reliability by filling the gaps between production and demand. The aim could be to electrify rural areas and/or to be independent from the main-grid. Installations might vary in terms of energy/power ratio according to the available resources (RES, genset, PV, wind or hydro turbines, etc.). Generally, they can range from tens of kW (small system) up to tens of MW (big islanded systems). Discharge phases can last up to days because they might have to sustain the loads even in the worst-case scenario of no energy production (e.g. RES+EES plants).

Figure 2.7 resumes graphically the different mentioned applications in terms of the typical power/energy ratings. From overlapping with Figure 2.6 it is possible to state that: (i) SMES have a great opportunity especially for voltage support where capacity is not an issue; (ii) TES and MES (with the exception of flywheels) have a good match with high demanding applications (both for power and energy ratings) like renewable energy integration, load-levelling and energy arbitrage; (iii) BESS are well suited for almost all

Table 2.7 Investment cost of main EES technologies, author elaboration based on [96]

Technology	Current and estimated cost [€/kWh]				Delta [%]
	2016	2020	2025	2030	
PHS	18	18	18	18	+0
CAES	45	41	39	37	-17
Flywheels	2500	2200	1900	1600	-36
NaS	450	370	270	200	-55
NaNiCl$_2$	340	270	200	145	-57
Lead-acid (Flooded-AGM)	125/225	110/190	85/150	65/120	-48/-47
Li-ion (various chemistries)	300/890	240/750	170/560	125/430	-58/-52
Flow Battery (VRB, ZnBr)	295/760	230/590	155/405	105/275	-65/-64

the mentioned applications but with particular predisposition for renewable integration, frequency regulation, off-grid systems, peak-shaving.

Among BESS, lithium-ion appears to be the most suitable technology for stationary applications: its characteristic area overlaps almost the whole application area of Figure 2.7. However, lithium-ion BESSs cover less than 30% of current stationary installations around the globe [85]. The main motivation is represented by the high cost of installation if compared with the other EES technologies. Table 2.7 shows that in 2016 the specific cost of lithium-ion BESS was the highest one (except for flywheels) with an average value (that include the 6 chemistries detailed in section 2.3) of 600€/kWh, 3 times higher than lead-acid BESS. Nevertheless, much attention from researchers, producers and system integrators is given to this technology since a huge cost decrease is forecasted in the next decades. Projections to 2030 show that lithium-ion BESS will be interested in the highest cost reduction of nearly 60% [96] that will drive its specific cost to be quite comparable with all the other EES technologies This fact, together with the best overall performances as detailed above, will put Li-ion in a probable monopolistic position for stationary applications.

2.5 Summary

This chapter has provided a comprehensive overview about Electrical Energy storage technologies. More attention has been dedicated to BESS with special focus on Li-ion chemistries. The different available cathode, anode and electrolyte materials have been presented by concentrating also on the expected performances, market share, producers and costs. Finally, the discussion has been contextualized towards stationary applications. The typical features of storage technologies have been matched with the requirements of possible final applications. This has highlighted the feasibility of BESS in addressing the needs of the today's electric power system scenario, in terms of expected performances and reliability. Given the high performances and the expected huge decrease in the specific cost, Li-ion technology is forecasted to be the most prominent option for renewable integration, frequency regulation, off-grid systems and peak-shaving.

CHAPTER 3

Performance evaluation of lithium-ion cells

Chapter 2 highlights that BESS are very suited for stationary applications among all EES technologies. Moreover, lithium-ion based chemistries appear to be the most prominent option for the near future. Manufacturers and analysts declare high energy density, power density, efficiency, lifetime that makes of Li-ion batteries the perfect candidate for several applications, including stationary ones.

Nevertheless, there are several existing limiting factors that are impacting on the diffusion of Li-ion BESS in today's markets: (i) the relatively high CAPEX for the integrated system despite a learning rate of lithium-ion battery cells of 21.6%, very similar to the one observed for PV cells [1]; (ii) the lack of a stimulating regulatory framework [7], [8], [10], [97] and (iii) the lack of technical information as regards to the real performances of BESSs in the field. The latter represents a strong barrier to the deployment of BESS independently from their CAPEX because the real storage performance, such as the efficiency and the expected lifetime, affects the overall system OPEX. Unless these parameters are correctly evaluated, the decisions on the installation of BESSs can be highly risky.

Nowadays, performance characterization of lithium-ion cells is left on the manufacturers' side, who provide information as regards to energy density, power density, efficiency, cycles to failure and others. However, no uniformity is found in manufacturer's datasheets that helps in categorizing the different products according to the final application. This fact is justified by the lack of standardized testing procedures to compare different cells for a specific usage in spite of an abundant literature on the characterization of lithium-ion battery cells. In [98] the authors assessed the performance of three different lithium-ion cells for plug-in hybrid electric vehicles (PHEV) under the IEC 62660-1 standard [99]. This standard defines ad-hoc test conditions for lithium-ion cells in EVs application. There is therefore no guarantee that the test results are applicable in other applications. In [100] the authors tested various cells and modules and claim to have used "consistent sets of test procedures intended to determine their performance characteristics for automotive applications". They develop their own testing procedures starting from the USAB/DOE programs [101] which developed an Evs battery test procedure manual. In [102] the authors developed specific testing procedures for both automotive and stationary applications. In [103], [104] different performance testing

protocols for lithium-ion cells are proposed. Another task defines the battery efficiency measurement under different test conditions, such as: fast charge test, aging test, actual operation test and battery vibration test [105]. In [106] the ISO/CD 12405-1/2 and IEC 62660-1 (section 7.8.1.2 "Energy efficiency test - test by temperature") standards are compared and the measurement of efficiency is defined for the pulse tests under different C-rates[2] (ranging from 1/3 C to 10 C), current profiles, temperatures (from -20°C to 45°C) and SoC levels[3] (from 20% to 100%).

Given the unconsolidated framework, in this chapter, a technological comparison among three different lithium-ion chemistries is presented by analysing their performance at cell level. This approach eliminates the influence of the module-level battery management system (BMS), which can restrict or change the operating conditions of the electrochemical cells. The technological comparison criteria are the energy density, power density, and efficiency. The IEC 62660-1 international standard has been used as a preliminary term of reference [99]. Then, two novel testing procedures, which are believed to be more suitable for stationary applications, are presented. In section 3.1 and section 3.2 all testing procedures are detailed with the support of real experimental test examples. In section 3.3, the related results are presented and discussed. Finally, in section 3.4, measurements of lithium-ion BESS performances in real-application (frequency regulation) are analysed.

3.1 Laboratory set-up

The chapter is based on real lab measurements that have been obtained in the framework of the collaboration between the Politecnico di Milano (Electric Power Systems research group) and CSEM-PV Center (Swiss Center for Electronics and Microtechnology) using cutting edge machineries at the Energy Storage Research Center (ESReC) located in Nidau, Switzerland (Figure 3.1):

- PEC- ACT 0550 battery tester equipped with 20 parallel, 5V-50A channels. PEC- ACT 0550 is a fully programmable machine and each channel can be programmed and used independently by the user. The machine has 100 µsec based internal sampling, control and capacity calculations and the FPGA hardware controls both current and voltage with a ± 0.005% FSD accuracy on the voltage readings and ± 0.03% FSD accuracy on current readings.
- ESPEC-ARU 1100 climatic chamber with a volume of 1100 L and a temperature range of -45°C/180°C. Temperature change rate is between 4K/minute and 18/K minute

Table 3.1 collects all the characteristics about the different tested chemistries (full details from the datasheets are collected in Appendix E). Specifically, the tested Li-ion cells are the following ones:

---

[2] C-rate is normally used to define the magnitude of current-based charge/discharge processes. It is the ratio between the current and the nominal cell's capacity:

$$C - rate = \frac{I_{ch/disch}\,[A]}{C_{nom}[Ah]}$$

[3] SoC is useful indicator that defines the ratio between the available capacity and the nominal capacity of the cell:

$$SoC\,[\%] = \frac{C_{actual}\,[Ah]}{C_{nom}[Ah]}$$

- Lithium Nickel oxide (LNCO): Boston Power SWING5300 [107]. It is an LNCO cell with complex layered Lithium Nickel oxide ($LiNi_{0.8}Co_{0.2}O_2$) as the cathode, graphite as the anode, Lithium hexafluorophospate ($LiPF_6$) as the electrolyte and Polyvinylidene fluoride (PVDF) as the separator [108].
- Lithium Iron Phosphate (LFP): A123 ANR26650 [109]. It is an LFP cell with $Li_{0.1}FePO_4$ structure as cathode, graphite as anode and carbonate-based Li-salt as electrolyte. Doped Nanophosphate™ is used to reach higher performances instead of conventional phosphates.
- Lithium Titanate Oxide(LTO): GWL POWER LY-LTO-30Ah [110]. It is an LTO cell that uses nano particles of the mixture of lithium titanium oxide compounds (e.g. Li_2TiO_3, Li_4O_4Ti, $Li_4Ti_5O_{12}$) as cathode, unknown cathode structure (not-declared by manufacturer) and dry powder electrolyte.
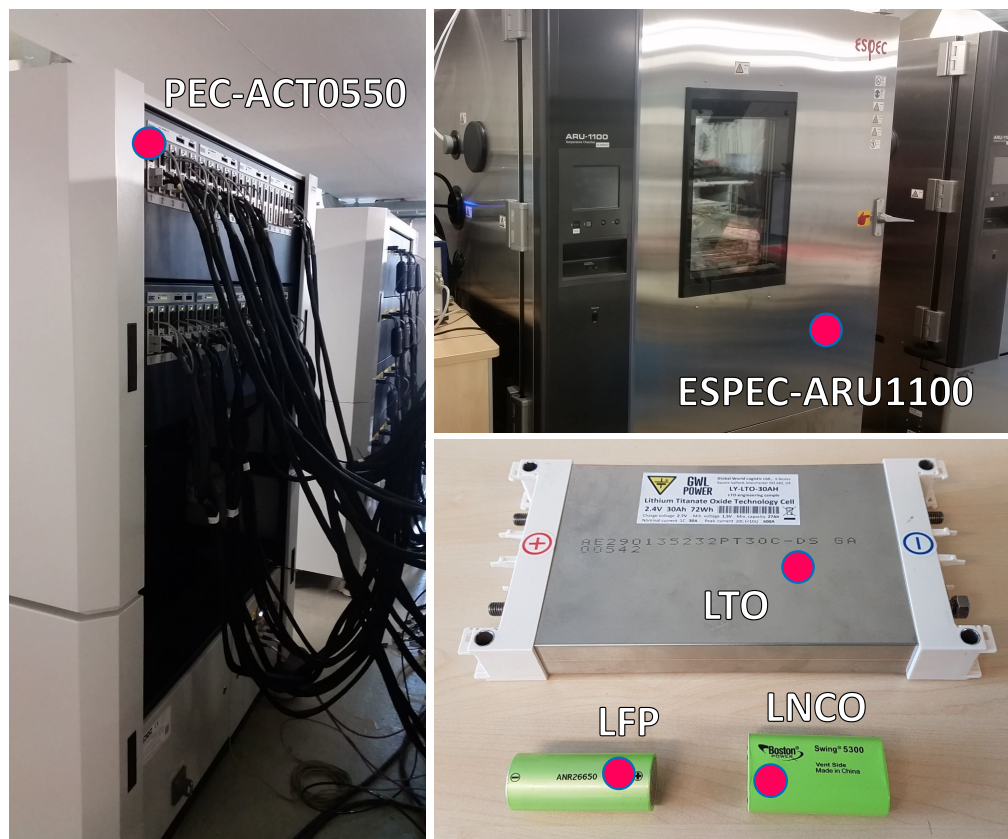

Figure 3.1 Experimental setup at ESReC lab located in Nidau, Switzerland

Table 3.1 Lithium-ion cells specifications from manufacturers' datasheets (Appendix F)

Cell	Voltage Range [V]	Capacity [mAh]	Energy [mWh]	Energy Density [Wh/kg]	Power Density [W/kg]	Operating Temp. [°C]	Cycles (DoD)
LNCO	2.75 – 4.2	5300	19345	207	1000	-20 / +60	>1000 (100 %) >2000 (90%) >3000 (80%)
LFP	2 – 3.6	2500	8250	108	2600	-30 / +55	>1000 (100%)
LTO	1.85 – 2.75	30000	72000	45	900	-20 / 45	>10000 (80%)

3.2 IEC 62660-1 test procedure

The IEC 62660-1 international standard is designed for the characterization of lithium ion cell in Hybrid Electric Vehicles (HEVs) and Battery Electric Vehicles (BEVs). The standard distinguishes between three main categories of tests:

- Specific performance tests: characterizing the device in terms of energy and power densities and efficiencies. These tests last at maximum a few days and they aim at characterizing the battery performance depending on temperature and current for a specific life time condition;
- Storage tests: which last about one month and mainly aim at evaluating the retention capacity as well as the power density when the battery is subjected to high ambient temperature without cycling;
- Cycle life tests: which last about six months and aim at evaluating the degradation of battery performance due to battery cycling. Measurements aim at evaluating capacity, dynamic capacity, and energy efficiency in both charge and discharge.

In the following, the focus is on the performance tests, leaving to following chapters the analyses about the storage and cycling tests (Chapter 7). Specifically, the standard distinguishes between: capacity tests (section 7.2 of IEC 62660-1), power tests (section 7.4 of IEC 62660-1) and efficiency tests (section 7.8 of IEC 62660-1).

Capacity test

The capacity test allows the gravimetric and volumetric energy densities computation. It involves the repetition of the same procedure at different ambient temperatures (-20°C, 0°C, 25°C, 45°C) and for two different discharged currents (1/3 C, 1 C). The test procedure is made up of the following steps (Figure 3.2):

1. Thermal stabilization[4] at the chosen temperature.

Full charge phase:
- Discharge the cell down to its low voltage limit with a constant current of 1/3 C.
- Charge the cell as indicated by the manufacturer. The charge phase is normally divided in two subsequent steps:
    - Constant Current (CC) phase in which the cell is charged by controlling the current flow until it reaches its maximum voltage limit.
    - Constant Voltage (CV) phase in which the cell is charged by controlling the voltage until the current decreases under a specific threshold (typically a percentage of the rated capacity).

    In the case of LNCO cell the cell is charged at 0.7C until it reaches 4.2V, then the cell is maintained at 4.2V until the drained current is below 50mA (~1%).

Discharge down to its low voltage limit with a CC of 1/3 C.
Full charge phase as indicated by the manufacturer.
Discharge down to its low voltage limit with a CC of 1 C or 1/3C

The energy density (gravimetric) ρ_{ed} is then computed as follows:

$$\rho_{ed} = \frac{\int IV(t)dt}{W} \tag{3.1}$$

Where the numerator is computed for the two current rates prescribed in steps 3 and

---

[4] Thermal stabilization is considered to be reached if after an interval of 1 h, the variation of the cell temperature is lower than 1 K.
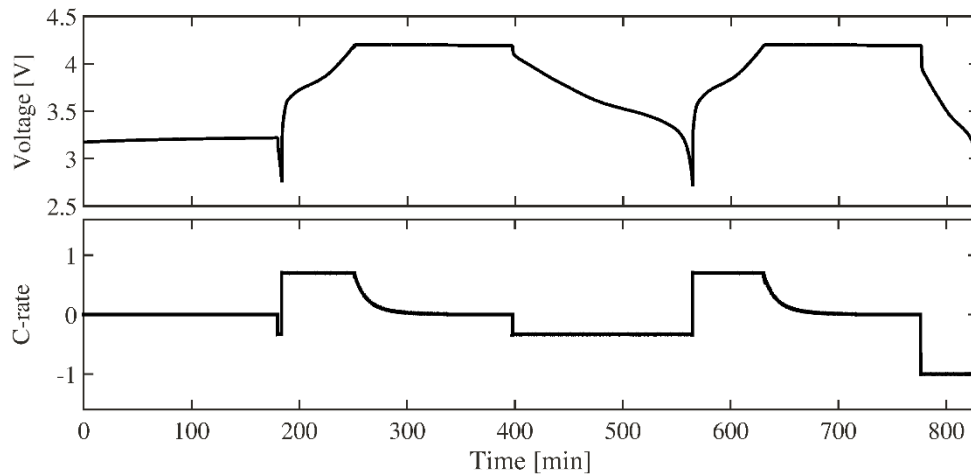
Figure 3.2 Example of capacity test procedure IEC 62660-1 on LNCO cell

5, while the denominator is the weight W of the cell.

Power test

The power test allows the gravimetric and volumetric power densities computation. It involves the repetition of the same procedure at four different ambient temperatures (-20°C, 0°C, 25°C, 45°C) and for three different states of charge (SoC; 80%, 50%, 20%). The test procedure is made up of the following steps (Figure 3.3):

1. Thermal stabilization at the chosen temperature.
2. Full charge phase (point 2 of the capacity test).
3. Discharge at CC of 1/3 C until the selected SoC is reached.
4. Pulsing periods phase:
   - Discharge at given C-rates for 10 s.
   - Pause for 10 s.
   - Charge at given C-rates for 10 s.
   - Pause for 10 s.
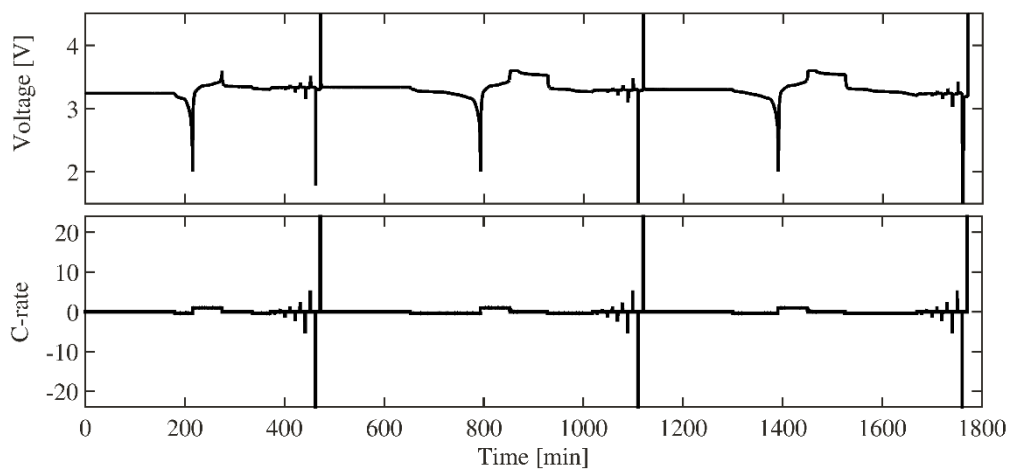   - Repeat at the following C-rates: 1/3 C, 1 C, 2 C, 5 C, maximum current (Imax)

Figure 3.3 Example of power test procedure IEC 62660-1 on LFP cell

53

declared by the manufacturer.
5. Discharge at CC of 1/3 C until the minimum voltage.
6. Repeat from point 2 for the next SoC condition.

The gravimetric power density ρ_{pd} is computed as follows:

$$\rho_{pd} = \frac{V_{end} \cdot I_{max}}{W} \tag{3.2}$$

Where V_{end} is the measured voltage at the end of the pulsed period.

Efficiency test

The efficiency test allows the evaluation of the coulomb and energy efficiencies. It involves the repetition of the same procedure at different ambient temperatures (-20°C, 0°C, 25°C, 45°C). The test procedure is made up of the following steps (Figure 3.4):
1. Full charge phase (point 2 of the capacity test).
2. Thermal stabilization of 16 hours at the chosen temperature.
3. Discharge at CC of 1/3 C until the minimum voltage.
4. Resting time of 4 hours.
5. Full charge phase as prescribed by the manufacturer.
6. Resting time of 4 hours.
7. Discharge at CC of 1/3 C until the minimum voltage.

The Energy efficiency is computed as follows:

$$\eta_e = \frac{(\int IV(t)dt)_{DISCH}}{(\int IV(t)dt)_{CH}} \tag{3.3}$$

Where the numerator is the discharge energy of step 7 and the denominator is the charge energy of step 5.

3.3 Additional test procedures for performance evaluation

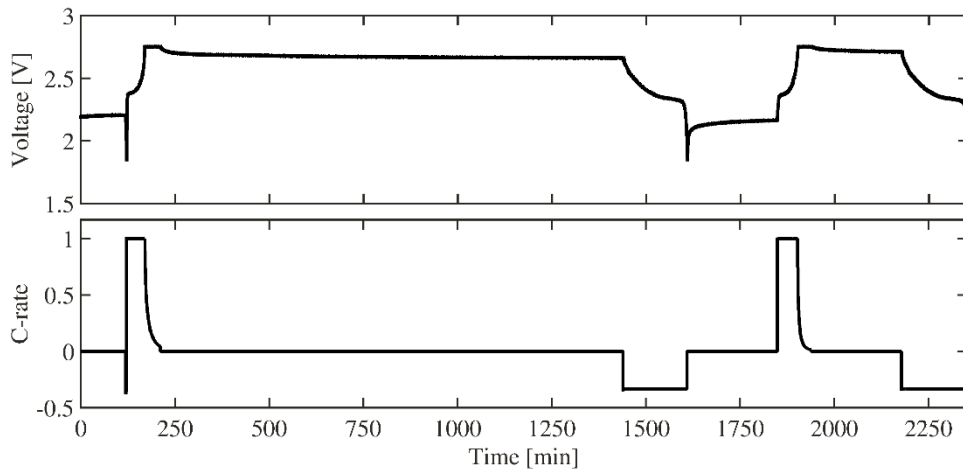The IEC 62660-1 procedure do not accurately represent the cell performance outside

Figure 3.4 Example of efficiency test procedure IEC 62660-1 on LTO cell

the operating conditions of automotive applications. The main limiting factors are:

- The current rates used for the evaluation of capacity and efficiency are very low. Energy densities are computed at a maximum of 1 C while energy efficiencies are evaluated at 1/3 C.
- The charging process is a full-charge process (CC+CV) that represents the typical use in EV applications: after driving periods the EV is normally left in charging stations where the BESS is charged as best as possible (i.e. as indicated by the manufacturer).

Hereinafter, two alternative procedures are proposed that want to fully characterize electrochemical cells performances independently from the specific final application.

Ragone test

Ragone test involves the computation of the energy density as a function of the power density. It requires the repetition of the same procedure at four different ambient temperatures (-20°C, 0°C, 25°C, 45°C) and different power density values (see Table 3.2). The test procedure is made up of the following steps (Figure 3.5):

1. Thermal stabilization at the chosen temperature.
2. Full charge phase (point 2 of the capacity test).
3. Discharge at CC of 1/3 C until the minimum voltage.
4. Charge at a specific power density until the maximum voltage
5. Full charge phase as prescribed by the manufacturer
6. Discharge at a specific power density (the same value of point 4).
7. Discharge at CC of 1/3 C until the minimum voltage.
8. Repeat from point 4 for the next power density value.

The energy density is then computed as in equation (3.1) given the measurements of step 6 for each value of power density. By relating the different obtained values, it is possible to outline the Ragone plot.
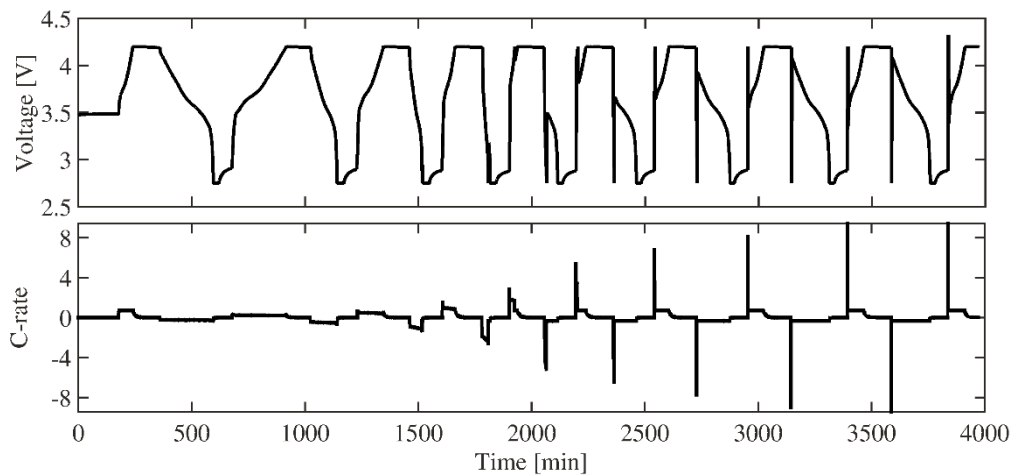

Figure 3.5 Example of Ragone test procedure on LNCO cell

Table 3.2 Power density values adopted in Ragone tests for LNCO and LFP lithium-ion cells

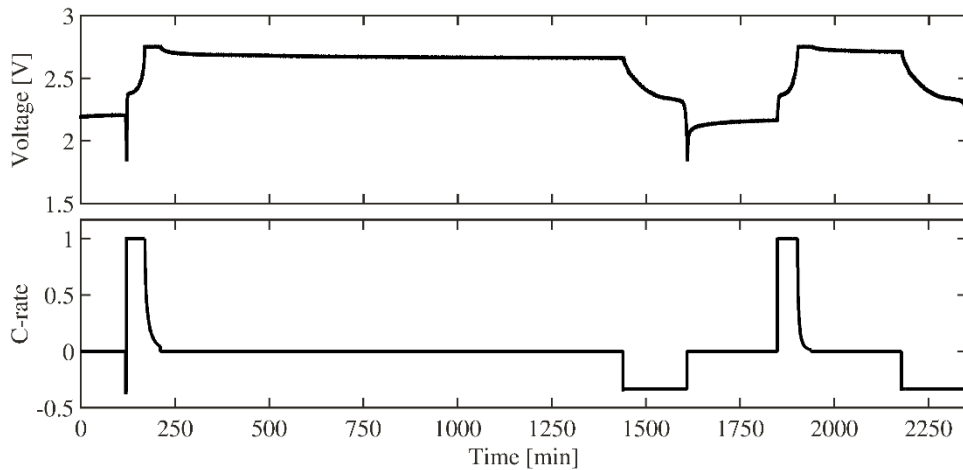| Cell	Power density [W/kg]
LNCO	50 – 100 – 400 – 800 – 1000 – 1200 – 1400
LFP	50 – 100 – 400 – 800 – 1200 – 1600 – 2000 – 2800 - 3200

Figure 3.6 Example of Efficiency curve test procedure on LFP cell

Table 3.3 C-rates values adopted in efficiency curve tests for LNCO and LFP lithium-ion cells

Cell	C-rates
LNCO	0.1C – 0.5C – 1C – 2C – 4C
LFP	0.5C – 1C – 2C – 5C – 10C

Efficiency curve test

This test aims at providing energy efficiency values as a function of the C-rate. It involves the repetition of the same procedure at four different ambient temperatures (-20°C, 0°C, 25°C, 45°C) and different C-rates values (Table 3.3). The test procedure is made up of the following steps (Figure 3.6):

1. Thermal stabilization at the chosen temperature.
2. Full charge phase as prescribed by the manufacturer.
3. Cycling between the voltage limits (CC mode only) until the regime condition is reached at the specific C-rate. [5]
4. Computing the energy efficiency as in equation (3.3).
5. Repeat point 3 for the next C-rate

3.4 Discussion on performances

Energy/Power performances

Energy density and power density are meaningful indicators used to compare the ability of different electrochemical devices in sustaining prolonged periods of charge/discharge

---

[5] The regime condition is reached when the coulombic efficiency is in the range of 100%±0.1%. Coulombic efficiency is defined as follows:

$$\eta_c = \frac{(\int Idt)_{DISCH}}{(\int Idt)_{CH}},$$

If the coulombic efficiency is far from the unit, it means either that strong parasitic reactions take place in the cell or the cell has not reached a steady state condition yet. The latter is typical after a slow charge process followed by a discharge at high C-rate: the strong asymmetry of the working cycle brings the coulombic efficiency to values consistently less than the other ones.
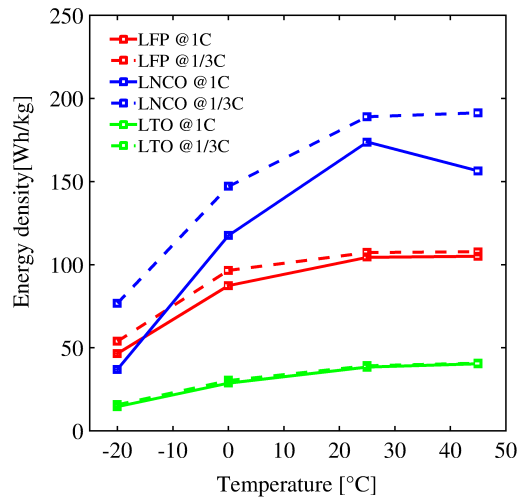
Figure 3.7 IEC 62660-1: capacity test results on 4 lithium-ion cell at 1/3C and 1C

conditions or in answering to high currents peaks.

IEC 62660-1 results (Figure 3.7) shows that all the cells:

- underperform at very low temperatures. At -20°C there is a significant decrease of the energy content: the energy density is reduced in all cases: LNCO (-52%), LFP(-48%), LTO (-59%);
- perform better at higher temperature but may degrade faster [73], [111];
- perform better at lower C-rate. LNCO shows a decrease of 10% in the energy density when moving from 1/3 C to 1 C discharge rate, while LFP, LTO tolerate higher currents and show less reduction in energy density.

In standard conditions, one cell (the LNCO: 180 Wh/kg at 25°C) obtains better performance if compared to the others (LFP stands at values 1/3 lower while LTO technologies fall drastically in the energy performance). This can be explained by the peculiarities of each technology (see section 2.3).

The Ragone plot confirms the statement by fully characterizing the performance in terms of both energy and power density (Figure 3.8-A). The plateau before the "knee" represents the amount of energy storable in the battery, while the "knee" clearly indicates the limiting power at which to use the stored energy. At power greater than the "knee", only a portion of the stored energy can be used. The higher horizontal plateau confirms the better energy density of the LNCO cell if compared to the LFP, but a lower power density at which the full energy can be used (1000 W/kg vs 2000 W/kg).

Figure 3.8-B shows the Ragone plot for the same cell (LNCO) at different ambient temperatures. Again, the Ragone plot proves to be a comprehensive way to describe the cell performance. The decrease of the horizontal plateau provides the same information as the capacity test IEC 62660-1 (Figure 3.7), while the variation in the "knee" position highlights a decrease in the power performance with decreasing temperature. Overall, the cell is increasing its ability to release energy with temperature, ensuring more and more deliverable power.

Overall, BESS designers should not underestimate the differences in energy and power performances of the different available chemistries. Each technology responds differently to changes in external conditions. The specific application that decides the severity of operations, together with the environmental conditions have to be taken into account in the design phase. For instance, thinking about stationary applications, LFP technology fits better power-driven applications (e.g., frequency regulation), while LNCO is more
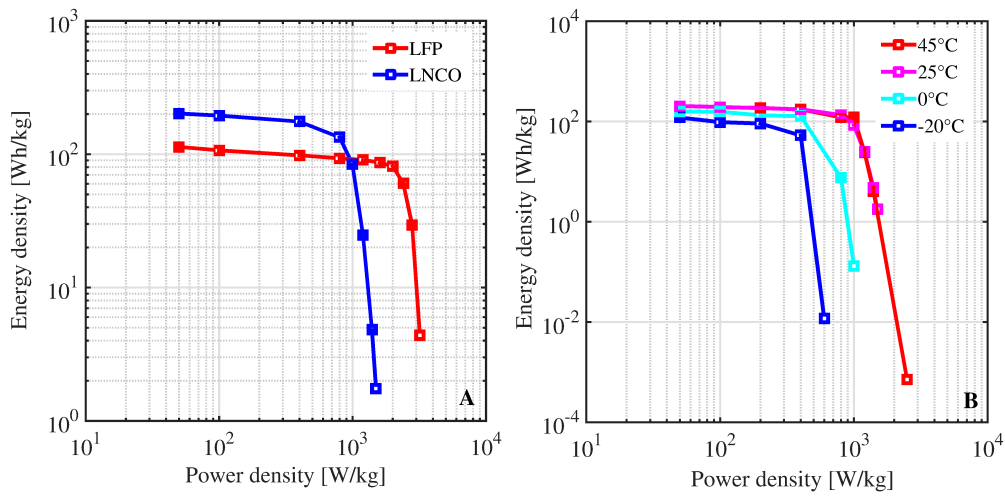
Figure 3.8 (A) Ragone plot for LNCO and LFP cells @ 25°C, (B) Ragone plot for LNCO at different ambient temperatures

suitable for energy-driven ones (e.g., load levelling).

Energy efficiency

If product datasheets published by cell manufacturers provide information on energy density and power density, the same cannot be said about the efficiency that is rarely present in the official documentation. Energy efficiency relates to the amount of extracted and injected energy between two SoC limits. IEC 62660-1 results (Figure 3.9) show that severe temperatures affect performance. At ambient temperature, the efficiency stands in the range of 92% to 97%. Low and high temperatures could impact up to 20 points of efficiency. Moreover, Figure 3.10-A and Figure 3.10-B show how efficiency is affected also by the specific operating conditions.

Specifically, Figure 3.10-A shows a clear dependence on the current rate. Lithium-ion cells can exhibit very low efficiencies compared to values reported in literature [112], [113]. The LNCO cell loses more than 20% of efficiency when the C-rate increases from
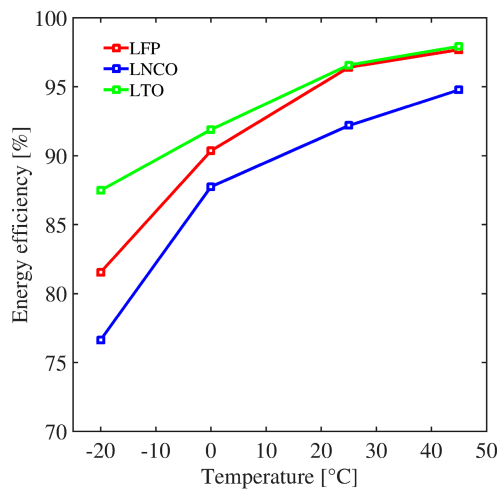

Figure 3.9 IEC 62660-1: efficiency test results (1/3C – DoD 100%) on 3 different Li-ion cell chemistries.
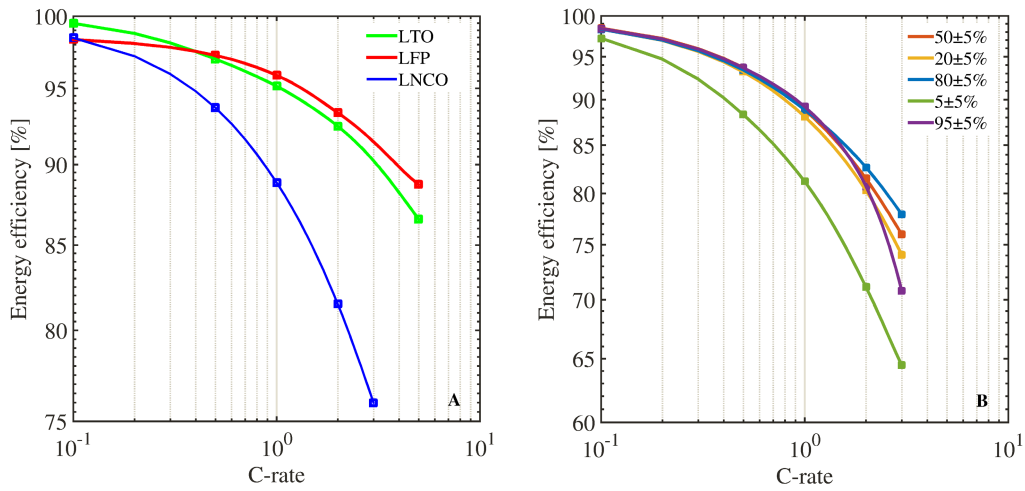
Figure 3.10 Energy efficiency measured at ambient temperature as function of the C-rate for (A) different Li-ion cell chemistries (DoD 100%), (B) different SoC (LNCO cell)

0.1C to 3C. LFP and LTO cells are less prone to this decrease due to a lower internal resistance, which results in a higher power density.

Additionally, Figure 3.10-B shows that also the SoC could affect energy efficiency. While, the variations in the efficiency are negligible for SoC levels in the range of 20% to 80%, a significant difference is observed at very low SoC (5% ± 5% SoC) where the measured efficiency for current rates between 0.5 C and 3 C is about 10% lower than the other SoCs. The same thing, but with minor extent, can be said for high SoC (95% ± 5% SoC) where the measured efficiency starts to deviate for c-rates above 1C.

This remarkable dependency from the operating conditions could have clearly a strong impact in the investment evaluation. Much attention is being paid to the capital costs (CAPEX) of BESS, that is the initial investment. However, the total cost of ownership of BESS includes other factors such as, in some cases, air conditioning to maintain the system in its operating temperature range, and in all cases by the cost of electricity loss over a charge/discharge cycles. Both are determined by the efficiency of the battery. BESS designers should then pay attention to the specific application for which the battery will be asked to work.

3.5 Performances in real-life application

Generally, in real applications, the currents fluctuate drastically and they cannot be fixed to desired values in the charging phase. For instance, in stationary applications, the primary control reserve (PCR) service is based on power injections that must follow variations in frequency. Since frequency deviations are stochastic, the current profile applied to a hypothetic BESS providing PCR can be extremely variable. This requires the BESS to operate continuously at variable C-rates in both charge and discharge conditions. In these cases, the efficiency will also fluctuate and it cannot be assumed constant.

Consequently, we tested the LNCO cells for PCR to better understand the performance in non-conventional applications[6]. We adopted a specific droop control law which takes into account the peculiarities of BESS when compared with traditional power

---

[6] The power injection from the BESS has been considered having negligible influence on the frequency, given the much smaller BESS power than grid power.
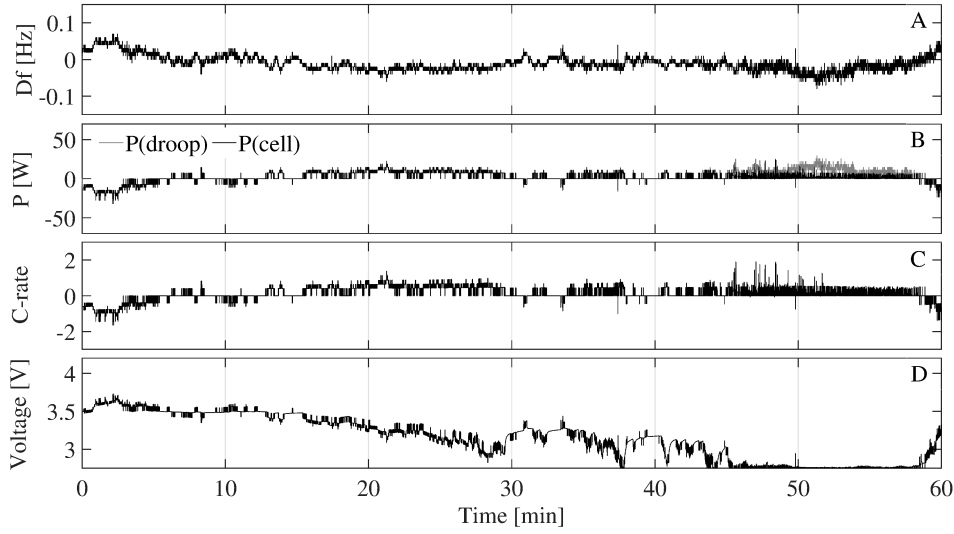
Figure 3.11 Input frequency deviation profile, power set point determined by the droop regulator, and measured power, C-rate and voltage on an LNCO cell used for primary control with a 200% regulation band

plants (more details about the theoretical assumptions can be found in Chapter 8). A BESS can in fact provide their full capacity for PCR. Once the maximum allowed C-rate is fixed, a BESS can operate from 0% to 100% of the current limit. Moreover, a BESS will normally operate at modest C-rates but, if required, can provide higher C-rates. In our tests, it is assumed that:

- The regulation band is linked to the maximum C-rate (i.e., maximum current I_{max}) the cell has to provide. A regulation band of 100% means that the cell can deliver a maximum current of 1C (the average C-rates during the PCR provision will be lower). Different configurations have been tested: from 50% to 300%.
- The dead band half-width Δf_{db} is 20 mHz. The droop σ is assumed constant at 0.21%. Therefore, the maximum allowed frequency deviations Δf_{max} (at which the cell will provide I_{max}) is of 100 mHz. The specific power profile (in p.u. of P_{max}) for PCR can be derived as follows:

$$\frac{\Delta P}{P_{max}} = \begin{cases} 0, & |f| < \Delta f_{db} \\ -\dfrac{\Delta f / 50}{\sigma}, & |f| > \Delta f_{db} \wedge |f| < \Delta f_{max} \\ 1, & |f| > \Delta f_{max} \end{cases} \tag{3.4}$$

- Given the selected maximum C-rate the power profile can be adapted to the particular battery/cell under test assuming that:

$$P_{max} = V_{rated} I_{max} \tag{3.5}$$

- The initial SoC corresponds to the open-circuit voltage of the cell being equal to the rated voltage.
- SoC limits are variable. Two different ranges have been tested: 0-100% and 20-80%. The frequency profile is derived from measurements taken at the Politecnico di Milano within the framework of the *IoT-StorageLab* (Appendix B), representative of the behaviour of the Italian power system. In Figure 3.11 an example of one hour of PCR is

Table 3.4: Measured and calculated efficiency of an LNCO cell used for PCR provision under a measured, 24-hour frequency deviation profiles and seven different sets of control conditions

Test N°	Regulation band	C-rate (average)	SoC min	SoC max	Efficiency at 25°C	Availability for PCR
1	50%	0.13	0%	100%	97.92%	100.00%
2	100%	0.26	0%	100%	96.15%	100.00%
3	100%	0.23	20%	80%	96.16%	92.14%
4	200%	0.47	0%	100%	91.24%	92.01%
5	200%	0.36	20%	80%	94.86%	80.10%
6	300%	0.62	0%	100%	88.00%	86.29%
7	300%	0.46	20%	80%	93.38%	76.84%

presented. It refers to a regulation band of 200%, meaning that a maximum C-rate of 2C is assumed. Given the rated voltage of the cell, the maximum power P_{max} is around 39W as per equation (3.5). We applied the droop law starting from the measured frequency deviation Df (Figure 3.11-A) to obtain the power (P_{droop} in Figure 3.11-B) that the cell must provide as per equation (6). However, the cell must respect the imposed SoC limits. P_{cell} is the real power provided for PCR (Figure 3.11-B). The difference with P_{droop} results in a service unavailability. The C-rate and voltage trends (Figure 3.11-C/D) reflect the operating state of the cell. In particular, the cell stays at the minimum SoC around the minute 50, which corresponds to the service unavailability visible on Figure 3.11-B.

Table 3.4 shows the measured efficiency on LNCO cell. The measured efficiency decreases with the increase in the C-rate, as expected as from Figure 3.10-A, and it increases if a narrow SoC range is used, according to Figure 3.10-B. Lower efficiency means more SoC fluctuations and more probability that the battery will reach its SoC limits being unavailable to provide the service, perhaps incurring in penalties. Therefore, the correct estimation of efficiency is of straightforward importance in order to estimate the correct operating costs of the BESS installation.

3.6 Summary

In this chapter BESS performances have been deeply discussed. Experimental measurements have been presented about a technological comparison among three different Li-ion chemistries. Energy density, power density and efficiency have been computed in different testing conditions (temperature, SoC, operating rate). The analyses have been carried out at cell level by following the IEC 62660-1 international standard in parallel with novel testing procedures. Lab measurements have been obtained in the framework of the collaboration between the Politecnico di Milano (Electric Power Systems research group) and CSEM-PV Center (Swiss Center for Electronics and Microtechnology). The results highlight the strong differences among chemistries. The careful analysis of the IEC 62660-1 testing protocols and the evaluation of the different operating conditions between automotive and stationary applications, suggest the need for additional testing procedures tailored for the latter. Consequently, two novel procedures to overcome the limitations of IEC 62660-1 have been proposed. The Ragone test that links energy density and power density to show the characteristics (energy vs. power) of each tested chemistry. The efficiency test as a function of the C-rate allows the correct evaluation of its average value for stationary applications, whereas the charge/discharge currents are highly variable. These testing procedures are demonstrated to be useful to system designers for a correct sizing as well as for the evaluation of the total cost of ownership of a BESS in specific final applications.

In general, all the lab tests performed and presented above represented the reference of comparison for the analysis and development of a critical bibliographic review that aim at identifying the appropriate mathematical models capable of reproducing the dynamic behaviour and final performances measured in the laboratory.

Review of approaches to battery modelling

Experimental measurements of Chapter 3 have demonstrated that BESS can show high variabilities in their performances, especially if used for unconventional applications (i.e. stationary, EVs etc.). Nominal data provided by manufacturers' datasheets are insufficient and far from being representative of the real battery behaviour. Performances as power density, energy density, efficiency and lifetime depend on many factors including temperature, current profile, SoC and Depth of Discharge (DoD). However, it is not plausible to map out the performances in all possible conditions through experimental approaches both for cost and time reasons.

Given this perspective, accurate battery modelling can help in different tasks: (i) predicting and analysing the battery behaviour in many different operational conditions by using specific sets of simulations; (ii) shortening development time of systems or components, (iii). finding optimal operation strategies (i.e. BMS development); (iv) identifying operating limits that allow to achieve best lifetime; (v) evaluating the techno-economic viability of battery systems in a specific application.

There are existing different technological levels of battery modelling: (i) the materials level in which the single electrodes/electrolytes structures and materials are investigated; (ii) the cell level in which the founding element of any BESS is described as seen at its terminals (e.g. performance test of Chapter 3 are at cell level); (iii) the module level in which the assembly of several cells together with the BMS is modelled as the main block within the BESS; (iv) the system level in which the BESS is modelled as a complete stack of modules including the battery inverter.

Battery modelling approaches can focus on one or more of the above technological levels while tackling different tasks. In this chapter, a literature review on battery modelling (mainly at cell level) is presented. The models have been grouped into four general different approaches: electrochemical models, empirical (analytical) models, electrical models and stochastic models. Moreover, two main tasks are identified for battery models: the estimation of the operating conditions (i.e. SoC estimation), the estimation of the lifetime (i.e. SoH estimation). These two main aspects create the frameworks of discussion through which the modelling approaches are deepened and compared.

4.1 Battery models: accuracy and computational effort

Battery modelling differs in regards to the degree of details they use to reproduce the battery behaviour. Some of them look at the battery like a "black-box" characterized by an energetic content that fluctuate during charge/discharge cycles, others reproduce the electric quantities seen at the battery terminals (i.e. voltage and current), some others go deeply into the chemical representation dealing with reactant concentration and electrodes materials. However, higher degree of precision means generally higher elaboration/simulation time that can influence the usability of the proposed model in the final applications.

Over the years, various models were developed for different areas of application. They aim at studying, estimating and predicting the operating conditions and aging of a battery. We can group them in four main families/categories [114]–[116]:

- *Electrochemical models:* which are known as the most accurate but difficult to develop. They consider the chemical reactions by accounting for mass, energy and momentum balances for each species, phase and component of the cell. Therefore, electrochemical modelling typically involves a system of coupled partial differential equations that must be solved in time and spatial dimensions. They are able to predict local distribution of concentration, electrical potential, current and temperature inside the cell, besides current and voltage at the external terminals. Therefore, they tend to be relatively complex and they typically have various parameters to determine. Despite the chance of gathering reasonable values from literature, the parameters must be evaluated through several experiments in order to develop the full model [117]. Given the inherent complexity, they are mostly used in the structural design of batteries. For instance, they can be used to evaluate the sensitivity of the reaction rate to different electrode structures.

- *Analytical models*: which are based on an abstract vision of the electrochemical cell behaviour. The battery is described by few analytical equations which do not consider electrochemical processes, but they are empirically fitted. These models usually focus on the evaluation of the SoC of the battery based on energy balances. Voltage or current characteristics of the battery are normally neglected. Nevertheless, in some in-depth cases, they can account for the nonlinearities inherent to the battery operations. Due to the simplicity of these models, they are well suited for energy planning studies and first choice for sizing tools [118]. However, the simpler models adopted could result inaccurate: the errors in predicting battery performance could be relatively high.

- *Stochastic models*: which aim at representing charging and discharging phenomena as stochastic Markovian processes. The complex electrochemical reactions are assumed to be significantly affected by random variables as ambient temperature and usage profiles [119]. The operation of the battery is modelled by describing the various states the device can be in, together with the consumption rates in those states and the transition probabilities between the states. In practice, the battery is usually represented by a Markov chain with N+1 states of charge, enumerated from 0 to N. The number of the battery state is linked to the number of units of charge available in the battery [120]. This approach can be particularly accurate in predicting end-of-discharge (EoD) and end-of-life (EoL) parameters. However, these models do not take into account the physical aspects of battery operations, their usage must be carefully evaluated.

- *Electrical circuit models (also electrical models)*: which focus on the electrical properties of a battery. In these models, an equivalent electric circuit is used to represent the battery dynamics by reproducing voltage and current characteristics at
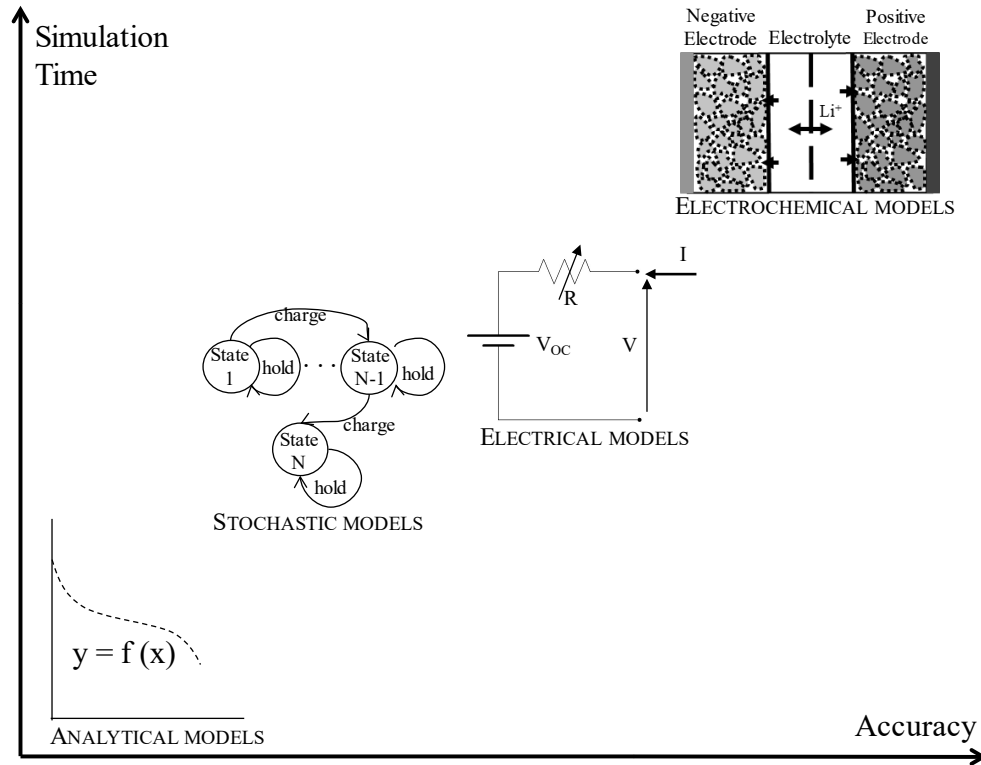
Figure 4.1 Accuracy vs. simulation-time for different battery modelling approaches

the external terminals. These models could be very simple, with few circuital elements (e.g. voltage source to model SoC and a resistance in series for losses), or more complex, with each circuital element related to a precise physical phenomenon occurring in the cell (e.g. Warburg impedance). These models are computationally less expensive than electrochemical models. However, if their development, (i.e. the elements' parameters identification process that can take quite some effort) is well done, they can reach a good degree of accuracy. The main drawback lies in the need of a great amount of data, especially if the objective is to assess the on-line update of the model during its lifetime. However, due to the wide spectra of possible equivalent circuits, these models find application in a broad range of sectors, comprising battery monitoring and design. [114]

Figure 4.1 resumes the above-mentioned approaches comparing them in terms of accuracy vs. simulation-time. Electrochemical models are the most advanced ones but out of the scope of this thesis given their very high time to obtain any usable information. Empirical models seem instead to be good candidates especially for their fast simulation time. However, their results should be validated comparing them with more accurate models. Given the similar simulation times between stochastics and electrical model, electrical models will be chosen as the main candidate for BESS modelling in the part II of the thesis.

4.2   Modelling of operating conditions (SoC estimation)

BESS models should be able to capture those quantities which characterize battery operations. The two most important are the voltage and the capacity, the product of which can be related to the energetic content. These quantities change during battery operations:
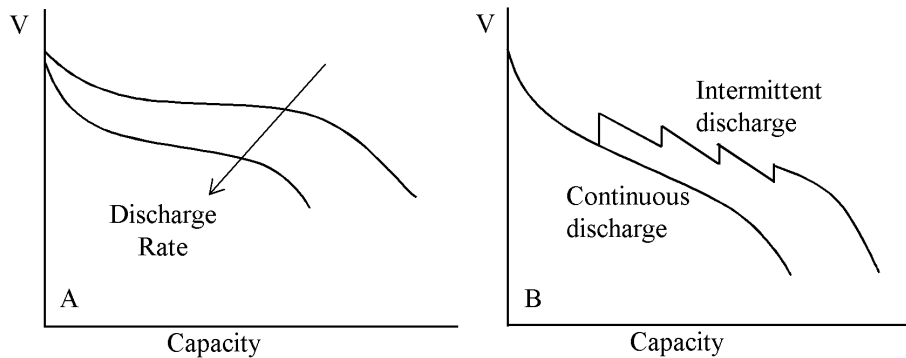
65

Figure 4.2 nonlinear battery behaviours: (a) rate capacity effect; (b) recovery effect

charge or discharge processes increase or decrease the available capacity; operating currents affect the voltage shown at the battery terminals; operating temperature affect the overall performances. This means that estimating the operating conditions of a battery is not straightforward.

The main challenge of any model is the estimation of the actual condition of the battery, which is normally represented by the SoC indicator. SoC estimators are usually the core of BMS systems. Apart from fulfilling the task of limiting the operating range of the cells (i.e. Voltage limits), BMS must detect the actual status of any cell that belongs to the monitored module/pack. This serves to activate proper strategies for equalizing and balancing the charge levels among the cells and increase the available capacity at module level. The more accurate the SoC estimation, the more capacity can be fluxed and the less safety margins have to be used to avoid unwanted damage to the system. This fact directly impacts on the reliability, availability and ultimately on the total cost of the BESS.

SoC estimation deals with the capacity of a battery. However, capacity is a relative quantity since it is defined for a specific rating of use: usually the nominal capacity on a datasheet is defined for a specified value of current. The lower the current, the higher the available capacity shown by the battery. As the intensity of the current is increased, the deviation from the nominal condition can became significant, affecting severely the SoC estimation. This is known as *rate capacity effect* and is shown in Figure 4.2-A. The capacity lost can be recovered by following alternative discharge procedures. If the cell is allowed to relax by following the so-called pulsed discharge rate, the rate capacity effect can be compensated to a certain extent. This other non-linear effect is called *recovery effect* and is shown in Figure 4.2-B.

In the next sections, it is detailed how the proposed modelling approaches describe the battery operations and deal with SoC computation. It is also shown how they take into account the described non-linearities.

Electrochemical models

Using electrochemical modelling means to describe a battery through its electrochemical governing equations. This allows to set up a problem consisting of a system of partial differential equation, to be solved in time and space domain. In general, some founding equations must be highlighted from which to start the electrochemical modelling process.

First, the *thermodynamic* principles are investigated. The two half- cell reactions that take place at the electrodes are studied at equilibrium. The *Nernst law* gives the

equilibrium potential difference for the specific cells:

$$E_{eq} = E_+^\circ - E_-^\circ - \frac{RT}{n_e F} ln \prod_{i=1}^{M} a_i^{v_i}$$

(4.1)

Where F is the Faraday constant, n_e is the number of electrons involved in the overall red-ox reaction and a_i represents the activity coefficient of the species i, raised at its stoichiometric coefficient. E_+° and E_-° are the equilibrium electrode potential measured with respect to a reference electrode that by convention is the hydrogen one, that has "zero" potential.

If Nernst's law describe reactions at equilibrium and the maximum energy release for a given reaction [121], *kinetics* governs the non-equilibrium conditions at electrodes and in electrolyte. Once a current is drawn from (or injected into) a battery, the equilibrium electrode potential is affected by a term called "overpotential" η, negative for reduction and positive for oxidation. For example, when a battery is discharging, the terminals voltage is lower than the Open Circuit Voltage (OCV). The current density can be directly related to the forward and backward reaction rate constants, to the activities of reactants and products, and to the potential gradient as per *Butler-Volmer equation* [122]:

$$i = i_f - i_b = n_e FSC_0 k_f^0 e^{-\frac{\alpha z F}{RT}(E^0 + \eta)} - n_e FSC_R k_b^0 e^{\frac{(1-\alpha)z F}{RT}(E^0 + \eta)}$$

(4.2)

where i_f and i_b are the forward and backward currents related to the two half reactions which can be expressed by the concentration of the oxidizing and reducing species (C_O and C_R) and the reaction rates as a function of the temperatures as per *Arrhenius law*.

When the exchange current is high ($i = i_f$) and very far from the equilibrium, the Butler-Volmer equation can be approximated with the *Tafel equation*:

$$\eta = \frac{RT}{\alpha z F} ln(i_0) - \frac{RT}{\alpha z F} ln(i)$$

(4.3)

In many studies, the loss of overpotential associated to kinetics of reactions at the interface electrode/electrolyte is called "activation polarization".

The last important phenomenon for evaluating losses in a cell is the *mass transport* process to and from electrode surfaces. Mass transport of charged species and reactants follows the *Nernst-Planck equation*:

$$\frac{\partial c_i}{\partial t} = z_i F \nabla(u_i c_i \nabla \emptyset) + \nabla(D_i \nabla c_i) + R_i$$

(4.4)

Where: c_i is the concentration of species i; D_i is the diffusion coefficient of ion i [cm^2/s]. In conditions of electro neutrality ($\nabla \emptyset = 0$), no species generated or depleted $R_i = 0$, one dimensional hypothesis, and constant diffusion coefficient D_i, can be simplified to the *Fick's second law* [122]:

$$\frac{\partial c_i}{\partial t} = D_i \frac{\partial^2 c_i}{\partial x^2}$$

(4.5)

The difference in concentration existing between the electrode surface and the bulk of the electrolyte results in a concentration polarization which impacts on the

overpotential ($E = E_{eq} + \eta$). The SoC indicator is strictly related to concentration of reactants. Consequently, its evolution in time has to be determined if one wants to assess the SoC trend.

In practical uses, the structure of the cell is usually simplified and given load profile (i.e. application) must be assumed to make the problem numerically solvable. The most common approaches (mainly used for Li-ion cells) are the following:

- *Pseudo two-dimensional model (P2D)*. Electrodes are assumed to be composed of identical spherical particles. Ions can move through two spatial coordinates: a radial coordinate *r* (across the spherical particles of active materials in the electrodes) and a linear coordinate *x* (across the cell from the negative to the positive electrode). It is called pseudo 2D model since the radial coordinate does not represent a new dimension. Authors in [123] where among the first authors to conceive a model based on these assumptions. They developed "*dualfoil*": a Fortran program based on their electrochemical model. It is widely used to simulate battery response to a certain load profile (power or current) and check the accuracy of other simplified models.
- *Single particle model* (*SP*): electrodes are assumed to be composed of one single spherical particle whose area is equivalent to the surface area of the solid active material in porous electrode. Porosity is neglected and ions surface concentration is assumed constant along the *x*-axis of the electrode. The solving process is much faster than the P2D model but this model is less accurate especially at high discharge or charge currents [124].

In general, electrochemical models require a large set of input parameters and have a great computational complexity when compared to the other modelling approaches. Finite element, partial differential equation solvers are needed in order to simulate battery operations. Some examples found in literature are [125]: (i) the finite-difference method *dualfoil* [126], developed in Fortran and based on the Newman's BAND subroutine in which the model is discretized with a determined number of nodes in the spatial direction for each variable; (ii) finite volume method (FVM) that discretizes time with various schemes; (iii) COMSOL Inc. Multiphysic [127] which employ a finite element method (FEM) and offer an implementation for the P2D models [128]; (iv) Finite difference method (FDM) or reformulation schemes in spatial coordinates using adaptive solver such as FlexPDE [129] and DASSL [130]. The inherent complexity makes electrochemical models unsuitable for real time monitoring and/or sizing tools, in which a balanced compromise between accuracy and simulation-time is crucial. They are usually employed for cell design purposes to enhance cell geometry and material developments. Moreover, they can be used as a reference term to validate the accuracy of other modelling approaches.

Analytical models

Few equations (with different possible degree of details) are used in order to describe battery behaviour. Values of parameters are empirically found by experimental data. The SoC is computed through charge or energy balances. Due to the simplicity of these models, they are the ones more often employed in dimensioning tools. Their simplicity comes however at the expenses of accuracy and errors in predicting battery performance could be high. In the following, four different approaches of growing complexity are presented.

Empirical models

Empirical models consider a steady-state operation of the battery since they compute the amount of energy that flows through the battery and updates the change in the battery

SoC over a given time step [131]–[133]. There is no direct reference to electrical quantities like voltage and current, but the battery is described as a system that, due to non-ideal behaviour, dissipates some energy. In most of the cases, SoC is assumed coincident with the State of Energy (SoE) and updated as follows:

$$SoE(t) = SoE(t-1) + \frac{\Delta E(\eta)}{E_n} \tag{4.6}$$

Where E_n is the BESS nominal energy and ΔE is the variation of energy in the given time-step that is assumed efficiency dependent. It has to be multiplied by the efficiency when power is provided to the battery and divided by the efficiency when released.

A round trip efficiency η_{RT} can be experimentally defined as the ratio of energy provided during discharge over energy absorbed during charge, at a given operating rate[7] and/or DoD. Round-trip efficiency can be considered as constant [134], or a decreasing function of charge/discharge current or power [135]. Quadratic functions of c-rate have been demonstrated to be suitable to fit experimental data in Chapter 3 (Figure 3.10):

$$\eta_{RT} = 1 - \gamma \cdot (C-rate)^2 \tag{4.7}$$

Describing battery behaviour by its efficiency allows to roughly estimate the SoC starting from the manufacturer's datasheet or simplified experimental tests (no complex parameters evaluation is required). However, battery dynamic response, as well as voltage characteristics are totally ignored.

Peukert's model

Peukert's law was developed in order to model the *rate capacity effect* (i.e. non-linear effect that account for the change in capacity at different discharge rates). The actual capacity of a battery is given by:

$$C_{ref} = I^k \Delta t \tag{4.8}$$

Where k is the Peukert coefficient: $k = 1$ in case of an ideal battery, whose capacity is independent on the current; $k > 1$ for real batteries. k varies with temperature and also with aging (k increases with the lifetime of the battery). In general, the higher the current and the higher k, the shortest the time Δt to arrive at complete battery charge/discharge and the smaller the actual discharged capacity.

SoC could be computed with the so-called coulomb counting method:

$$SoC(t) = SoC(t-1) + \frac{I\Delta t}{C_{ref}} \tag{4.9}$$

Where an average value of I during the time-step can be computed in the case of variable current.

The overall output of Peukert's law is similar to the variable efficiency described in the previous subsection. The difference is that the emphasis is on accumulated charge instead of stored energy.

---

[7] E-rate is assumed equal to the C-rate by using a constant nominal voltage:

$$E - rate = C - rate = \frac{I(k)}{C_n}\frac{V_n}{V_n} = \frac{P(k)}{E_n}$$

Sheperd model

Sheperd's model describes battery behaviour by using electrical quantities [136]. However, it does not belong to electrical models because it reproduces the voltage characteristic through analytical equations rather than electrical circuits. It follows:

$$V(t) = V_{nom} - RI(t) - \frac{\mu}{SoC(t)} \tag{4.10}$$

Where $V(t)$ is the battery voltage at time t, V_{nom} is the rated voltage, R represents the internal resistance of the cell, $I(t)$ is the cell current and μ is a parameter to fit and adapt the model to real measurements. This equation is assumed valid both during charge and discharge.

In [137] authors tested the Sheperd's model obtaining good results during discharge while significant errors during charge. The same authors proposed an improvement based on correction factors that account for temperature, currents and SoC. In [138] another modification is proposed based on a parametric representation of the charge/discharge curve shape: a first exponential trend followed by a linear one (Figure 4.2-a). the voltage is described in the following form:

$$V(Q_i) = V_{nom} - RI(t) - K\frac{Q}{Q - Q_i} + Ae^{-BQ_i} \tag{4.11}$$

where Q is the battery capacity and Qi is the actual battery charge (by coulomb counting method), A is the amplitude of the exponential zone and B [Ah^{-1}] is the time constant inverse of the exponential zone.

KiBaM model

In this model the authors describe the battery with an hydraulic equivalent circuit [139]. The battery is treated as a two-tank system: one with the available charge (q_1), immediately usable by the load, and the other one with the chemically bound charge (q_2). The tanks are divided by valve with a fixed conductance *k'* (which corresponds to the rate constant of the chemical reactions). The rate at which bound charge becomes available is proportional to the difference in "head" of the two tanks (h_2-h_1). The battery is considered totally discharged when $q_1=0$. SoC can be evaluated as:

$$SoC = \frac{q_1}{q_{1,max}} \tag{4.12}$$

Given a constant charge/discharge current, the equations describing the battery behaviour are the followings:

$$\frac{dq1}{dt} = -I - k'(h1 - h2) \tag{4.13}$$

$$\frac{dq2}{dt} = k'(h1 - h2) \tag{4.14}$$

The parameters which need to be found are q_{max} which is the maximum capacity of the battery, *c* which is the capacity ratio (i.e. the fraction of total charge in the battery which is readily available) and the rate constant *k'*.
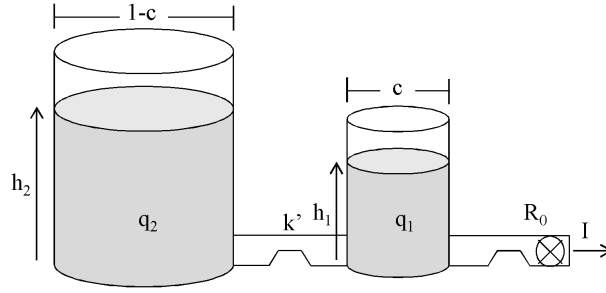
Figure 4.3 Physical picture of the KiBaM model as proposed in [139]

KiBaM model accounts for the *Rate capacity effect*: at high discharge rates, the available tank empties quickly and very little of the bound energy can be converted to available energy before the available tank is empty; at slower discharge rates, more bound energy can be converted to available energy before the available tank empties, so the apparent capacity increases. KiBaM model accounts also for the *recovery effect*: when a load is applied to the battery, the available charge reduces, and the height difference between the two tanks grows. When the load is removed, charge flows from the bound-charge well to the available-charge well until *h1* and *h2* are equal again. So, during an idle period, more charge becomes available and the battery lasts longer than when the load is applied continuously.

Voltage variation over time is also computed within KiBaM model as a linear function:

$$E = E_{min} + (E_{max} - E_{min})SoC - IR_o \tag{4.15}$$

Where R_0 is the internal resistance. This model was proposed by the authors as a valid substitute of electrical models given the small number of parameters required, often derived simply by manufacturer's data. For this reason, KiBaM is the reference model also for some of the well-known sizing tools [118]. One of the main drawbacks is that it is mostly applicable to lead acid batteries and not easily extendible to other technologies (e.g. Li-ion).

Diffusion Model

This model is based on the diffusion of the ions in the electrolyte [140]. It was validated with data of Li-ion batteries [141]. The authors describe the evolution of the concentration of active species in the electrolyte during battery discharge. Processes occurring at the electrodes are assumed to be identical and the symmetry of the battery allows to consider only one electrode.

Figure 4.4 shows the steps occurring in the semi-cell during discharge. At first the battery is full charged and the concentration of electroactive species is constant. When a load is applied, the chemical reaction occurring at the electrode starts consuming species near to its surface. A gradient is created across the electrolyte and this allows ions to move by diffusion. When the load is removed, the battery has time to recover part of the charge by redistribution of electroactive species in the electrolyte (i.e. *recovery effect*).

The concentration of the electro-active species at time t and distance x is denoted by *C(x,t)*. The maximum length is *w*. When the battery is completely charged, concentration is constant over the length of the electrolyte: *C(x,0)=C**. The battery is considered empty when *C(0,t)* drops below $C_{cut-off}$ and the reaction can no longer be sustained.

After solving the diffusion equations described by Fick's law (equation (4.5)), an
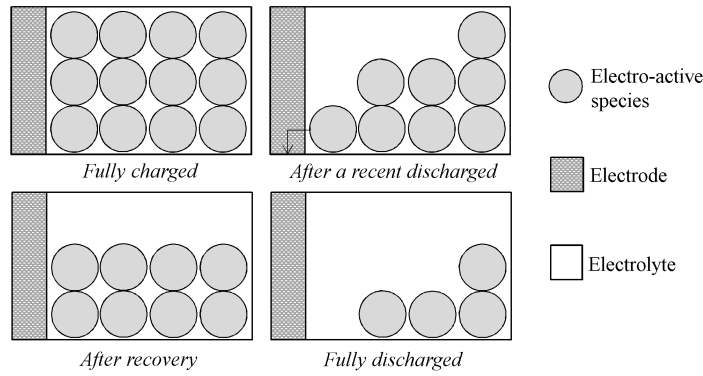
Figure 4.4 Physical picture of the diffusion model as proposed in [140]

expression for σ, the apparent charge lost until time t, can be found of the form:

$$\sigma(t) = l(t) + u(t) = \int I(t)\,dt + \int I(t)a(t)\,dt \qquad (4.16)$$

The apparent charge lost can be separated into two parts: the charge lost to the load *l(t)*, which is simply the integral of the current over time, and the unavailable charge *u(t)*. The first is the charge used by the device, effectively gone out from the battery, the second is the charge which stays unused in the battery (i.e. *rate capacity effect*). These concepts of available and bound charge are the ones already discussed in the KiBaM model, which can be thought of a discretization of the diffusion model.

This model has the advantage of being physically justified since it is developed starting from physical laws that describe processes occurring in the cell. However, it is simplified if compared to electrochemical models, entailing less equations and a much shorter computational time. The drawback of the model is the absence of voltages in the model outputs. It can instead be used to compute battery discharge time, as a substitute of Peukert's law, to optimize battery management systems.

In [114], the authors compared Peukert's model, KiBaM model, Diffusion model and *Dualfoil* electrochemical model in order to predict battery lifetime. As expected, Peukert's law resulted the less accurate model, having the bigger error with respect to *Dualfoil*. Kibam and diffusion model appeared instead to have very similar results, that matched well to the *Dualfoil* electrochemical model.

Stochastic models

Stochastic models describe battery system as a whole, modelling not only battery behaviour but also the stochastic nature of random usage profile. They describe the battery in mathematical terms, employing a high degree of abstraction. Authors in [120] were among the first to develop and improve a stochastic model for non-rechargeable batteries. Other authors adapted their model in order to apply it to rechargeable ones [119]. In general, SoC is predicted by exploiting the theory of Markov chains.

Specifically, the amount of charge available in a battery is divided into *N* states of a Markov chain (Figure 4.5-a). When the battery is in state 0, it means that SoC = 0 and that the battery is completely discharged. State *j* represents an arbitrary SoC. When, instead the state of the battery is *N*, the battery is completely charged (SoC is considered in relative terms, related to the actual maximum capacity).

The basic of this model is the charge unit, that is the amount of charge necessary to transmit a data packet (typical in the TELCO sector). During each time step, the charge
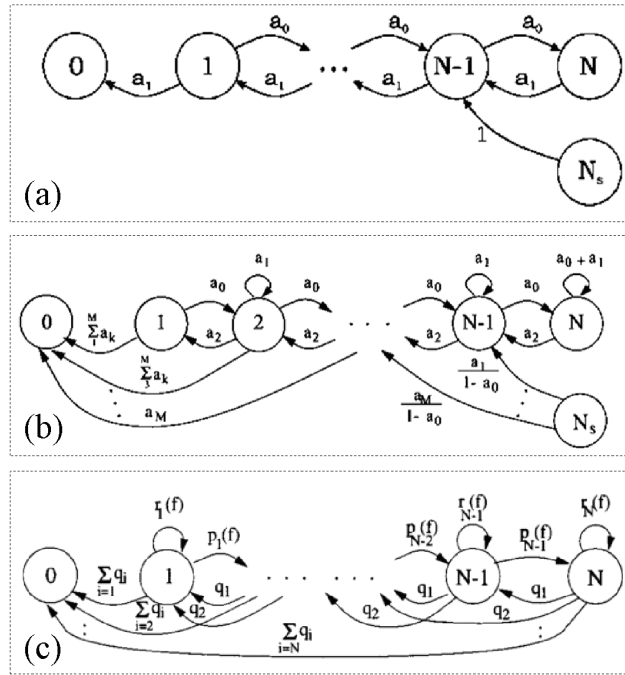
Figure 4.5 Representation of stochastic battery models: (a) Basic Markov chain; (b) Extended Markov chain presented in [120]; (c) extended Markov chain presented in [142]

unit has a probability $a_1=q$ to be consumed, leading the battery to a lower state of charge and $a_0=1-q$ to be recovered. EoD is reached when the battery arrives to state 0 or when the maximum of T charge units has been consumed, T equals the theoretical capacity($T>N$). N is in fact the amount of charge recoverable with continuous discharge, and it can differ from the charge obtained via pulsed discharge, due to the advantages of the *recovery effect*. The major findings of the work are two parameters [114]:

- m_p that is the predicted amount of transmitted charge units.
- G that is the gain obtained from a pulsed discharge if compared to a constant discharge. Defined as m_p/N. $G =1$ for continuous discharge and greater than one for pulsed discharge, reaching a maximum value of T/N.

The same authors, proposed more advanced models, able to predict battery behaviour also in more complex situations:

- The first change (Figure 4.5-b), applied in [120] consists in considering each time step the possibility that more than one packet can be trasmitted arriving to a maximum number of packets of M≤N. This allows taking into account the discharge at high currents (i.e. *rate capacity effect*)
- A second change (Figure 4.5-c) applied in [142] considers that the probability to recover is not constant but a decreasing exponential function of SoC, depends also on the total discharged capacity. If the SoC is represented by the state j of the system, the discharged capacity is taken into account via the number of phases f. The higher f, the higher the amount of consumed charge units and the lower the *recovery effect*.

In general, stochastic models are suitable to be used in real time BMS, due to low time consumption if compared with electrochemical models [142]. However, they do not represent the physical phenomena behind BESS operations. For this reason, stochastic models could be integrated with electrical or analytical models in order to describe the necessary battery characteristics.

For instance, in [116] a KiBaM-based stochastic model is developed. The authors coupled a stochastic model with the previously described KiBaM model. Battery behaviour is described by a Markov process. It is assumed that the bound charge and available charge (i.e. SoC) change their states according to probabilistic laws. Moreover, during idle periods, the battery has a certain recovery probability, dependent on the SoC. Three are the possible transitions that the battery can experience: (i) the idle period in which the battery recovers charge (with probability of recovery p_r): an amount Q of charge is transferred from bound to available charge and no current is extracted; (ii) the idle period during which the battery does not recover charge (with probability of non-recovery p_{nr}); (iii) the period in which a load is applied (with probability that charge units are required in the time step q_l): the charge transferred from the two tanks in agreement with kiBaM model funding equations. Overall, the hybrid model is claimed to be able to represent the statistical nature of the load (thanks to its half-stochastic nature) and the real-operations of the battery (thanks to its half-analytical nature) in a more accurate way than with a simple stochastic model.

In [143] the authors proposed an electrical circuit model integrated with a stochastic model. The scope of the work is to provide a real-time estimation of SoC in EVs. The authors model the battery with the simplest equivalent circuit model: a voltage source in series with a resistance (see electrical models in next section). SoC is given by a discretization of the coulomb counting equation (4.9), while the dynamic behaviour is represented by a Markov chain that changes during time according to external and internal factors. The model has been validated and it is claimed to predict accurately the SoC of the battery. It allows avoiding error measurements that appear when calculating SoC using only the coulomb counting method.

Electrical models

Electric circuit modelling is one of the most common approaches investigated nowadays. Batteries can be represented by equivalent electric circuits composed of circuital elements which, if opportunely tuned, can reproduce the same characteristics of voltage and current as seen from external terminals. Thanks to their flexibility, relative simplicity (when compared to electrochemical models) and high accuracy, electrical models can cover a wide range of applications. They are particularly used in real-time applications, such as in EVs to predict the current condition of the battery pack [144]–[146].

There is a wide range of circuital models, with a different degree of complexity. The simplest ones, with few constant circuital elements, are far from describing the real physics of the battery, and they could be compared with empirical models. The most advanced models are composed of circuital elements that directly reflect electrochemical characteristics of the cell. They can have a grade of accuracy almost similar to electrochemical models, but they require the determination of many parameters resulting in time-consuming simulations. Parameters need to be experimentally estimated taking into account the various operating conditions (SoC, SoH, temperature). The simplest but time-consuming strategy is the offline estimation, with the creation of lookup tables or polynomial function. It is also possible to estimate parameters online in case of adaptive models [147].

Electric circuits are composed of two main parts to proper reproduce battery steady-state and dynamic behaviours respectively: (i) the circuital element that represent the equilibrium voltage of the cell (i.e. OCV), directly related to the energy content of the cell (i.e. the SoC); (ii) other circuital elements that represent the overpotential with respect to equilibrium condition.

In literature, two main families of battery electrical models are used to differentiate the way in which the OCV is represented [148], [149]:

- *Active models*: OCV is modelled by an ideal source that is typically a voltage generator, with voltage varying according to SoC. In this case the battery is seen as DC electric generators driven by chemical reactions.
- *Passive models*: OCV is modelled as the voltage drop across a capacitor of big-variable capacitance (called incremental, differential or intercalation capacitance [150], [151]). Such passive element represents the charge stored in the cell in a chemical way rather than an electric way. Capacitance and voltage drop across the capacitor vary with the SoC.

Regardless of the specific category, the techniques used to estimate the other circuital elements are the same and can be divided into: time domain and frequency domain techniques [115], [145]:

- *Time domain*: circuits are built using serial and parallel networks of resistances and capacitors. The values of circuital elements are usually found by fitting discharge curves in different conditions [152].
- *Frequency domain*: circuits are built with complex impedance expressions which can be approximated, but not in an exact way, with resistances and capacitors. Sometimes circuital elements remain expressed in the frequency domain. Constant Phase Element (CPE) and the Warburg Impedance (WI) are typical options used in this category. Electrochemical Impedance Spectroscopy (EIS) is the most used technique in order to give each element a precise physical meaning and to estimate the value of parameters (basics of EIS are detailed in Annex C) [153].

As regards to SoC indicator, electrical models estimate the SoC as function of the electrical quantities (i.e. OCV): SoC is derived and not computed. For this reason, they are often coupled to other approaches that use the coulomb counting method (equation (4.9)) [154]. Coulomb counting is actually fast and easy to implement but it is often subject to mistakes due to systematic errors in current measurements that affect the integral computation. An electrical model is then used to check the accuracy of SoC estimation in specific conditions and to recalibrate the integral if needed.

Active models

Active models are characterized by the presence of an ideal source to represent the charge stored in the battery, typically a voltage generator. This could ideally provide an infinite amount of energy and it is not representative of the real battery physics. They are mostly developed in the time-domain and they are composed of resistors and capacitors to reproduce the dynamic phenomena. R and C parameters are found by fitting experimental tests in different conditions. However, there also exist examples also of models that make use of complex impedances (i.e. expression in the frequency domain) that are found with sophisticated experimental techniques like EIS.

The first and simplest electric model is shown in Figure 4.6-a: the R_{int} *model* constituted by a voltage source (V_{oc}) and an internal resistance (R_{int}) [147]. Because of its few constituent circuital elements, this model cannot consider the dynamic response of the battery. However, the accuracy of the model can be increased when parameters depend on temperature, SoC and SoH [147]. The crucial aspect is the element R_{int} that can be determined with different methods: pulse characterization, thermal methods (i.e. Joule losses method) and EIS [155]. In the last case, different values of resistances which correspond to different excitation frequencies are determined. Then, the value of R_{int} is chosen among them which is in agreement with the typical solicitation in the final application (i.e. typical periods of the discharge charge cycles). Generally, the R_{int} *model*

can be adapted to several technologies: in [145], it has been used to model lead acid batteries applied in UPS application or traction vehicles. While in [156], it has been used for simulating high power Li-ion batteries in HEV application.

Another type of active model is the so-called *Thevenin model* which is mainly composed of three parts (Figure 4.6-b) [157]: (i) a voltage source for open-circuit voltage V_{oc}; (ii) the internal resistances that include the ohmic resistance R_o for losses in electrolyte and conductors, and the polarization resistance R_p associated to the electrochemical reaction; (iii) the equivalent capacitance C_p that is used to describe the transient response during charging and discharging. Different from R_{int} model, *Thevenin model* accounts for transient response with a single RC branch, with a single time constant:

$$\dot{V}_p = -\frac{V_p}{R_p C_p} + \frac{I}{C_p}$$

$$V = V_{oc} - V_p - IR_o$$

(4.17)

The parameters (R_o, R_p, C_p) can be assumed to be constant or dependent from SoC, temperature, charge/discharge rates, SoH. These dependences can be experimentally determined and then taken into account via lookup tables [157]. Applications of this model in PV-BESS systems, portable BESS-powered systems and real-time simulation of HEVs and EVs are found in literature [145].

Further evolution of the previous models is the *DP model* (double-polarization) which is similar to *Thevenin model*, with an additional RC group (Figure 4.6-c) [158]. This last element is added in order to make a distinction among the polarization phenomena occurring in the battery and being faithful in representing the transient phenomena especially for Li-ion cells. The first RC group, with a smaller time constant, is related to electrochemical polarization, while the second RC group has a bigger time constant and it characterizes the diffusion processes occurring inside the cell. This kind of polarization is called concentration polarization.

In general, the higher the number of RC groups in series, the more accurately the model reflects the transient behaviour of the battery. In [159]**,** the authors propose a model with 5 RC groups: Three of them model the diffusion processes while the other two the electrochemical reactions. The more sophisticated the model, the higher the number of parameters to be determined and the more difficult the use of the model in order to simulate and estimate the battery operation. For this reason, the *Thevenin* model or the *DP model* are often preferred.
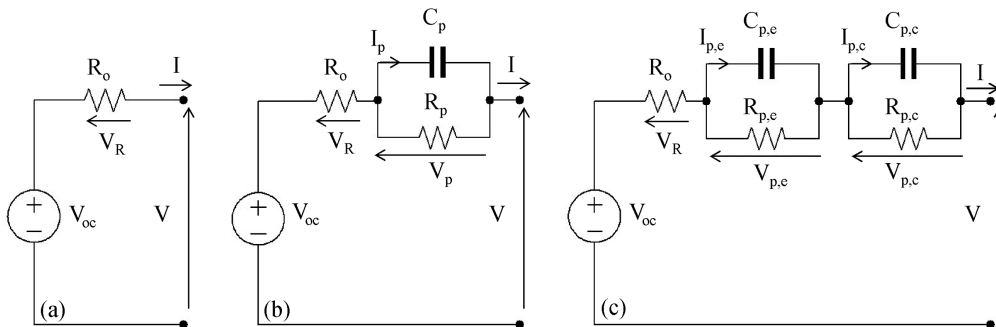

Figure 4.6 Examples of electrical active model developed in the time-domain: (a) R-int model, (b) Thevenin model, (c) DP model
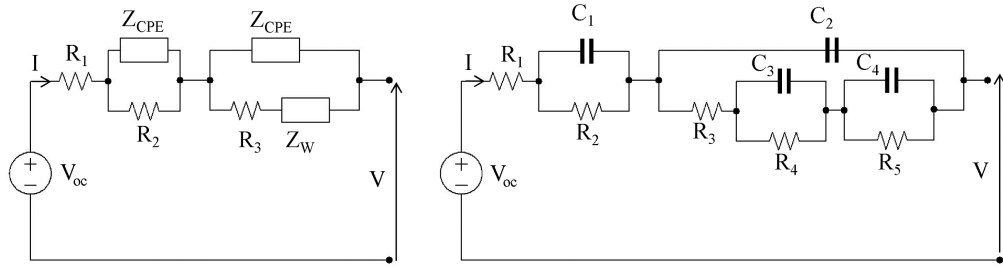
Figure 4.7 Example of electrical active model developed the frequency-domain (left) and its equivalent circuit in the time-domain (right)

If the above models are derived in the time-domain, a typical active model in the frequency domain is proposed in [160], as a possible improvement for real-time BMS systems. The model structure is shown in Figure 4.7. The parameters are empirically found by fitting of EIS experiments and expressed as function of SoC and temperature. Element Z_W is the so-called Warburg impedance that is used to account for diffusion phenomena (more details about Warburg impedances will follow in Chapter 5). While the two R-Z_{CPE} couples account for the electrochemical reactions in the two electrodes. *CPE* (Constant Phase Element) impedance models an imperfect capacitor. It is used when the shape of the R-C semi-circle in EIS (see Appendix C) is not perfect but slightly "depressed". Its expression is given by:

$$Z_{CPE} = -\frac{1}{(j\omega)^{\alpha}C} \tag{4.18}$$

Where α is less than one in the CPE but equal to one for a perfect capacitor.

Authors propose also the equivalent circuit in the time-domain for simulation purposes: CPEs, given the non-intuitive electrical representation, are adapted with perfect capacitors, while Warburg impedance is represented with two parallel RC elements. Therefore, the main difference with previous models lie in the parameters identification procedure (frequency-domain nature) rather than the final model configuration which resembles the one of Figure 4.7. Finally, SoC is computed by the coulomb counting method and authors claimed that the model is able to accurately predict the output voltage of LMO and NMC chemistries in EV applications.

Passive models

Passive electrical models use only passive circuital elements to represent the battery functioning, including the energetic content. This is done by using a big capacitor of variable capacitance: the charge stored in this capacitor is assumed equivalent to the charge stored in the battery via electrochemical reactions. The capacitor is used to describe the SoC instead of the voltage generator in active models. The value of the capacitance is variable with the OCV and can be derived from discharge curves. It is often called intercalation capacitance because it describes the accumulation and depletion of Li-ions within the electrode [150], [161].

Passive models developed in the time-domain are very similar to active models developed in the same domain. They are made of RC groups in series according to the level of accuracy required. As stated in [145], the model can be simplified to a single capacitance in series with a resistance when a low degree of accuracy is tolerated (Figure 4.8-a). C_0 is the bulk capacitance of the cell and R_0 is the internal resistance. As for an active model, the value of resistance can be found via different techniques, among which
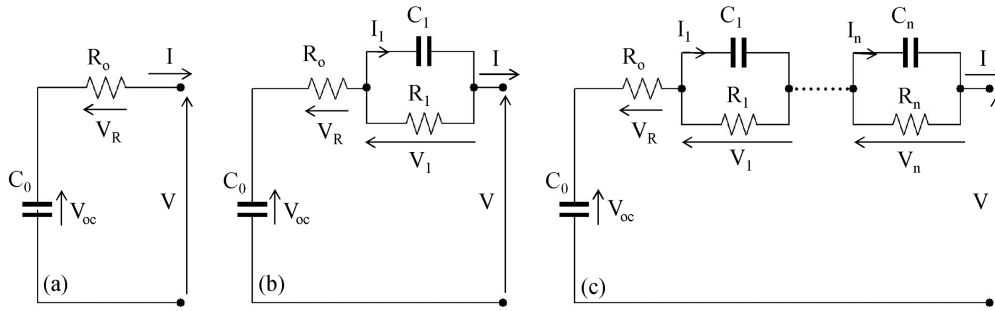
Figure 4.8 Examples of electrical passive model developed in the time-domain with different degree of complexity

it is relevant to mention EIS.

Models that resemble the *Thevenin models* can be found in the passive form (Figure 4.8-b). The only difference is that OCV is represented by a capacitor rather than a voltage source. The others circuital elements are basically the same: a resistance to account for ohmic losses, a RC group to represent the transient behaviour. All the parameters, including the big capacitance of the main capacitor, are derived from discharge curves obtained in different testing conditions. Also in the case of passive models, the accuracy can be enhanced by increasing the number of RC groups (Figure 4.8-c) [162].

Passive models developed in the frequency-domain distinguishes from the other three families (i.e. active-models/time-domain, active-models/frequency-domain, passive-models/time-domain) because they aim at describing the battery operations by modelling its physical phenomena. Thus, the electrical models use elements that singularly represent one or more electrochemical phenomena avoiding ambiguous elements which are far from being representative of a battery. They usually use OCV characteristics to find OCV related to SoC, then OCV is summed to overpotential to compute battery terminal voltage.

The reference model was developed in 1947 by John Edward Brough Randles, but it is still referred to today works. The so-called *Randles model* well represents the interfacial electrochemical reactions in presence of semi-infinite linear diffusion of electroactive particles to flat electrodes (Figure 4.9-a) [163]. This circuit is developed to reproduce the behaviour of a half battery cell and it is composed of four main elements: (i) Z_w is the Warburg impedance element that models diffusion processes occurring at electrodes; (ii) R_{ct} is the charge transfer resistance at the electrodes that models the electrochemical reactions; (ii) C_{dl} is the double layer capacitance that models the capacitive effect between the electrode-electrolyte interface; (iv) R_o represents ohmic losses in wires, electrodes and electrolyte.

Ideally the full cell is composed of two identical half cells, with the same Randles structure but different parameters' values. In Figure 4.9-b, the impedance of the whole battery is represented. Inductances show their effect only at high frequencies and are due to battery current collectors and cables. However, it is difficult to separate the impedance measurement of the negative and the positive electrode for sealed cells (i.e. Li-ion batteries, AGM lead-acid batteries, etc.). Therefore, the Randles model of the first order is widely used as a representative lumped model for an electrochemical cell.

In practice, *modified Randles models* are used and applied to specific technologies. In [164] a model for Li-Ion cells is presented. The authors describe each process occurring in the cell via the physical governing equations in order to define the impedances that form their proposed model. It has a strong physical basis. The model presents an anode impedance and a cathode impedance connected in series, the ohmic resistance and
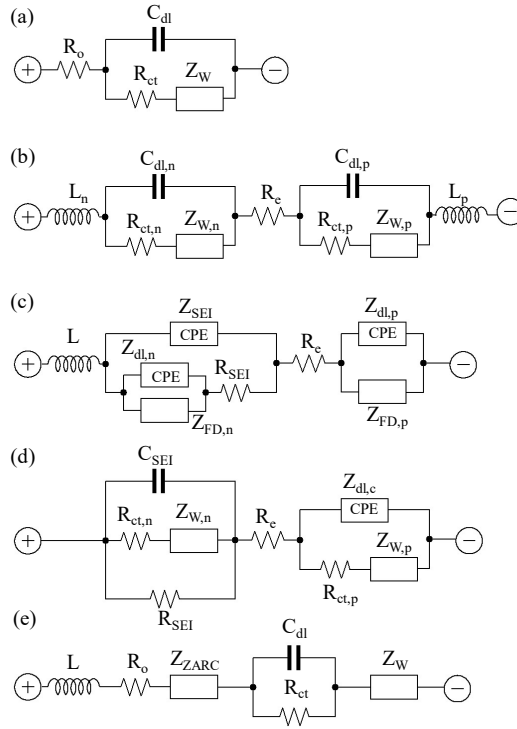
78

Figure 4.9 Examples of electrical passive model developed in the frequency-domain: (a) Randles model (half-cell), (b) Randles model (full-cell); (c-d-e) modified Randles-like models

inductance (Figure 4.9-c). Specifically the electrodes impedances include: (i) Z_{FD} that is the faradaic impedance present at both anode and cathode, it can be derived from electrochemistry using Butler-Volmers and Fick's law (equations (4.2)(4.5)); (ii) the double-layer impedances: CPE is used to describe this dispersed capacitance on the assumed rough electrode surface; (iii) the effect of SEI (solid electrolyte interface) film at anode. SEI is a protective layer that is formed by reduction reactions of electrolyte components at the electrolyte/electrode interface [165].

In [166] another modification to *Randles model* for Li-ion cells is presented (Figure 4.9-d). The anode part of the circuit slightly differs from the original model. The anodic electrochemical reaction and SEI formation reactions happen in parallel. The first one is composed by the couple composed of a charge transfer resistance and a diffusion impedance in the Warburg form ($R_{ct,n}$, $Z_{W,n}$), while the second one is composed of a resistance in parallel with a capacitor (R_{SEI}, C_{SEI}).

In [167] the authors develop an innovative electrical model for Li-ion batteries based on EIS measurements (Figure 4.9-e). As in Randles circuit, inductance and ohmic resistance are present. The other part of the circuit slightly differs from Randles model: Z_{zarc} stands for the "depressed" arc in the Nyquist plot at high frequencies (Z_{zarc} can be represented by a resistor in parallel with a CPE element), but the authors give no physical meaning to this impedance. The RC group comprises the double layer capacitance and charge transfer resistance. Finally, the Warburg impedance represents diffusion at low frequency. Differently from Randles model, Warburg impedance is in series with the other circuital elements and it represents the diffusion phenomena happening across the cell. By using the depicted model, the authors claimed to have reached sufficient precision in reproducing all the relevant processes happening inside a Li-ion cell.

In all the above Randles-like models it is not clear how the SoC is estimated. In some

works, the SoC is found by an integration of the current [168]; then, by using lookup table, the OCV is inked to SoC; the output voltage is determined by taking into account the voltage drops over all the circuital elements. In some others, the key lies in the Warburg impedance that physically represents the phenomena of intercalation and thus the capacity (i.e. intercalation capacitance). In the time domain, it is demonstrated that the Warburg impedance can be represented by a series of RC groups (more details will follow in Chapter 5): a big capacitance (also called intercalation capacitance) is then used to represent OCV and thus the storage capacity. SoC is derived with look-up tables or a fitting function. The output voltage is given by the sum of the potential drop over each element.

The latter case can be found in some works in which the big capacitance is explicitly shown in the model. A first notable example is the *SAFT RC model* (Figure 4.10-a) [158] that is based on a two-capacitance model which reproduces well the behaviour of the high power cells developed by Saft Groupe S.A. Figure 4.10-a. C_b is the bulk capacitance that represents the charge chemically stored in the battery, being so responsible to describe the OCV as a function of temperature; C_c is a smaller capacitance that accounts for the surface effects of the cell (i.e. double-layer), diffusion and chemical reactions; while the resistors represent losses associated to various parts of the cell. SoC is related to OCV by using OCV tests [156].

In [169], the authors derive the *energetical model*: an electrical model whose development starts directly from Fick's law (equation (4.5)). The strong physical basis of this model makes it accurate and comparable with electrochemical models. The model's configuration is different from the classical Randles scheme. However, similar elements can be found (Figure 4.10-b): R_o is the resistance representing ohmic losses in electrolyte and electrodes; C_{dl} is the double layer capacitance; C_{int} is the intercalation
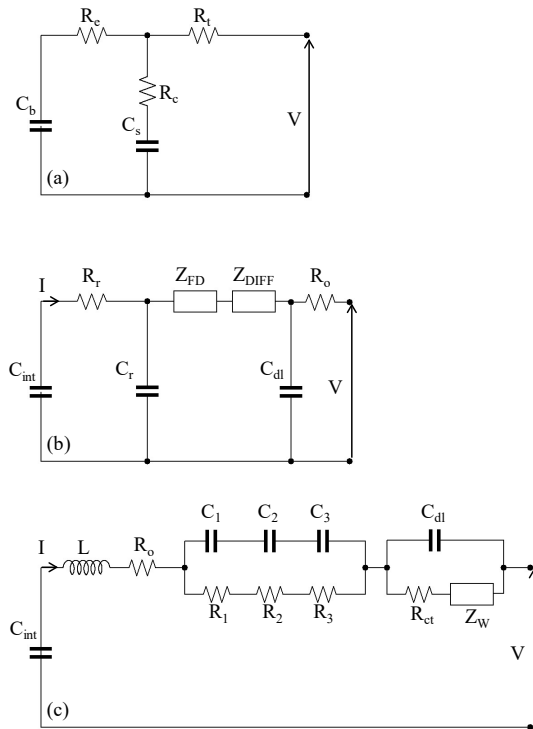

Figure 4.10 Examples of electrical passive model developed in the frequency-domain: (a) SAFT RC model; (b) energetical model; (c) model presented in [151]

capacitance: the term that accounts for charge availability (i.e. the SoC); Z_{FD} is the Faradaic impedance; Z_{DIFF} is the impedance representing diffusion in porous electrodes; finally, R_r and C_r represent the relaxation branch, taking into account the phenomenon of relaxation.

In [151], the authors developed an equivalent circuit model with the aim of improving BMS. The parameters were evaluated with EIS, at various SoC and temperatures. Authors give to EIS graph a physical meaning: the low frequency portion represents the diffusion of lithium ions into the porous electrode matrix; extremely low frequencies signify the intercalation capacitance of the electrode, which describes the accumulation of lithium ions within the host material. Specifically, the model is composed of the following elements (Figure 4.10-c): L incorporates the inductive behaviour due to geometry of the electrodes; R_o is the solution resistance in representing the ohmic losses; R-C circuits (R_n and C_n) in parallel denote the slow migration of Li-ions through surface films of the electrodes; charge transfer resistance (R_{ct}) and a double layer capacitance (C_{dl}) of electrodes; Warburg impedance (Z_W) for diffusion processes of the anode and cathode; and finally intercalation capacitance (C_{int}) which describes the accumulation and depletion of Li ions within the electrodes. The intercalation capacitance is included in this model to show the variation of open circuit potential with SoC.

4.3 Modelling of aging (SoH estimation)

Apart from dynamic modelling, BESS models should also be able to represent degradation during cycling. Modelling of aging is becoming important especially in EVs application. Monitoring and estimating change of performance during operation can improve BMS and safety [170]. For this reason, it is easier to find literature that refers to automotive sector rather than stationary applications.

In general, two are the main mechanisms that influence battery aging:

- Cycle aging that describes the impact of BESS utilization periods and is influenced by the operating conditions (currents, SoC, temperatures).
- Calendar aging that describes the impact of BESS storage periods. In this case, the impacting factors are the storage conditions (ambient temperature and SoC level).

From a final application perspective, two are the main issues brought by aging of BESS:

- *Capacity fade* that limits the energy performances. It involves the reduction of the available capacity over time. BESS end of life (EoL) is defined when the capacity fade has reached a specific threshold (usually 80%). The most used indicator to update aging status is the SoH that is the ratio between the current capacity and the rated capacity.
- *Power fade* that limits the power performances. It involves the increase of impedance over time and consequently a worsening of the overall efficiency of the device. The most used indicator is the SoH_R (or SoR) that is the ratio between the current cell resistance and the initial one.

In general, aging phenomena occur mainly at the electrodes, differently between anode and cathode and among the different technologies. Focusing of Li-ion we can distinguish [165]:

- Formation of surface layers both at anode and cathode. At anode, it is typical due to SEI formation that takes place mainly in the first few charge/discharge cycles, leading to a rapid decrease in battery capacity at the beginning of its life. The layer partly protects the anode from further oxidation, but it continues to grow during the whole life of the battery, playing a major role on the impedance increase. In particular, cracks

can propagate through the SEI layer when the battery is subject to high stresses (e.g. high currents). At cathode, it is typically seen happening for LNCO chemistries and is due to electrolyte oxidation reactions. It is enhanced by high temperatures and high SoC.

- Graphitic anode exfoliation and cracking: caused by electrolyte reduction inside graphite and gas evolution. The consequent loss of active material leads to capacity fade. It is enhanced by high SoC.
- Dendrite growth: Lithium deposits on the surface of graphite layer instead of intercalating into the lattice of the carbon. Li metal will subsequently react with electrolyte. It might occur at a low temperature and high discharging rate accelerating capacity fade.
- Cathode disordering, typical of Lithium metal oxide structures.
- Metal dissolution: typical of LMO chemistry. At elevated temperature metal dissolves in the electrolyte, leading to capacity fade.
- Change in porosity: volume changes of active material during charge and discharge cycles affect the structure of the electrodes. High current rate associated with high cycle depth and high SoC enhance the phenomenon leading to impedance rise.
- Current collector corrosion: there might be reactions between a current collector and electrolyte that lead to loss of contact between current collector and electrodes. This phenomenon is enhanced at low SoC and leads to an increase of the impedance.

In literature, many different approaches have been used to model aging mechanisms and estimate battery SoH [170] [171]. Parameters of the adopted battery model (see previous sub-section) must be changed with time or with cycles. A full charge-discharge cycle is defined when the throughput Ah are equal to two times its nominal capacity (C_n). Therefore, the number of cycles n that a BESS has cycled until time t is given by:

$$n = \int_o^t \frac{|I(t)|dt}{2C_n} \qquad (4.19)$$

In the following, aging modelling for Li-ion cells is described in agreement with the four approaches adopted in the previous sub-section.

Electrochemical models

Electrochemical modelling aims at describing degradation phenomena through equations based on electrochemical principles. This set of equations are usually connected as subsystem to the governing equations of the electrochemical model of earlier subsection. Ex situ techniques (X-ray diffraction, scanning electron microscopy, transmission electron microscopy, x-ray photoelectron spectroscopy, etc.) can reveal the operation and degradation process. From this analysis, it is possible to obtain information about the structural change and parameters variation of materials [172]. However, this kind of technique must be performed on samples that have been disassembled and cannot operate anymore. Developing degradation model using these detailed data could be particularly laborious. Another option could be to exploit EIS technique to evaluate the changes in the electrochemical model parameters due to degradation [173].

In [174], authors attempt to describe the cell calendar aging for the LCO chemistry. They refer only to the Lithium corrosion phenomenon at negative electrode which is related to side reactions occurring between electrolyte and lithium, causing capacity loss. They claim to have found a general equation to calculate Lithium corrosion curves as a function of time and temperature. This finding is used to forecast capacity fade, but it is

not added to a general electrochemical battery model. If a new chemistry is adopted, then the experiments have to be performed again to deduce the new equation coefficients.

Authors in [175] considers degradation phenomenon at cathode as the most crucial one, whereas the aging effect for the anode is neglected for simplicity. In the electrochemical model, Kalman filter is used to estimate two crucial parameters: the cathode porosity and electrolyte conductivity. During operation, some particles will be isolated from the conductive area or will crack, reducing cathode effective porosity. Thus, the capacity fade is modelled as reduced cathodic porosity and loss of active insertion material. Moreover, cycle aging causes the overpotential to rise. Thus, the power fade is modelled by a decrease in electrolyte conductivity.

In [176] degradation modelling is included in a P2D model in order to assess the change of battery operating performance. Butler Volmers' kinetics is defined separately for Li-ion intercalation reaction and parasitic reactions. Moreover, SEI formation is modelled as an additional resistance (proportional to the film thickness) that leads to an overpotential rise. Capacity loss is then given by the integral of the parasitic reaction's current over time. The model, comprising a total of eight variables was simulated with COMSOL Inc. Multiphysic [127]. The model is claimed to be quite accurate but it considers only one degradation mechanism; a proposed improvement considers a comprehensive analysis of the whole battery aging process.

Analytical models

These models correlate capacity and power fade rates with a combination of stress factors (i.e. temperature, SoC, number of cycles) which have a great influence on battery lifetime. They can deal separately with calendar and cycle aging (distinction typically found for lithium-ion batteries) or they take into account the life of the battery as a whole. They rely on experimental data in which the chosen BESS technology has been cycled in several external conditions. Some of them, propose equations based on the purely best data fitting method, some others seek to relate observed trend with a physical meaning. Moreover, two different sub-categories can be highlighted:

- Analytical models which evaluate capacity fade and power fade indicators by updating parameters on-line during the simulation (e.g. updating the remaining capacity due to the capacity loss).
- Analytical models which evaluate battery residual lifetime by assessing the maximum number of cycle and calendar lifetime but do not update battery characteristics.

Equivalent full cycles to failure

This method is the simplest approach to predict battery lifetime [132]. It estimates the number of full charge-discharge cycles N until the battery reaches a defined maximum number of cycles (i.e. EoL). The maximum number of cycles can be set from a datasheet or from international standard rules. SoH is written as a linear function of the number of cycles. At cycles n, SoH can be determined as follows:

$$SoH(n) = SoH_0 - \frac{SoH_0 - SoH_{min}}{N_{max}^{cycles}} \cdot n$$

(4.20)

Actually, this model does not consider the decrease of capacity and power in time and the consequent changes in battery operation.

Empirical models

Empirical models derive mathematical expressions for capacity and power fade by

fitting experimental measurements. These equations are easy to use but they are strongly dependent on the specific battery technology. Moreover, they typically entail long testing periods for parametrization.

In [177] the authors describe cycle aging for LFP chemistry as dependent on various parameters, such as temperature, DOD and current. The model evaluates the number of cycles to failure for each condition; however, this evaluation is not used to predict the power and capacity fade but to update the Peukert coefficient (see *Peukert model* in section 4.2)

In [178] power fades due to calendar aging is estimated for NCA chemistry through the following equation:

$$P_{fade}^{calendar}(t,T,SoC) = \frac{e^{\left(b_0+b_1\frac{1}{T}\right)}}{1+e^{\left(b_2+b_3\frac{1}{T}\right)}} - e^{\left(b_4+b_5\frac{1}{T}+b_6SoC\right)}t^{1.5} \qquad (4.21)$$

Where b_x are the sets of parameters needed to fully characterize the specific technology. Two degradation processes contribute to the power fade: the first term of the equation represents the fast degradation mechanisms and is strongly enhanced by high temperature. The second term represents the slower degradation processes and it depends on time.

Authors in [179] derive equations for LFP chemistry for both capacity and power fade during calendar and cycle aging to analyse different driving profiles for HEVs applications. As regards to calendar aging they found link with storage temperature, SoC and time:

$$C_{fade}^{calendar}(t,T,SoC) = (a_1 SoC^{a_2} + a_o)(a_3 T^{a_4} + a_5)t^{0.8} \qquad (4.22)$$

$$P_{fade}^{calendar}(t,T,SoC) = \left(\frac{b_1 SoC^{b_2} + b_3}{b_4} b_5\right)\left(e^{b_6 T}\right)t \qquad (4.23)$$

Where a_x and b_y are the sets of parameters needed to fully characterize the specific technology. Power fade is found to be linearly dependant with the storage time while capacity fade depends on $t^{0.8}$. On the contrary, cycling aging is found to be dependent on temperature, DoD and cycle number (cycling rate was not taken into consideration because the test were all made at the same current).

$$C_{fade}^{cycling}(n,T,DoD) = (c_1 e^{c_2 T})(c_3 DoD^{c_4})n^{0.5} \qquad (4.24)$$

$$P_{fade}^{cycling}(n,T,DoD) = d_1\left(d_2 e^{d_3} + d_0\right)d_4\left(e^{d_5 DoD}\right)\left(n^{d_6 T - d_7 DoD - d_8}\right) \qquad (4.25)$$

Where c_x and d_y are the sets of parameters needed to fully characterize the specific technology. Both calendar and cycling aging are found to be dependent on the number of cycles n. In particular, capacity fade with the square of n. A comprehensive lifetime model is then developed by combining the two aging mechanisms: equation (4.22) and equation (4.23) are used when the battery is working, while equation (4.24) and equation (4.25) are employed during battery rest periods. The main limitation of this model is the remarkable amounts of parameters that need to be mapped in all the different conditions of SoCs, DoDs, time, cycles, etc.

Semi-empirical models

Different from purely empirical models, semi-empirical models are based on a physical description of battery degradation. The modelling approach consists on the establishment of analytical equations and parameter estimation through data fitting. The majority of the works consider that the reaction rate of parasitic/unwanted processes (e.g. electrolyte decomposition and SEI formation) exponentially increase with temperature according to Arrhenius law. Moreover, many studies use a correlation between capacity fading and the square root of time: the corrosion rate at the anode is found to be dependent on $t^{0.5}$.[174].

In [82], the authors developed a semi-empirical models based on LFP chemistry. They discovered that DoD influence on capacity fading was negligible. Starting from Arrhenius law they proposed a power law equation for the capacity loss, depending on T, C-rate and *Ah* throughput:

$$C_{fade}(Ah, T, Crate) = \left(a_1 e^{\frac{a_2 + a_3 Crate}{RT}} \right) Ah^{0.55} \tag{4.26}$$

The authors found an empirical relation between activation energy and C-rate that suggests that higher currents induce higher stresses accelerating chemical processes involving lithium consumption. In the subsequent work [180], the same authors made a step further. They considered calendar and cycle aging separately, as follows:

$$C_{fade}(t, Ah, T, Crate) = \left[(a_2 T^2 + a_1 T + a_0) e^{(b_1 T + b_0) Crate} \right] Ah + f e^{-\frac{E_a}{RT}} t^{0.5} \tag{4.27}$$

In [181] a semi-empirical model is developed which is based on an *energetical model*. They assumed that calendar aging is mainly driven by SEI growth and the consequent lithium ions loss. Therefore, lithium ions loss is presumed to depend on the square root of time, as previously stated. Moreover, they assume an exponential dependency of the aging on the SoE (i.e SoC) and on the temperature (i.e. Arrhenius law). The expression for calendar aging is:

$$A^{calendar}(t, T, SoE) = A_0 \left(e^{\frac{SoE + SoE_0}{b}} \right) \left(e^{\frac{T_B + T_0}{c}} \right) t^{0.5} \tag{4.28}$$

Where A_0 coefficient corresponds to initial battery lifetime, SOE_0 and T_0 are the initial SoE and temperature. The aging per cycle is a cubic function of cycle depth and cycle current. Therefore, cycle aging can be expressed as:

$$A^{cycling}(n, DoD, I) = \sum_{n=1}^{N} a_n(DoD_n, I_n) \tag{4.29}$$

Then, authors superimpose the effect of calendar and cycle aging in single factor A^{aging}. The SoH indicator is computed as follows:

$$SoH = 1 - A^{aging} \tag{4.30}$$

The maximum storable energy is then reduced by aging through SoH (i.e. capacity fade).

In [182], authors propose a semi empirical model adaptable to different Li-ion chemistries, useful to predict battery EoL in a wide operating range. They define a

degradation function f_d which is the sum of calendar and cycle aging:

$$f_d(t, SoC, T) = f_t(t, SoC, T) - \sum_i^N n_i f_c(DoD, \overline{SoC}, T) \qquad (4.31)$$

Cycle aging function f_c depends on stress factors which are DoD, average SoC and temperature, while calendar aging function f_t depends on time, SoC and T. As usual, a great number of parameters must be determined, making the model quite accurate in predicting the lifetime of lithium-ion batteries. The model has been proposed to evaluate battery capacity fading in the context of grid services such as frequency control in a regulation market.

Finally, one of the most accurate analytical model present in literature is the Weighted Ah aging model presented in [183]. Authors proposed a heuristic model to predict lifetime in applications with irregular operating conditions. Each *Ah* throughput of a battery is multiplied by a factor that represents the conditions to which the battery is subjected during cycling. The more severe operating conditions are, the higher the weighting factor is. Aging is found to depend mainly on DoD and current rate. Different from other empirical models, aging effects are taken into account starting from a physical analysis of the battery behaviour. The strong electrochemical background makes it quite accurate even though it remains easy to use. For this reason, the model is particularly suitable for sizing tools and system simulations.

Stochastic models

In Stochastic model, the aging process is written as a general expression by the combination of charge/discharge processes, SoC and SoH at the previous time-step with their transition probability. Markov chains are used to express the evolution of the batteries' health indicator SoH, similarly to SoC estimation described in the previous section.

In [184], a stochastic model is proposed for the optimal management of harvesting-based wireless sensors devices, accounting for battery lifetime while guaranteeing a minimum quality of service. The authors described the degradation process as a Markov chain. They define the battery health state $H(k)$ at time k, taking values from 0 to H_{max}. The maximum battery capacity at time k is:

$$C_{max}(k) = -\frac{H(k)}{H_{max}} C_{max} \qquad (4.32)$$

The health states are part of a Markov chain, where the transition probability from one state to another is independent on the history of the battery but depends on the current cycling condition (e.g the DoD or temperature). The authors extract the transition probabilities from the manufacturer's data. [184].

Electrical models

In this approach, aging modelling means to update the circuital parameters of a predefined electrical model (see section 4.2). Cells are typically subject to accelerated aging conditions (high temperature and cycling rate) and subjected to reference performance tests after determined time periods [178]. EIS studies are also used to detect the aging phenomena happening in the cell. Changes in the Nyquist diagram are used to understand which phenomenon can be linked to which section of the electrical model

[185], [186]. In general, circuital elements vary in agreement with the same stress factors described for analytical models. For this reason, aging trends of the model's parameters could be totally empirical or based on some physical considerations. Specifically:

- Capacity fade is usually referred to the changes in the discharge curves in active models, while at the variation of the intercalation capacitance over cycling in passive models [187], [188], [161].
- Power fade is related to an increase of the impedance of the cell. EIS evolutions in time is usually assessed. Depending on the reference electrical model, the equations are referred to single or several circuital elements.

In literature, different studies ([185], [189] [190]) evaluate the increase of the cell's internal resistance during lifetime. The underlying electrical models is the *R_{int} model* (Figure 4.6-a). Resistance measurements are done by EIS or by applying pulsed current of predefined length computing the ratio $\Delta V / \Delta I$. Impedance increase due to cycle aging and calendar aging can be studied separately or together. For instance, typical expressions for calendar aging are of the form [185]:

$$R(t, T, SoC) = (a_0 e^{a_1 T})(b_0 e^{b_1 SoC})t^{0.8} \tag{4.33}$$

In other works [191], [192], authors uses the *Thevenin* model (Figure 4.6-b) as reference to model degradation for NCA and NMC. In the first study [191], they focus on thermal aspects. Only R_p is assumed to change with time, while R_o and V_{oc} curve are assumed constant because claimed to be an intrinsic parameter of the cell which do not vary with temperature. In the second work instead [192], which is proposed to be used for dynamic simulation of EVs, they go more into detail by adding relation for capacity fading and R_o:

$$C(n) = C_0 + K_{C,N} n \tag{4.34}$$

$$R_o(n, SoC) = R_{0,0} + k_{R,n} n + k_{R,SoC} SoC \tag{4.35}$$

Where $k_{x,y}$ are coefficients that can be extracted from the manufacturer's datasheet or experimentally determined. Nominal capacity is used to estimate SoC and thus OCV through the Coulomb Counting method. Its value, together with resistance value, is updated during battery lifetime.

In [193], the authors studied degradation of NMC cells. With the help of EIS studies, they focus on the increase of impedance at a low frequency value f^* (0.1Hz), because they claimed it is the one mostly contributing to degradation. The real part of the impedance is described by empirical equation:

$$Re_{f^*} Z(t, T, SoC) = A(T, SoC)t^{0.5} + B(T, SoC)$$

$$A(T, SoC) = a_1 \cdot SoC + a_2 \cdot T + a_3 \cdot T \cdot SoC \tag{4.36}$$

$$B(T, SoC) = b_1 \cdot SoC + b_2 \cdot T + b_3 \cdot T \cdot SoC$$

In[194],the process of calendar aging is described to predict remaining life in EVs applications for Li/SOCl$_2$ batteries. The variation of all circuit elements depends on storage temperature, time and SoC (i.e. voltage). Aging assessment is done through EIS technique. It is assumed that all the parameters, Resistances, L and capacity, follow the same aging trends:

$$f_{cal}(t, T, V) = f_{cal}(t_0, T, V)[1 + B(T, V)F(t)] \qquad (4.37)$$

Where f_{cal} is used to update all the model's parameters on-line during simulation; B is the key factor used to find the best fitting trend for all circuital elements; $F(t)$ describes time dependence and it can have different shapes according to dominant aging process.

4.4 Summary

In this chapter, a comprehensive literature review on battery modelling (mainly at cell level) has been presented to create a framework of reference on which to base the modelling steps of part II of the thesis. The models have been grouped into four general approaches: electrochemical models, analytical (empirical) models, electrical models and stochastic models. Two main tasks have been identified for battery models: the estimation of the operating conditions (i.e. SoC estimation) and the estimation of the lifetime (i.e. SoH estimation). Each modelling family/category has been discussed in all its features by detailing literature examples, typical equations, methodologies, available software/tool. *Electrochemical models* have been found to be the most accurate since they account for the electrochemical processes behind battery operations; however, they are difficult to develop and they bring to a very high simulation time which make them unsuitable for techno/economic analyses but more suitable for material development purposes. *Stochastic models* describe battery operations by using transition probabilities between possible states. This approach can be particularly accurate in predicting end-of-discharge and end-of-life parameters in real-time applications; however, their usages must be carefully evaluated since they do not take into account the physical aspects behind battery operations. *Analytical models* have been described to be based on few equations which do not take into account electrochemical processes, but they are empirically fitted from experimental measurements. Due to their simplicity, they are well suited for techno/economic analyses and energy planning studies; several available tools have been found to rely on analytic models. Their simplicity comes however at the expenses of accuracy: the errors in predicting battery performance can be relatively high. Finally, *electrical models* have been presented as a last alternative to model electrochemical cells/batteries. They are based on equivalent electric circuits that aim at reproducing the responses at the external terminals. Electrical models have been detailed in all the possible configurations: active or passive, time-domain based or frequency-domain based. A different level of complexity can be found in literature that is generally proportional to the number of circuital elements used to build the model. They are found to be computational less expensive than electrochemical models but more accurate than analytical models. For this reason, they are well suited for a wide range of possible applications: from design/energy analyses to real-time monitoring.

Overall, this chapter has highlighted the necessity to implement and compare different BESS models in order to understand the accuracy in reproducing the expected behaviour and performances (by referring to the experimental data of Chapter 3) with respect to the required computational time. The objectives of the remaining parts of the thesis are: (part II) to develop a proper model for Li-ion BESS, (part II) to develop proper methodologies to evaluate the proper design of BESS in real applications). The first objective requires the identification of the best modelling approach that is worth investigating. Given the high flexibility (i.e. different level of details achievable) and the good compromise between simulation time and accuracy, an electrical model will emerge as the best choice both for dynamic modelling (investigated in Chapter 5 and Chapter 6) and lifetime (investigated in Chapter 7). The second objective will require complex techno-economic

analyses entailing long simulations. For this reason, electrical models will be compared with analytical models to assess the accuracy in evaluating BESS performances for two different real applications (Chapter 8 and Chapter 9) within a reasonable time.

Part II: A Novel Electrical Model for Lithium-Ion Cells

Part II offers the modelling framework about BESS and represents the main element of originality of the thesis. Starting from theoretical fundamentals that aim at bridging the gap between electricals and electrochemical models, a novel electrical model for lithium-ion cells based on experimental measurements is presented, discussed and validated. Lifetime modelling elements are also proposed to create a wider background useful for application-oriented analyses, techno-economic analyses and investment evaluations.

In Chapter 5, the main theoretical pillars which are necessary for a proper electrical modelling process are investigated. There must be a clear link in between the equations describing the electrochemical phenomena and the derived elements in the electrical model.

In Chapter 6, theoretical analyses of Chapter 5 are coupled with experimental measurements and applied to build a novel electrical model for Li-ion technology. In this way, all the electrical parameters depend on physical quantities, avoiding misleading interpretations of electrochemical phenomena. The model is composed of impedance blocks connected in series and accounts for the dynamic response of battery cells as a nonlinear function of state of charge (SoC). The model's parameters are determined by a specific procedure based on EIS and OCV measurements which is presented and applied to a commercial lithium-ion cell (lithium nickel oxide). The model is developed in the frequency domain and validated in the time domain to show the capability in estimating the voltage at the device terminals, efficiency, power and energy density under different operating rates and SoC.

In Chapter 7, lifetime modelling of Li-ion technology is investigated through experimental measurements. Testing results on Li-ion technology, which come from an innovative aging procedure, are presented and used to discuss about the main aging effects. Three lifetime modelling approaches are proposed which are linked to experimental measurements and characterized by a different degree of complexity in order to create a comprehensive electrical modelling approach.

Physics of battery for impedance based modelling

Chapter 4 offered a comprehensive review of battery modelling approaches. They differ for the degree of details used to reproduce the battery behaviour and for the elaboration/simulation time required to obtain the results. Electrochemical models and analytical models represent the extremes: the first is by far the most accurate since it includes the chemical equations that govern the battery functioning, while the second is the fastest and the most used in simulation programs.

Electrical models aim at providing a good compromise between electrochemical and analytical models. They aim at faithfully reproducing the dynamic behaviour while allowing reasonable simulation times. However, electrical modelling can be misleading unless interpreted with due caution. On one hand, substantial limitations may arise when electrical models are developed without considering the fundamental electrochemical processes. In this case, the accuracy might result limited to the condition for which the model was developed and the overall performance might not be so far from the ones achievable with analytical models. On the other hand, if a strong physical background is linked to the model elements (detailed experimental analyses are required) final performances might be very close to the ones achievable with electrochemical models.

Chapter 5 aims at bridging the gap between electricals and electrochemical models. The following sub-sections will present those theoretical fundamentals that are needed for a proper electrical modelling process. The description of these phenomena is used to derive the associated electrical representations in form of equivalent impedance circuits.

5.1 Underlying nexus for electrical modelling

As already introduced in Chapter 3 and Chapter 4, a battery is a complex non-linear dynamic system. The voltage at the battery terminals is non-linear with the current absorbed or delivered and it is mainly dependent on the current amplitude, temperature, SoC and SoH.

The physics of a battery system involves two main phenomena: charge transfer and transport of mass. Second-order effects are the double-layer effect and electric/magnetic effects. Different time constants characterize all these effects so that different dynamics
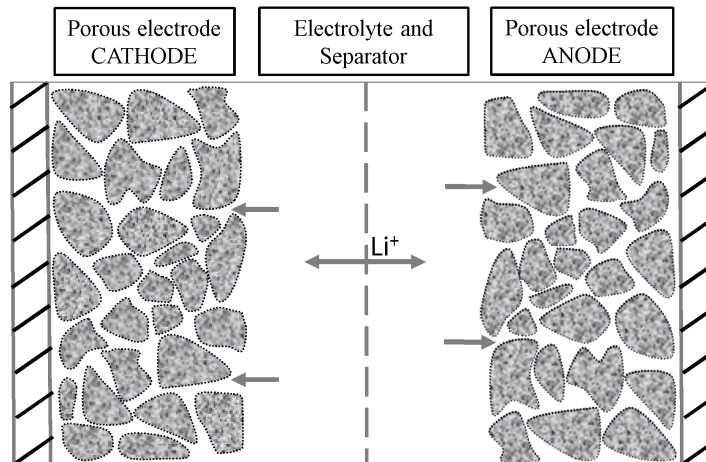
Figure 5.1 Schematic representation of the structure of an electrochemical cell.

describe the battery system during its operations.

Charge transfer considers the redox reactions occurring at the electrode/electrolyte interface. The oxidation number of the active materials involved in the reaction changes: electrons are released or consumed at both electrodes. The electrons are collected through the current collectors and the current flows externally to the battery. In parallel to the charge transfer effect is the double layer effect that takes into account the separation of charge carriers at the electrode/electrolyte interface [195]. When an electrode is immersed in the electrolyte, ions in the solution face the electrode surface at a distance of few nanometres. The result is a significant capacitive effect that takes place due to the large surface area of porous electrodes. The effect occurs at both electrodes, namely the double layer effect.

Reagents and products have to be continuously taken to and from the electrode/electrolyte interface in order to sustain the reaction (Figure 5.1). Different mechanisms of mass transport at distinct locations of the battery are involved, mainly inside the electrodes and in the electrolyte.

In the electrodes, the solid-state transport of charge carriers takes place [196]. The two main mechanisms of diffusion in a solid state material are the vacancy/defect-mediated mechanisms, and non-vacancy/non-defect-mediated mechanisms [197]. During the charge process of a lithium ion battery, for example, lithium ions at the cathode electrode have to cross through the crystalline structure before reaching the electrode/electrolyte interface where the redox reaction takes place. Diffusion of a Li-ion is strongly dependent upon the interaction potential between the Li-ion and the host material structure. Diffusion in solid state materials is strongly affected by temperature and follows an Arrhenius like relations.

In the electrolyte, ions have to cross all the electrolyte volume moving from cathode to anode during the charge process and vice versa during discharge. Diffusion in liquids is often hindered by solvated molecules and, compared to diffusion in solids, it is much less dependent on temperature [198]. Two are the forms of mass transport for charge carries in the electrolyte of electrochemical batteries: diffusion and migration. Diffusion occurs when charge carriers are subjected to a concentration gradient, while migration occurs per effect of an applied external field.

In absence of mass transport phenomena, the pure electric/magnetic effect is predominant. It takes into account the internal device resistance and inductance.

In order to quantify the rate of the different transport phenomena, the relationship

Table 5.1 Typical conductivity values for material used in electrochemical cells [199].

Material	Conductivity [S/cm]	
Cathode material	$10^{-10} - 10^{-1}$	
Anode material	$10^{-9} - 10^{2}$	Ionic conductivity
Solid electrolyte	$10^{-7} - 10^{-3}$	
Liquid electrolyte	$10^{0} - 10^{1}$	
Metal collector	$\sim 10^{5}$	Electronic conductivity

between the ionic conductivity and the diffusion coefficient has to be considered. This is done by the Nerst-Einstein equation:

$$\Lambda = c_i \cdot n_i^2 \cdot D_i \cdot \frac{F^2}{R \cdot T} \tag{5.1}$$

Where: Λ is ionic conductivity [S/cm]; c_i is the concentration of species i [mol/cm^3]; n_i charge number of ion I; D_i is the diffusion coefficient of ion i [cm^2/s]; F is the Faraday's constant [C/mol]; R is the gas constant [J/(K mol)]; T is the temperature [K].

Table 5.1 presents the ionic conductivity of different materials [199]. Cathode materials have the slowest diffusion coefficient that is at least one order of magnitude slower than liquid electrolyte materials. Electronic diffusion is much faster: three orders of magnitude greater in the worst case. In between anode and cathode, usually the cathode material is the one limiting the dynamics of the entire system[8]. From these data, it is possible to deduce the speed of the different dynamics involved in the battery operations. This creates a nexus between the electrochemical process and the electrical model building process.

During the cell operation, each phenomenon of above is reflected in an over voltage potential that can be measured at the battery terminals. A general formulation is:

$$\mathrm{E} = E_0 - [(\eta_{ct})_a + (\eta_{ct})_c] - [(\eta_c)_a + (\eta_c)_c] - R_i i \tag{5.2}$$

Where: E_0 is the standard potential of the cell at a specific temperature; $(\eta_{ct})_a$,$(\eta_{ct})_c$ are the over voltage at the anode and cathode respectively due to the charge transfer process and double layer effects; $(\eta_c)_a$,$(\eta_c)_c$ are the concentration polarization at the anode and cathode respectively due to mass transport mechanisms; R_i is the internal resistance of the cell equal to the sum of the collector, electrolyte and active mass resistance.

5.2 Electric and magnetic phenomena

Electric and magnetic phenomena consider the ohmic-inductive behaviour of a cell. The inductive behaviour is due to the motion in space of electrons in a three-dimensional space so that an equivalent internal inductance can be modelled. The total inductance of a cell is in the range of 10 to 100 nH/cell and it is negligible in the typical ranges of use of battery systems [198]. The resistance, in series to the inductance, is the total ohmic resistance of the collector, electrolyte and active mass.

The equivalent model is depicted in Figure 5.2.

---

[8] In term of correct BESS manufacturing, similar diffusion coefficients for the two electrodes are required in order to guarantee a symmetric operation of both electrodes.
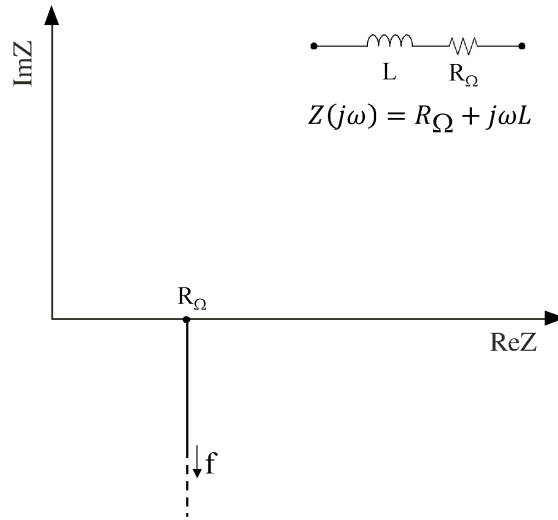
Figure 5.2 Equivalent impedance model for electric and magnetic phenomena

5.3 Electrode kinetics phenomena

The redox reaction, which involves the charge transfer between electrode and species in the electrolyte, can be written as:

$$Ox + ne^- \leftrightarrow Red \tag{5.3}$$

with O and R the oxidized and reduced species respectively and n the number of electrons e^- involved in the reaction. Oxidation and reduction, which take place at the electrode/electrolyte interfaces, generate the specific forward (i_f) and backforward (i_b) currents [A/m]. They can be defined as follows:

$$i_f = nFSk_f c_O \tag{5.4}$$

$$i_b = nFSk_b c_R \tag{5.5}$$

Where S is the equivalent reaction surface [m²], c_O and c_R are the concentrations of the oxidising and reducing species [mol/m³] and F is the Faraday constant. k_f and k_b are the forward and backforward rate constants [1/s], as per the Arrhenius law:

$$k_f = k_f^0 e^{-\alpha n \frac{F}{RT}\left(E-E^0\right)} \tag{5.6}$$

$$k_b = k_b^0 e^{(1-\alpha) n \frac{F}{RT}\left(E-E^0\right)} \tag{5.7}$$

Where, E^0 is the standard potential [V] of the redox process, k_i^0 are the rate constants at potential E^0, α the transfer coefficient, R the universal gas constant and T is the absolute temperature [K]. The transfer coefficient α determines what fraction of the electric energy, which results from the displacement of the potential from the equilibrium value,

affects the rate of electrochemical transformation.

At the equilibrium, the forward (i_f) and backward (i_b) are equal. At non-equilibrium, the faradaic current i (i.e. total current as per the redox reactions at the electrode surface) can be derived as follows [122]:

$$i = i_b - i_f = nFS\left(k_b c_R - k_f c_O\right) \tag{5.8}$$

In general, it is possible to express the current variation Δi as a function of the concentrations i of the species involved and of the variation of the electrode potential ΔE [122]:

$$\Delta i = \sum \left(\frac{\partial i}{\partial c_i}\right)\Delta c_i + \left(\frac{\partial i}{\partial E}\right)\Delta E + (higher\ order\ terms) \tag{5.9}$$

And, by neglecting the higher order terms, the impedance Z is derived as:

$$Z = {1} \Big/ {\frac{\partial i}{\partial E}} \left[1 - \sum \left(\frac{\partial i}{\partial c_i}\right)\frac{\{\Delta c_i\}}{\{\Delta i\}}\right] \tag{5.10}$$

This equation is made of two terms: the first one represents the charge transfer resistance; while the second one in square brackets contains the influence of diffusion effects in the electrolyte and electrodes. The time constant of diffusion effect is far greater than the one of electrode kinetics, thus the two effects can be studied separately. The value of the resistance R_{ct} can be obtained by deriving equation (5.10):

$$\frac{1}{R_{CT}} = \frac{\partial i}{\partial E} = \frac{n^2 F^2 S}{RT}\left(\alpha k_f c_O + (1 - \alpha)k_b c_R\right) \tag{5.11}$$

As mentioned before, in addition to the faradaic current i, there exists the non-faradaic current due to the double layer effect. Assuming that the faradaic current is decoupled from the non-faradaic one, the double layer effect can be taken into account with a capacitor element C_{DL} in parallel to the charge transfer resistance R_{CT}. Therefore, the whole kinetics effects at the single electrode can be represented by a parallel R_{CT} - C_{DL} circuit with time constant τ, as depicted in Figure 5.3

At very high dynamics the impedance associated to the capacitor tends to be a short circuit so that the total current of the battery is equal to the non-faradaic current. In other words, the current of the battery comes from the electrostatic charge stored in the double layer capacitor and not from the redox reaction. When the battery is subjected to a current step, the total current is equal to the faradaic current after a time greater than five times the time constant τ.

In the complex plane the impedance is represented by a semicircle of radius R_{CT}. At very high frequencies the impedance approaches the origin while at very low frequency it approaches the resistance value R_{CT}. The maximum amplitude of the imaginary parts is $R_{CT}/2$ and it happens for the frequency $f_0 \sim 1/(\tau)$.

5.4 Diffusion phenomena

Diffusion processes can be found at different locations in an electrochemical cell [200]:
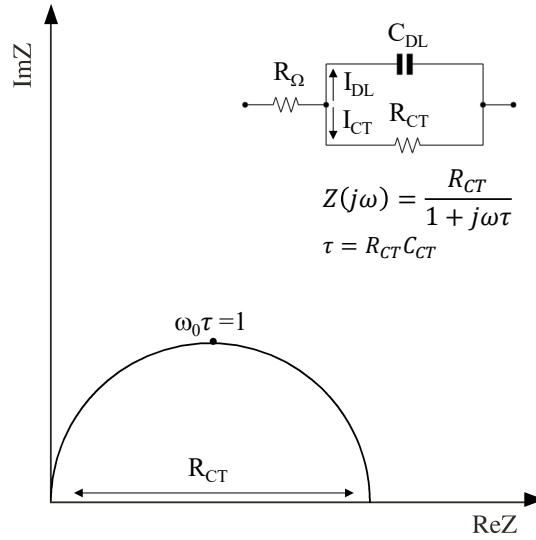
Figure 5.3 Equivalent impedance model for electrode kinetics phenomena

- In the free electrolyte between the two electrodes. The ions must migrate from the cathode to the anode and vice versa.
- In the electrolyte inside porous electrode. Since the geometry influences the boundary conditions, the diffusion process is influenced as well.
- In the active material inside the electrodes. Charge carriers fill and empty the crystalline structure at both electrodes during the charge and discharge processes.
- In the SEI (Solid Electrolyte Interface [201]) in case of lithium-ion batteries;

The Nerst-Planck equation describes in one dimension (x) three factors: the rate of accumulation of a species i in a given volume per effect of an electrostatic field E which is applied between electrodes, the change in the concentration gradient, and any other terms R_i that lead to the production or deletion of the species i, such as chemical reactions.

$$\frac{\partial c_i}{\partial t} = n_i F u_i \frac{\partial c_i}{\partial x} E + D_i \frac{\partial^2 c_i}{\partial x^2} + R_i \tag{5.12}$$

where u_i is the mobility of the species i. In absence of an electric field E and terms in R_i equations (5.12) reduces to Fick's second law [122]:

$$\frac{\partial c_i(x,t)}{\partial t} = D \ \frac{\partial^2 c_i(x,t)}{\partial x^2} \tag{5.13}$$

The temporal evolution of the concentration of the species i is the product of the diffusion coefficient D by the change in the concentration gradient over the x dimension, which is the distance of the electrolyte from the surface where the reaction takes place (x=0).

Solutions of the diffusion equation are required in the frequency domain. The Laplace transform of equation (5.13) is an ordinary differential equation:

$$s\{c_i\} - c_i(t=0) = D \frac{d^2\{c_i\}}{dx^2} \qquad s = j\omega \tag{5.14}$$

Where $\{c_i\}$ is the Laplace transform of c_i. General solutions of equation (5.14) are of

the form:

$$\{\Delta c\} = A e^{-\sqrt{\frac{j\omega}{D}}x} + B e^{\sqrt{\frac{j\omega}{D}}x} \tag{5.15}$$

With $\{\Delta c\}$ the Laplace transform of the excess concentration, $\Delta c = c(x,t) - c(x,0)$. From an impedance-perspective study, the interest is on the excess of concentration. Specifically, to identify the variation of the system response to external stimuli, that is the voltage variation Δv at the battery terminals due to the variation of the current variation Δi. In this way, it is possible to calculate the equivalent impedance.

The A and B coefficients are constants determined by the three following boundary conditions, with the hypothesis of one dimensional geometry [153] (Figure 5.4):

- Semi-infinite boundary condition which is the case for infinitely extended electrolyte $(x \rightarrow \infty)$.
- Finite-length boundary conditions which can be divided in [202], [203]:
  - Reflective boundary conditions: electrolyte with finite extension x=l and limited by a non-permeable wall at x = l (i.e. the impermeability of ions at the current collector of electrodes).
  - Transmissive boundary conditions: electrolyte with finite extension x=l and constant activity or concentration at x = 0. It is typical for the diffusion of charge carriers through a permeable membrane, (i.e. the ions that cross the separator moving from one electrode surface to the other).

Semi-infinite boundary condition

This is the case for $\Delta c \rightarrow 0$ as $x \rightarrow \infty$. From equation (5.15) it results B=0 and the solution is:

$$\{\Delta c\} = -\frac{1}{\sqrt{\frac{j\omega}{D}}} \frac{d\{\Delta c\}}{dx} \tag{5.16}$$

But the current variation $\{\Delta i\}$ is proportional to the concentration variation $\{\Delta c\}$:

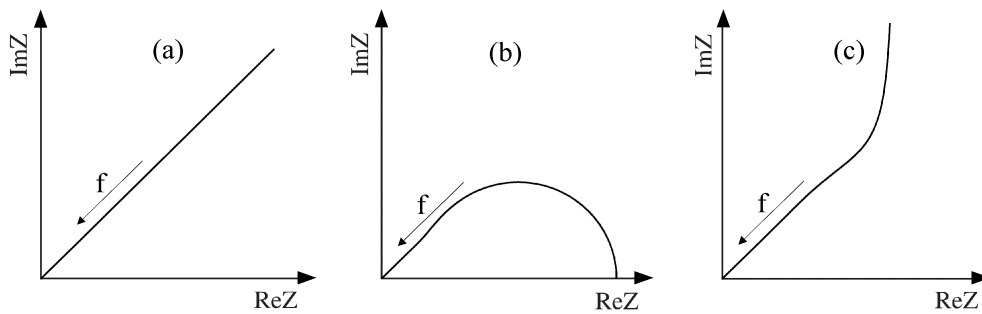$$\{\Delta i\} = -nFD \frac{d\{\Delta c\}}{dx} \tag{5.17}$$

Figure 5.4 Nyquist plot of the impedance describing the diffusion phenomena for three boundary conditions: a) Semi-infinite, b) Finite-length transmissive boundary, c) Finite-length reflective boundary

By assuming small perturbations around equilibrium, it is possible to write:

$$\frac{\{\Delta v\}}{\{\Delta c\}} = \frac{dE}{dc} \tag{5.18}$$

and to derive the equivalent impedance in the Laplace domain as [122]:

$$Z'(j\omega) = \frac{\{\Delta v\}}{\{\Delta i\}} = \frac{dE}{dc}\frac{1}{nF\sqrt{j\omega D}} \tag{5.19}$$

dE/dc represents the change in electrode potential with concentration in [V/mol/m^3]. The electrode surface S has to be introduced in the expression to derive the total impedance in [Ω]. For an ideal solution:

$$\frac{dE}{dc} = \frac{RT}{nFc} \tag{5.20}$$

The total impedance is:

$$Z(j\omega) = \frac{\sigma}{\sqrt{j\omega D}} \quad with \quad \sigma = \frac{RT}{cn^2F^2S} \tag{5.21}$$

The complex impedance is therefore inversely proportional to the square root of frequency. In the complex plane, it is a straight line inclined at $\pi/4$ to the real axis (Figure 4.3-a). From an electrical point of view.

Transmissive boundary condition

This represents a finite-length condition. It is assumed a constant activity or concentration at x = 0. In this case the impedance is [122]:

$$Z_{D,T}(j\omega) = \sigma\frac{\tanh\left(l\sqrt{\frac{j\omega}{D}}\right)}{\sqrt{j\omega D}} \tag{5.22}$$

The Nyquist plot of the impedance $Z_{D,T}$ is depicted on Figure 4.3-b. It approaches the one of infinite boundary conditions for high frequencies. It is possible to derive the following limiting factors $R_{D,T}$ and $C_{D,T}$ by studying the following limits[9]:

$$\lim_{\omega\to 0} Re\{Z_{D,T}(j\omega)\} = R_{D,T} = \sigma\frac{l}{D} \tag{5.23}$$

---

[9] The solution has been derived by using the following limits:

- $\lim_{\omega\to 0} Re\left\{\frac{\tanh(\sqrt{j\omega\theta})}{\sqrt{j\omega\theta}}\right\} = 1$
- $\lim_{\omega\to 0} -\frac{1}{\omega} Im\left\{\frac{\tanh(\sqrt{j\omega\theta})}{\sqrt{j\omega\theta}}\right\} = \frac{\theta}{3}$

$$\lim_{\omega \to 0} - \frac{Im\{Z_{D,T}(j\omega)\}}{\omega \cdot \left(Re\{Z_{D,T}(j\omega)\}\right)^2} = C_{D,T} = \frac{l}{3 \cdot \sigma} \tag{5.24}$$

By defining the time constant $\tau_{D,T}$, it is possible to write the reflective boundary impedance $Z_{D,T}(j\omega)$ as a function of its limiting factors:

$$\tau_{D,T} = R_{D,T} C_{D,T} = \frac{l^2}{3D} \tag{5.25}$$

$$Z_{D,T}(j\omega) = \frac{\tau_{D,T} \tanh\sqrt{3 \cdot j\omega\tau_{D,T}}}{C_{D,T}\sqrt{3 \cdot j\omega\tau_{D,T}}} \tag{5.26}$$

Note that the electric impedance measurable at the electric terminals is a function of the electrochemical parameters as well as the geometry of the diffusion process. By anti-transforming equation (5.26), it is possible to derive the expression of the reflective boundary impedance in the time domain [204].

$$Z_{D,T}(j\omega) = \frac{k_2}{\sqrt{i\omega}} \tanh\left(\frac{k_1}{k_2}\sqrt{i\omega}\right) \; \to Z_{D,T}(t) = \frac{2k_2^2}{k_1} \sum_{n=1}^{\infty} e^{-\frac{(2n-1)^2\pi^2 k_2^2}{4k_1^2}t} \tag{5.27}$$

By comparing equation (5.27) with equation (5.26) the coefficients k_1 and k_2 can be computed as follows:

$$k_1 = R_{D,T} \quad and \quad k_2 = \sqrt{\frac{R_{D,T}}{3 \cdot C_{D,T}}} \tag{5.28}$$

The impedance $Z_{d,t}(t)$ can then be written as:

$$Z_{D,T}(t) = \frac{2}{3 \cdot C_{D,T}} \sum_{n=1}^{\infty} e^{-\frac{(2n-1)^2\pi^2}{12R_{D,T}C_{D,T}}t} \tag{5.29}$$

The impedance $Z_{D,T}(t)$ can be represented with an electric circuit made by a serial connection of infinite parallel R_n, C_n elements, described by:

$$h(t) = \frac{1}{C_n} \sum_{n=1}^{\infty} e^{-\frac{1}{R_n C_n}t} \tag{5.30}$$

By comparing equation (5.30) with equation (5.29), it is possible to derive the values of each single resistor and capacitance of the series:

$$C_n = \frac{3 \cdot C_{D,T}}{2} \quad and \quad R_n = \frac{8R_{D,T}}{(2n-1)^2\pi^2} \tag{5.31}$$

The electric model representing the case of a diffusion with a finite length

Figure 5.5 Equivalent electric circuit representing the diffusion process with a finite length transmissive boundary condition

transmissive boundary condition is depicted in Figure 5.5.

Reflective boundary condition

This is a second finite-length condition for which it is valid that $dc/dx = 0$. Ho et al. [205] derived the impedance as follows:

$$Z_{D,T}(j\omega) = \sigma \frac{\coth\left(l\sqrt{\frac{j\omega}{D}}\right)}{\sqrt{j\omega D}} \tag{5.32}$$

The Nyquist plot of the impedance $Z_{D,R}$ is depicted on Figure 4.3-b. It approaches the one of an infinite boundary conditions for frequencies tending to infinite. By studying the limits [10], it is possible to derive the limiting factors $R_{D,R}$ and $C_{D,R}$:

$$\lim_{\omega \to 0} Re\{Z_{D,R}(\omega)\} = R_{D,R} = \sigma \frac{l}{3D} \tag{5.33}$$

$$\lim_{\omega \to 0} -\frac{1}{\omega \cdot Im\{Z_{D,R}(\omega)\}} = C_{d,r} = \frac{l}{\sigma} \tag{5.34}$$

By defining the time constant $\tau_{D,R}$, it is possible to write the reflective boundary impedance $Z_{D,R}(j\omega)$ as a function of its limiting factors:

---

[10] The solution has been derived by using the following limits:

- $\lim_{\omega \to 0} Re\left\{\frac{\coth(\sqrt{j\omega\theta})}{\sqrt{j\omega\theta}}\right\} = \frac{1}{3}$

- $\lim_{\omega \to 0} -\frac{1}{\omega \cdot Im\left\{\frac{\coth(\sqrt{j\omega\theta})}{\sqrt{j\omega\theta}}\right\}} = \theta$

$$\tau_{D,R} = \frac{l^2}{D} = 3R_{D,R}C_{D,R} \tag{5.35}$$

$$Z_{D,R}(j\omega) = \frac{\tau_{D,R}\coth\sqrt{j\omega\tau_{D,R}}}{C_{D,R}\sqrt{j\omega\tau_{D,R}}} \tag{5.36}$$

By anti-transforming equation (5.36), it is possible to derive the expression of the reflective boundary impedance in the time domain [204].

$$Z_{D,R}(j\omega) = \frac{k_2}{\sqrt{i\omega}}\coth\left(\frac{k_1}{k_2}\sqrt{i\omega}\right) \;\rightarrow\; Z_{D,R}(t) = \frac{k_2^2}{k_1} + \frac{2k_2^2}{k_1}\sum_{n=1}^{\infty} e^{-\frac{n^2\pi^2 k_2^2}{k_1^2}t} \tag{5.37}$$

By comparing equation (5.37) with equation (5.36) the coefficient k_1 and k_2 can be found as follows:

$$k_1 = 3R_{D,R} \quad and \quad k_2 = \sqrt{\frac{3R_{D,R}}{C_{D,R}}} \tag{5.38}$$

The impedance $Z_{d,r}(t)$ can then be written as:

$$Z_{D,R}(t) = \frac{1}{C_{D,R}} + \frac{2}{C_{D,R}}\sum_{n=1}^{\infty} e^{-\frac{n^2\pi^2}{3R_{D,R}C_{D,R}}t} \tag{5.39}$$

The second term in equation (5.38) can be represented with an electric circuit made by a serial connection of infinite parallel R_n, C_n elements, described by:
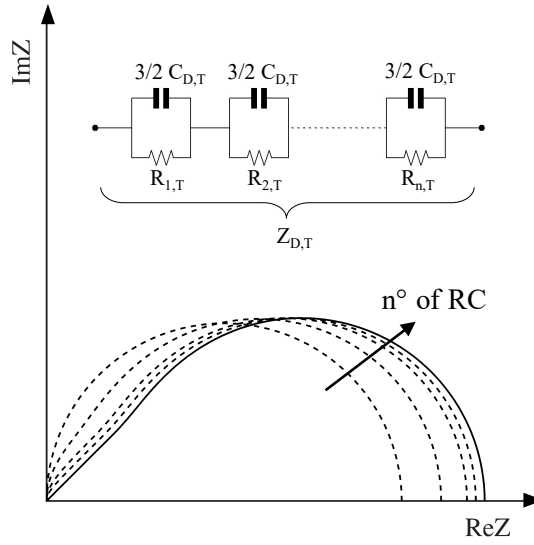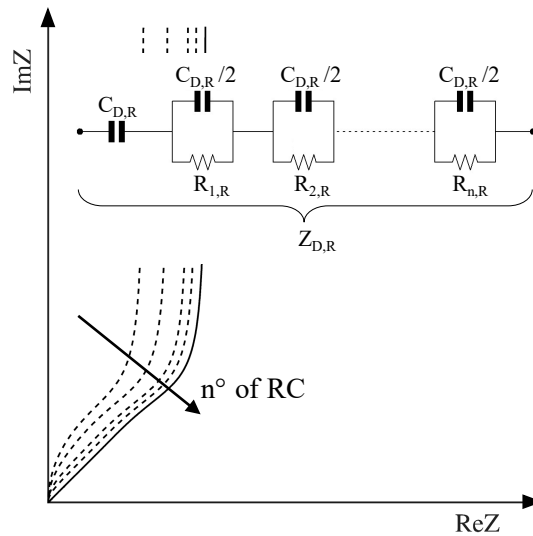

Figure 5.6 Equivalent electric circuit representing the diffusion process with a finite length reflective boundary condition

Table 5.2 Equivalent capacitance C$_{D,eq}$ as function of frequency.

Frequency	$C_{D,eq}$ / $C_{D,R}$
$1 / \tau_{D,R}$	0.95
$10 / \tau_{D,R}$	0.35
$100 / \tau_{D,R}$	0.11

$$h(t) = \frac{1}{C_n} \sum_{n=1}^{\infty} e^{-\frac{1}{R_n C_n} t} \tag{5.40}$$

Then, by comparing equation (5.39) with equation (5.39), it is possible to derive the values of each single resistor and capacitance of the series:

$$C_n = \frac{C_{D,R}}{2} \quad and \quad R_n = \frac{6 R_{\mathrm{D,R}}}{n^2 \pi^2} \tag{5.41}$$

The electric model representing the case of a diffusion with a finite length reflective boundary condition is depicted in Figure 5.6.

The capacitance element $C_{D,R}$ is the limit of the equivalent impedance for frequency tending to 0 as per equation (5.34). Equivalent circuit in Figure 5.6 shows that $C_{D,R}$ is a series element; thus, it does not change its voltage when no current is flowing. In other words, the amount of charge remains unchanged. From an electrochemical perspective, the capacitance $C_{D,R}$ is the parameter able to take into account the amount of charge stored in the active material, thus in the battery electrodes.

The time constant $\tau_{D,R}$ define the rate of the diffusion process with a reflective boundary condition. By considering the equivalent capacitance:

$$C_{D,eq} = -\frac{1}{\omega \cdot Im\{Z_{D,R}(\omega)\}} \tag{5.42}$$

$C_{D,eq}$ (jω) approaches the limiting capacitance $C_{D,R}$ for frequencies lower than the characteristic one of $1/\tau_{D,R}$ (Table 5.2). For instance, the equivalent capacitance reduces at 35% for frequencies one decade greater than the characteristic one. With reference to Figure 5.6, it means that the full charge stored in $C_{D,R}$ is fully accessible only for a frequency lower than $1/\tau_{D,R}$, while only a fraction is accessible at greater frequencies.

5.5 Summary

In this chapter, the main theoretical pillars which are necessary for a proper electrical modelling process have been provided. The underlying physics about electrochemical cells functioning have been covered in depth. The main phenomena have been identified (electric and magnetic phenomena, electrodes kinetics phenomena and diffusion phenomena) are discussed. Diffusion phenomena are discussed for three different boundary conditions: semi-infinite, transmissive and reflective. The main novelty is represented by the approach used to link electrochemical phenomena to the electrical modelling approach. The equivalent impedance representation is proposed for each phenomenon, which must be characterized by clear links in between the characterizing equations and the derived circuital elements in the electrical model.

CHAPTER 6

Novel electrical model for Lithium-ion cell

Chapter 5 provided the fundamentals which are necessary for a proper electrical modelling process. In this chapter, a novel lithium-ion cell model derived from such a theoretical framework is proposed. The novelty lies in the fact that each single block of the electrical model has a close link with a specific electrochemical phenomenon. The focus is on cell level rather than module for several reasons: (i) device response is only a function of electrochemistry, no influence from BMS; (ii) ease of access: electrochemical cells are small and easy to test; (iii) lower current and voltage that allow to test more devices in parallel, (iv) costs.

The modelling approach, which is based on the Electrochemical Impedance Spectroscopy (EIS) measurements (basics of EIS is detailed in Appendix C), is composed of the following steps (Figure 6.1):

- As a first step, it is necessary to define the specific electrochemical technology to be tested and modelled. Each chemistry has its own peculiarities: a model developed for the Li-ion chemistry could be inaccurate for the lead-acid chemistry and vice versa.
- The second step is represented by the interpretation of electrochemical phenomena as shown in Chapter 5.
- The third step is the definition of a suitable electric model which is able to describe typical EIS of the chosen technology. This step represents the core of the whole procedure. By linking any interpretation to the underneath theoretical framework, ambiguous circuits are avoided by default. For instance, the model cannot contain resistors, capacitances or inductance with negative values, which clearly have no meaning from the physical point of view.
- The fourth step is represented by measurement sets. In this case, the modelling is based on EIS measurements which investigate the impedance response for different battery SoC, SoH and temperatures in the frequency domain.
- The fifth step is the fitting process between the measurements and the proposed model in order to identify the model parameters, which must have a clear physical meaning.
- The sixth and last step is the model validation in the time domain. This is done by comparing the simulated and measured response (i.e. voltage at terminals) to injected or adsorbed current profiles.

```
┌─────────────────────────────────┐
│      Technological selection    │
│      (electrochemical cell)     │
└─────────────────────────────────┘
                 │
                 ▼
┌─────────────────────────────────┐
│    Electrochemical Phenomena    │
│          interpretation         │
└─────────────────────────────────┘
                 │
                 ▼
┌─────────────────────────────────┐
│  ELECTRICAL MODEL FORMULATION   │
│        (frequency domain)       │
└─────────────────────────────────┘
                 │
                 ▼
┌─────────────────────────────────┐
│        Experimental tests       │
│        (SoH, Temp, SoC)         │
└─────────────────────────────────┘
                 │
                 ▼
┌─────────────────────────────────┐
│   Model parameters identification│
│          (fitting process)      │
└─────────────────────────────────┘
                 │
                 ▼
┌─────────────────────────────────┐
│         Model validation        │
│          (time domain)          │
└─────────────────────────────────┘
```
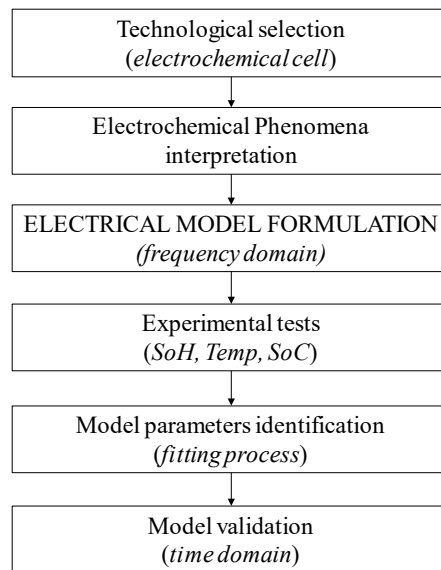
Figure 6.1 Modelling approach and validation

As anticipated, in the following sub-sections the modelling approach of Figure 6.1 is detailed and applied to build a novel model for Li-ion cells.

6.1 Electrical model formulation

In this section, we present and motivate the novel model that is applied for Li-ion technology. The Reference framework for the analyses is the one proposed in Chapter 5, while the physical interpretation is based on EIS measurements. By looking at the characteristic frequency ranges, it is in fact possible to discern between the different electrochemical phenomena. As presented in Table 5.1, different conductivities belong to the different cell materials and this fact has a close link with the impedance spectrum shape. For instance, diffusion phenomena inside the electrolyte have a diffusion rate one order of magnitude slower than those ones in the electrodes. Therefore, we expect to find characteristic regions in the impedance plot which reflect these differences.

Figure 6.2 shows a typical EIS for Li-ion cell. We can distinguish 4 different phenomena, that are interpreted as follows:

- Electromagnetic phenomena: they reflect the inductive and resistive behaviours of the battery at very high frequencies. The resistance R_Ω is the sum of the electrolyte, active mass of the electrodes, separator and current collector resistances. These phenomena occur for frequencies higher than kHz.
- Charge transfer and double layer phenomena: they take into account the kinetics of the redox reactions at the anode and cathode electrodes. These phenomena occur in the frequency range of tens of kHz down to hundreds of Hz.
- Diffusion in the electrolyte phenomena: they take into account the diffusion of ions in the electrolyte from the electrode/electrolyte interface towards the bulk of the electrolyte. These phenomena occur in the frequency range of tens of Hz down to hundreds of mHz.
- Diffusion in the electrodes phenomena: they describe the diffusion of charge carriers in the electrode structure. These phenomena take place at a very low frequency (from some hundreds of mHz to DC regime) where the impedance approaches a purely capacitive behaviour.
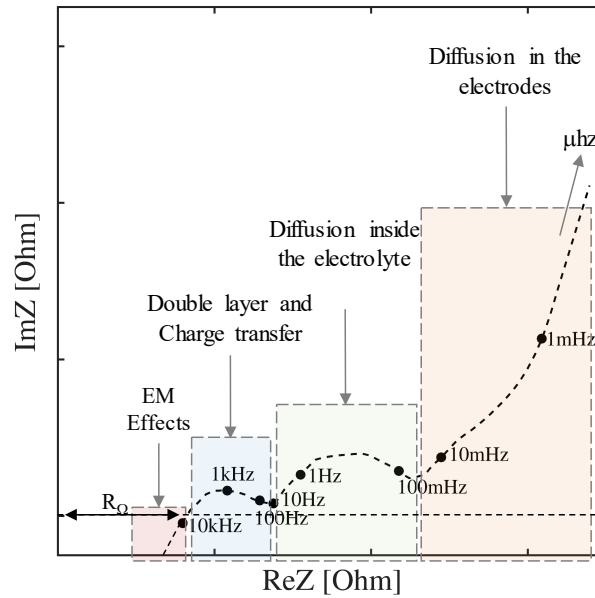
Figure 6.2 Typical impedance trend for a lithium ion battery at a specific temperature and SoC

The proposed electric model faithfully represents the electrochemical physics of Chapter 5 and Figure 6.2. It is valid in the frequency range from kHz to DC at a specific temperature, SoC and SoH. Since the time-constants of the characteristics phenomena are well separated, the model is based on series blocks, each one reproducing one specific dynamic. Figure 6.3 show the proposed electric model in its five blocks:

- The first block consists of a pure resistor that models the electromagnetic effects. The inductance is neglected because a battery is rarely used at very high frequencies in real applications (the battery will behave like a resistance with no capacity). Moreover, it is worth noting that the equivalent inductance of any external circuit, which normally surrounds a cell, is much higher than the equivalent internal one.
- The second and third blocks are two parallel *RC* branches that model the charge transfer and double layer capacitance at the two-electrode surface. The model requires two blocks because typically the equivalent impedance in this frequency range is not a perfect RC-type shape but resembles a depressed arc. This means that the rate of charge transfer processes is not the same at the two-electrode surface. This fact results in a superposition between the correspondent semi-circles [200].
- The fourth block models the diffusion of charge carriers from the electrode surface towards the bulk of the electrolyte and vice-versa. The equivalent circuit is the anti-transform of the $Z_{D,T}(j\omega)$ impedance. Simulation results show the series of infinite *RC* branches can be limited to five without affecting the accuracy of the model in the time domain.
- The fifth block models the diffusion of the charge carriers in the crystalline structure of active material. In this case the diffusion is of a reflective type due to impermeability of current collectors to the ions. It is represented by the anti-transform of the $Z_{D,R}(j\omega)$ impedance, and also in this case the number of parallel RC branches can be limited to five.

Overall, the model consists of nine independent parameters. Since EIS changes with respect to temperature and SoC, the nine parameters cannot be assumed constant. A set of EIS measurements is needed to map the impedance response at different operating conditions (e.g. at different battery temperature and SoC).
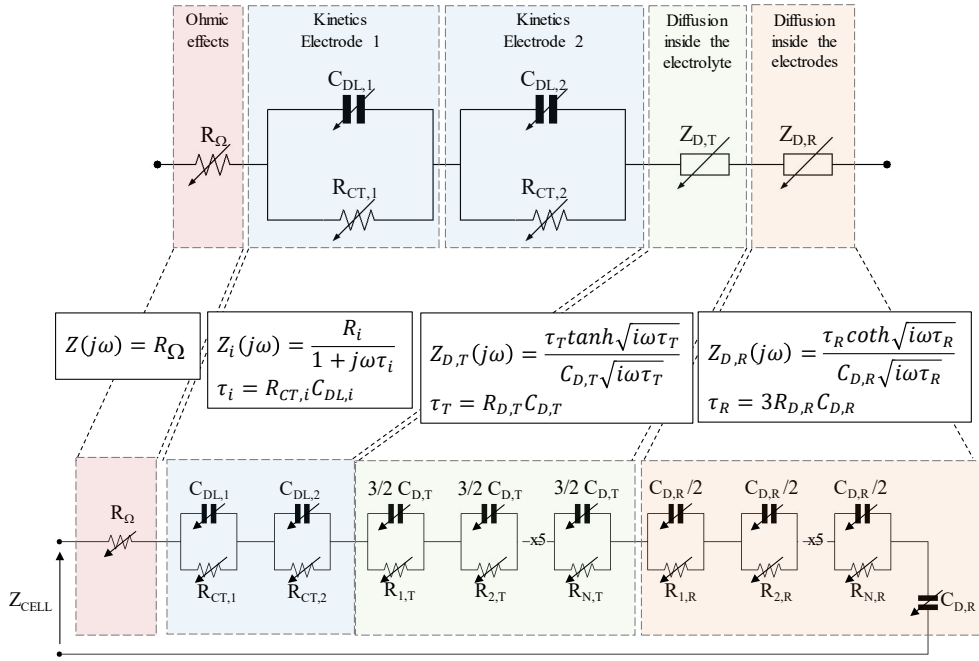
Figure 6.3 Proposed electric model for lithium-ion cells in the frequency-domain (top) and time-domain (bottom)

The model impedance in the frequency domain can be written as:

$$Z_{cell}(j\omega) = R_\Omega + \cfrac{1}{\cfrac{1}{R_{CT,1}} + j\omega C_{DL,1}} + \cfrac{1}{\cfrac{1}{R_{CT,2}} + j\omega C_{DL,2}} + \cfrac{R_{D,T}\tanh\sqrt{j\omega R_{D,T}C_{D,T}}}{\sqrt{j\omega R_{D,T}C_{D,T}}}$$
$$+ \cfrac{3R_{D,R}\coth\sqrt{j\omega 3R_{D,R}C_{D,R}}}{\sqrt{j\omega 3R_{D,R}C_{D,R}}}$$

(6.1)

The model does not contain any voltage generator to represent the open circuit voltage (OCV). Therefore, it belongs to the family of passive electric models (see section 4.2). The OCV of the device is taken into account by the parameter $C_{D,R}$. This parameter represents the equivalent capacitance per effect of the diffusion of charge carriers in the active material (reflective boundary type). This effect takes place at very low frequencies when ions intercalating in the electrodes face the impermeable current collector. The amount of energy stored in a battery cell is strictly related with the amount of available charge carriers in the electrodes. The equivalent capacitance measured at very low frequency takes into account this effect, thus the parameters $C_{D,R}$ represents the capacity in [F] of the battery and ultimately the parameter is used to update the SoC.

6.2 Measurements on Lithium-ion cells

In the following sections, we present the measurements performed on Li-ion technology. These sets of measurements are at the basis of the subsequent modelling phase. Specifically, they are of two types:

- GEIS measurements: that aim at fully dynamically representing cell behaviour (see Appendix C). This is done by performing: (i) time-consuming tests (namely LONG GEIS) that aim at fully characterizing the cell dynamics up to a very low frequency;

Table 6.1 Gamry Instruments© Reference 3000™ settings for long GEIS tests and fast GEIS tests

Reference 3000™ settings	LONG GEIS	SHORT GEIS
Number of samples	3	1
AC current (rms)	10 mA	10 mA
DC current	0 mA	0 A
Points per decade	5	5
Frequency range	10kHz – 10μHz	10kHz – 10mHz
SoC [%]	0 / 50 / 100	0 / 20 / 50 / 80 / 100
Ambient temperature [°C]	25	-20 / 0 / +25 / +45
Estimated test time	300 hours	0.3 hours

(ii) shorter tests (namely SHORT GEIS) that aim at differentiating the dynamic response at different SoCs and temperature conditions.

- OCV measurements: aim at identifying the OCV as function of the removed charge. OCV and SoC are closely related to each other: a value of SoC is given for a specific value of OCV and vice versa.

All the measurements have been run on a specific Li-ion cell: the BOSTON POWER SWING5300™ [107] (details about the cells in appendix E).

EIS measurements

EIS measurements have been performed with the Gamry Instruments© Reference 3000™ Potentiostat/Galvanostat/ZRA. LONG and SHORT GEIS tests measure the frequency response of the device respectively in the frequency range of 10^5 - 10^{-5} Hz and 10^5 - 10^{-2} Hz. While each LONG GEIS test is time consuming and lasts about 12 days, SHORT GEIS are faster (roughly 20 minutes) and therefore are repeated also at different ambient temperatures. The rms value of AC current has been chosen small enough to limit the cell SoC variation at a maximum 1% of the nominal capacity even in the worst-case scenario of the smallest frequency (10μHz).

The GEIS measurements have been performed at different levels of SoC. The SoC regulations have been done by first charging the cell as indicated by the manufacturer[11] so that the cell can be assumed to be at SoC 100%, then by discharging (CC mode) at specific C-rate (1/3C) for the time t_{SoC} as follows:

$$t_{SoC} = \frac{100 - SoC_i}{100} \frac{1}{C_{rate}}$$

(6.2)

Where SoC_i is the desired level of SoC at which to perform the GEIS measurements.

Long GEIS measurements

The experiments have been performed at standard ambient temperature of 25°C for three different levels of SoC. As mentioned in Table 6.1, a very low frequency range has been adopted aiming at fully characterizing the dynamic of the Li-ion cell under analysis.

---

[11] The charge phase is normally divided in two subsequent steps:
a) Constant Current (CC) phase in which the cell is charged by controlling the current flow until it reaches its maximum voltage limit.
b) Constant Voltage (CV) phase in which the cell is charged by controlling the voltage until the current decreases under a specific threshold (typically a percentage of the rated capacity).
In the case of the BOSTON POWER SWING5300™ cell, the manufacturer indicates to charge at 0.7C until the cell reaches 4.2V, then to keep the cell at 4.2V until the drained current is below 50mA [107].
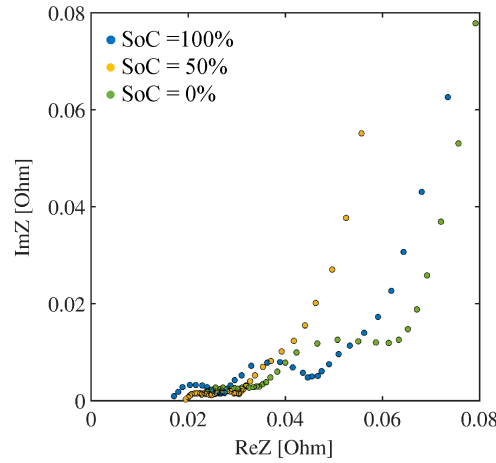
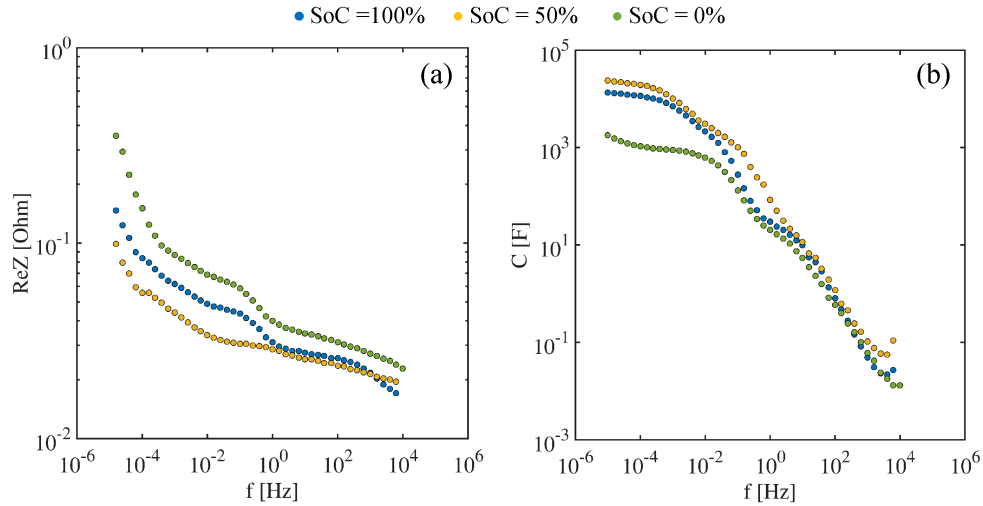Figure 6.4 Nyquist plot of 3 BOSTON POWER SWING5300™ cells for three levels of SoC (0%, 50%, 100%) at 25°C

Figure 6.5 Equivalent resistance (on the left) and capacitance (on the right) of 3 BOSTON POWER SWING5300™ cells for three levels of SoC (0%, 50%, 100%) at 25°C

The GEIS frequencies span from 10^5 to 10^{-5} Hz, theoretically embracing the whole dynamic response, from purely ohmic phenomena until the intercalation effects of charge carriers in the electrodes.

Given the very long time required to perform a single GEIS measurement (almost 12 days), three BOSTON POWER SWING5300™ cells have been tested in parallel at the different SoC levels[12]. It cannot be guaranteed the three cells are identical due to the dispersion in the cells manufacturing process: Therefore, some biases are surely introduced in the measurements. However, given our data, the cell capacity dispersion is negligible since the standard deviation is of about 0.2% of the nominal capacity.

The Nyquist plot of the selected cells is depicted on Figure 6.4. The shape of the GEIS measurements is preserved in the three experimental tests. We can distinguish the presence of three characteristic trends: (i) a first semi-circle at high frequency that appear

---

[12] The measurements have been carried out exploiting the stack mode cell connection of the Gamry Instruments© Reference 3000™ that allows to measure the impedance of different cells series connected up to 30V.

to be slightly depressed; (ii) a second semi-circle at medium frequency; (iii) a vertical slope for a very low frequency. Semicircles are more depressed at the SoC of 50%.

The Bode plot of Figure 6.5 unveils more information. Figure 6.5-A and Figure 6.5-B show that both resistance and capacitance follow a ladder-like shape with a decrease of frequency. This confirms that the dynamic response turns at some characteristic frequencies, allowing to infer that different electrochemical phenomena are behind these sudden changes. Moreover, we can highlight that:

- The relationships between both resistance and capacitance with frequency depend on the specific SoC at which the EIS is taken.
- The ohmic resistance increases with the decrease of the SoC.
- The final plateau in the equivalent capacitance suggests that the full capacity of the cell can be derived from measurements at a very low frequency, where the cell can be modelled as a capacitor (SoC dependent).

SHORT EIS measurements

The second set of EIS experiments have been performed at four different ambient temperatures for five different levels of SoC (Table 6.1). A narrower frequency range (from 10^5 to 10^{-2} Hz) has been adopted in order to appreciate (in a reasonable amount of
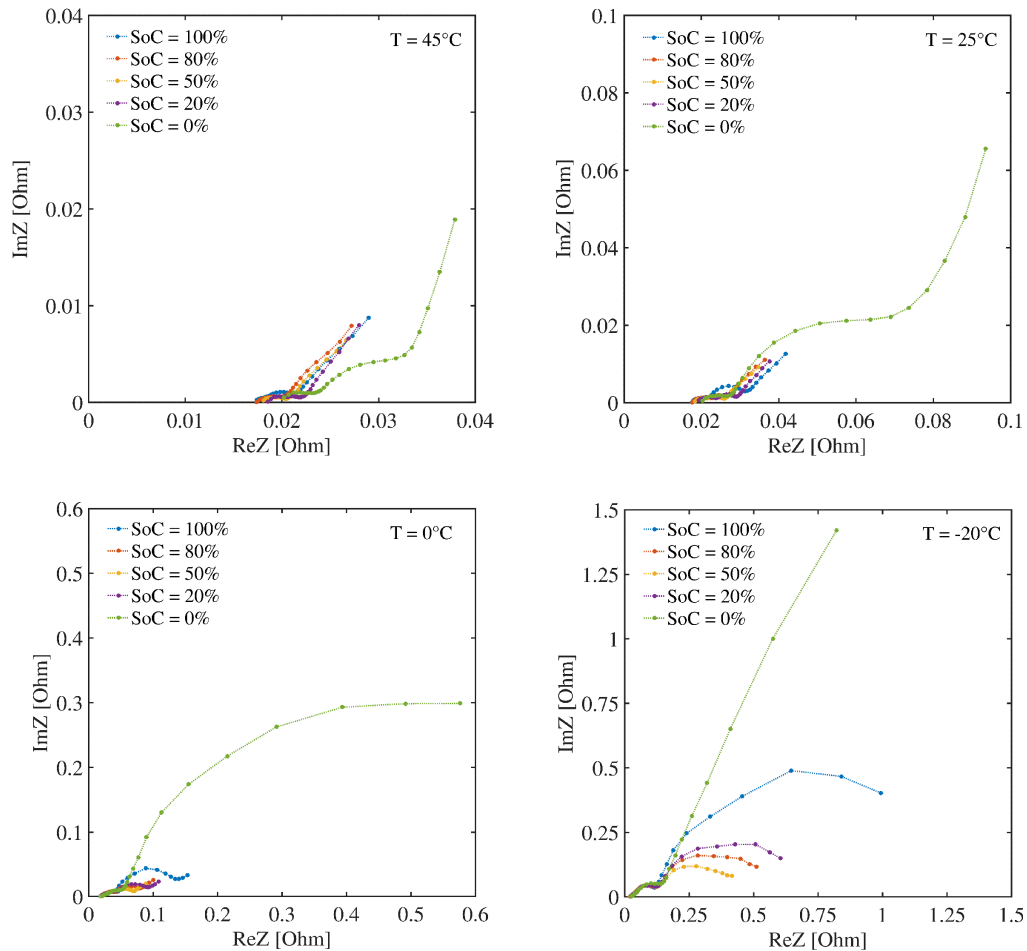

Figure 6.6 Nyquist plot of BOSTON POWER SWING5300™ cell at different ambient temperatures for five levels of SoC

time) the variation in the cell behaviour with respect to different external conditions. In this case, the measurements have been repeated on the same cell to avoid any biases.

The Nyquist plots of Figure 6.6 show that the typical shape of the diagram is preserved even at a different ambient temperature: the semicircle-like shapes in the middle-high frequency range are always present. Deviations emerge with respect to the magnitude of the impedance that heavily decreases with the temperature. At the lowest frequency (10 mHz), the resistance and capacitance respectively increases and decreases at about the same ratio (15-35 times) when the temperature moves from 45°C to -20°C.

By lowering the temperature, the same electrochemical process takes place at a lower frequency. At 45°C and 25°C, the investigated frequency range is sufficient to depict the entire first two semicircles followed by the beginning of the vertical slope (as already discussed in Figure 6.4). When lowering the temperature, only a part of the dynamic cell response is represented in the same frequency range. For instance, the second semi-circle bagan at just -20°C for frequencies around 10 mHz, while the same semicircles were more than over at 25°C. This fact can be easily explained considering the influence of temperature on the diffusive processes of charge carriers: lowering the temperature means to decrease the ions mobility in accordance with the Arrhenius law. The resulting dynamic response of the cell is reduced as a consequence.

Open Circuit Voltage (OCV) measurements

The OCV voltage measurements aim at identifying the OCV as a function of the removed charge. OCV tests have been performed by discharging the cell at a very low current rate of C/100 (53 mA). The results of Figure 6.7 show the high non-linearity trend of the OCV curve for the tested cell.

When performing an OCV test, a very long time (one hundred hours) is required to fully discharge or charge the cell. This means that a powerful analogy exists between the LONG EIS measurements and the OCV test. The explanation of this correspondence lies in the analysis of the dynamic of the OCV measurement:

- LONG EIS measurements are performed with very small AC current to avoid change in the SoC. Measurements are done at a constant OCV that is preserved at all frequencies.
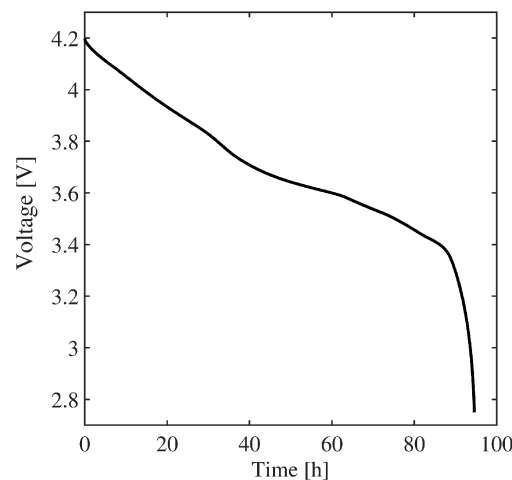- During the OCV test the current is small enough to impact negligibly on the voltage.

Figure 6.7 Voltage of the BOSTON POWER SWING5300™ cell when discharged at a current rate of C/100 at 25°C

The measured terminal voltage can be assumed equal to the OCV. Considering the typical values for the cell resistance, the voltage drop is less than 0.1% of the nominal cell voltage.

▪ The OCV test imposes a square current profile that has a fundamental at 1.38 µHz. The fundamental as well as the meaningful harmonics are all in the region of very low frequencies where the phenomena of diffusion in electrodes take place. Such a value of frequency belongs to the region of very low frequencies explored also by the LONG EIS measurements.

Given these findings, we expect that the capacitance $C_{D,R}$, which is identified at very low frequencies by using LONG EIS measurement, can be assumed equal to the capacitance $C_{D,R}$ *(OCV)* computed from an OCV measurements. This fact can be explained by the equivalent circuit of Figure 6.3. At very low frequencies, the capacitances of all the parallel *RC* branches are open circuits and all the current moves through the resistances. At low dynamic, the OCV measurement is then equal to the voltage across the capacitance $C_{D,R}$.

6.3 Parameters identification procedure

The model parameters are identified thanks to the EIS and OCV measurements. SHORT EIS have been used to identify all the model parameters with the exception of the diffusive capacitance $C_{D,R}$ which has been identified by means of the OCV measurements.

EISs have been fitted with the model in equation (6.1). We exploited the *fminsearch* algorithm in MATLAB® to minimize the difference between the model impedance Z and the measured one. At each iteration, the algorithm searches for the best set of parameters which minimize the errors defined as follows:

$$err = \sum_{i=f_{max}}^{f_{min}} \sqrt{Re\left(Z_{meas,i} - Z_{mod,i}\right)^2 + Im\left(Z_{meas,i} - Z_{mod,i}\right)^2} \qquad (6.3)$$

The procedure has been applied on the 5 SHORT EIS of BOSTON POWER SWING5300™ cell at 5 different levels of SoC (at the ambient temperature of 25°C). Figure 6.8 and Figure 6.9 show the results of the fitting process. The model is able to faithfully represent the measurements in all the tested conditions with minimum deviation (R^2 always above 99%). Some deviations are registered only at a very low level of SoC, especially in the resistance estimation.

The fitting process returns the model parameters which have validity in the domain expressed by the EIS measurements. Table 6.2 shows the parameters values for the 5 different SoCs which correspond to a specific OCV value. The resistance parameters increase with the decrease of the SoC, this highlights that low levels of SoC have a bad influence on the cell performance. Conversely, no common trend can be inferred about the capacitance: double layer capacitances decrease with the SoC, while diffusive capacitance $C_{D,T}$ presents a minimum for average levels of SoC.

In Figure 6.10 the trends of parameters within the entire OCV range (i.e. SoC range) are presented. By performing a second fitting process, namely "over-fitting", it is possible to define the correspondent interpolating functions which are in the form:

$$y = a_0 + a_1 x + a_2 x^2 \qquad (6.4)$$
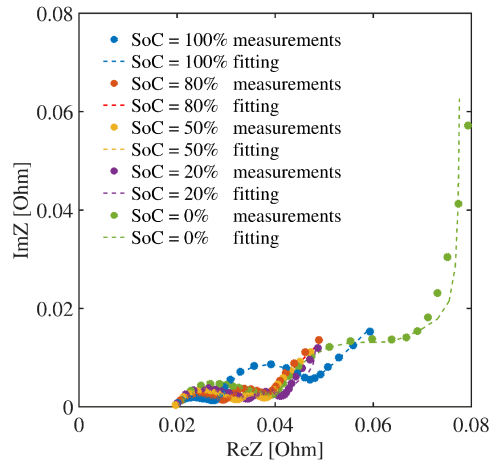
Figure 6.8 Nyquist plot comparing the EIS measures with the model fitted data for the BOSTON POWER SWING5300™ cell at different SoCs
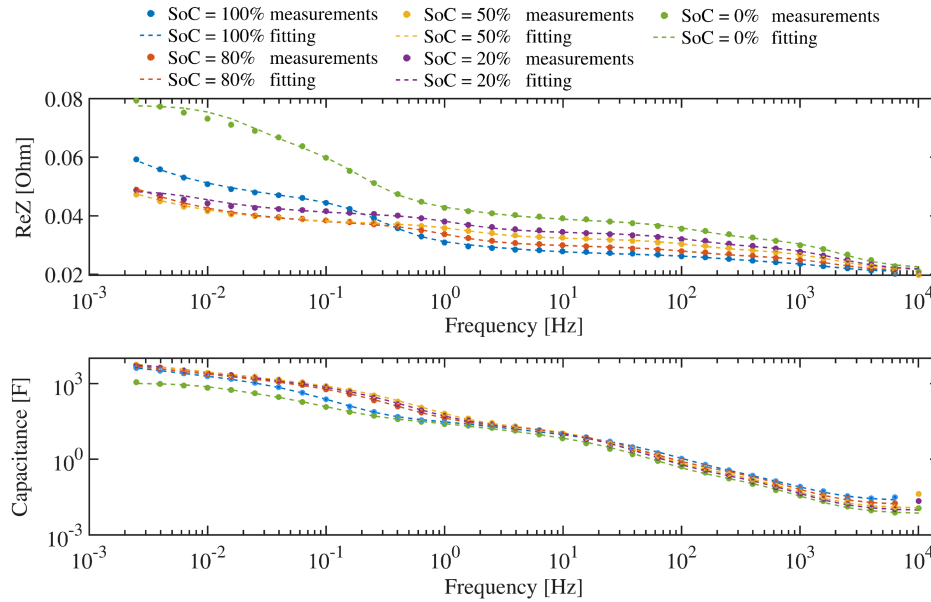
Figure 6.9 Bode plot comparing the EIS measures with the model fitted data for the BOSTON POWER SWING5300™ cell at different SoCs

Table 6.2 Model parameters identified by fitting the SHORT EIS measurements of BOSTON POWER SWING5300™ cell at different SoCs

Parameter	SoC = 100%	SoC = 80%	SoC = 50%	SoC = 20%	SoC = 0%
OCV [V]	4.1744	3.9595	3.6675	3.5226	3.0934
R_Ω [Ω]	0.0207	0.0209	0.0213	0.0215	0.0221
$R_{CT,1}$ [Ω]	0.0034	0.0049	0.0065	0.0077	0.0097
$C_{DL,1}$ [F]	0.0264	0.0168	0.0121	0.0098	0.0075
$R_{CT,2}$ [Ω]	0.0020	0.0026	0.0034	0.0040	0.0052
$C_{DL,2}$ [F]	0.3766	0.4631	0.3437	0.2814	0.2118
$R_{D,T}$ [Ω]	0.0173	0.0074	0.0052	0.0062	0.0186
$C_{D,T}$ [F]	25.1545	17.1120	15.3869	16.1848	33.5702
$R_{D,R}$ [Ω]	0.0079	0.0076	0.0161	0.0245	0.0641
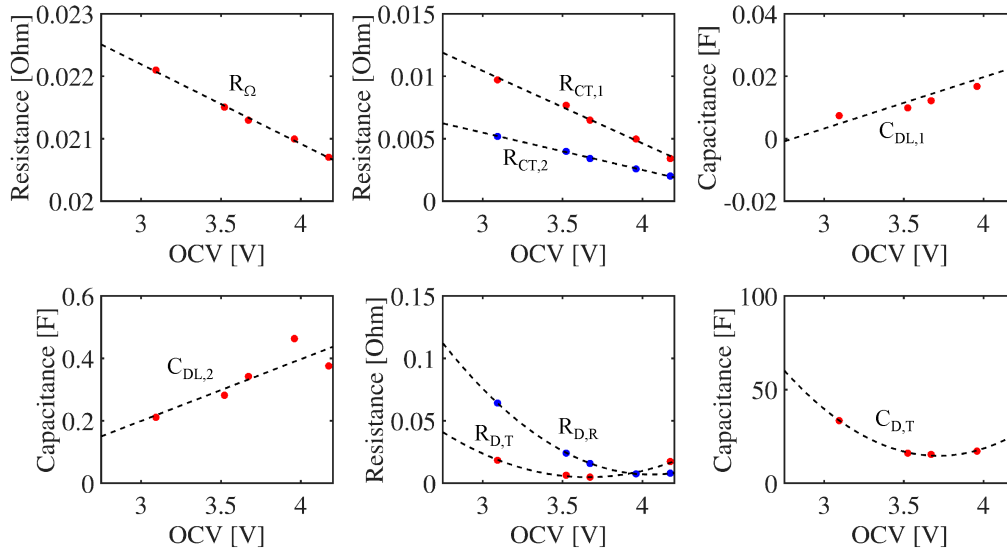
Figure 6.10 Model parameters as a function of the OCV for the BOSTON POWER SWING5300™ cell. The dotted pattern is the trend line as per linear or quadratic approximation

Where a_0, a_1 and a_2 are defined in Table 6.3 for each specific parameter. The derived functions are then used in the model to describe the parameters in all the possible SoC conditions.

As mentioned before, the only parameter that is defined separately is the $C_{D,R}$. This capacitance is derived by differentiating the entire OCV curve obtaining the so-called intercalation capacitance (IC) [150], [151]:

$$C_{D,R}(OCV) = \frac{dQ}{dV} \tag{6.5}$$

Figure 6.11-a shows the trend of the IC. Each peak corresponds to a quasi-horizontal region of the OCV curve of Figure 6.7. In these regions, for the same imposed charge $Q=I \cdot dt$, the cell shows smaller changes in the OCV (i.e. SoC) that is a greater IC [F].

Given the high non-linearity of the parameter $C_{D,R}$, an interpolating function (like for the other parameters) might not be representative of the real OCV behaviour. For this reason, the full mapping of the IC curve is required in the model. This is the reason why IC curve is done through the OCV measurement of section 6.2 rather than the LONG EIS measurements. Unlike LONG EIS measurements, which last about 12 days to measure the impedance of a single OCV (SoC) value, the OCV measurements take about 8 days

Table 6.3 Model parameters identified by fitting the SHORT EIS measures of the BOSTON POWER SWING5300™ cell at different SoCs

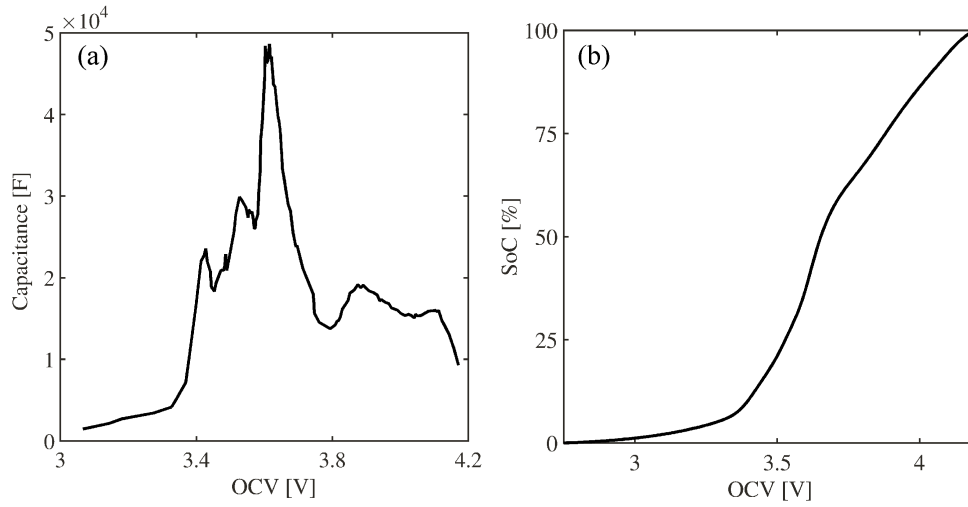| Parameter	fitting	a_0	a_1	a_2
R_Ω	Linear	0.0260	-0.0013	0
$R_{CT,1}$	Linear	0.0279	-0.0058	0
$C_{DL,1}$	Linear	-0.0461	0.0165	0
$R_{CT,1}$	Linear	0.0145	-0.0030	0
$C_{DL,1}$	Linear	-0.3939	0.1980	0
$R_{D,T}$	Quadratic	0.5915	-0.3207	0.0438
$C_{D,T}$	Quadratic	688.7170	-362.8400	48.8301
$R_{D,R}$	Quadratic	1.0254	-0.5025	0.0620

Figure 6.11 (a) Intercalation capacitance $C_{D,R}$ (OCV), (b) OCV-SoC relationship for BOSTON POWER SWING5300™ cell

Table 6.4 Model parameters identified by fitting the SHORT EIS measures of the BOSTON POWER SWING5300™ cell at different levels of SoC

Parameter	SoC = 100% (OCV = 4.151 V)	SoC = 50% (OCV = 3.655 V)	SoC = 0% (OCV = 3.036 V)
$C_{D,R}$ (long GEIS)	13.08 kF	23.13 kF	0.95 kF
$C_{D,R}$ (OCV)	12.03 kF	35.15 kF	1.46 kF

to measure the full response at a very low frequency but spanning all the ranges of SoC between 100% and 0%, thus with relevant benefits in terms of time.

The correspondence in between the parameters $C_{D,R}$ *(OCV)* and $C_{D,R}$ obtained respectively through the LONG EIS and OCV measurements have been experimentally verified. Table 6.4 shows a good match: the capacitance is lower at the cell limits while higher at medium levels of SoC. The differences can be explained by two main reasons: (i) non-uniformity in the tested cells: LONG EIS measurements are based in three different cells, while for the OCV measurements a fourth cell was used; (ii) non-uniformity in test conditions: in the LONG EIS test the minimum frequency was around 10 µHz while the fundamental frequency of the OCV test is 1.38 µHz. Figure 6.5 shows that the equivalent capacitance is going to rise up by lowering the frequency beyond the µHz region. This explains the higher values of the capacitance $C_{D,R}$ estimated by the OCV measurements for SoC levels of 0% and 50%.

SoC evaluation

Given the passive nature of the proposed electric model, the SoC is not represented by an external voltage source but by the parameters inside the model itself. Since OCV is the electrical quantity that represents the SoC, the model should be able to account for the OCV. During the OCV measurements, that is for very low frequencies and current, the capacitances of all the parallel *RC* branches of the electrical model (Figure 6.3) are open circuits and all the current flows through the series resistances. Therefore, the OCV is equal to the voltage across the capacitance $C_{D,R}$ .It is then possible to find the relationship between OCV-SoC directly from the OCV curve (Figure 6.7) as presented in Figure 6.11-b. This relationship is used in the model (i.e. simulations) to directly derive the SoC from the OCV estimation.

6.4 Validation

The model has been built in the frequency domain. However, its accuracy has to be verified in the time domain. Two are the peculiarities of the model:

- the ability in reproducing the full impedance in the frequency range from tens of μHz up to 10kHz. In the time domain, we expect the ability in simulating the battery terminal voltage for all possible solicitations: from very slow constant charge/discharge profiles up to highly pulsing profiles.
- the ability in estimating the OCV and in reproducing the SoC of the cell. The $C_{D,R}$ is the element devoted to account for the SoC (no voltage generator is present in the model). In the time domain, we need to exclude the presence of any drifting effect in the SoC estimation. Voltage drift is a common problem of battery models when subjected to consecutive charge/discharge cycles.

The validation has been done on two levels: (i) validation in the time-domain in which we compare measured voltage responses per effect of different current/power profiles with the simulated ones; (ii) validation of the performances in which we verified the ability of the model in estimating the performance of the cell in terms of energy density, power density and efficiency.

Validation in the time-domain

Four different tests have been performed to validate the model in the time domain and its ability in simulating the voltage at the cell terminals:
1. Square current profile tests: to verify model accuracy in reproducing the solicitations deriving from fast square current profile (30 secs steps) and slow square current profile (5 mins steps) at different C-rates.
2. Constant current tests: to verify the model accuracy at constant current for full charge-discharge cycles at different C-rates.
3. Arbitrary profile test: to test the model accuracy with an arbitrary current profile, that is for test conditions closer to final application.

The accuracy of the model is evaluated by means of the RMSE indicator:

$$RMSE = \sqrt{\frac{\int_0^T \left(X_{measurements}(t) - X_{model}(t)\right)^2}{T}} \qquad (6.6)$$

Where X is the terminal voltage.

Square current profile tests

In this section, we validate the model for two different square current profiles: fast and slow. The main cycle foresees charge and discharge steps (separated by a resting period) at different current rates (0.1C, 0.5C, 1C, 2C, 3C and 4C). Charge/discharge steps last 30s in the fast case, 5 minutes in the slow case.

The current profile has an average value which equals to zero so that the average cell SoC does not change (by neglecting losses). The tests are performed at a different level of initial SoC. The accuracy of the model is then evaluated by spanning different current rates.

The results of the fast square current profile tests are shown on Figure 6.12 at five levels of SoC (100%, 80%, 50%, 20% and 0%). Accuracy is greater when SoC is in between 20% and 100% with RMSE value always below 10mV (less than 0.3% of the nominal voltage). Errors are notable especially during the charging phases at high

Figure 6.12 Simulated and measured voltage of the BOSTON POWER SWING5300™ cell when cycled with the fast square current profile. Four current steps (0.1C, 0.5C, 1C and 2C) of 30s charge and discharge spaced with a 30 s rest period for different SoC (100%, 80%, 50%, 20% and 0%)

currents (note that manufacturer instructs to charge at 0.7C [108]). At very low SoC (i.e. 0%) the RMSE value increases up to 75 mV (2%). This is due to additional non-linearities that are currently not taken into account by the model.

The results of the slow square current profile tests are shown on Figure 6.13 at three levels of SoC (80%, 50% and 20%). The average error in the three tests is 26mV (0.7%). Higher errors are confirmed when the cell attains the SoC limits of 100% and 0%.

Constant current tests

In this case we perform multiple full charge/discharge cycles at difference C-rates (0.1C, 0.5C, 1C and 2C), in between the operating limits of the cell. Again, Figure 6.14 shows that the model presents remarkable deviations for low levels of SoC (SoC < 5%). Globally, the RMSE value is lower than 50mV (less than 1.4%) over a period of 24hrs
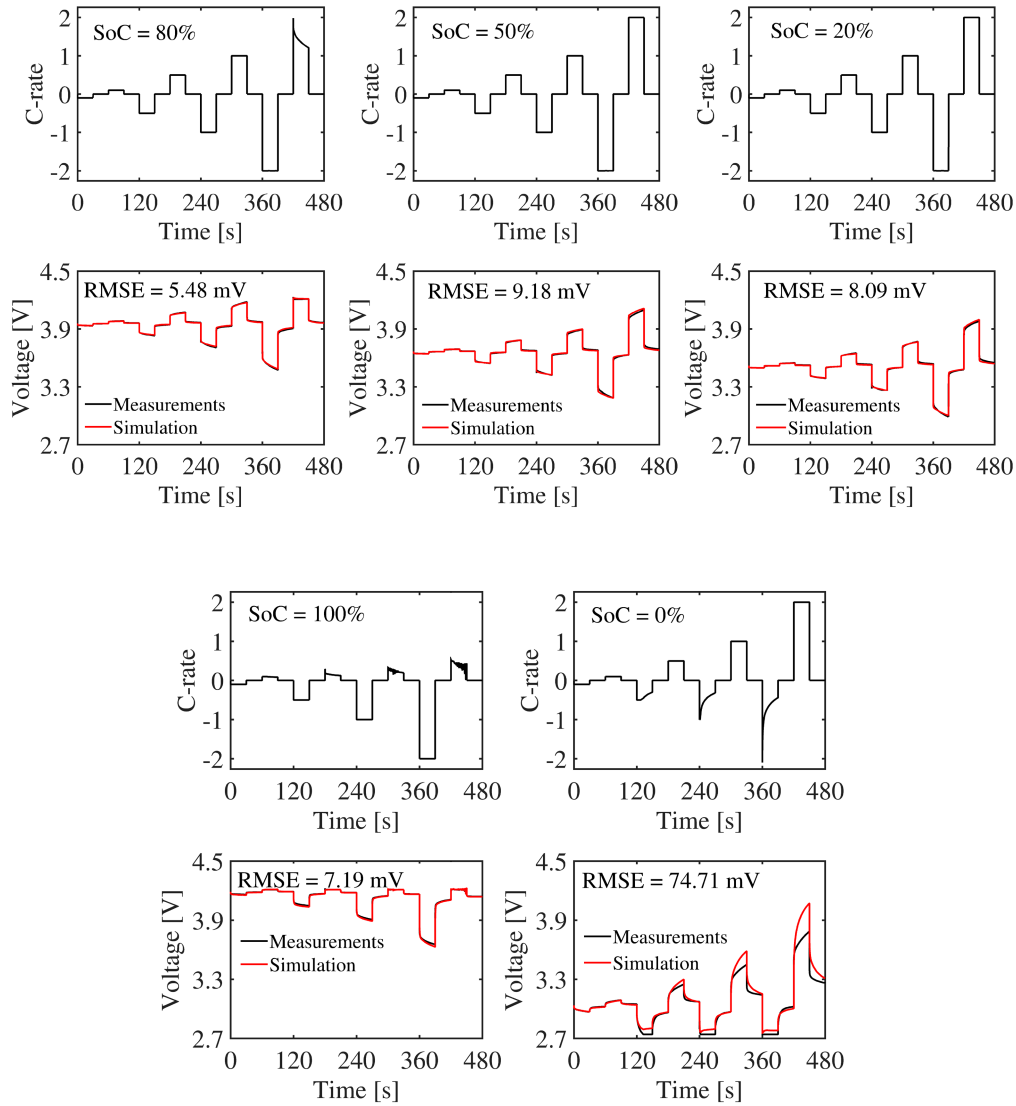
Figure 6.13 Simulated and measured voltage of the BOSTON POWER SWING5300™ cell when cycled with the slow square current profile. Four current steps (0.1C, 0.5C, 1C and 2C) of 5min charge and discharge spaced with a 5 min rest period for different SoC (100%, 80%, 50%, 20% and 0%)

test. Moreover, no drifts of the simulated voltage are registered: the model is able to follow the SoC trend without accumulating errors.

Arbitrary profile test

Finally, we validate the model considering an arbitrary current profile from real application. Specifically, the test emulates the typical stochastic current profile derived from the grid application of PCR already presented in Section 3.5. The battery is charged/discharged according to a specific control law proportional to the deviation of the grid frequency from the nominal value. Since frequency deviations are stochastic, the current profile applied to the BESS in operations can be extremely variable.
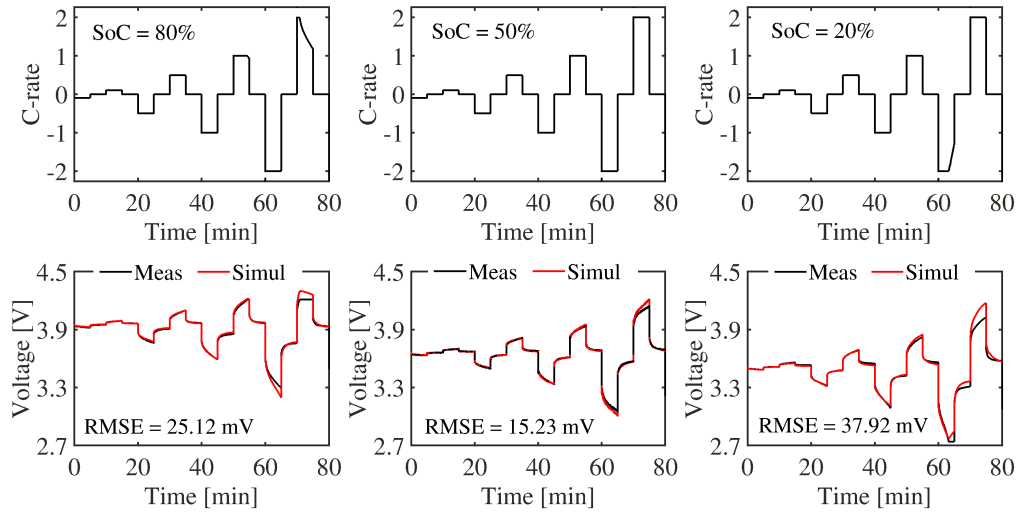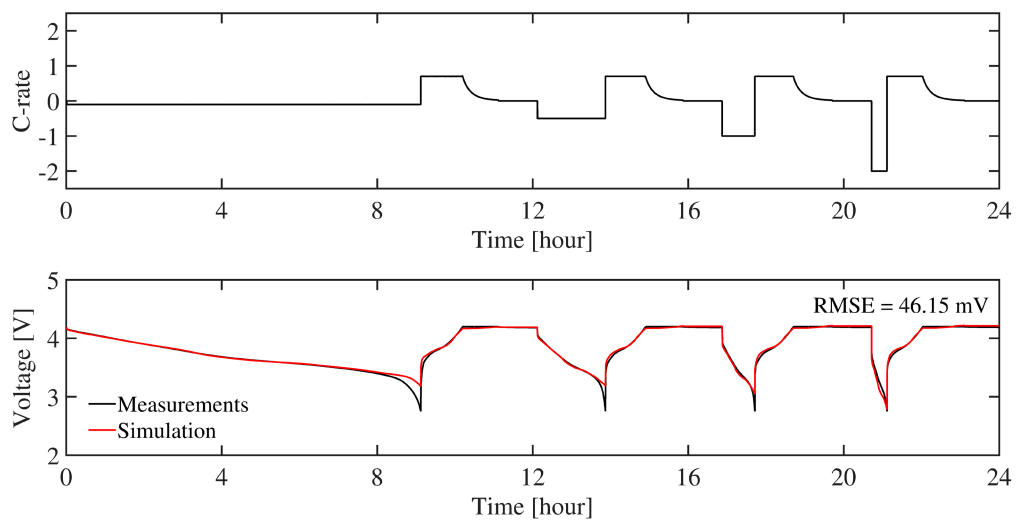

Figure 6.14 Simulated and measured voltage of the BOSTON POWER SWING5300™ cell when cycled with the constant current test. Four discharge C-rates (0.1 C, 0.5 C, 1 C and 2 C) and only one charging rate of 0.5 C between the voltage limits of 2.75 V and 4.2 V

119
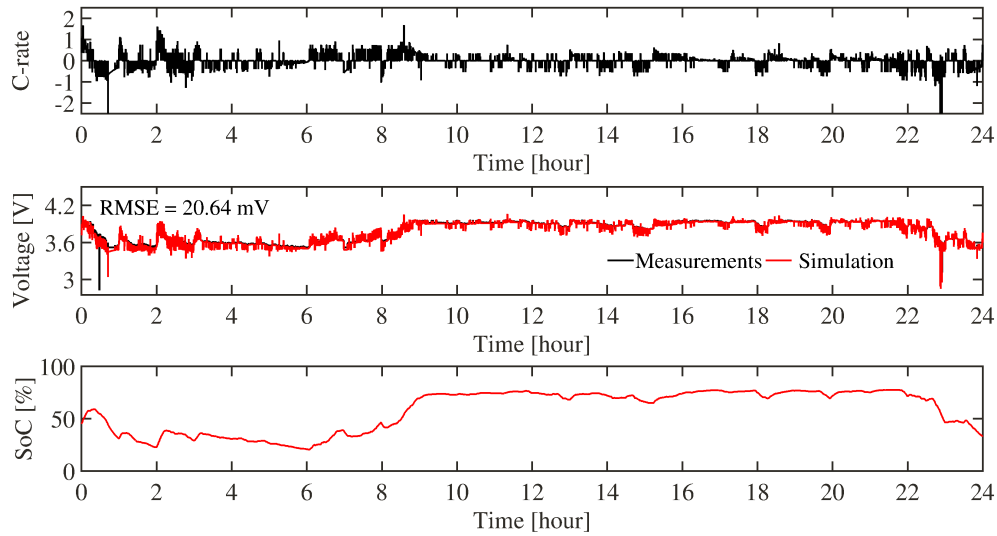
Figure 6.15 Simulated and measured voltage and SoC of the BOSTON POWER SWING5300™ cell per effect of an arbitrary current profile derived from the frequency regulation application

The C-rate and voltage trends are depicted on Figure 6.15. The RMS error is 20.64 mV (0.6%) over 24 hours confirming a very good accuracy of the model. We report also the computed SoC, which is estimated from the OCV as per Figure 6.11-b. The model is able to provide reliable information about the SoC that can be used to assess the effectiveness of the battery in the final application. For instance, in the PCR application, the model can be used to detect the periods of unavailability that would lead to penalties or extra-costs (as investigated in Chapter 8).

Performance estimation

The model has also been tested to estimate the expected cell performances: energy density, power density and efficiency.

Figure 6.16 shows a comparison between the Ragone diagram derived from
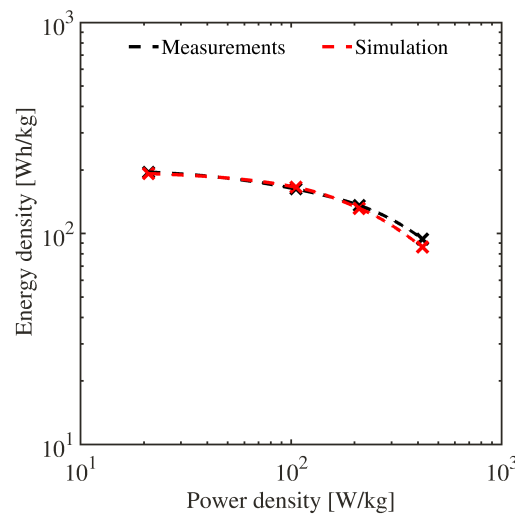
Figure 6.16 Simulated and measured energy density and power density of BOSTON POWER SWING5300™ cell

120

Table 6.5 Measured and simulated efficiency of the BOSTON POWER SWING5300™ cell in the constant current tests

C-rate	Measurements			Simulation			Error
	Charge Energy [mWh]	Discharged Energy [mWh]	Efficiency	Charge Energy [mWh]	Discharged Energy [mWh]	Efficiency	
0.1	1.88E+04	1.84E+04	97.56%	1.85E+04	1.81E+04	98.25%	0.69%
0.5	1.67E+04	1.53E+04	91.97%	1.71E+04	1.56E+04	91.62%	0.35%
1	1.48E+04	1.28E+04	86.48%	1.47E+04	1.24E+04	83.97%	2.52%
2	1.12E+04	8.85E+03	78.82%	1.10E+04	8.12E+03	73.61%	5.21%

measurements and simulations. Given the accordance between the curves, we can state that the model is able to estimate energy density and power density with minor errors. Overall, the RMSE error on the energy density is around the 2.4% of the nominal value (210 Wh/kg as declared by the manufacturer [107]). Deviations are found only for high levels of power (i.e. higher levels of average C-rate) as emerged also in the square current profile tests.

Efficiency estimation has been evaluated for two different testing conditions: (i) full charge/discharge cycles at different C-rates and (ii) arbitrary profile. Table 6.5 shows that the model is able to estimate the efficiency especially for lower current rates. The small errors (less than 1%) are probably due to inaccuracy at very low SoC (as already explained in the previous sections). The error increases considerably with the C-rate as per effects of the nonlinearities with the current which are currently not considered in the model.

Table 6.6 shows the efficiency estimation in the case of the previous mentioned arbitrary profile of PCR service. Tests have been repeated at maximum C-rate in between 0.5 and 2C and for two different limits of SoC (0-100% and 20-80%). Results indicate a better accuracy of the model when the battery is cycled in between 80% and 20% SoC (error is less than 0.5%). When approaching the limits of 0% and 100%, additional nonlinearities take place and the error can increase up to 2.2%.

Overall, it is possible to state that the proposed novel model is able to reproduce the full dynamic response of the cell and to simulate the real performances under different external signals. The full dynamic response of lithium-ion batteries has been presented.

Qualitative comparison with battery models from literature

It is interesting to compare the novel Li-ion model with some of the existing battery models presented in Chapter 4. Several aspects are considered to evaluate the models capabilities: (i) the ability to estimate the SoC and the voltage response at the device

Table 6.6 Measured and simulated efficiency of the BOSTON POWER SWING5300™ cell in the arbitrary profile tests

C-rate (max)	C-rate (average)	SoC min	SoC max	Efficiency		Absolute Error
				Measured	Estimated	
0.5	0.13	0%	100%	97.92%	97.74%	0.18%
1	0.26	0%	100%	96.15%	95.20%	0.95%
1	0.23	20%	80%	96.16%	96.35%	0.19%
2	0.47	0%	100%	91.24%	89.98%	1.26%
2	0.36	20%	80%	94.86%	94.45%	0.41%
3	0.62	0%	100%	88.00%	85.85%	2.15%
3	0.46	20%	80%	93.38%	92.87%	0.51%

Table 6.7 Qualitative comparison of different battery models. Evaluation scale: 5-very good, 4-good, 3-fair, 2-poor, 1-very poor, 0-absent (i.e. the feature is not modelled)

Model	SoC estimation	Battery Voltage response	Rate capacity effect	Recovery effect	Performances estimation		Develop. easiness	Comp. speed
					Efficiency	Energy/Power densities		
Electrochemical (P2D model)	5	5	5	5	5	5	1	1
Empirical (Peukert's model)	1	0	1	0	0	0	5	5
Sheperd model	1	1	1	0	1	0	4	4
KiBaM model	2	0	3	3	2	2	3	4
Electrical 1 (single R-C model)	3	2	2	0	3	3	3	3
Electrical 2 (SAFT RC model)	5	4	3	3	3	3	2	2
Electrical 3 (Novel model)	*5*	*5*	*4*	*2*	*4*	*4*	*2*	*2*

terminals, (ii) the ability to reproduce the two most important nonlinearities: the rate capacity effect and the recovery effect, (iii) the ability to estimate the overall performances: energy density, power density and efficiency; (iv) the easiness in the model development (experimental tests, conception, validation); (v) the computational speed achievable during simulations. These features have been used to qualitatively compare (i.e. through a comparative evaluation scale) the novel Li-ion cell model with six different battery models discussed in section 4.2: an electrochemical model (the *P2D model*), an empirical model (the *Peukert's model*), the *Sheperd model*, the *KiBaM model* (see Figure 4.3), a simplified electrical model (the single R-C electrical model of Figure 4.8-a) and a more complex electrical model (the *SAFT RC model* of Figure 4.10-a).

Table 6.7 shows the comparison. Electrochemical models guarantee the maximum level in all the indicators except for the development easiness and usability. They are very complex to develop and this fact reflects in a very high computational effort that make them unsuitable for simulation purposes. Analytical models (i.e. *Peukert's model, the Sheperd model*, the *KiBaM model*) are less accurate in reproducing the battery behaviour, but they are much faster and much easier to develop. Moreover, some of them can reach a moderate level of precision (e.g. the *KiBaM model* faithfully represent the rate capacity effect and the recovery effect) still being employable in simulations. Finally, as already showed in Figure 4.1, electrical models stand a compromise: they are not as accurate as electrochemical models nor as fast ad easy as analytical models. They are fairly good in all the indicators of Table 6.7 with an important distinction: simplified electrical model like the single R-C model are less accurate but faster than more complex electrical models like the *SAFT RC model*. In general, they can be used for simulation purposes by accepting longer simulation time in favour of more reliable results.

Within this framework, the novel electrical model developed in this chapter is comparable with complex electrical models. In fact, if compared with simplified electrical models (i.e. the single R-C model), it presents higher accuracy and higher computational effort. Specifically:

- The SoC estimation and the modelling of the voltage response are characterized by high precision, thanks to the electrochemically-driven modelling process used to develop the model (see section 6.1). For this reason and with regard to only these two features, the proposed model can be considered similar to electrochemical models.

- The nonlinearities are modelled with acceptable level of details: the rate-capacity effect is well accounted as shown in Figure 6.14, while the recovery effect modelling needs improvements since no specific circuital section is dedicated to model this issue. As regard to nonlinearities, the model offers better capabilities if compared to analytical models but still far from the ones achievable with electrochemical models.
- The final performances (i.e. energy density, power density and efficiency) are accurately estimated. The Ragone diagram of Figure 6.16 and Table 6.6 proved the ability of the model in reproducing the expected performances for industrial applications. This fact emphasizes the capability of the proposed model, especially if compared with empirical models where energy, power and efficiency characteristics must be assigned as input to the model rather than obtained from the model as output.
- The development effort is remarkable. Intensive experimental tests and long conceptual analyses are required to end up with a proper model. As regard of this aspect, the electrical model proposed is more similar to electrochemical models than analytical models. This can represent a limitation but also an opportunity to investigate faster testing procedures.
- Computational effort is high. The complexity of the model makes it slower than simplified electrical models or analytical models, but still much faster than electrochemical models. This fact, makes of the proposed model a good instrument for short/medium term simulations and a proper term of reference to validate simplified electrical models for long term simulations.

6.5 Summary

In this chapter, a novel electrical model representative of the entire Li-ion technology has been presented. The model has been developed in the frequency domain by means of EIS measurements and it has been based on the theoretical framework presented in Chapter 5. The proposed model belongs to the family of passive electrical models and is capable of simulating the full dynamic response of lithium-ion batteries. It is composed of 5 impedance blocks connected in series. Each block is derived from electrochemical equations which describe the dynamic processes of charge transfer and transport of mass. The SoC is estimated by the voltage of a nonlinear capacitance, thereby addressing the intercalation of ions into the electrode structure. Totally, the model consists of an incremental capacitance parametrization table and eight RC parameters. A procedure to estimate the parameters of the model have been presented and applied on a commercial lithium-ion cell (lithium nickel oxide). Finally, validation of the model has been carried out in the time domain showing high accuracy in estimating the voltage at the device terminals, efficiency, power and energy density under different operating rates and SoCs. Specifically, different tests at 25 °C were carried out. The error in predicting the output voltage and the overall battery efficiency is less than 0.6% when the battery is cycled through SoCs between 20% and 80% and less than 2.2% when the SoC limits of 0% and 100% are used. The very high accuracy demonstrated by the proposed model is essential in assessing the technical and economic viability of battery systems.

CHAPTER 7

Elements on lifetime modelling

While previous Chapter 5 and Chapter 6 were dedicated to dynamic modelling of Li-ion technology, this Chapter focuses on lifetime modelling of the same. The analyses are directly linked to experimental measurements. At the moment of the thesis writing, several tests are still running (since February 2017 - 8 months). Depending on the cycling conditions they have completed hundreds of cycles, in the range 400-800. The first obtained results have been used to propose lifetime modelling approaches to be used for simulation purposes. Thus, the general objective of this chapter is to extend the dynamic modelling analyses of the previous chapter by including elements of lifetime modelling. This serves to create a wider background useful for application-oriented analyses, techno-economic analyses and investment evaluations.

The chapter is structured in three main parts: (i) the aging testing procedure specifically developed to test Li-ion cells with different cycling conditions; (ii) the early results which are used to discuss about the main aging effects; (iii) the proposal of three lifetime modelling approaches with different degrees of complexity.

7.1 Aging test procedure

Chapter 3 exhaustively proved that energy density; power density and efficiency are strongly linked to operating conditions. The same can also be said for lifetime of electrochemical devices. Severe charge/discharge cycles can lead to accelerated degradation [111], [206]. In some conditions, the cell can last thousands of cycles while in other only hundreds. This fact affects strongly the operational costs (OPEX) since it is based on the right evaluation of the expected lifetime to account for replacement costs. Estimation of lifetime is even more difficult if we contextualize the problem towards real applications. Applications that requires fluctuating power requests (e.g. ancillary service) will create a non-standard cycling condition that makes the expected lifetime estimation not straightforward at all.

Chapter 4 detailed the main mechanism of battery aging and how they can be modelled. In the following, the analyses are focused on cycling aging while calendar aging is left for further insights. Experimental tests have been thought to give numerical extents to the two main degradation effects: capacity fade and power fade.

In order to ensure consistency with the previous modelling phase of Chapter 6, we tested the same Li-ion technology, LNCO chemistry, BOSTON POWER SWING5300™
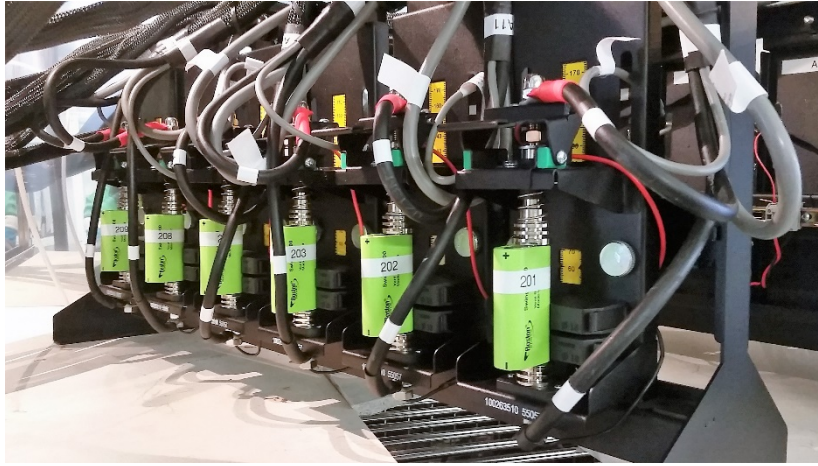
Figure 7.1 Brand new BOSTON POWER SWING5300™ cells before starting aging tests procedure at 25°C

(appendix E). The measurements have been obtained in the framework of the collaboration between the Politecnico di Milano (Electric Power Systems research group) and CSEM-PV Center (Swiss Center for Electronics and Microtechnology) at the Energy Storage Research Center (ESReC) located in Nidau (CH). All the tested cells have been cycled with a PEC- ACT 0550 battery tester starting from a brand new condition at fixed ambient temperature of 25°C, set by the ESPEC-ARU 1100 climatic chamber. Figure 7.1 shows a picture of the lithium-ion cells under aging test. Table 7.1 resumes the different test conditions: four different C-rate and three different DoD. However, not all the possible combinations have been tested, but only six can be separated in two main cycling conditions:

▪ Variable C-rate / Fixed DoD: 4 different cells cycle at different C-rate (0.25C, 0.5C, 1C, 2C) with DoD = 100% that means cycling between SoC = 0% and SoC = 100%.

▪ Fixed C-rate / variable DoD: 3 different cells cycle at fixed C-rate of 1C and variable DoD: 100%, 60%, 20%. This means that the cells are cycling in between different SoC limits: respectively 0-100%, 20-80%, 40-60%.

A specific aging test procedure has been developed not only to cycle the cells with the two above cycling conditions, but also to compute the expected aging phenomena. The procedure is repeated each 100 cycles (cycles are computed as per equation (4.19)), meaning that the aging parameters are updated each 100 cycles. The aging protocol is divided in five sub-procedures, each one responsible of providing information as regards to one specific aging aspect (Figure 7.2):

▪ Sub-procedure A is responsible for the capacity measurements. Available capacity is updated at the beginning of each set of a hundred cycles. Capacity is obtained by charging the cell as instructed by the manufacturer (CC-CV, 0.7C-4.2V 50mA cut off) and by discharging at 0.5C till the voltage limit (2.75V).

Table 7.1 testing condition matrix for the 6 BOSTON POWER SWING5300™ cells under aging tests at 25°C

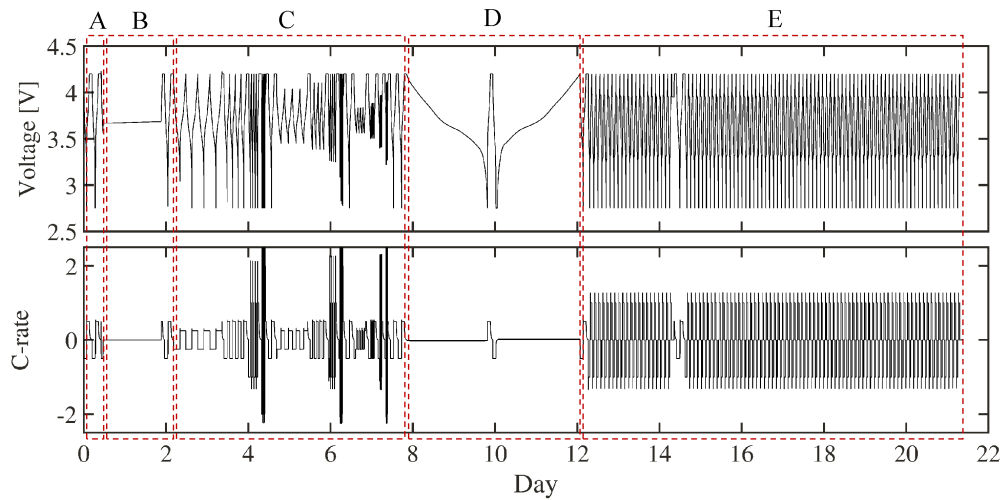| DOD	C-rate			
	0.25C	0.5C	1C	2C
100%	Cell 1	Cell 2	Cell 3	Cell 6
60%	-	-	Cell 4	-
20%	-	-	Cell 5	-

Figure 7.2 Example of aging test procedure on LNCO cell #3 with the five sub-procedures (from A to E) highlighted in red

- Sub-procedure B is responsible for resistance and EIS measurements. Measurements are taken in specific conditions:
  - Resistance at SoC=50%. The resistance is derived by measuring the voltage drop consequent to a step current profile of 100ms. The measurement is taken directly from the PEC- ACT 0550 battery tester.
  - GEIS at SoC=50% in the range 10kHz-10mHz through the Gamry Instruments© Reference 3000™. GEIS are done by pausing the PEC- ACT 0550 battery tester.
- Sub-procedure C is responsible for efficiency estimation that serves to evaluate the degradation in the efficiencies of the cells. The sub-procedure structure is like the one presented in section 3.2 (4 different C-rates: 0.25C, 0.5C, 1C, 2C) but repeated for three different levels of DoD: 100%, 60%, 20%.
- Sub-procedure D is responsible for OCV computation. OCV tests have been performed by discharging and charging the cell at a very low current rate of C/50.
- Sub-procedure E is responsible for the proper cycling phase. Whereas sub-procedures from A to D are identical for all cells, sub-procedure E is different for each cell in accordance with Table 7.1. Overall, the cycling phase weight for less than 50% of the whole aging test time (Figure 7.2), but almost 75% of the total cycled capacity. This difference is due to the long time required for some of the sub-procedures: the OCV procedure (sub-procedure D) involves only 2 cycles out of 100 but it lasts 4 days (almost 20% of the total time).

7.2 Discussion on aging effects

Given the aging procedure, the early results (up to 700 cycles) are presented which are used to discuss about the main aging effects as measured at external terminals of the cells.

Capacity fade

Decrease in cell capacity is of substantial importance in BESS applications. Less storage ability means less capability to accept or provide power for the time required by the specific application. This means a higher probability of service interruption or general unavailability due to reached SoC limits. The capacity fade is strictly related to the
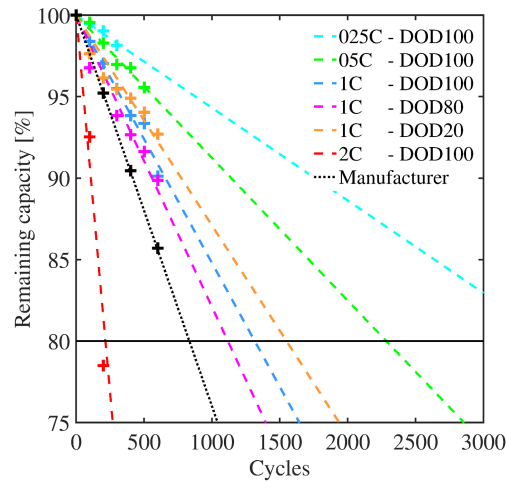
Figure 7.3 Capacity fade trends for the BOSTON POWER SWING5300™ cells under testing condition of Table 7.1

Table 7.2 Capacity fade index per cycle and cycle life for the BOSTON POWER SWING5300™ cells under testing conditions of Table 7.1

	0.25C DoD100	0.5C DoD100	1C DoD100	1C DoD60	1C DoD20	2C DoD100
Capacity fade Index [%/cycle]	-5.7E-03	-8.7E-03	-1.5E-02	-1.8E-02	-1.3E-02	-9.3E-02
Cycle life (80% capacity)	3520	2280	1310	1110	1550	210

specific cycling conditions. According to sub-procedure A of the aging test, the capacity has been computed each 100 cycles for all the tested cells. Therefore, the number of points depends

on the time required to finish each set of 100 cycles (roughly 30 days for 0.5C cycling regime, 20 days for 1C, 15 days for 2C). The main highlights are:

The trend of the capacity fade can be assumed linear (Figure 7.3). The manufacturer's data confirm the statement as shown by the black dotted line [107][13].

- It emerges a clear influence on the C-rate. The capacity fade index (i.e. the angular coefficient of the curve) increased by the cycling rate (Table 7.2). Moving from 0.25C to 2C the fade increase of almost 20 times, while only 3 times moving from 0.25C to 1C. This confirms that high currents are not well tolerated by the LNCO cell, especially if repeated constantly as in the proposed aging test procedure.
- Projections say that the cycle life of the tested cells range from 200 to 3500 cycles according to the specific C-rate condition (Table 7.2). The cycle life is computed by dividing the capacity fade index [%/cycle] by the conventional maximum capacity fade of 20% at which cells are considered dead (i.e. 80% of remaining capacity).
- No clear influence is found that relates the degradation with the DoD. The three tested conditions show deviations that would bring in a maximum difference of about 400 cycles. More cycles are needed to understand if a lower DoD impacts the degradation mechanism along the aging.

---

[13] The cycling conditions provided by the manufacturer are the following:
Charge: CC-CV, 0.7C-4.2V 50mA cut off
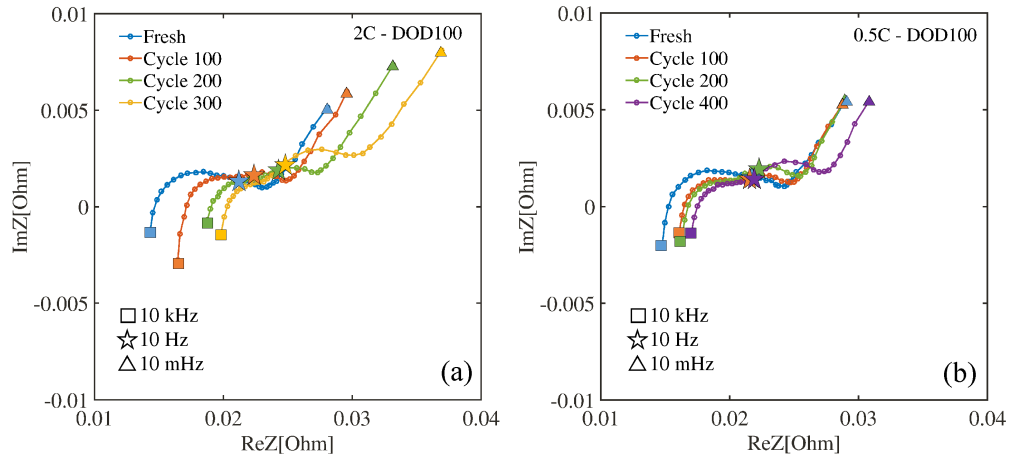Discharge: 0.5C to 2.75V
Temperature: 23±2 °C

Figure 7.4 Nyquist plots at different cycle numbers for two different cycling conditions: 2C-DoD100 (a) and 0.5-DoD100 (b)

Power fade

As detailed in section 4.3, power fade is related to an increase of the impedance of the cell. According to sub-procedure B of the aging test, GEIS measurements have been repeated each 100 cycles for all the tested cells.

In brand new condition, the Ohmic resistance R_Ω for the six tested cells resulted to be about 14.83 ± 0.8 mΩ while the manufacturer declares a "*Nominal cell impedance*" of 15.5 mΩ [107]. Deviations can be traced back to the manufacturing process. Figure 7.4 shows the impact of different cycling conditions on the shape of the EIS measurements. On the one hand, Figure 7.4-a shows the evolution of Nyquist plot of cell #6 from a fresh to a "conventionally-dead" condition (2C-DOD100 cycling rate brought the cell under 80% capacity in less than 300 cycles as per Figure 7.4-a). On the other hand, Figure 7.4-b shows the same evolution on cell #2 which is cycling at ¼ of the cycling rate of the previous case. In this case the cell is not dead yet, but after 400 cycles it is at 97% of its initial capacity. In both cases two main trends can be identified:

- The increase of the resistance that shifts the Nyquist plot towards the right side of the graph. This is the main expected phenomenon that impacts on the power capability of the device (i.e. power fade).
- The swelling of the diffusive section (transmissive type of section 6.1) that emerges with cycling and it is almost not present in fresh conditions. At the moment of the thesis writing, no further investigations have been carried out regarding the physical meaning behind any shape change of EIS. By rapidly searching in literature, it might be explained by SEI growth with cycling [207].

Efficiency reduction

In some cases, aggregated indicators are needed to describe cell degradation over time. Efficiency is often an option. Given the increase in the overall cell impedance as shown in Figure 7.4, cell's efficiency is expected to decrease with cycles. With respect to sub-procedure C of the aging test, efficiency curves evolutions can be traced for the tested cells (Figure 7.5). As depict in the two graphs, the fresh cells started all from the same conditions. Some differences have been only found at higher currents. This can be due to deviations in manufacturing process. In details:

- Figure 7.5-a highlights that severe cycling condition impact more on the efficiency.
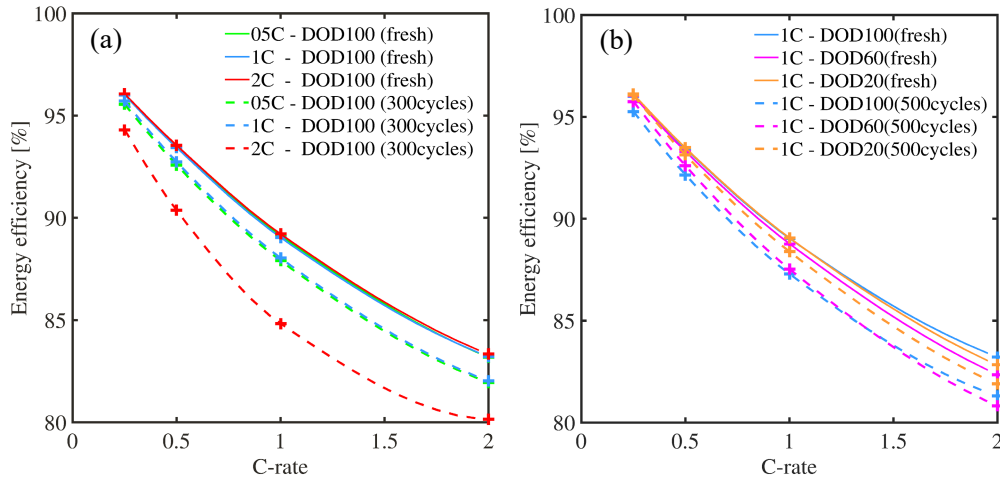
Figure 7.5 Efficiency curves trend at 25°C for different C-rate (a) and different DoD (b) for the BOSTON POWER SWING5300™ cells under testing condition of Table 7.1

Cell #6 (2C-DoD100, assumed dead after 300 cycles) lost 5 points of efficiency along its lifetime. Cell #3 (1C-DoD100) lost 1 point of efficiency in 300 cycles. By linearizing the loss and by considering the projected EoL of the cell, we can infer a total loose of 4 points of efficiency through its lifetime.

- Figure 7.5-b confirms that no clear tendency can be inferred from the influence of the DoD on the cell performances. It might be stated that cycling conditions at very low DoD are positively affecting the efficiency degradation. Also in this case, more cycles are needed to better evaluate the trends.

OCV curves shape

Aging effects emerge also from OCV curves: change in the shape corresponds to change in the IC curve peaks that have been widely studied by several recent works [150], [161], [188], [208]. According to the sub-procedure D of the aging test, OCV curves have been repeated every 100 cycles for all the cells tested. Figure 7.6 shows the impact of
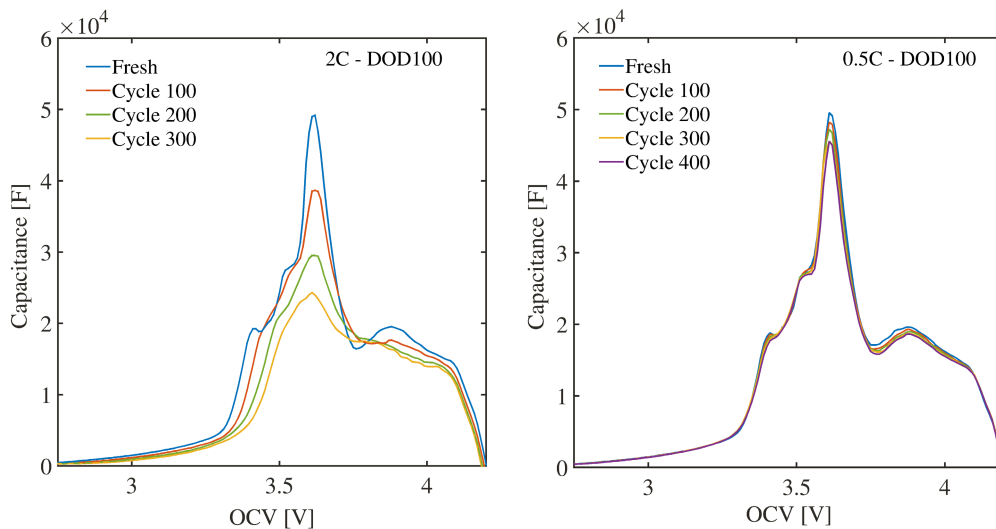
Figure 7.6 IC curves at different cycle number for two different cycling conditions: 2C-DoD100 (a) and 0.5-DoD100 (b)

different cycling conditions on IC curves. The reduction of available capacity as per Figure 7.6-a has an impact on the slope of the OCV curve. Consequently, IC curves show lower peaks as the aging increases. The reduction of peaks is greater if the cycling condition is stronger (Figure 7.6-a) and smaller if the cycling rate is lower (Figure 7.6-b). It is worthwhile to highlight the different reduction trends among the three main peaks of the IC curve. This can be explained by different degradation mechanisms that occur inside the cell.

7.3 Proposed approaches to lifetime modelling

In the following sections, lifetime modelling approaches will be proposed based on the measurements and findings of the previous sections. The purpose is to extend the dynamic modelling analyses of earlier chapters by including elements of aging modelling. This serves to create a wider background useful for the application-oriented analyses of Part II of this thesis (Chapter 8 and Chapter 9). In the next sub-sections, three approaches will be proposed and compared. They differ for the level of complexity they use to compute *capacity fade* and *power fade*:

- Empirical approaches (Figure 7.7-A) consider a steady-state operation of the battery. There is no direct reference to electrical quantities such as voltage and current, but the battery is described as a system that, due to non-ideal behaviour, dissipates some energy. Given the lower computational burden due to easier models (if compared to electrical model), these approaches are often preferred for simulation purposes (see Chapter 4).
- Electrical approaches (Figure 7.7-B) consider the full BESS dynamic response over the entire lifetime of the BESS. Aging phenomena are taken into account by updating the parameters of the electrical model. In this way, *capacity fade* and *power fade* phenomena are intrinsically modelled. This modelling approach is by far the most accurate (see Figure 4.1). However, given the huge amount of data/measurements necessary to correctly update the parameters, it is computational intensive and often preferred for on-line diagnostics (e.g. EVs application) rather than simulation analyses.
- "Hybrid" approaches (Figure 7.7-C) combine simplified electrical models with empirical functions to account for aging phenomena. *Capacity fade* and *power fade* are directly linked to update of the model parameters. Given the lower computational burden if compared to (full) electrical approaches, they can be suitable in some types of studies like planning analyses (preliminary to the final deployment of the systems).
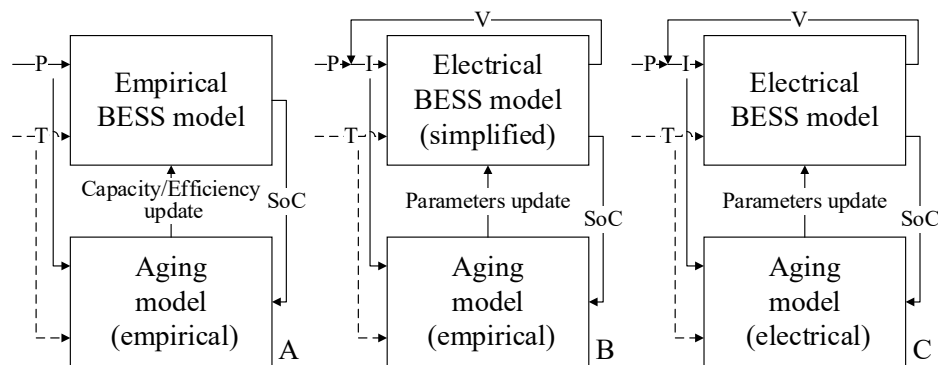

Figure 7.7 Proposed approaches for lifetime modelling of Li-ion BESS: empirical approach (A), electrical approach (B), "hybrid" approach (C).

In this case, the engineer/analyst is probably not interested in the full dynamic response of the battery, but in having accurate information as regards of the expected energy/power performances and thus reliability of the BESS in the final application.

Lifetime modelling with empirical approach

As detailed in Chapter 4, empirical models correlate aging phenomena with a combination of stress factors which have a great influence on the battery. Mathematical expressions are derived to describe capacity and power fade directly from the measurements.

Given the aging results of the previous section, Figure 7.3 and Table 7.2 suggest a possible empirical modelling of the *capacity fade* based on the influence of the current rates. A fitting function is derived which is able to identify the capacity fade index given the operating conditions (Figure 7.8). In simulations, this means that the SoH indicator at time-step k can be updated from time-step $(k-1)$ in the different cycling conditions as:

$$SoH(k) = SoH(k-1) - a_1 e^{a_2 Crate(k)} n(k) \qquad (7.1)$$

Where n are the equivalent cycles during time step k as per equation (4.19) and a_1, a_2 are experimental coefficients (as showed in Figure 7.8).

However, some cautions have to be used at very low currents: a capacity fade index at null current has absolutely no physical meaning (the fitting function identifies around 400k cycles for the current approximating zero). Conceptually, the capacity fade at zero current is due to the calendar aging effect. This effect should be evaluated in time and not cycles (see chapter 4): BESS will last for a limited amount of years if not used. In our case, roughly 5000 cycles are estimated in cycling condition of 0.01C. Assuming a corresponding cycling time of 200 hours, it would mean an expected life of almost 110 years, clearly does not make sense. A good compromise, which matches with real installations, could be to assume a maximum number of deployment years EoL_{max}. At low currents, no matter the cycling conditions, the BESS is replaced every EoL_{max}.

Besides capacity fade, empirical approaches usually account also for efficiency decrease in cycles. Figure 7.5 suggests that efficiency is decreasing differently with the cycling conditions. This is because the phenomenon is nothing but the consequence of the increase of the cell impedance. As already mentioned, when dealing with empirical
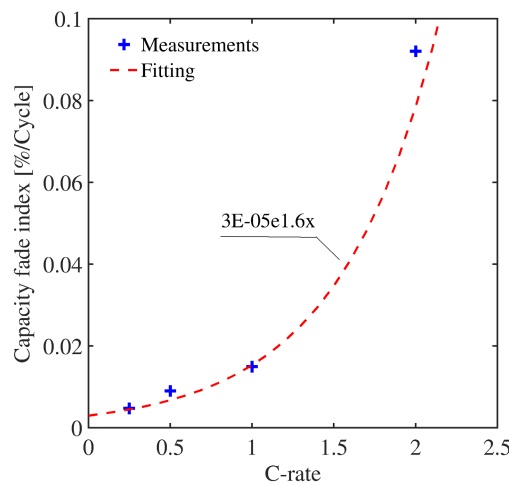

Figure 7.8 Capacity fade index trends for the BOSTON POWER SWING5300™ cells under testing condition of Table 7.1

Table 7.3 Model parameters identified at SoC=50% by fitting the GEIS measurements of the BOSTON POWER SWING5300™ cell #6 at different aging conditions

Parameter	Fresh	Cycle 100	Cycle 200	Cycle 300	Cycle 400
OCV [V]	3.6815	3.6928	3.7392	3.7717	3.6675
R_Ω [Ω]	0.0152	0.0173	0.0194	0.0205	0.0213
$R_{CT,1}$ [Ω]	0.0029	0.0016	0.0016	0.0012	0.0065
$C_{DL,1}$ [F]	0.0936	0.1011	0.3964	0.5686	0.0121
$R_{CT,2}$ [Ω]	0.0023	0.0018	0.0014	0.0010	0.0034
$C_{DL,2}$ [F]	1.1853	2.8184	4.3238	4.3588	0.3437
$R_{D,T}$ [Ω]	0.0024	0.0032	0.0036	0.0059	0.0052
$C_{D,T}$ [F]	14.0376	15.4427	15.7484	16.1156	15.3869

models, aggregated parameters, which handle complex degradation phenomena with simple equations, are much appreciated. In this case efficiency decrease represents *power fade*: the more the efficiency decreases the less the battery is able to sustain power for a given time without reaching its SoC limits. Therefore, empirically modelling the efficiency means to map the curve of Figure 7.5. In real application, the efficiency curve will evolve differently according to the specific operating conditions.

Lifetime modelling with electrical approach

This modelling approach requires an electrical model as a starting point. For the sake of simplicity, the electrical model developed in Chapter 6 is taken as a reference. Degradation mechanisms are accounted for by updating the parameters of the model during cycling. Parameters are found by running the fitting procedure of section 6.3 on each EIS and OCV measurements. Post elaboration of the obtained results should then provide the trend of parameters as a function of the cycling rate. Table 7.3 shows the results of the cell #6 (strong cycling rate 2C-DOD100)[14]. The model is able to fit the cell dynamic response through its lifetime. Data highlight the expected increase of the ohmic resistance together with the increase of all the capacitance and corresponding resistances. Further investigations that explain the physical meaning behind the variations of the parameters are left for future works.

In this modelling approach, *capacity fade* and *power fade* phenomena are intrinsically modelled by updating the model parameters. Power performances are taken into account by updating the real part of the impedance, while capacity variation by the reduction of the capacitance of the cell $C_{D,R}$ as determined in OCV tests of Figure 7.6.

The drawback of this approach is the huge amount of measurements needed to map the aging effects. OCV and EIS measurements are usually not available in literature. Moreover, measurements are used to create a map of possible aging conditions of the cell. Then, according to the specific cycling conditions (i.e. application), one should update the model by extrapolating the right set of parameters. This process needs complex functions which increase considerably the simulation time if compared to empirical approaches.

Lifetime modelling with "hybrid" approach

Electrical-based approaches are very precise but complex and time-consuming.

---

[14] Differences are present in the values of the parameters between Table 7.3 and Table 6.2, even if the tested cells are of the same brand: the BOSTON POWER SWING5300™. One year has passed between the lab tests for cell modelling (chapter 6) and lab tests for aging characterization (chapter 7). Meanwhile, the factory has changed the production site. Differences can be explained by some changes in the manufacturing process.
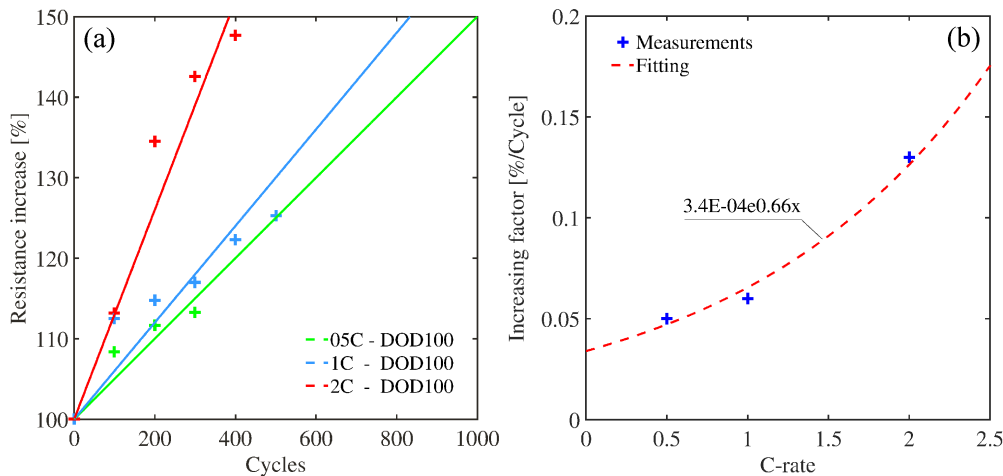
Figure 7.9 Resistance increment (a) and resistance increase index trends (b) for three BOSTON POWER SWING5300™ cells under testing conditions of Table 7.1

Empirical-based approaches are faster but they entail simplified models which do not take into account any dynamic behaviour. In this sub-section a hybrid-based approach is presented which wants to find a suitable compromise. This approach is based on two main assumptions: (i) it requires a simplified electrical model like the *R-int model* or the *Thevenin model* (see section 4.2); (ii) it uses empirical functions, which are derived from simplified aging tests, in order to update the model's parameters. Here below the approach is exemplified by using a simple R-C circuit (Figure 4.8-a).

Power fade is modelled through empirical functions which describe the impedance increase through simplified resistance measurements. While electrical-based approaches need intensive EIS measurements campaign, in the hybrid approach no EIS mapping is required. However, a characteristic solicitation, which depends on specific applications, must be defined to measure the proper value of the resistance R. The characteristic dynamic behaviour of the typical current/power profiles[15] can be found through proper analyses (e.g through FFT analyses). Overall, the approach is based on:

- One single EIS measurement in fresh conditions in order to characterize the dynamic response of the device at different SoCs. If available, one can also exploit literature data that refer to the same battery or similar chemistries.
- The mapping of the resistance at the characteristic frequency in different cycling conditions.
- The update of the initial EIS measurement (limited to the characteristic frequency) according to the cycling results of the previous step.

Figure 7.9-a shows the resistance rise in different cycling conditions at the characteristic frequency of 10 Hz (in accordance with sub-procedure B of the aging test). If a linear trend is assumed, a resistance increase index can be derived as shown in Figure 7.9-b. The relative interpolation function can then be used to update the SoR indicator of the model. In simulations, this means that SoR indicator at time-step *k* can be updated from time-step *k-1* in different cycling conditions as shown in:

---

[15] If we assume energy planning analyses, minute/hour based profiles are usually used for simulations. This means that the characteristic frequency to assess the resistance of the model will be in the order of mHz.
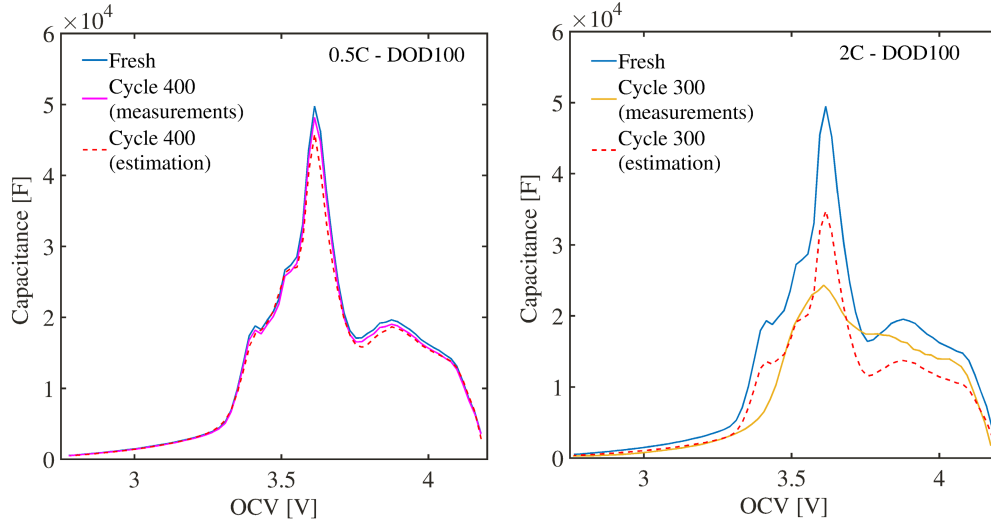
Figure 7.10 Measured and estimated IC curves at different cycle number of two different cycling conditions: 2C-DoD100 (a) and 0.5-DoD100 (b)

$$SoR(k) = SoR(k-1) + b_1 e^{b_2 Crate(k)} n(k) \qquad (7.2)$$

Where n are the equivalent cycles during time step k as per equation (4.19) and b_1, b_2 are experimental coefficients (as shown in Figure 7.9-b). The SoR indicator is then used to update the resistance at the different SoC.

Capacity fade is modelled through capacity-based measurements (sub-procedure A of aging test) as in empirical models but the derived equation (7.1) is used to update the IC curve. The modelling approach is based on the following steps:

- A first OCV measurement that serves to characterize the OCV-SoC relationship in fresh conditions and to compute the IC curve. If available, one can use literature data about similar chemistries.
- The mapping of the capacity fade at different cycling conditions as already presented in Figure 7.3.
- The update of the IC curve according to the cycling results of the previous step (Figure 7.10). The IC curve is reshaped by exploiting the interpolation function of Figure 7.8.

However, Figure 7.10 shows the limitations of the proposed hybrid approach. If the cycling regime is not severe (0.5C-DOD100), the IC curve trend is almost preserved, even after several cycles (Figure 7.10-a). On the contrary, in case of severe cycling condition (2C-DOD100), the estimation deviates considerably (Figure 7.10-b). According to measurements (the yellow line is the IC curve measured after 300 cycles, while the red dotted line shows the estimation based on the capacity fade index), the shape of IC during cycling is affected by a remodulation rather than a simple translation. For this reason, an intrinsic error affects the model: the hybrid approach cannot fully represent the phenomena behind the battery degradation.

Nevertheless, Table 7.4 shows that the remaining capacity (the area under the IC curve) is well estimated even in the case of severe cycling conditions (Figure 7.10-b). The measured capacity from IC curve (i.e. OCV measurements) was 70.5% of the initial one, against 70.3% of the estimated one. This confirms the ability of the hybrid approach in representing the capacity fade during aging.

In general, the proposed hybrid modelling approach can have several advantages:

Table 7.4 Measured and estimated capacities at different cycle number for two different cycling conditions: 2C-DoD100 (a) and 0.5-DoD100 (b)

Cycle	Measurements from IC curve [mAh]		Estimation from fade indicator [mAh]	
	0.5-DoD100	2C-DoD100	0.5-DoD100	2C-DoD100
0	5212	5238	5212	5238
100	5129	4709	5189	4848
200	5037	4131	5123	4112
300	5024	3696	5054	3683
400	4939	-	5043	-

- It does not require to run EIS measurements along the lifespan of the device as in impedance-based approaches (it requires only one EIS measurement in brand new condition). Resistance measurements to update for the cycling effect can be performed by conventional cycling machineries (e.g. PEC- ACT 0550 battery tester).
- Being based on an electrical model, even though simplified, it takes into account the power capability of the battery. Empirical models account only for efficiency decrease, but they do not relate it with physical limits (i.e. voltage limits).
- The approach can be implemented starting from manufacturer and the available literature data.

7.4 Summary

In this chapter, lifetime modelling of BESS has been investigated. The discussion has been grounded on experimental measurements carried out within the framework of the collaboration between the Politecnico di Milano (Electric Power Systems research group) and CSEM-PV Center (Swiss Center for Electronics and Microtechnology). The aging testing procedure, developed expressly to test Li-ion cells (LNCO chemistry) with different cycling conditions at ambient temperature, has been presented. Testing results gave evidences regarding the main aging effects: capacity fade, power fade and efficiency decrease. They are found to be highly dependent on the cycling rate. Projections stated that the cycle life range from 200-4500 cycles according to the specific operating conditions. No clear influence has been found instead relating to the degradation with the DoD. Aging tests allowed also to map the OCV/EIS curves evolution during aging; however, no further investigations have been carried out about the physical meaning behind it, leaving it to further developments. Nevertheless, the first obtained findings (at the moment of writing of the thesis the aging tests are still ongoing) have been used to propose three lifetime modelling approaches which attain different degrees of details. They are: the empirical approach, the electrical approach and the "hybrid" approach. Each of them have been discussed as regards of experimental efforts required to develop the model, accuracy and expected computational time. The "Hybrid" approach is demonstrated to be a suitable compromise between empirical and electrical models. It can reach higher levels of accuracy if compared to empirical models, but with lower computational burden if compared with electrical models. In general, this chapter contributed in creating a wider modelling background useful for application-oriented analyses, techno-economic analyses and investment evaluations. The modelling approaches of Figure 7.7 will be exploited in Part III of this thesis to handle complex simulations. Empirical and electrical approaches will be compared in the assessment of the BESS performances in two different real applications: (i) a grid-tied application: BESS for the provision of the PCR service (Chapter 8), (ii) an off-grid applications: BESS coupled with PV in microgrid systems (Chapter 9).

Part III: From Modelling to Applications: Approaches to BESS Proper Design

Part III offers the design framework of the thesis by bridging the modelling phase with the final applications and emphasizing BESS design criteria. Two different stationary applications are discussed that show how proper BESS model can influence the design conclusions. In both cases, the proposed novel model is compared with traditional or well-established literature approaches to compute techno-economic results. Therefore, each chapter of this part is structured according to: context analysis of the specific application, the description of the BESS model, case study presentation, discussion. Overall, the analyses of part III are centred on electrochemical batteries, considering power electronics well-established with respect to both industrial applications and mathematical modelling (i.e. simplified model of the power electronics has been adopted). Nevertheless, power electronics could impact on electrochemical cells performances: this is one of the possible future development of the PhD work.

The two selected stationary applications (i.e. cases studies) are:

- *Grid-tied application*: BESS providing Primary Control Reserve (PCR) service. PCR is chosen as one of the most investigated applications of BESS today. Business cases are already present in several regulatory frameworks that motivate the techno-economic analyses developed in Chapter 8 of the thesis.
- *Off-grid application*: PV-BESS power plants providing energy supply for rural electrification purposes. Off-grid power systems represent another important industrial sector for BESS. The right design is crucial to come up with a reliable system. This fact motivates the analyses of Chapter 9 of the thesis.

Chapter 8 deals with the PCR application. A proper methodology is proposed which includes: a specific control mechanism; an unconventional droop-control law that takes into account the specific features of BESS; proper BESS models developed on the basis of the previous chapters findings. The procedure has been applied to the Italian context. Simulations have been run to discuss about: the influence of different BESS models in the evaluation of the reliability for PCR service; the correct BESS design from a techno-economic point of view; the proper control mechanisms to increase BESS availability. The analyses are based on real measurements taken at the Politecnico di Milano within the framework of the *IoT-StorageLab*. The methodology is proposed in form of a computational tool in MATLAB®Simulink® named BESS4PCR.

Chapter 9 deals with off-grid power systems for rural electrification in Developing Countries (DCs). The aim is to address the robust design of off-grid systems by including the majority of available inputs of these contexts. A novel sizing methodology is proposed composed of four blocks which separately face the different design phases. The procedure has been applied to size a PV+BESS microgrid system to supply power to a rural village of Tanzania. Simulations are run to discuss: the impact of different BESS models on the system energy design; the evaluation of the correct system design by accounting for different scenarios of load evolution. The analyses are based on real data

gathered within the framework of the *Energy4growing* project. The methodology is proposed in form of a computational tool in MATLAB® named Poli.NRG (POLItecnico di Milano –Network Robust design).

CHAPTER 8

BESS for grid-tied applications: PCR service

In this Chapter, BESS in grid-tied applications for Primary Control Reserve (PCR) service is discussed. The general objective is to identify the presence of business cases for the application, specific objectives are: (i) to evaluate the influence of different battery modelling in the evaluation of the service provision; (ii) to identify control strategies able to maximize the availability and profitability, (iii) to evaluate the correct BESS design from a techno-economic point of view. The analyses are based on real measurements taken at the Politecnico di Milano within the framework of the *IoT-StorageLab* (Appendix B). The study approach is proposed in the form of a computational tool in MATLAB®Simulink® named BESS4PCR developed by the author within his PhD research project.

The chapter is organized in five sections: Section 8.1 provides a contextualization of the proposed BESS application, a focus on the PCR service and on the regulation mechanism in place in Europe, a short review on the available study of BESS for PCR with specific attention on the possible control strategies. Section 8.2 describes the methodology used to model the PCR service in case of provision from BESS, which includes (i) controllers that use internal and external signals to detect the best working conditions, (ii) droop-control laws with fix or variable droop modes of operations, (iii) battery model able to compute and update the SoC. Section 8.3 presents the battery models adopted for simulations: the novel model of Chapter 6 is compared with empirical models. Section 8.4 introduces the tool based on the proposed methodology which is applied on a case study that refers to the Italian context. Finally, Section 8.5 presents the main results of simulations: (i) a detailed comparison of the different battery models in the evaluation of reliability indicator for PCR service; (ii) an evaluation of the correct BESS design from a techno-economic point of view; (iii) The analysis of the variable-droop control mechanism to increase BESS availability.

8.1 Context analysis

The general framework of battery energy storage systems for ancillary services

Power systems currently undergo considerable changes in operating requirements

because of an increasing amount of discontinuous distributed generation (DG), mainly renewable energy sources for electricity (RES-E). The integration of RES-E into power system grids affects optimum power flow, power quality, voltage/frequency control and system economics. RES-E traditionally have priority in load dispatching because their production must be exploited when available. This brings about a reduction of available resources necessary for the safe and reliable operation of an interconnected power system. Moreover, RES-E plants usually connect to the grid via a static converter. Thus, the inertia level of the whole power system reduces, causing the frequency to drop faster after an outage. For this reason, the Transmission System Operators for Electricity (ENTSO-E), with key legal mandates from the European Agency for the Cooperation of Energy Regulators (ACER), are increasingly considering extending the participation in ancillary services provision to DGs [7], [8], [97].

After the European energy sector unbundling process, ancillary services include both mandatory services and others subjected to market-based competition. They allow the local Transmission System Operator (TSO) to control frequency and stability of the system, voltage along the transmission network, loading of the power lines and to restart the system in certain circumstances. The primary control reserve (PCR) is one of these services. In Italy, the PCR is a mandatory service every traditional power plant (not RES-E), with rated active power greater than 10 MW, has to guarantee [10].

Technical issues arise when considering the suitability of DGs equipment to function effectively as part of the electricity system and to provide ancillary services [16], [209]. This topic is part of the theme about the evolution of existing electrical systems towards the smart-grid paradigm [210]. Taking Italy as an example, regulations have been introduced in order to set the duties of the DGs in order to ensure the security and stability of the network [9], [211], [212]. Today, RES-E plants have to deal with the unpredictable nature of the primary resources; therefore, stringent regulations can strongly affect their operations and profits. For instance, asking RES-E plants to contribute to PCR or to sustain voltage dips means forcing them to limit their active power injection which is an incentive for them (e.g. Green certificates, feed-in premium). If the service remuneration from the ancillary service market is insufficient to cover the losses, the profitability of these systems will decrease.

Battery energy storage systems (BESSs) are the most promising technology to enable RES-E to meet this challenge. As seen in section 2.4, BESSs can provide high power capability in relation to energy capacity. They are therefore suited to a variety of grid uses, such as PCR and secondary control reserve, voltage regulation, peak shaving, load shifting and energy trading [213]. Generally, they can operate both as individual units or associated with RES-E plants. In the second option, the presence of BESS can make the ancillary services market more attractive for the RES-E owner. BESSs allow a more flexible use of the RES-E plant without limiting the exploitation of the primary source. Moreover, in a future scenario with a higher share of RES, it may be necessary to increase the ramp rates of units providing PCR. Such fast ramp rates could be provided by many EES technology, but especially BESSs.

This perspective is supported by recent evolutions in the EU and Italian regulatory framework, foreseeing new roles and opportunities for all the electric power systems players involved. A clear example in this direction is the Winter Package presented by the EU Commission [214], which envisages an update of current EU rules to allow renewable producers (RES-E based power plants) to fully participate in all market segments, with a progressive shift from centralized conventional generation to decentralized. In Italy, a first important step in this direction has been made recently by the Energy Authority (AEEGSI) through the consultation document (DCO) 298/16/R/eel [215]. AEEGSI proposed a reform of the regulatory framework for the dispatching

service currently in force, with the purpose to enable the active participation of final users, RES power plants and ESS (BESS included) to the management of the power system. These new players will be allowed to sell services designed to balance generation and consumption on the Ancillary Services Market.

PCR service: a viable opportunity for BESS

The PCR service is identified as one of the most promising, and economically interesting, regulation services for BESSs [216]. Nowadays, large scale BESSs for PCR are representing a growing business model [217]: PCR is identified to have the highest financial benefit for the BESS owner over a period of 3-5 years [218]. The purpose of PCR is to maintain the power balance on the electric network, ensuring that the amount of the electric power injected by all the power generators is equal to the electric power required by the loads. Power generators must follow their specific droop-control law. Traditionally, the droop-control differentiates among droop, regulation-band and dead-band (Figure 8.1):

- *The regulation-band* (ΔP_{max}): which is the maximum upward or downward power (ΔP_{max}) that the generator must make available when the frequency deviation exceeds a defined threshold. It is normally expressed per unit of the nominal power of the generator P_n.
- *The dead-band*: this is a small band around the nominal frequency (in Italy at $\pm$ 20 mHz), in which no power needs to be provided in order to preserve the power plant apparatus.
- *The droop*: this is the slope of the curve. It describes the capacity of the power generator to act slowly rather than faster to a change of frequency. The definition is given by:

$$\sigma = -\frac{\dot{\Delta f}}{\dot{\Delta P}} \tag{8.1}$$

Where the frequency variation Δf, per unit of the nominal value of 50Hz, is divided by the variation of the electrical power ΔP, measured in stable working conditions and per unit of the nominal power of the generator P_n.

In several countries BESSs already have the opportunity of offering PCR. In some cases, BESSs are equated to traditional power plants and they compete economically within a common ancillary service markets; in other cases, "ad-hoc" regulating mechanisms have been developed that are tailored on BESS characteristics.
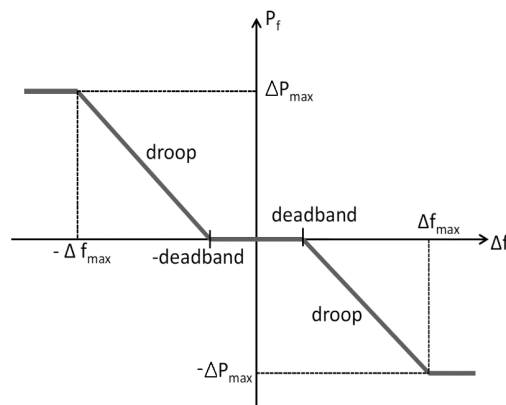

Figure 8.1 droop control law

In Italy, the requested performances are coded by the TSO Terna S.p.A. in Section A-15 of the Italian Grid-Code [10]. The dead-band is fixed in the range of ± 20 mHz. The regulation-band is about ±1.5% of the nominal power for traditional power plants. Moreover, the generators are requested to maintain the level of power for at least 15 minutes consecutively. The droop angles is not fixed to single values, but a traditional power generator must theoretically provide the capability of operating with any degree of droop between 2% and 8%. In practice, the PCR service is shared among all the power plants according to their predefined droop values. Remuneration of PCR has been defined by the Italian Energy Authority (AEEGSI) in a specific resolution [219]. Such a resolution is not devoted to creating a PCR market mechanism, vice versa the goal is to identify adequate reimbursement mechanisms for PCR regulation from traditional power plants (in particular, an advanced meter is required in order to measure properly the contribution of each generation unit to the PCR service [220]).

In Germany, the TSOs published a specific regulation for BESS providing PCR [217], [221]. Every participant had to follow a particular droop control law. Outside the dead band the power provided must increase up to 100% of the offered capacity. The BESS must be able to provide the power in 30 seconds or less and to maintain the set-point for at least 30 minutes in both positive and negative directions. Power provision in the range of dead-band and variations up to 20% in the droop control law are accepted in order to regulate the SoC.

In UK, the TSO National Grid and regulator OFGEM established a new method of providing the PCR service: the Enhanced Frequency Response (EFR) [222], [223]. The service is available in two variants and service providers can use them in order to maintain an optimal level of SoC. Regulation must be provided in reaction to frequency deviations from 50 Hz greater than ±0.05 Hz (service 1) or ±0.015 Hz (service 2). BESSs must be capable of detecting a change in system frequency within 500ms and capable of providing the contracted regulating power within 1 second. Specific droop control law fixes the working points as percentages of the BESS capacity.

More recently, as a pilot project of ENSTO-E, TSOs of Germany, Austria, the Netherlands and Switzerland have started a joint ancillary service market for PCR in April 2015 which in 2017 includes also Belgium and France [224], namely the Central Europe mechanism. This creates the largest market for PCR in Europe with a common demand of 1400 MW which is procured via a common internet platform through an anonymous tendering process [225]. The PCR cooperation is based on weekly auctions. The contracted PCR volume is the sum of each TSO PCR demand. The offers are selected with an algorithm which minimizes the total procurement cost, while respecting the PCR import/exports limits per Country. Suppliers are paid a fixed price per MW of "standby" reserve for the whole tendering period. Updated data say that the prices have ranged from 3000 to 5000 €/MW per week in the period May 2015 - July 2017 [226]. Since BESSs can provide high power capabilities in relation to energy capacity, services generating profits based on power is a real opportunity for the BESS owner. Additionally, capacity constraints are normally not stringent thereby allowing an economic operation of BESS (investment costs are proportional to capacity) [227].

Apart from the specific regulating mechanism in place, the PCR provision will be allowed as long as BESSs fulfil technical and commercial requirements set by the TSO. The most challenging requirement for BESS is service continuity. In fact, even if a zero-mean ancillary service signal is presumed, the battery will constantly decrease in the SoC level due to the internal efficiency that affects charge and discharge processes. In the end, the battery will reach its capacity limits cutting the service provision and incurring penalties that reduce the profits. For this reason, the investigation of the technical and economic performances of BESS in the provision of PCR is assuming higher relevance

as a research topic.

Regulating strategies to enhance BESS competitiveness

The effective exploitation of the regulation resources can be enhanced through the development of proper SoC control strategies that assure service continuity and competitiveness. Literature separates between [216], [228]–[235]:

▪ *Scheduled strategies:* which define a pre-defined number of charging periods (e.g. [236]).

▪ *Dead-band strategies:* which propose charging or discharging the battery by changing the BESS set point only when the grid frequency is within the dead-band. In [230] the authors use fixed SoC limits in order to (i) prevent overcharge conditions and the consequent use of dissipation resistors, (ii) anticipate the charge phase. Additionally, they allow selling relatively small amounts of energy on the electric market to stay within SoC limits. In [216] an adjustable SoC limit is proposed by following the expected frequency profile based on load forecasting and power production planning.

▪ *Dynamic strategies:* these strategies force the frequency input signal to be zero-mean by introducing set-point adjustments. The assumption is that TSOs generally allow power plants to make some changes in their schedule. It is then proposed to enable storage systems to add a time-dependent offset to the frequency control signal in order to promote charging and discharging processes that keep the SoC within acceptable levels. The adjustment of the working point has to be considerably slower than the associated service. BESS would help compensate fast components of supply-demand mismatch, while passing slow components to slower units. In [231] the authors propose adjustments when the BESS reaches specific SoC levels. The offset variation is slow enough for slower plants to follow and it has to stay flat for a certain period between two ramps of different signs. In [232] they propose a similar approach but the power set-point is based on a moving average of the previous period. They can control the ramp rate of the offset by increasing or decreasing the averaging period. The calculation takes into account also losses during charging and discharging processes;

▪ *Model Predictive Control (MPC) based strategies:* used since the 1980s, in recent years they have entered the power system balancing models [233]. By relying on dynamic models of the processes, they allow the current time-step to be optimized, while considering future time-steps. MPC has the ability of anticipating future events and can take control actions accordingly. In [234] an MPC algorithm is able to manage and allocate control reserve power efficiently, taking into account BESS constraints such as SoC limits, ramp capabilities and power/capacity limits. In [235] a model that consists of a control system model, an MPC-based controller, and a frequency predictor are presented. The authors claimed an optimal operation of BESS that prolong the lifetime and optimize the total costs.

Some of these strategies have already been analysed in real case studies. In [237] the authors present 1MW/0.58MWh BESS application able to work in 3 different configurations: MV direct coupling, LV coupling with load support, and island mode operation. They claim to use a dynamic recharge strategy that uses frequency measurements and droop-control directly implemented in the power conversion system. The charge of the battery is activated when SoC in not between the interval 45% - 65%. The presented BESS passed all prequalification requirements posed by the TSO for the provision of PCR (including minimum ramp rate and reaction time requirement). In [238] findings of different BESSs for PCR are presented. The authors simulate BESS operation using dead-band strategies with unlimited capacity, limited capacity and with or without

SoC control. Then they carry out a cost-benefit analysis comparing the economic returns in the Italian context. In [239] LFP batteries providing EFR in the UK system are investigated. The simulations outcome resulted in a optimal EPR of BESS around 0.43. The SoC-set point is set between the interval 50-60% to guarantee the service continuity. Moreover, two time intervals are defined to provide the service continuously and to bring the battery back to initial SoC when needed. In [240] the authors describe the case of 1.6MW/0.4 MWh BESS participating to the market. The main components are the over-frequency droop and the SoC controller. The first one uses over-frequency periods to charge the battery (reference SoC is 90%) while the second one starts SoC restoration after 15 minutes of delivering power even if the under-frequency period has not ended. In [241] the authors analyse a 1MW/0.25 MWh BESS (LTO technology) installed on the island of Hawaii. It is designed to provide multiservice: PCR and peak-shaving. The battery stored 1.5 GWh of energy in three years, which correspond to an intensive use (around 5 cycles per day) but the capacity decreases to 95% of the initial capacity. Finally in [242] the authors present an economic assessment of BESS within the Central Europe capacity market for PCR. Simulations evaluate the NPV in case of minimum bid size of 1MW (contracted period of 1 week) for two different BESS configurations: 1MW/2MWh and 2MW/2MWh. Their conclusions show no business cases under the current market conditions. However, the authors state that the actual BESS model is unable to reveal the differences behind the two tested configurations. A more detailed BESS model is necessary to improve the results to account for cycling rate, temperature and DoD in SoC and SoH estimations. They claim that "this will be essential for more accurate statements regarding system dimensioning and cost-effectiveness".

8.2 The proposed methodology

Given the above framework, this section presents a methodology of studying BESS capabilities in providing PCR service both from technical and economic points of view. The focus is on BESS in individual configurations, but it can be extended in the case of BESS supporting RES-E power production. Real metered profiles will be used to test different control logics through the definition of controllers, regulation and battery models. The whole methodology is represented in Figure 8.2 and it has been implemented in a tool, namely the BESS4PCR tool.

The methodology is based on several techno-economic assumptions that are compliant with the Italian regulating framework.

Technical assumption

BESS differs considerably from traditional power plants in the provision of PCR. Specifically:
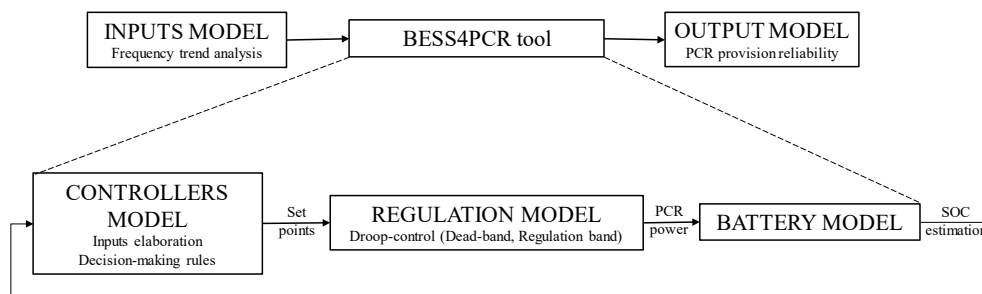

Figure 8.2 Structure of the methodology of studying BESS in providing PCR service

1. The concept of rated power of BESS is not straightforward. A battery is normally defined in terms of nominal capacity. The nominal power is usually derived from the Energy to Power ratio (EPR). The EPR can vary considerably according to the specific technology: lithium-ion technology can sustain much lower EPR if compared to lead-acid technology [237]. Thus, it is necessary to distinguish between the regulating power which is the power BESS will make available for PCR (ΔP_{max} in Figure 8.1) and the nominal power that is related to the regulation-band.

2. Given a predefined regulating power (e.g. 1MW), the regulation-band can be optimized in relation to the specific application BESS is installed for. If in an individual configuration, BESS can use up to all the rated power for the PCR (e.g. a regulation band of 100%. that corresponds to a nominal power of 1MW); if in BESS + RES-E configuration, only a fraction of rated power will be used for PCR and the remaining part for other purposes (e.g. a regulation band of 25% that corresponds to a nominal power of 4MW). Analyses/simulations are needed to understand the right regulation-band that minimizes the investment.

3. Since BESSs connect to the grid through interface converters, it is possible to exploit the resulting benefits of their fast response time. Modifications to the traditional droop-control law can be introduced, specifically in the droop that can vary according to specific logics (i.e. variable-droop).

Given the findings, the proposed methodology is based on three pillars: the regulating power (P_{Reg}) the regulation-band (ΔP_{max}) and the EPR. Once the three parameters are set, it is possible to determine the corresponding BESS P_n-E_n configuration to be analysed in the PCR provision. The nominal power (P_n) and energy (E_n) can be in fact derived from the regulation band and EPR factor:

$$P_n = {P_{Reg}} \big/ {\Delta P_{max}} \tag{8.2}$$

$$E_n = P_n \cdot EPR \tag{8.3}$$

For instance, if a BESS with EPR=1 is deployed with a regulation-band of 50% to provide P_{Reg} of 1MW, it means that the installed BESS is of 2MW/2MWh.

As regards to droop angles, the Italian Grid-Code has been taken as a term of reference which states that DGs droop must be set to a fixed value between 2% and 5% [9]. The same limits are respected also in the case of PCR provision from BESS. By keeping the frequency saturation limits constant *(Δf_{max} in Figure 8.1)*, it is in fact possible to derive the droop-range once a specific regulation-band is assumed. For instance, a droop-range [0.12% - 0.3%] is computed for a regulation-band of 0.25 p.u. as per equation (8.1).

Finally, two different regulation strategies can be used to define the specific droop to be adopted: fix-droop strategy or variable-droop strategy. In the first case, the droop is fixed to a single value within the droop range. In the second case, a specific controller defines a droop-factor (*DF*) which takes into account the actual SoC (estimated by the battery model) and the grid frequency. At a decrease of SoC the DF should (Figure 8.3):

- gradually decrease when the delta-frequency is positive (thus absorbing more and more energy from the network) in order to restore the SoC;
- progressively increase when the delta-frequency is negative (thus delivering less and less power to the network) in order to save the SoC.

Once the controller has chosen the most suitable DF value, the droop is computed as follows:

$$\sigma(t) = \sigma_{min} + DF(t) \cdot (\sigma_{max} - \sigma_{min}) \tag{8.4}$$
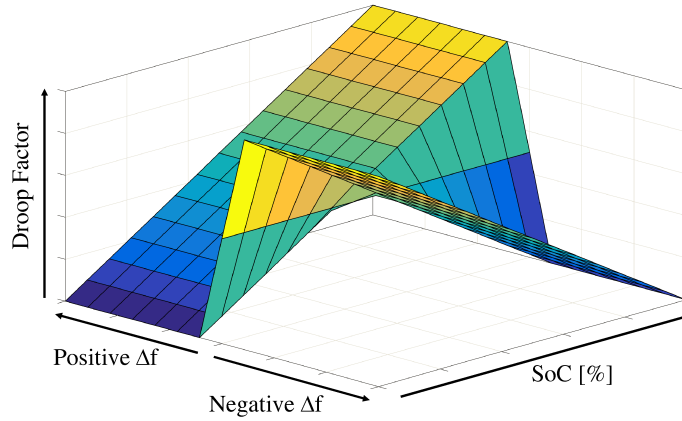
Figure 8.3 Variable-droop regulation strategy. Droop is function of Δf and SoC.

Economic assumptions

Economic analyses are based on different hypotheses which want to remain at a general level. The idea is to avoid limiting the analyses to a specific market mechanism already in place because market structures are going to quickly change driven by a relevant electric grid evolution caused by RES-E growth.

An economic gain for the PCR service has been introduced as "Revenue of PCR" (*RoPCR*), presuming it to be proportional to the regulating power provided by the BESS (P_{Reg}). Such a model is similar to the Central Europe mechanism [226]. Moreover, a market structure based on the regulation-band provided by the player is considered to be a simple, effective and transparent option for the PCR service. Since the tool assumes a constant regulating power for each BESS configuration (cfr. technical assumption), design criteria are based on the minimization of the total costs.

Analytically, the Net Present Values (NPV) can be computed as follows:

$$NPV = Inv + \sum_{y=1}^{T} \frac{CF(y)}{(1+r)^y} + RV(T) \quad [\text{€}]$$ (8.5)

$$Inv = c_{BESS}(y_P) * E_n$$ (8.6)

Where *Inv* is the initial investment cost that is proportional to the installed capacity E_n given the specific cost of BESS (see Appendix D). *CF(y)* is the net cash flow during the year *y* and *r* the discount rate. *RV(T)* represents the residual value of the assets (i.e. BESS) at the end of the investment term *T,* as per Appendix D. Cash flows can be computed by accounting for penalties and replacement costs:

$$CF(y) = RoPCR(y) - C_P(y) - C_R(y)$$ (8.7)

Where $C_P(y)$ considers the penalties associated to outages of BESS in providing PCR service (i.e. when the BESS has reached its technical limits), while $C_R(y)$ accounts for replacement costs of BESS by taking into account the projected BESS cost at the specific year *y* (see Appendix D).

Penalties are based on the Loss of Regulation (LoR) that computes the PCR not provided (due to exceeded BESS limits) as a percentage of the expected PCR energy.

$$LoR \ [\%] = \frac{E_P}{E_{PCR}} \qquad\qquad (8.8)$$

Where E_{PCR} is computed as follows:

$$E_{PCR} = \int_{t=start}^{t=end} \dot{\Delta P} \ P_n \ dt \qquad\qquad (8.9)$$

and E_P is the E_{PCR} not provided because of attained BESS limitations. Thus, the calculation/expression depends on the specific BESS model adopted (details about BESS models will follow in section 8.3).

The energy not provided is assumed to be valorised at the price p_{LoR} set by the regulator. The penalties can be computed as:

$$C_p = LoR \ \cdot E_{PCR} \ \cdot p_{LoR} \qquad\qquad (8.10)$$

Analyses and comparisons between the different regulating strategies will be based on the NPV values and break-even points. However, LoR and C_R values depend highly on the BESS modelling. Different SoC trends result actually in different LoR estimations, while aging evaluations impact on the number of replacements within the investment period. Correct BESS models are needed for a proper design that aims at maximizing the investment values for the BESS owner.

8.3 BESS models adopted

While the techno-economic assumptions of previous sections are essential to build a framework of analysis that follow the PCR service regulations, BESS models are of fundamental relevance for deriving reliable techno-economic analyses which would lead to investment decisions. SoC and SoH indicators from the model are in fact used to estimate LoR and replacement costs C_R.

Two different BESS modelling approaches will be analysed and compared in the following sections: empirical and electrical. In both cases, the BESS model receives the power set point ΔP (per unit of the nominal power) from the regulation model and must give the updated battery SoC as output. What changes is the way in which the SoC is estimated (i.e. the modelling approach). Eventually, these differences will result in marked deviations in LoR estimation. One of the main tasks of this chapter is in fact to verify the sensitivity of different modelling approaches on the optimum design evaluation. Specifically, two different empirical models (model 1 and model 2) are developed and compared with one electrical model (model 3).

In both cases, the Li-ion technology has been chosen as reference for the modelling phase. Specifically on the Li-ion LNCO chemistry from Boston Power SWING5300 [107] which has also been used for the modelling phase of Chapter 6 and the aging modelling of Chapter 7. As emerged in section 2.4, it is plausible to expect that Li-ion BESS will be the first choice for PCR provision.

The electrical model

The electrical model (model 3) is essentially the one proposed in Chapter 6. The Li-ion cell model is used as the elementary block of the BESS. This is a realistic assumption since BESS are constituted by thousands of cells (in the range of 15,000-150,000 cells/MWh in case of Li-ion BESS). For instance, two very different BESSs of 10MWh

and 500kWh are constituted of the same cells of fixed capacity, but in different numbers. If the service to provide remain the same (i.e. 1 MW), this means that the cells will have to provide different levels of power (higher for the smaller BESS). In this way, the macroscopic effect at BESS level are preserved to the cell level. Specifically, the real power P_{cell} required from or injected to cell (generators convention) is computed as follows:

$$P_{cell} = \frac{E_{n,cell} \cdot \dot{\Delta P}}{EPR} = \frac{C_{n,cell} \cdot V_{n,cell} \cdot \dot{\Delta P}}{EPR} \tag{8.11}$$

Where $E_{n,cell}$ $C_{n,cell}$ and $V_{n,cell}$ are respectively the nominal energy [Wh], capacity [Ah] and voltage of the cell. Once P_{cell} is computed and the current set-point I_B can be computed by dividing by terminal voltage.

Note that the BESS configuration P_n-E_n is scaled down to cell level by neglecting all those modelling steps that are proper of the battery pack level like the balancing and equalization of the cells. No proper BMS is implemented but a simplified PI regulator is introduced to prevent any current supply or adsorption when the cell voltage reaches its limits (the one provided by the manufacturer). As in real-operations, the BESS limitations are then linked to the cell voltage limits rather than SoC limits. The LoR is updated when the voltage reaches the limits, even if the SoC has not reached saturation. Therefore, the E_P (i.e. LoR) is estimated as follows:

$$E_P = \int_{t=start}^{t=end} \dot{\Delta P}\, P_n\, dt \Bigg|_{(V < V_{min})\, V\ (V > V_{max})} \tag{8.12}$$

SoC estimation is derived from the OCV cell as detailed in Chapter 6.

The empirical model

The empirical model is based on the steady-state operation of the battery since it computes the amount of energy that flows through the battery and updates the change in the battery state of charge over a given time step. The real power ΔP_B (in p.u. of the nominal power) required from or injected to the battery (generators convention) is computed as follows:

$$\dot{\Delta P_B} = \begin{cases} \dot{\Delta P}\, \eta_{CH}, & \dot{\Delta P} < 0 \\ \dot{\Delta P}\, /\, \eta_{DISCH}, & \dot{\Delta P} \geq 0 \end{cases} \tag{8.13}$$

where η_{CH} and η_{DISCH} are respectively the BESS charge and discharge efficiencies. On this point, the two proposed empirical models are differentiated as regards to the efficiency values:

- Model 1 assumes a fixed value of round-trip efficiency η_{RT}= 95% that is claimed to be typical for Li-ion BESS for PCR provision [242]. The hypothesis of full symmetry between charging and discharging processes is used to derive the single efficiencies for equation (8.13):

$$\eta_{CH} = \eta_{DISCH} = \sqrt{\eta_{RT}} \tag{8.14}$$

- Model 2 assumes a variable efficiency linked to the operating conditions during the specific time-step. The reference trend is derived from performance tests of Figure

7.5 where the efficiency is a function of the registered C-rate. Since electrical quantities are not considered in empirical models, the C-rate is approximated by $\Delta\dot{P}_B$. The efficiency expression[16] can be written as:

$$\eta_{CH} = \eta_{DISCH} = \sqrt{-b_3\Delta\dot{P}_B{}^3 + b_2\Delta\dot{P}_B{}^2 - b_1\Delta\dot{P}_B + b_0} \tag{8.15}$$

Then, the SoC variation at each time-step can be computed as follows:

$$\Delta SoC = \frac{\int_t^{t+1}\Delta\dot{P}_B\,P_n\,dt}{E_n} \tag{8.16}$$

In this case, BESS limitations are linked to SoC limits. Therefore, the E_P (i.e. LoR) is estimated as follows:

$$E_P = \int_{t=start}^{t=end}\Delta\dot{P}\,P_n\,dt\,\Bigg|_{(SoC < SoC_{min})\,V\,(SoC > SoC_{max})} \tag{8.17}$$

Lifetime modelling

Given the very high details required to simulate PCR application (i.e. to verify the BESS response each second), the computational effort is very high. For this reason, simulations are run for a reference period that is assumed representative during the whole plant lifetime. Consequently, the three models do not take into account neither the capacity fade effect nor the power fade effect. For instance, in the case of model 3, the full electrical modelling approach proposed in Figure 7.7 cannot be applied because the impacts of the variations on the resistors and capacitors parameters is not extensible over the entire lifetime. Nevertheless, the cycling counting during the reference period has been performed as follows:

$$cy_{sim} = \frac{E_{PCR}(1 - LoR)}{E_n} \tag{8.18}$$

cy_{sim} is then used to assess the expected BESS lifetime as follows:

$$LT_{BESS} = \frac{cy_{max}}{cy_{sim}} \tag{8.19}$$

Where cy_{max} is the maximum number of cycles that is differentiated between the different models:

- Model 1 assumes constant cy_{max} which is based on the maximum number of cycles as claimed in literature and/or by the manufacturer's data for similar studies.
- Model 2 and Model 3: assume a variable value of cy_{max}. The value comes from aging test results of Table 7.2 and is linked to the specific working conditions registered during the simulation (i.e. the average $\Delta\dot{P}_B$ for empirical models or average C-rate for electrical model).

---

[16] With $[b_3; b_2,; b_1; b_0]$ = [-4.0E-3, +3.1E-2, -1.4E-1, +1E0];

Table 8.1 Main characteristics of the BESS models adopted in the proposed methodology

Model #	Model name	SoC estimation	SoH estimation
M1	Empirical(FIX)	– Energy balance – SoC limits – η_{RT} = 95%	– Cycles counting – cy_{max} = fix
M2	Empirical(VAR)	– Energy balance – SoC limits – η_{RT} = f(c-rate)	– Cycles counting – cy_{max} = f(c-rate)
M3	Electrical	– Voltage limits – SoC = f(OCV)	– Cycles counting – cy_{max} = f(c-rate)

For instance, if the simulation provides 20 cycles/month and the maximum number of cycles is estimated in 2000, the lifetime of BESS is estimated in 100 months. This means that the BESS will be replaced every 8,3 years and C_R (i.e. NPV) can be updated accordingly.

Table 8.1 resumes the main assumptions of the three models adopted in the simulations.

8.4 Case study

The methodology of section 8.2 and the different BESS models of section 8.3 have been merged in the BESS4PCR tool and implemented in MATLAB®Simulink® (Figure 8.4). The BESS4PCR has been used to run different sets of simulations which are detailed as follow.

In addition to the models already explained (i.e. controller model, regulation model and battery model), the battery inverter has also been modelled in its efficiency and its response time. It is a simplified model since it is not the scope of this thesis to investigate more appropriate inverter models, which, however, might be matter of future improvements in the methodology herein presented. The response time is modelled by a transfer function that imposes the signal from the regulation model on the battery model, with a setting time of 200 ms (time constant of 40 ms). The efficiency is expressed as a function of the nominal power of the inverter that is assumed equal to the regulating power (Figure 8.5). In fact, it is not the scope of this thesis to investigate more appropriate inverter models, which, however, might be matter of future improvements in the methodology herein presented.

In the analyses, I/O models and their mutual effects (i.e. the effect of the BESS power injections on the system frequency) are neglected. In other words, the simulations are in "open-loop", meaning that the battery power output does not affect the input frequency to the controllers (i.e. no I/O model). This is because the goal is to investigate the effect
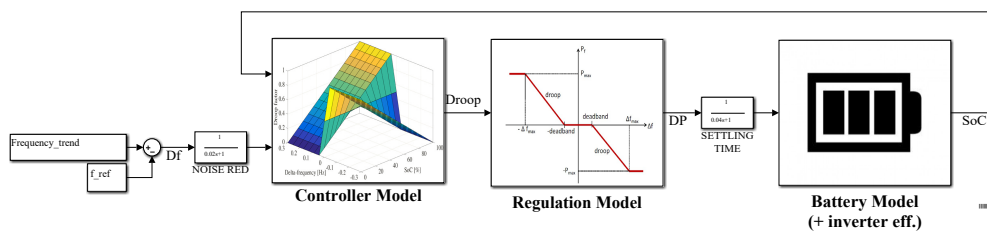
Figure 8.4 The BESS4PCR MATLAB®Simulink® tool
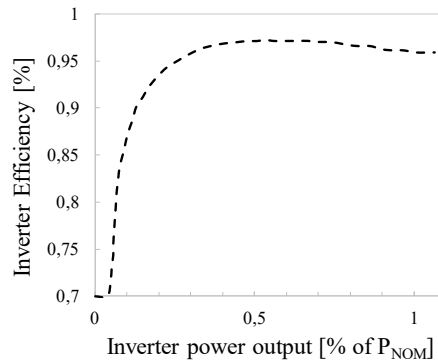
Figure 8.5 Inverter efficiency curve as a function of inverter nominal power adopted in BESS4PCR tool

of the regulation on the BESS itself.

Frequency trend analyses in Italy

As already mentioned, it is quite complex to evaluate properly the BESS performances due to the stochastic nature of the frequency signal. Therefore, simulations must rely on real data which are able to embrace the real working conditions of a BESS in providing the PCR service.

For this reason, lab activity within the framework of the *IoT-Storage Lab* (Appendix B) was devoted to measure the electrical frequency on the Italian power system. Data have been acquired with a 1 Hz sampling time without interruptions for 1 month, during the period between February and March 2017, as reported in Figure 8.6-a.

The acquired data have been subdivided into 30 single daily profiles in order to compare them and to find a common behaviour in the daily trend. The mean value and the standard deviation for each frequency sample have been computed considering the 30 days monitored, obtaining the daily profile shown in Figure 8.6-b, which can be considered representative of the mean power system behaviour. Results clearly show that there are several periodic trends. Periodic fluctuations can be observed at the beginning of each hour: the frequency rises or decreases sharply, and, after a transient behaviour, it returns close to the initial value. Periodic oscillation of 30 min and a 15 min are also
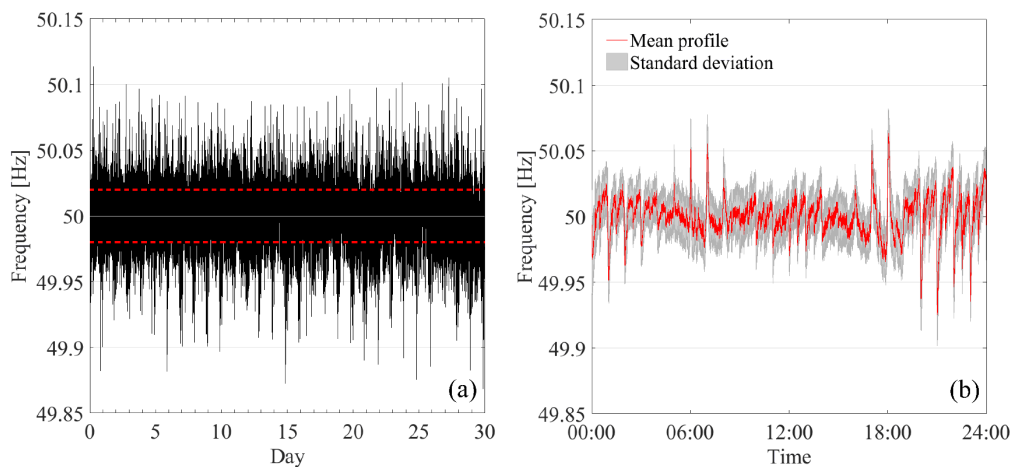
Figure 8.6 Frequency profile measured on 30 days in February/March 2017. Daily mean frequency profile (a) and its standard deviation (b)

151

observed. Currently, all these trends are correlated with the market structure in place in Italy: the Day Ahead Market is arranged in hourly sessions, while the Ancillary Services Market are based both on hourly sessions and on quarter-hour sessions.

Moreover, during the night and central hours of the day the frequency is commonly higher than 50 Hz and it decreases sharply at the beginning of the hour; on the contrary, the frequency has a typical value lower than 50 Hz in the early morning and in the late afternoon, but it increases suddenly when a new hour begins. Furthermore, the observed variations are higher during the night due to a lower system inertia.

All these findings clearly impact on the provision of PCR service especially if provided by unconventional apparatus like BESS. The deeper and longer the periods of frequency outside the dead-band are, the faster the SoC will reach its limits incurring in economic penalties. Simulations of the next sections will be therefore based on these real measurements (i.e. 30 days, $\Delta t = 1s$) embracing the Italian framework. The results obtained on the simulated month will then be assumed representative during the whole plant lifetime.

Set-up of the simulations

The parameters adopted in the simulations (Table 8.2) are compliant with the current regulation rules in Italy and plausible if related to the discussed applications. Some of them (SoC range, lifetime, etc.) are a direct consequence of the assumed technology type that is lithium-ion (note that the model used for the simulation is the one determined in Chapter 6 for the LNCO chemistry from the Boston Power SWING5300 [107]). As mentioned in the economic assumptions of section 8.2, the analyses are based on the same regulating power of 1MW and EPR=1. In all the simulations, BESS starts with half of its usable capacity exploiting the whole SoC range: from 0% to 100%. Economics are based on an investment period of 10 years which is equal to the maximum BESS lifetime. Revenue for PCR is set to 3,5 k€/MW per week (around 20€/MW per hour) as an average value of data published in [226]. The analyses are based on the variation of three variables: the regulation-band, p_{LoR} and the droop.

The regulation-band adopted in the simulations ranges from 10% to 200% (Table 8.3). From equations (8.2) and (8.3), this means that different BESS P_n-E_n configurations are

Table 8.2 Parameters adopted in the simulations with the BESS4PCR tool

Description	Parameter name	Value
Regulating Power	P_{Reg}	1 MW
Energy-Power ratio	EPR	1 h
Initial State of Charge	SoC_start	50 %
Maximum SoC	SoC_max	100 %
Minimum SoC	SoC_min	0 %
Dead-band	db	±0.02 Hz
Regulation-band	ΔP_{max}	Variable (See Table 8.2)
Droop (FIX strategy)	σ	Fix or variable (See Table 8.2)
Maximum lifetime	$LT_{BESS,max}$	10 ys
Round-trip efficiency (M1)	η_{RT}	95 %
Maximum number of cycles (M1)	cy_{max}	5000 [107]
Internal rate of return	r	6 %
Valorisation of LoR	p_{LoR}	Variable (scenario analysis)
Revenue of PCR	RoPCR	3500 €/MW per week
Investments term	T	10 y
Simulation span	ΔT	30 d
Time-step	Δt	1 s

Table 8.3 regulation-bands, droop-ranges, BESS and cell configurations (for electrical model based simulations) adopted in the simulations with the BESS4PCR tool.

Regulation Band	Droop angles		BESS level config.			Cell config.	
	σ_{min} [%]	σ_{max} [%]	P_{Reg} [MW]	P_n [MW]	E_n [MWh]	P_{reg} [W]	E_n [Wh]
10%	0.300	0.750	1	10	10	1.934	19.345
25%	0.120	0.300	1	4	4	4.836	19.345
50%	0.006	0.150	1	2	2	9.673	19.345
100%	0.030	0.075	1	1	1	19.345	19.345
150%	0.020	0.050	1	0.67	0.67	12.897	19.345
200%	0.015	0.038	1	0.5	0.5	38.690	19.345

analysed: from 10MW-10MWh to 500kW-500KWh. If the biggest configuration is a pure arbitrary choice, the smallest should respect the specific regulation in place. In Italy BESS should provide PCR for 15 minutes consecutively. Therefore, the maximum allowable constant discharge power must be $2E_n$: in these conditions, the battery will completely charge or discharge in 15 minutes starting from an average SoC=50%. Given a regulating power of 1MW the smaller BESS can be of 500KWh, exactly as in the worst scenario that assumes a regulation-band of 200%. Once the regulation-band is determined for the specific simulation, the droop angles change as per equation (8.1). In case of fix-droop strategy, the droop has been fixed at the mean value of the specific droop range; while, in the case of the variable-droop strategy, the droop moves between the maximum (σ_{max}) and minimum (σ_{min}) following equation (8.4).

Finally, in case of simulations based on the cell model of Chapter 6, the BESS configurations are scaled down to cell level as explained in section 8.3.

8.5 Simulations, results and discussion

The results obtained by running different simulations through the BESS4PCR tool are presented. Specifically, the discussions will be focused on three different layers of analysis:

1. The LoR estimation with different BESS models. The six BESS configurations of Table 8.3 are simulated. The focus is on the LoR estimation achievable with the three different BESS models presented in section 8.3 and section 8.4. The simulations are carried out with a fixed-droop strategy. Results will demonstrate the high impact of the BESS modelling on the LoR computation.
2. Optimal BESS design. Given the LoR estimated by the different BESS models, the discussion moves on to economic analyses. The NPV as a function of the regulation-band is derived. Results will show that the optimal regulation-band (i.e. optimal BESS design) changes with the BESS modelling approach. Moreover, sensitivity analysis highlight that the same differences are even more remarkable with a higher level of p_{LoR} set by the regulator.
3. Variable-droop control strategy analysis. Given the optimal regulation-band, fix-droop strategy and variable-droop strategy are compared. Results show that variable-droop helps to improve SoC control enhancing the profitability of BESS.

LoR estimation with different BESS models

In this first sub-section, a detailed comparison of different battery models in the evaluation of BESS reliability for PCR service is presented. The results demonstrate the different impact of electrical and empirical models. Simulations have been run for all the
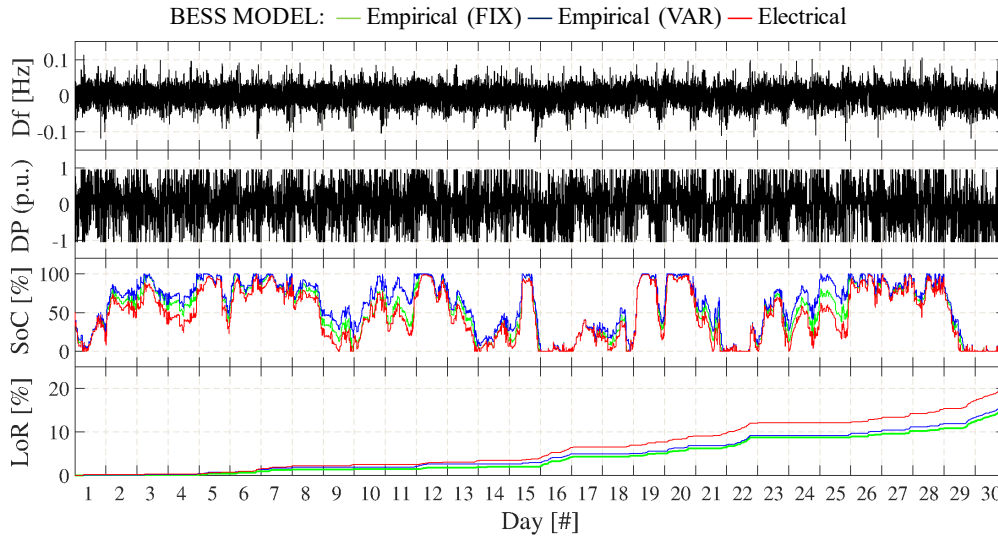
Figure 8.7 30-days simulation at 100% regulation-band: DF and DP input profiles and computed SoC and LoR with different BESS modelling approaches

six configurations of Table 8.3.

Figure 8.7 shows the case of a 100% regulation-band as reference for discussion. ΔP trend is the same for all the three models since it is derived from the frequency deviation *Δf* by equation (8.1), while SoC is determined differently in agreement with the different modelling approaches (see section 8.3): empirical models simply update SoC analytically, while the electrical model base the account on voltage limits. This turns in similar SoC shapes that depend on the particular frequency profile, but different trends: saturation periods are different among the models. For instance, day 25 shows a great variability in the SoC estimations: empirical model with variable efficiency (M2) is almost at its maximum SoC while electrical (M3) and empirical with a fixed efficiency (M1) are far behind. These differences are mirrored in the LoR estimations. Table 8.4 groups the main results of the simulation. The highest value of LoR is reached by the electrical model (21%), while empirical models M1 and M2 attain lower levels: M1 has

Table 8.4 simulation results at 100% regulation band: comparison between different modelling approaches

Results	Model		
	M1-Empirical(FIX)	M2-Empirical(VAR)	M3-Electrical
Regulation band	100 %	100 %	100 %
Sigma (σ)	0.05 %	0.05 %	0.05 %
E_{PCR} [MWh/d]	3.23	3.23	3.23
E_P [MWh/d]	0.51	0.53	0.68
LoR	15.8 %	16.4 %	21.0 %
C-rate (average)	0.39	0.39	0.33
Efficiency	95.0 %	-	90.4 %
Cycles (Cy_{sim}) [#/d]	1.36	1.35	1.27
Maximum cycles (cy_{max})	5000	3539	3886
BESS lifetime (LT) [y]	10	7.3	8.5
Simulation time [s/d][17]	16.7	21.8	1142

[17] Intel® Core™ i7-4790 CPU @ 3.6GHz, RAM 16 GB.

Figure 8.8 30-days simulation, electrical BESS model performances at different regulation-bands: input ΔP, C-rate and Voltage at cell level; estimated SoC and LoR

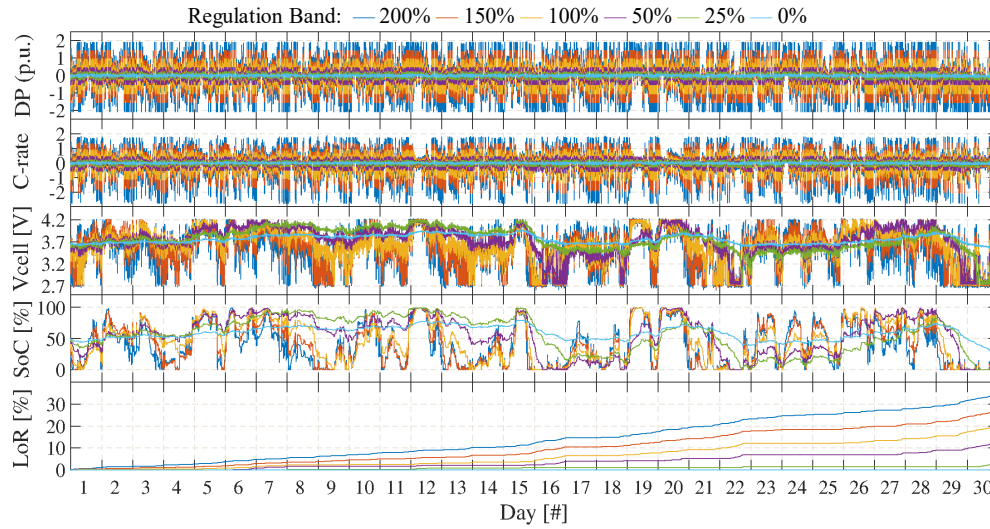the lowest value but very close to M2, respectively 15,8% and 16,4%. This means that the assumption of η_{RT}= 95% for M1 is realistic for the PCR application.

Lower LoR means higher regulating energy to the grid, more cycles per day and higher average C-rate. This fact affects directly the lifetime computation (and economic analyses) since the number of maximum cycles cy_{max} depends on the cycling rate (in case of M2 and M3). Empirical model M1 (characterized by a fix value for cy_{max}) results in a BESS lifetime of 10 years that correspond to the investment term. Empirical model M2 and electrical model M3 are based on values of Table 7.2 and thus related to the average C-rate registered during the simulation (i.e. the cycling severity). In these cases, BESS lasts 7,3 or 8,5 years respectively. The lifetime is very different between the modelling approaches impacting on the replacement costs: replacements are more or less frequent depending on this estimation.

Overall, it is possible to state that electrical model can enhance the accuracy in the final results by better simulating the real behaviour of BESS. However, as shown in Table 8.4, this result can be obtained at the expense of a considerably higher simulation time. Simulation with electrical model are 50-70 times longer than simulation with empirical models.

Simulation over 30 days of analysis with the 18 possible configurations (6 regulations band, 3 modelling approaches) have been performed with electrical and empirical models. Figure 8.8 shows the results obtained with electrical model. As detailed in section 8.3, the analyses are scaled down at cell level. The input of the model is the current (C-rate) that is determined by dividing ΔP (in per unit of the cell nominal power $P_{n,cell}$) to the cell voltage. The model outputs are the terminals voltage, The SoC and the LoR. As expected, the higher the regulation-band, the higher the C-rates, the larger the variations of SoC, the greater the LoR. Table 8.5 groups the main results of the simulations of Figure 8.8. The LoR reaches up to 36% in the worst scenario that is for the highest regulation band of 200% (i.e. 0.5MW/0.5MWh BESS), while it considerably reduces up to 0% for lower regulation bands (e.g. the 10% case, 10MW/10MWh). Different regulation bands, which corresponds to different BESS configurations, result in different cycling estimations: fractions of cycles per day are consumed when the regulation band is set to a very low value, while up to 2 cycles per day are cycled when

Table 8.5 simulation results with electrical model at different values of regulation band

Results for M3	Regulation band					
	10%	25%	50%	100%	150%	200%
Sigma (σ) [%]	0.52	0.21	0.11	0.05	0.04	0.03
E_{PCR} [MWh/d]	3.23	3.23	3.23	3.23	3.23	3.23
E_P [MWh/d]	0	0.12	0.43	0.68	0.92	1.18
LoR [%]	0.0	3.7	13.3	21.0	28.5	36.5
C-rate (average)	0.04	0.10	0.18	0.33	0.47	0.61
Efficiency [%]	99.0	97.6	95.2	90.4	85.7	81.6
Cycles (Cy_{sim}) [#/d]	0.16	0.39	0.70	1.27	1.73	2.05
Maximum cycles (cy_{max})	6230	5693	5001	3886	3086	2486
BESS lifetime (LT) [y]	10	10	10	8.5	4.9	3.4

the regulation band is progressively increased. This fact, coupled with the decrease of the maximum cycles (cy_{max}), affect the lifetime estimations. Life expectancy varies from 10 years for the lower regulation bands to 3 years in the worst case.

By coupling the above results with the ones obtained with the other models, it is possible to map the LoR as a function of the regulation band. Figure 8.9 highlights the different trends between the two modelling approaches: logarithmic for empirical models and linear for the electrical model. The lower LoR values computed by the empirical models are due to the LoR estimation based only on SoC limits. Empirical models do not account for the influence of higher current on the BESS, while electrical models account for the greater voltage excursions to evaluate if the voltage limits are reached and to account for LoR.

Given the technical analyses that arise from the different modelling approaches, one might want to understand if any business cases exist in using BESS for PCR. An economic analysis should then be coupled with the technical one.

Optimal BESS design for PCR provision

From a techno-economic point of view, the evaluation of the correct BESS design (i.e. the optimal regulation band) means to compute NPVs as detailed in equation (8.5) for different scenariosof analysis. Figure 8.10 shows the estimated NPVs as a function of the regulation-band for the three different modelling approaches. Two scenarios are analysed as regards to C_P computation (equation (8.10)): (a) refers to a valorisation of LoR which
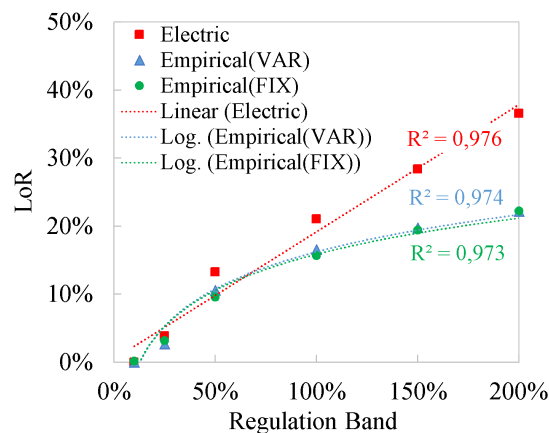

Figure 8.9 Estimated LoR Curves as function of the regulation-band with different BESS modelling approaches

is derived directly from the Italian regulating framework (p_{LoR} = 140 €/MWh) [220], while (b) represents a prospective scenario in which the penalization has a strong impact (p_{LoR} = 500 €/MWh). In both cases, the influence of C_P on NPV becomes visible for regulation bands greater than 50% because LoR does not support not-negligible values. At lower regulation bands the curves are overlapped because the NPV depends only on the investment cost: LoR penalizations are practically absent and replacements costs are null since the BESS lifetime is equal to investment terms (a low regulation band in fact means a shallow cycling rate).

Figure 8.10-a shows that at the current value of penalization, BESS installations are convenient on a 10-year investment perspective in 4 out of 6 possible configurations: a regulation band in the range 50%-200% ensure NPV around 0.5-1 M€. Small differences are present within the models. M2 and M3 are practically overlapped: the weight of C_P is so small that the differences in the LoR estimations do not emerge on the NPV curves. M1 differentiates from M2 and M3 because of the assumed fixed cy_{max}. In M1, higher severity on cycling rate do not bring to a shorter BESS lifetime. This affects C_R estimation which increase linearly with the regulation-band. Therefore, the empirical models totally based on manufacturer's data would lead to choosing the smallest BESS configuration possible (i.e. 0.5MW/0.5MWh), which corresponds to a regulation-band of 200%. On the contrary, the other models show an optimal configuration around 110% (i.e. 0.9MW/0.9MWh).

Figure 8.10-b shows different results. In this case, all models show their own curve with clear and separated optimum points. By assuming a higher penalization for the service not provided, C_P becomes comparable with $RoPCR$ and C_R. In this case, also NPV of M1 decreases at a high regulation band. However, with this scenario, the profitability is reduced to values slightly above zero. Moreover, the range of allowable regulation-bands (i.e. BESS configurations that would bring to positive NPV) is narrowed in M2 and M3. Optimum points stand at 70% (i.e. 1.4MW/1.4MWh) for M3, 75% (i.e. 1.3MW/1.3MWh) for M2 and 120% (i.e. 0.8MW/0.8MWh) for M1. This highlights the importance of proper estimation of LoR (i.e. proper modelling) in case the regulating framework changes towards some stricter rules. The risk in fact is to end up with an undersized BESS solution that will negatively affect the final performances once deployed. In the following section, the electrical model M3 is chosen as a reference for further improvement in the regulating strategy.

Variable-droop strategy analysis

The results of the previous sub-section show the presence of business cases for two
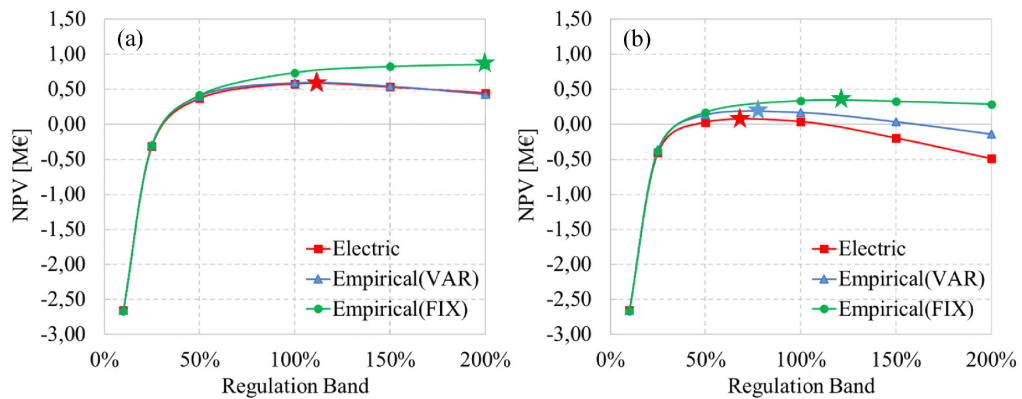

Figure 8.10 Estimated NPV curves as function of the regulation-band with different BESS models; two valorisations of LoR are assumed: (a) p_{LoR} = 140 €/MWh, (b) p_{LoR} = 500 €/MWh
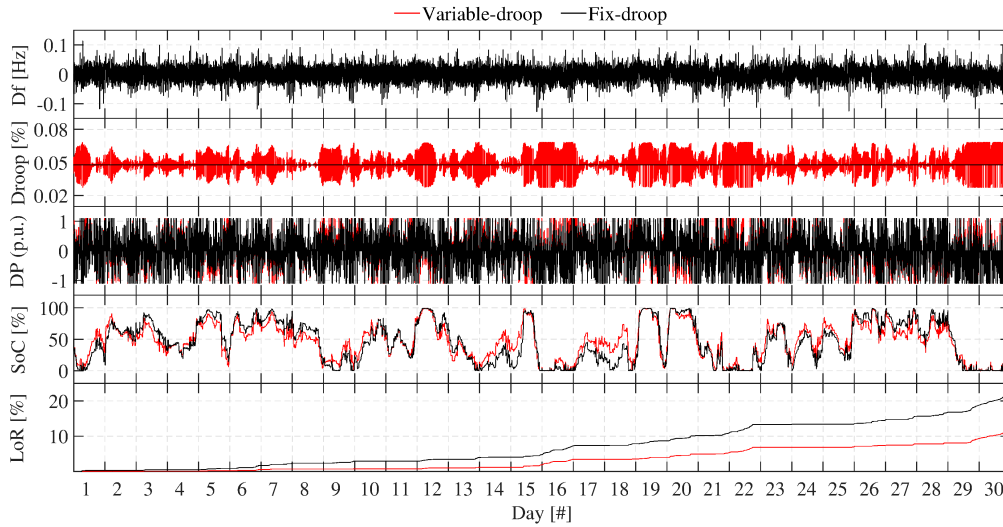
Figure 8.11 30-days simulation at 110% regulation-band with different regulation strategies: Droop, ΔP, SoC and LoR computed for the same frequency profile.

different regulating scenarios. Proper control strategies can be then put in place to increase profitability. One possible choice could be to adopt a variable-droop mechanism to limit the LoR as presented in section 8.2. The general idea is to let the BESS exploit all the possible droops as a function of the actual SoC and frequency deviation Δf (Figure 8.3). For instance, if the battery is about to reach the minimum allowable SoC and the grid frequency is under 50 Hz, it should provide as little power as possible (saving SoC and incurring in lower LoR) by keeping the droop to the maximum value. In the same way, if the grid frequency is above 50 Hz, it is advisable to change the droop to the minimum value in order to charge the battery as much as possible, while providing PCR. In this way, the variable-droop helps to improve SoC control.

In this framework, BESS with the optimal configuration as emerged from scenario (a) of Figure 8.10 (i.e. 0.9MW/0.9MWh) has been simulated with or without variable-droop controls strategies. Simulations rely on the electrical model of section 8.3 given its higher reliability in the LoR estimation. Figure 8.11 shows the difference between fix-droop

Table 8.6 simulation results with different regulation strategies for a 1MW/1MWh BESS

Results	Regulating strategy	
	Variable droop	Fixed droop
Regulation band [%]	110	110
Sigma (σ) [%]	0.027- 0.068	0.065
E_{PCR} [MWh/d]	3.15	3.23
E_P [MWh/d]	0.38	0.72
LoR [%]	12.0	22.3
Efficiency [%]	89.4	89.3
C-rate (average)	0.38	0.36
Cycles (Cy_{sim}) [#/d]	1.59	1.49
Maximum cycles (cy_{max})	3561	3717
BESS lifetime (LT) [y]	6.2	6.9
Simulation time [s/d][18]	1308	1142

[18] Intel® Core™ i7-4790 CPU @ 3.6GHz, RAM 16 GB.

Figure 8.12 Estimated NPV trends and pay back time with variable-droop or fix-droop strategies; Two valorisations of LoR are assumed: (a) p_{LoR} = 140 €/MWh, (b) p_{LoR} = 500 €/MWh

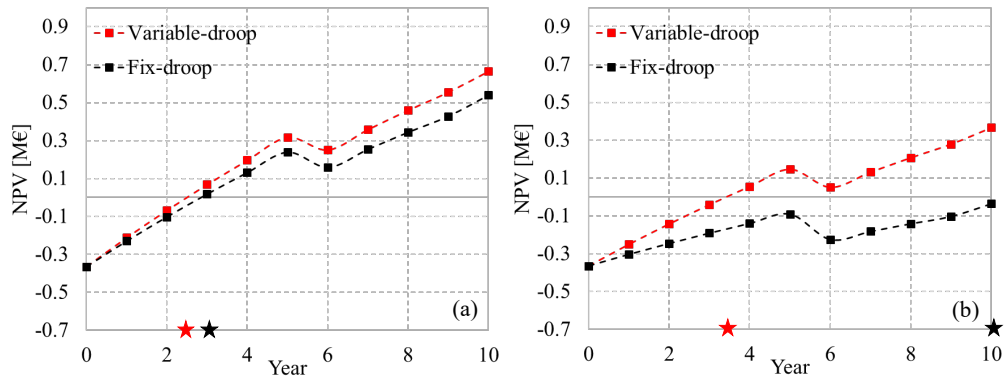strategy and variable-droop strategy. As highlighted by red lines, in both high and low SoC conditions the electrical model works close to the extreme values of the droop range (0.027%- 0.068% from equation (8.4)) in order to avoid SoC limits. Days 16 and 20 are illustrative of this behaviour: SoC is at its limit; however, variable droop-strategy allow BESS to exploit favourable values of Δf to charge or discharge quickly, avoiding unwanted LoR. Variable-droop strategy almost halves the loss of regulation during the simulation. However, for the controller to be effective, even the frequency trend needs to be favourable at the same time. Actually, if low-frequencies are much more frequent than high-frequencies, the variable-droop operation can only help to retard reaching the minimum allowable SoC.

Table 8.6 includes the main results of the simulations. The whole energy that must be provided for PCR service is different between the two strategies because it depends on the value of the droop that will affect the ΔP. E_{PCR} for variable-droop strategy is in fact 2% lower than the fix-droop strategy. However, cycles and average C-rate per day are respectively 6% and 5% higher due to the lower LoR that means lower unavailability time. This will affect the BESS lifetime which is 6.2 years compared to 6.9 years.

All these findings should be taken into account to evaluate the correspondent business cases. The same scenarios of Figure 8.10 are analysed. Figure 8.12-a shows that there is very little difference present in the pay-back-time (PBT) at current regulatory framework (scenario a): independently from the adopted regulation strategy, the investment will pay back in less than 3 years. Simulations show again a great profitability of BESS for PCR at the assumed market mechanisms (i.e. constant RoPCR and decreasing cost of BESS during the plant lifetime). Profitability is increased in the case of a variable-droop strategy that shows a value of the investment 15% higher if compared to a fixed-droop strategy.

In the case of a more stringent regulating framework (scenario b), simulations show that a variable-droop is a necessary strategy to preserve the profitability of the installation (Figure 8.12-b). By reducing the LoR, it guarantees a low level of CP allowing a PBT very similar to the previous scenario: 4 years instead of 3 years. On the contrary, a fix-droop will be affected by the high weight of penalties that will put at risk the investment: NPV is estimated lower than zero over the 10 years of investment.

In conclusion, simulations demonstrate that business cases are present when BESS is analysed for PCR provision. However, the profitability is very much linked to the BESS model and the regulation strategy adopted. Empirical models that are usually adopted in literature tend to overestimate the optimal BESS design while underestimating the BESS unavailability periods. Electrical models can represent a viable option for this kind of

analyses since they reproduce the real behaviour in the real-life application. The opportunity of proper models is even more motivated when regulating frameworks become stringent and penalties become non-negligible in the investment evaluation.

By referring to the Italian context, coupled with hypotheses and data that belongs to the Central Europe mechanism, the simulations highlight that the right BESS design is for a regulation band of 110% that correspond to a BESS of 0.9MW/0.9MWh. This optimal BESS design is estimated to be worth around 0.6-0.9 M€ on a 10 year investment term, depending on the adopted regulation strategy. The variable-droop mode of operation in fact improves the BESS performance avoiding part of the penalties related to full charge or discharge conditions. Moreover, it allows the BESS owner to maintain profitability also in the case of a changed regulating framework.

8.6 Summary

In this chapter, the final application of Grid-connected BESS for Primary Control Reserve (PCR) has been discussed.

After a brief contextualization about today's regulatory framework related to BESS for ancillary services, followed by a short review on the available studies in literature, a proper methodology to study BESS for the provision of PCR has been proposed, which includes: (i) controller which uses internal and external signals to detect the best BESS working conditions, (ii) unconventional droop-control law with fixed or variable droop modes of operations, (iii) different battery models (empirical and electrical) able to compute and update the SoC. The proposed methodology is part of the approaches for the optimum control of BESS operations. When compared with the related literature, this methodology aims at understanding how BESS features could be used to the advantage of the BESS owner. Thus, attention has been focused not only on the SoC control but also on the expected economic benefits for the BESS owner. The analyses have been based on real measurements taken at the Politecnico di Milano within the framework of the *IoT-StorageLab* (Annex B). The methodology has been proposed in the form of a computational tool in MATLAB®Simulink® named BESS4PCR and applied to the Italian context.

Several simulations on a 30-day basis (sampled at 10 Hz) have been presented to discuss about: (i) the influence of different BESS modelling approaches on the evaluation of reliability for the PCR service; (ii) the correct BESS design from a techno-economic point of view; (iii) proper control mechanisms to increase BESS availability (i.e. Loss of Regulation (LoR)). Results showed that different BESS models highly affect the LoR estimation. Differences can reach up to 20%. It is shown how empirical models do not account for the influence of higher operating rates on BESS performances, while electrical models evaluate if the correspondent greater voltage excursions have caused an unavailability state due to voltage limits. BESS optimal design evaluations have been carried out through investment evaluations that take into consideration revenue for PCR, investment costs (i.e. BESS cost), penalties due to LoR, replacement costs and residual value of BESS. Results showed that the adopted BESS modelling approach highly influences NPV calculations. This is true especially when the penalization for LoR assumes modest values (e.g. 500 €/MWh). In this scenario, business cases (i.e. NPV > 0) are shown for a limited set of BESS configurations, again highly dependent on the BESS modelling approach adopted. If an electrical model is chosen as reference, simulations showed that an optimal configuration is 1.4MW/1.4MWh with NPV slightly above 0 over a 10 year investment term. Finally, a detailed analysis of BESS operations using a variable-droop control has been proposed. This control strategy has been shown to improve the BESS performances and profitability avoiding part of the penalties. LoR is

shown to be reduced by 10 points, NPV to be more than doubled and Pay-back-time to be almost halved.

Overall, grid-connected BESS have been shown as a promising technology to provide ancillary services as PCR to electric power systems, especially if proper control strategies are adopted to enhance BESS performances. However, analysts or engineers must pay attention to the BESS model which is used to derive investment evaluations. Electrical models are found to be a valid option in simulating the operation of a real BESS when the regulating framework (i.e. remuneration and penalty) is clearly defined. Empirical models represent a faster option in understanding the behaviour of the system but they can lead to undersize BESS solutions that will negatively affect the final performances.

CHAPTER 9

BESS for off-grid applications: PV-BESS systems for rural electrification

In this Chapter, the application of BESS within off-grid power systems in Developing Countries (DCs) is discussed. The goals are: (i) to propose a novel procedure for the robust design of off-grid electric power systems that want to be as general as possible providing reliable design outputs by including the majority of available inputs of DCs rural contexts; (ii) to evaluate the influence of different battery modelling in the sizing process. The analyses are based on real data gathered within the framework of the *Energy4growing* project (Appendix A). The study approach is proposed in the form of a computational tool in MATLAB® named Poli.NRG (POLItecnico di Milano –Network Robust desiGn), the development of which the author cooperated within his PhD research project.

The chapter is organized in five sections. Section 9.1 contextualizes the application in the framework of rural electrification. Then a brief literature review on the methodologies and software that already address this issue is presented and several issues are found that motivate an alternative design procedure. Section 9.2 describes the features of the proposed novel methodology for the robust design of off-grid electric power systems that are composed of four building blocks, which separately face the different design phases by taking into account the distinctive features of DCs rural contexts. Section 9.3 focuses on BESS modes and their appropriateness in Poli.NRG. In this kind of analyses, the detailed dynamic response of the battery is not an issue; however, reliable simulations able to forecast accurately the performances of the system: result quite useful for a proper investment evaluation. For this reason, a simplified electrical model derived from the one proposed in Chapter 6 is compared to empirical models which represent the first choice for a sizing tool in literature. Section 9.4 introduces the developed tool that applies the proposed methodology in performing a sizing of a PV+BESS microgrid system to supply electric power to a rural village of Tanzania. Finally, Section 9.5 presents the main results of simulations: (i) a detailed comparison of the different battery models aiming at understanding the impact on the system energy design; (ii); an evaluation of the correct system design by accounting for different scenarios of the load evolution.

9.1 Context analysis

BESS in the bottom-up electrification paradigm

Rural electrification represents one of the issues to be faced in order to provide modern energy services to 1.2 billion of people living in developing countries (DCs) that do not have access to electricity (data refer to 2013, [22]).

Two electrification approaches face this challenge, i.e. *top*-down and *bottom-up*. Specifically:

- *The top-down* (or centralized) approach to electrification is the one followed historically in developed countries. It stays at a high level (i.e. *top*) dealing with a large population of users (e.g. cities, agglomerations of villages, etc.) and using statistical estimations based on macroscopic data to forecast consumption. The building of huge power plants is then planned according to the country resources and fossil fuel supplies, while the service is brought to the single users (i.e. *down*) through a power system infrastructure.

- *The bottom-up* (or decentralized) approach to electrification looks at the specific features (i.e. resources and loads) of the targeted context to satisfy the electrical needs of single users or small communities. It starts from microscopic data (i.e. single electric appliances) to effectively catch the customer needs (i.e. *bottom*) and to match them with the available energy sources in the area of consumption. Normally, the potential applications are narrowed to small size off-grid power systems, tailored on the specificities of the customer(s). This approach aims at conceiving, sizing and designing these units as small cells of a wider architecture (i.e. *up*) [243]. In a long-term perspective, these units may have to be ready for mutual interconnections aiming at creating self-sufficient microgrids able to receive and perhaps sustain the national grid, once available. Nevertheless, today in place microgrids are designed and deployed without considering future connection capabilities to the main grid, critically bounding the effectiveness of the electrification process [244], [245].

Effort has been spent to evaluate which is the best planning/design procedure to proper address the rural electrification process [246]–[248]. It is now accepted that off-grid power systems based on Renewable Energy Technologies (RETs) represent the most viable solution in the medium-short term [23], [249]–[251]. Despite *top-down* approach could be more energy efficient and cost-effective in the long term, governmental weaknesses in facing the huge capital investments for power plants and power systems construction, have in the last decades speeded up the diffusion of decentralized off-grid systems (i.e. the *bottom-up* approach) [252]. According to the New Policy Scenarios of IEA World Energy Outlook 2014, stand-alone systems and microgrids (with a ratio of 2 to 1) are expected in fact to provide electricity to 70% of rural dwellers by 2040 [22].

Within off-grid systems, BESS may allow a cost-effective exploitation of RES-E since they help in mitigating both short-term fluctuations (to ensure the instantaneous power balance) and intermediate-term energy deficiency which are typical consequences of unpredictability of RES. Specifically, off-grid systems based on PV and BESS are becoming a solution of great interest for rural electrification. In this regard, three typical applications can be distinguished (Table 9.1):

1. The first application type is *solar home systems* (SHS). SHS are systems typically employed to provide basic power service to a single household, which are composed of PV modules, electro-chemical batteries, charger and end-use appliances. The smallest SHS are solar lanterns, which is a portable device comprising of a PV module up to about 10W, a single battery with a capacity ranging from few to ten Wh and a charge controller. These are *dc* systems with a voltage ranging from 2.4 to

Table 9.1 Typical off-grid applications for electrochemical-batteries and key features

	Application type	Storage capacity range	Power source size range	Typical power source Typical architecture
(1)	Solar Home Systems	from few Wh up to about 10kWh	from few to hundreds of W	PV Stand-alone, *dc*
(2)	Mid-size off-grid PV systems	from tens to hundreds of kWh	from few to hundreds of kW	PV Stand-alone, *ac*
(3)	Micro-grids	from tens to hundreds of kWh	from tens to hundreds of kW	Micro hydropower – Integrated PV, small wind, diesel/petrol generators Isolated grid, *ac*

12V often integrating battery, charger and a LED lamp in a single case [253]. The largest SHS reach up to hundreds of W for PV module(s) and several (tens) kWh battery capacity. When these sizes are employed, systems can be either *dc* or *ac*. In the first case, 12-24V systems can be adopted, while in the second one an inverter is required. Off-grid systems ranging in sizes of SHS are also employed for telecom systems, small schools, clinics, and small commercial activities. Moreover, SHS systems also find applications as a back-up system of the grid for urban area users.

2. The second application type is mid-size off-grid PV systems. They are isolated plants based on PV power sources that supply power to an *ac* system. In this case, PV installations range from a few to hundreds of kW with some larger cases reaching up to 1MW, while BESS capacity ranges from ten to hundreds of kWh. The demand for these systems comes from large households, but mainly from public institutions, schools, health centres, hospitals, small productive initiatives and site-specific activities such as mines, touristic resorts, and telecommunication. PV modules and batteries strings that are connected on a dc bus via solar controller / battery charger compose the basic scheme of these systems. Then *ac* power is supplied to the loads by means of an off-grid inverter. The voltage of the *dc* bus is defined by the inverter and typically increases with the rated power.

3. The third application type is represented by the RES application in *ac* micro-grids which address the power supply for remote villages, large school campuses, and hospitals. Traditionally hydropower systems (from a few to hundreds of kW) have been the main renewable source for micro-grids pending availability of suitable water streams [254]–[256]. These systems are typically designed as *run-off-river* (i.e. no upstream water basin is available) and they often employ electronic load controllers based on dump resistors to provide frequency regulation. Despite this solution goes to the detriment of efficiency (i.e. dump resistors dissipate energy in air or water), it allows having free-maintenance, low-cost and reliable system control. Besides hydropower systems, other RET are appearing in rural areas of SSA thanks to the decrease of costs, the development of technological solutions (mainly for the system control aspects) and the increased policy efforts and availability of suppliers. In fact, micro-grids integrating different energy sources (PV, small wind, petrol/diesel generators) are still rare, but are feasible as for the technological state of the art [247], [257]–[259]. The power size of these systems for rural electrification can range from ten to hundreds of kW while the storage ranges from ten to hundreds of kWh.

Besides the different applications, the study of the optimum sizing of BESS is the one concerning the technical issues regarding off-grid systems [260]. The design process of off-grid systems is not straightforward since it means matching unpredictable energy

sources with unknown or uncertain load demands and, at the end, providing the most favourable conditions in terms of reliability and costs [248], [249].

Off-grid systems design methodologies

Within the scientific literature, there are three main methods to design off-grid power systems [261]. Each of them require data about the user's load and energy resources. These input data may vary in terms of temporal detail and accuracy in measurement or estimation. They are:

▪ *Intuitive sizing methods*, based on simple algebraic relationships between load requirements and energy sources availability over a typical day. These methods have been applied for the sizing of stand-alone photovoltaic power systems for residential usage [262].

▪ E*nergy planning methods*, based on steady-state simulations (typical hourly time-step), heuristic or analytical optimization, and simple modelling of the components. Modelling of the components can be performed with different degree of details [263]. Production and load profiles are usually considered in their stochastic nature to evaluate the influence of different load profiles [264] or different resource profiles [265] on the design process. The most common objective functions are based on the loss of load probability [266] or on the levelized cost of energy [267].

▪ *Real-time power methods*, based on short-term simulations (typical time-steps on second or fraction of seconds) that rely on circuital models of detailed components. With this approach, the knowledge of the electrical power control and energy management strategy need to be well considered. The real-time approach allows to model the electrical and electronic devices as a synchronous generator [268] and converters for a maximum power point tracker [269].

Currently, commercial software based on the above presented methodologies are already available. Sinha and Chandel [270], and Khatib et al [261] reviewed software tools to size up off-grid power systems. *HOMER by NREL* [118] is the most used software for the simulation and optimization of off-grid hybrid power systems. The design optimization model determines the configuration that minimises life-cycle costs for a particular site application. *RETScreen by CANMET* [271] is a renewable energy decision support and capacity building tool. Each RET model is developed in Visual Basic within and individual Microsoft Excel spreadsheet. *TRNSYS by Solar Energy Lab* [272] was originally created to study passive solar heating systems, nowadays the software is also used to model solar energy applications with a very precise unit size. *iHOGA by the University of Zaragoza* [273] is a C++ based software tool that exploits genetic algorithm for the multi or mono-objective optimization of hybrid power systems. *HYBRID2 by WEC-MIT* [274] is a probabilistic/time series computer model that uses statistical methods to perform long-term performance, and economic analyses on various off-grid power system architectures. *SAM by NREL* [275] estimates performance and cost of grid-connected power systems. It runs system simulations over a one-year period, in time steps of one hour, in order to emulate the performance of the system. *PVsyst by PV syst SA* [276] is a software for the study of stand-alone and grid-connected solar systems. It performs hourly simulations of the plant importing weather data from different sources as well as the user-defined data.

However, the above methodologies and software do not consider some of the most important features of the rural electrification process:

▪ *Load consumption uncertainties*: when dealing with rural electrification analyses, information about users' loads is typically unavailable because electric consumptions do not exist or are limited to small sources. Therefore, consumption has to be properly

estimated being one of the main input data for the sizing process. Clearly, such estimates are prone to a significant degree of uncertainty, consequently a stochastic approach is necessary to properly evaluate the distribution of different load patterns the final users may require.

- *Load evolution scenarios*: Even if correctly estimated for an actual condition, an off-grid power system operates for several years (at least 10), and consequently it is not correct to consider a static picture of the user demand. As it is typically done for national energy planning, where different load evolution scenarios are considered, a fortiori analyses of several load demand evolution scenarios would positively affect the design phase even in rural contexts. Not considering this factor may have an impact on the power system reliability and cost-effectiveness over its entire lifetime. The load evolution scenarios can be traced in different ways: (i) by assuming possible socio-economic development trends, (ii) by using local surveys, (iii) by exploiting experts' opinions, (iv) by exploiting countries' energy planning studies [277].
- *Unpredictable energy sources:* off-grid power systems usually rely on RETs, this requires dealing with the energy resource data availability (i.e. mainly solar and wind). Typically, in rural areas of DCs, they have to be estimated by retrieving data from weather stations located in the main cities. Also, several databases, as well as a number of models, are available to facilitate the designer's computation [278]–[280].
- *BESS modelling*: The storage systems are the crucial element of any off-grid systems. System reliability and costs depend mainly on BESS performances and lifetime. Off-grid systems design procedures should implement accurate BESS models in order to embrace the unconventional working conditions in DCs scenarios and provide accurate results. Today the above mentioned commercial software use analytical models since they can provide acceptable results in a short time (see Chapter 4): *TRNSYS* adopts the *Sheperd model* for lead-acid batteries; *Sheperd model* is the reference choice also by *SAM* but with the modification proposed by Tramblay [138]; *HOMER* and *HYBRID2* adopt the *KiBaM model* both for lead-acid and Li-ion batteries; finally, *iHOGA* proposes different options to users for lead-acid batteries: *KiBaM*, *Sheperd model* with modifications proposed by Copetti [137] and *Schiffer model* [183], moreover it includes also three models for Li-ion batteries, with particular attention to LFP and LCO chemistries. No commercial software attempts to implement and compare different BESS modelling approaches for the sizing process of off-grid systems (i.e. stochastic, electric and electrochemical models are not investigated)

Therefore, comprehensive procedures that couple the atypical features of rural contexts (i.e. resources and loads) by including estimation errors into the design phase with proper component models are strongly required. For this reason, the next sections are focused on the proposition of a novel methodology for the robust design of off-grid electric power systems. The procedure wants to be as general as possible providing reliable design outputs by including the majority of available inputs of DCs rural contexts. It starts from microscopic data (i.e. single electric appliances) to effectively capture the targeted customer needs and matches them with the available energy sources of the targeted area. Simulations are carried out for different possible plant configurations and by assuming different BESS modelling approaches (i.e. empirical and electrical) to effectively capture the right final design.

9.2 The proposed methodology

This section introduces the whole procedure that addresses the design of off-grid power systems. It consists of four blocks, each one made of different sub-blocks that

singularly address one particular design phase. The whole methodology is represented in Figure 9.1 and it has been implemented in a tool, namely Poli.NRG tool.

- In the *data inputs gathering* block, all the necessary information regarding users' electric needs, fixed and variable equipment costs and weather data are collected. As regards to load consumption, the block can elaborate data collected through on-field surveys or taken from measurements in similar contexts.
- In the *inputs processing* block, users' electric needs and weather data are processed to obtain load and sources profiles. Specifically:
  - Daily load profiles are obtained by means of *LoadProGen* tool [281] which is able to formulate different realistic daily load profiles starting from field data. *LoadProGen* is based on a stochastic approach, it has been developed in 2015 at the Politecnico di Milano and has been integrated in the Poli.NRG tool.
  - Yearly load profiles are generated by considering intra-week variability and seasonal incidence on the user consumptions. This is done by exploiting *LoadProGen* to generate different "pools of daily load profiles" (e.g. week/winter pool, week/summer pool, weekend/winter pool, etc.) and then by randomly combining them until a yearly profile is obtained.
  - Lifetime load profiles are generated assuming load evolution scenarios over the plant lifetime.
  - Renewable source profiles are formulated according to specific models obtained from wheater stations or from databases.
- In the *system modelling and simulation* block, the operations of the specific off-grid power system are simulated according to specific models of components and dispatch strategies. The simulation engine investigates all the viable plant configurations taking into account the set of possible lifetime load profiles and the Renewable source profiles. This simulator has been implemented by the authors in an algorithm named *OpSim* (Operations Simulator), based on MATLAB.
- In the *output formulation* block, heuristic or mathematical optimization methods are used to find the most *robust design* for the context of analysis. Finally, a post-processing methodology is required to render the obtained results in easier indications or suggestions for decision makers.

In the next sections, each single block of Figure 9.1 is described (dashed blocks are not detailed since under development at the moment of the thesis writing). It is worthwhile to mention that Poli.NRG can be applied to any particular plant architecture
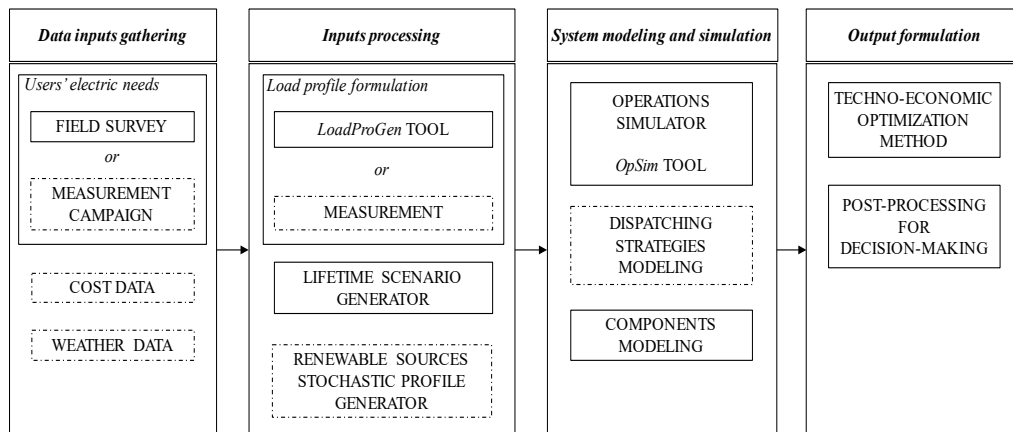

Figure 9.1 Structure of the novel procedure to address the design of off-grid power systems, the Poli.NRG tool

(stand-alone systems, microgrids, hybrid microgrids, off-grid systems with possible main grid interconnections, etc.). In the following, the example of a PV+BESS microgrid is used to detail the main aspects of the procedure.

Field survey

This block defines a set of parameters that allow modelling the users' electric needs (Table 9.2). These are the minimum requirement to compute the load profile(s) of a given group of consumers in rural areas and they can be assumed based on practical experience on similar context conditions or by surveys.

Targeted users are grouped into different user classes. Such classes are defined according to the fact that consumers within a class show a broadly similar demand behaviour. Then basic data regarding any single appliance i within each user class j of N users need to be collected or defined:

- The daily overall time each appliance is on, i.e. the functioning time (h_{ij}).
- The period(s) during the day when each appliance can be in use, i.e. the functioning window(s) ($w_{F,ij}$).
- Each appliance is modelled with its nominal power (P_{ij}). Furthermore, its functioning is considered as *on-off* mode allowing a minimum continuous functioning cycle (d_{ij}).

Measurement campaign

Alternatively to the field survey, a measurement campaign can directly provide the required information in the form of daily load profiles. However, those campaigns are not easy to carry out in rural areas either because there is no power supply at all, or because no measurement instruments are available on the field. Moreover, a significant amount of data (load curves) are necessary in order to properly evaluate the user's energy pattern, consequently, even if available, measures are typically inadequate for a reliable microgrid design.

Cost data

Specific costs of each system components, as well as replacement and maintenance costs, should be included as main inputs of the design procedure. For instance, in the case of an off-grid solar system, data related to PV, battery and inverter costs as well as maintenance costs are required.

Weather data

Weather data are required to allow the computation of RETs energy production. For instance, the mean daily irradiations [kWh/m^2/day] and numbers of cloudy days over the different months have to be provided in the case of a PV+BESS system.

Table 9.2 Parameters for modelling users' electric needs

Parameter	Note
I	type of electrical appliances (e.g. light, mobile charger, radio, TV)
J	specific user class (e.g. household, school, stand shop, clinics)
N_j	amount of users within each class
n_{ij}	amount of appliances within each class
h_{ij}	overall time each appliance is on during a day: *functioning time*
$w_{F,ij}$	period(s) during the day when each appliance can be on: *functioning windows*
P_{ij}	nominal power rate of each appliance
d_{ij}	*functioning cycle*, i.e. minimum continuous functioning time of the appliance once it is on

LoadProGen tool

Daily load profiles formulation is based on *LoadProGen which* has been presented and validated in [281]. It allows considering the uncertainty of the users' energy consumptions. It is based on the users' electric needs defined in the *field-survey*, which are then elaborated in order to introduce uncertainty on the values of functioning times (h_{ij}) and functioning windows ($w_{F,ij}$) respectively. Then, it builds up the coincidence behaviour of the appliances and the power peak value with regards to the correlation between number of users, load factor and coincidence factor.

The load profile of each single user class is formulated as follows:

▪ The total daily electric need of the user class, the possible theoretical maximum power peak and the peak time are computed. Then, the class coincidence factor is calculated according to the empirical correlation existing between the amount of users (N_j), the load factor ($f_{L,j}$) and the coincidence factor ($f_{C,j}$). The obtained value of the coincidence factor is employed to compute a reference value of the class power peak.

▪ The functioning of each appliance is defined by sampling randomly the switching on times within the relative functioning windows. Once the random sampling is carried out for all the appliances of the user class, the functioning of the single appliances are aggregated and the class daily load profile is computed. Then an iterative process is applied so that the resulting power peak matches, assuming a design error, the reference power peak.

▪ Repeating the previous computational steps for each user class and aggregating the different class profiles leads to compute the total daily load profile. The profile is based on a minute time step, i.e. it is constituted by a series of 1440 values representing the average load (W) over a minute. The minute time-step will increase the simulation time, but it will serve to enhance the accuracy of the results, especially for the correct estimation of the BESS performances. Then according to the needs, profiles can be averaged over different time step; typical load profiles for techno-economic sizing of off-grid power systems are based on hourly samples [282], [283].

The adopted stochastic approach formulates different possible load profiles all complying with the given input data. At the moment, the algorithm computes a different load profile each time it is run by acting on:

▪ The stochastic definition of the peak time and the switching on times of each appliance.

▪ The degree of uncertainty in the elaboration of the functioning times and functioning windows, which are key parameters for the electric needs modelling.

Lifetime scenario generator

The scenario formulation is made up of three main steps:

1. The intra-week daily consumption variability has to be addressed. By means of *LoadProGen*, two different daily load profile pools can be generated with respect to two different settings of the electric needs modelling for weekdays and weekends. For each pool, *i* daily profiles are formulated until they represent all the range of profile variations for the given input setting. *I* is the number of profiles *i* such that the relating average profile satisfies a convergence criterion. Specifically, the following conditions to identify the number *I* have been defined

$$\frac{\bar{y}(k)_n - \bar{y}(k)_{i+1}}{\bar{y}(k)_i} \leq 0.25\% \ for \ k \geq 95\% \qquad (9.1)$$

170

$$\frac{\overline{std}[y(k)_n] - \overline{std}[y(k)_{i+1}]}{\overline{std}[y(k)_i]} \leq 0.25\% \; for \; k \geq 95\% \tag{9.2}$$

Where k refers to the profile time steps, $\bar{y}(k)_n$ refers to the average load value of i generated daily profiles at the time step k, and $\overline{std}[y(k)_i]$ refers to the average standard deviation of the load value of i generated profiles at the time step k. I is the number of i profiles that fulfil the two conditions for at least 95% of the time steps.

2. The yearly load profiles are obtained by randomly drawing 365 daily load profiles from the two pools (weekdays and weekends). In this way, it is possible to define a finite number of equiprobable yearly load profiles. Optionally, the seasonal variation can be taken into account by creating more pools for the different seasons.

3. The lifetime load profile has to be created. Each yearly load profile has to be projected over the entire lifetime of the plant according to specific *load evolution scenarios*. By exploiting specific customers' questionnaire or some experts' opinions, different possible trends can be traced. For instance:
   – *linear function*: presuming that the consumption changes linearly during the years;
   – *logarithmic function*: assuming that the users will start to learn how to exploit the new electricity service after the installation, stabilising their consumptions after a while;
   – *step function*: presuming that the consumption will face a sudden change at a specific time due to new future connections;
   – *custom function:* suited to the specific context under analysis.
   – *estimated function:* derived from specific energy planning studies [284], [285].

At the end of the *inputs processing* block, the output can be represented by a 3d matrix (Figure 9.2). Each yearly load profile n, synthesized using the above step 1 and step 2, is projected over the lifetime following the s possible scenarios depicted in step 3. The result is an $n \times s$ lifetime load curves (LC_{ns}) matrix.

Renewable sources stochastic profile generator

By exploiting specific algorithms that generate synthetic hourly solar irradiation or real measured data from weather stations, this block reproduces the incident radiation on the surface of the PV array throughout the year for the specific location.

Components modelling

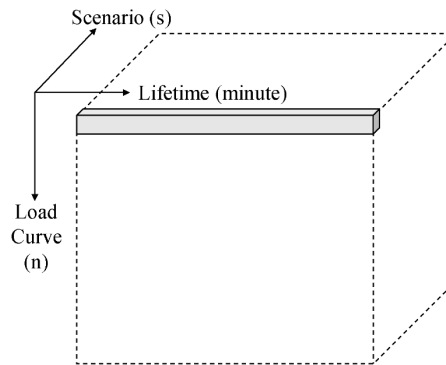This block collects mathematical models of the components. In the case of a

Figure 9.2 3d LC_{ns} input matrix as results of the input processing block

PV+BESS based microgrid, the main equations that define a PV generator, a BESS and an inverter [286], [287] are reported.

The estimation of the PV energy output for each time step k is computed as:

$$E_{PV}(k) = PV_{size} * \left(1 - \rho_T * \left(T_{Cell}(k) - T_{Rif}\right)\right) * \frac{H_\beta(k)}{h} * \eta_{BOS} \qquad (9.3)$$

Where $H_\beta(k)$ is the specific solar irradiation on a tilted surface for the chosen time-step k; PV_{size} is the rated power of the panels at an irradiance h of 1 kW/m^2, an ambient temperature of 25°C and an air mass value of 1,5; ρ_T is the temperature coefficient of power in respect to the solar cell temperature provided by the manufacturer (normally 0.35÷0.45 %/°C); η_{BOS} is the balance of system efficiency which embraces all the losses indirectly related to the sun energy conversion process.

The inverter size is defined according to the power peak occurring within the load profile and by considering the inverter efficiency (η_{Inv}). In fact, it is not the scope of this thesis to investigate more appropriate inverter models, which, however, might be matter of future improvements in the methodology herein presented.

BESS can be modelled with different degrees of details. Storage system modelling is in fact considered crucial for the off-grid system design. Empirical and simplified electric models of BESS are included as options in the Poli.NRG tool. The following section 9.3 is dedicated to detailing the modelling approaches used for BESS.

Dispatching strategies

This block refers to the operation modes which define the interactions of the different power sources in the energy system. In a PV+BESS system this is trivial because all the energy produced by the PV array is exploited by the load, otherwise stored. On the contrary, there are different options if a diesel generator is considered (PV+BESS+Diesel). One option is to switch it on when the BESS is discharged (load-following mode). A second option is to operate it in order to maintain a fixed level of available charge into the BESS (cycle charging mode). A third option is to use the generator to feed some priority loads (dedicated mode).

The simulation of plant operations

This block, which has been implemented in a tool (namely *OpSim*), simulates the off-grid power system lifetime operations. For a given load profile LC_{is} (Figure 9.2) and for given combinations of PV and BESS sizes: PV_{size} and $BESS_{size}$, *OpSim* provides techno-economic performance parameters (i.e. Loss of Load Probability, Net Present Cost and Levelized Cost of Energy) as output.

For each time step k (i.e. minute, $\Delta t = 60s$) of the load and solar resource profiles, the balance between generators energy production (i.e. PV, $E_{PV}(k)$) and loads consumption $LC_{ns}(k)$ is computed. The difference represents the amount of energy that flows through the BESS (charging or discharging):

$$\Delta E(k) = E_{PV}(k) - \frac{LC_{ns}(k)}{\eta_{Inv}} \qquad (9.4)$$

Then the BESS SoC can be updated by the specific BESS model adopted (see section 9.3) in the simulation. In all cases, the SoC is subjected to the following constraints:

▪ To respect the BESS technological limits (SoC levels and/or voltages depending on the BESS modelling approach adopted).
▪ To respect EPR$_{max}$ (maximum EPR) of the BESS. For instance, if the EPR_{max} is 0.5

and the $BESS_{size}$ is 1 kWh, the battery can provide or accept maximum 2 kW during the k time step.

With such constraints, the Loss of Load (*LL*) indicator, which represents the amount of energy required by the load that remains unsatisfied because the system is unable to supply it, is computed as follows:

$$LL(k) = LC_{ns}(k)\big|_{(BESS\ limits)\ V\ \left(\frac{\Delta E}{\Delta t} \geq \frac{BESS_{size}}{EPR_{max}}\right)} \tag{9.5}$$

For each simulation (one configuration of PV_{size} - $BESS_{size}$ within a particular LC_{ns}) the system reliability is considered by computing the *Loss of Load Probability*, which is the share of the electricity demand not fulfilled by the power system over its lifetime (*LT*) [288], [289]:

$$LLP = \frac{\sum_{k=1}^{LT} LL(k)}{\sum_{k=1}^{LT} LC_{ns}(k)} \tag{9.6}$$

Then the *Net Present Cost* (NPC), which is defined as the present value of the sum of discounted costs that a system incurs over its lifetime, is calculated [290]:

$$NPC = Inv + \sum_{y=1}^{T} \frac{CF(y)}{(1+r)^y} - RV(T) \quad [\text{€}] \tag{9.7}$$

$$Inv = c_{BESS}(y_P) * BESS_{size} \tag{9.8}$$

Where *I* is the initial investment cost that is proportional to the installed capacity E_n given the specific cost of BESS (see Appendix D). *CF(y)* is the net cash flow during the year y and $(1+r)^y$ is the discount factor. *RV(T)* represents the residual value of the assets (i.e. BESS) at the end of the investment term T as per Appendix D. Cash flows can be computed by accounting for penalties and replacement costs:

$$CF(y) = O\&M(y) + C_R(y) \tag{9.9}$$

Where *O&M(y)* are the operation and maintenance costs, while $C_R\ (y)$ accounts for replacement costs of BESS by taking into account the projected BESS cost at a specific year y (see Appendix D).

Moreover, the *Levelized Cost of Energy* (LCoE) is also computed since it is a convenient indicator for comparing the unit costs of different technologies over their life, and it is a reference value for the electricity cost that rural consumers would face [291], [292]. Moreover, it has also been employed as an objective function in a number of analyses that deal with renewable-based off-grid power systems (e.g. [293]–[295]):

$$LCoE = \frac{r * (1+r)^T}{(1+r)^T - 1} * \frac{NPC}{(1 - LLP) * \sum_{k=1}^{LT} LC_{ns}(k)} \quad [\text{€}/kWh] \tag{9.10}$$

Techno-economic optimization method

In order to manage the microgrid *robust design,* a heuristic optimization method has been developed (Figure 9.3). This method is able to find the optimal solution according
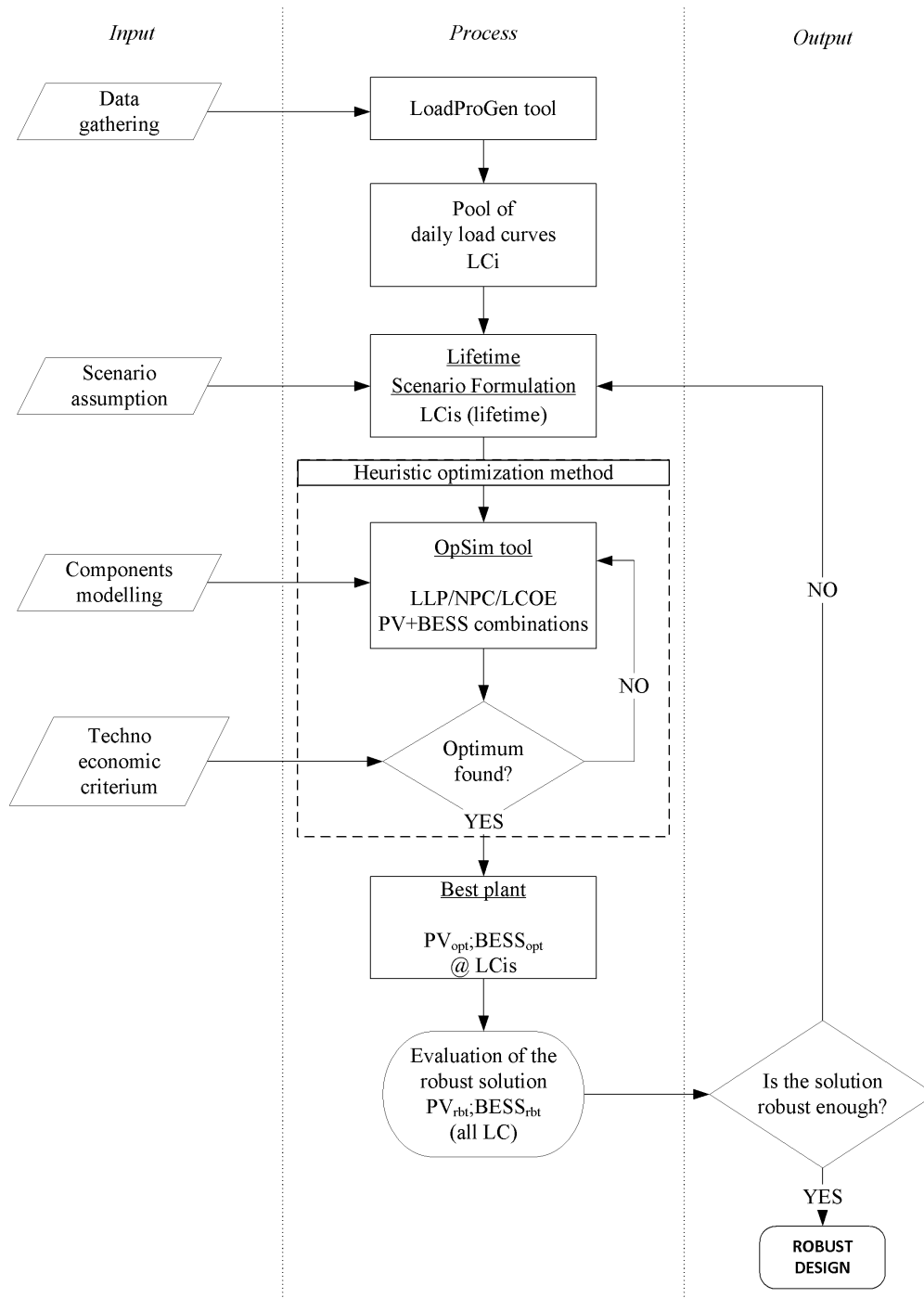
Figure 9.3 Poli.NRG procedure flow-chart for the robust design of PV+BESS based microgrid

to the techno-economic criterion by running the *OpSim* tool in an iterative way, by testing different combinations of the sizes of components (PV and BESS). The optimal solution is the specific combination of the sizes of components (PV_{opt} ; $BESS_{opt}$) which have the minimum NPC value while fulfilling the desired level of LLP [286].

The heuristic optimization method is based on a two step algorithm:

1. Definition of the searching space, i.e. the ranges of PV and BESS to be investigated.

2. Searching of the optimal combination within this searching space through an iterative process.

As regards to the first point, the minimum size of the PV plant has to be sufficient to produce the load consumption (including the acceptable loss of load):

$$PV_{min} = \frac{(1 - LLP) * \min\left(\sum_{k=1}^{LT} LC_{ns}(k)\right)}{\sum_{k=1}^{LT} E_{PV}(k)}$$

(9.11)

where the denominator is the total amount of energy produced during the system lifetime and the numerator includes the minimum amount of energy required by the load (considering all the scenarios under evaluation). The maximum size of the PV can be set as a multiple of the maximum power required by the load:

$$PV_{max} = w_{PV} * \max(LC_{ns})$$

(9.12)

where w_{PV} is a scaling factor that overestimates the size of the PV (with the purpose of adapting the searching space to the magnitude of the problem).

With respect to BESS, the minimum size is considered equal to zero, while the maximum size is considered as a multiple of the mean daily energy consumption (in order to consider the presence of a number of consecutive cloudy days).

$$BESS_{min} = 0$$

(9.13)

$$BESS_{max} = w_{BESS} * E_{load}^{day}$$

(9.14)

Where w_{BESS} is a scaling factor to overestimate the size of the storage system.

As regards to the second step, a heuristic procedure is used to look for the optimal combination (PV_{opt} ; $BESS_{opt}$) in agreement with the techno-economic criterion. The adopted algorithm is based on the imperialistic competitive algorithm [296].

The method employs an iterative process that progressively explores the searching space as shown in Figure 9.4. Two parameters characterize the algorithm: the number of
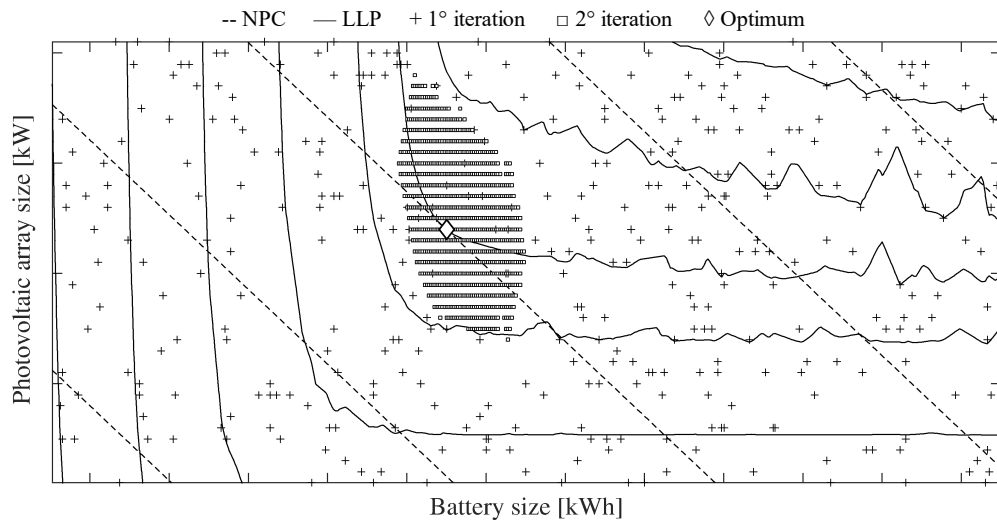

Figure 9.4 Heuristic optimization method based on LLP and NPC curve estimation.

combinations of PV-BESS that have to be evaluated in each iteration, and the number of combinations that after each simulation of the lifetime operations are considered as the best ones. When considering the first load profile, a number of combinations of PV-BESS (Z_{combs}) are selected randomly within the searching space (combinations with symbol + in Figure 9.4) and, for each of these configuration, *OpSim* computes the couple LLP and NPC. This allows to create a first scattered (i.e. first iteration) matrix of LLP (solid black line) and NPC (dotted black line) values: an estimation of the probable optimal solution can be carried out. The purpose of the following iterations (i.e. second iteration) is to explore the surrounding PV-BESS combinations to check if the solution can be confirmed or improved. For instance, in the second run of *OpSim tool,* the PV-BESS combinations that have to be simulated are the ones identified previously plus a number of combinations selected randomly around them (combinations with symbol □ in Figure 9.4). In this way, a better estimation of the LLP and NPC is available and the vector of best options can be updated. The optimal solution (PV_{opt} ; $BESS_{opt}$) is found where the line of maximum LLP is tangent with the minimum possible NPC (symbol ◊ of Figure 9.4)

Finally, the same heuristic procedure is repeated for the next *n* lifetime load profile LC_{ns} (see Figure 9.2) by fixing the evolution scenario *s*. The new optimum points are likely to be different because of the different load profile. Consequently, the optimum points create an *area of solutions* instead of a single deterministic solution. The most *robust solution* (PV_{rbt} ; $BESS_{rbt}$) within the area of solutions is computed as the most frequent solution among the obtained optimal solutions (PV_{opt} ; $BESS_{opt}$) for each simulated lifetime load profiles.

New *n* lifetime load profiles LC_{ns} are tested until a specific convergence criterion is fulfilled. *N* is the number of profiles *n* such that the simulation of a new LC_{ns} would not increase the robustness of the solution. Specifically, the following convergence conditions to identify the number *N* are defined:

$$\frac{std[\, PV_{rbt}(n-1,s)] - std[\, PV_{rbt}(n,s)]}{std[\, PV_{rbt}(n-1,s)]} \leq j_{conv} \; \forall \; scenario \qquad (9.15)$$

$$\frac{std[\, BESS_{rbt}(n-1,s)] - std[\, BESS_{rbt}(n,s)]}{std[\, BESS_{rbt}(n-1)]} \leq j_{conv} \; \forall \; scenario \qquad (9.16)$$

Where (*std[PV$_{rbt}$(n,s)]* ; *std[BESS$_{rbt}$(n,s)])* indicates the standard deviations of the *robust solution* given the new *n* simulated profiles over the given scenarios *s*. *N* is the number of *n* profiles at which the *robust design* is defined.

Finally, according to the different evolution scenarios *s* and following the same method, different a*rea of solutions* can be computed in parallel. This recursive process will create a *map of solutions* in the searching space that shows how the *robust design* changes due to future change in the electric consumptions (i.e. scenarios of load evolution).

It is worthwhile to mention that the above recursive procedure is complex and time-consuming. A non-negligible simulation time is required to complete a set of simulations for a given load profile *n*. Z_{combs} plants have to be simulated (with minute time-steps) over the entire lifetime of the plant (e.g. 20 years) for each load evolution scenario. This brings about issues related to the modelling of the components which have to be reliable and simple at the same time, in order to have a correct compromise between robustness of the solution (enhanced by a proper modelling phase) and simulation-time.

Post-processing for decision-making

An analysis of the results for each scenario is carried out to support the decision maker's choice. In particular, the obtained *robust solutions* are compared with respect to:

- The variation in the load consumption required by customers;
- The variation on the sizing of the system components due to the different scenario hypotheses assumed;
- The variation on the LCoE among the different scenarios given a fixed level of LLP.

The purpose of this step is to provide the decision-makers with more detailed information in order to identify the design of the off-grid power system that best suits the targeted context.

9.3   BESS models adopted

For application of EES within electrification approaches in DCs, selecting the best technology in terms of performance and durability is not the top priority; but cost and availability on site play a relevant role in the final decision. Therefore, the battery technology choice is usually defined by the economic capacity of the donor or investor. Thus, lead-acid batteries (In particular VRLA), which have benefited from years of development with inevitably cost reduction and global spread, still represent the most appropriate choice for all the applications (SHS, mid-size PV systems, micro-grid, and grid-ties back-up systems) [24], [25].

As regards to lithium batteries, they are rarely seen in DCs applications despite leveraged kWh costs of Li-ion BESS are comparable to lead-acid batteries (when considering the higher depth of discharge, lifetime and number of cycles) [17]. The initial investment cost is a barrier for both investors and donor agencies. However, due to the current experienced reduction in the overall cost of lithium-ion technology (Figure 1.2-B), it is presumable to forecast that Li-ion BESS will have a relevant share in the sector of off-grid system in the near future. In this section, Li-ion is chosen as technology of reference for the BESS modelling phase within the methodology for the robust design of off-grid power systems. Specifically, the following models are based on the Li-ion LNCO chemistry from the Boston Power SWING5300 [107] which has been used for the modelling phase of Chapter 6 and aging modelling of Chapter 7.

As already mentioned for grid-tied applications in section 8.3, BESS models are of fundamental relevance for obtaining reliable information which would support the decision makers and lead to investment decisions. SoC and SoH from the BESS model are in fact used to estimate LLP and NPC which are the indicators at the basis of the techno-economic analysis of section 9.2.

Two different BESS modelling approaches will be compared: empirical and electrical. In both cases, BESS models will have to fulfil the energy balance *ΔE(k)* between production (PV) and demand (load) and update SoC and SoH indicators. The differences lie in the way in which the SoC and SoH are estimated (i.e. the modelling approach). Eventually, these differences will result in marked deviations in LLP and NPC estimations. Main task of this chapter is to verify the sensitivity of different modelling approaches on the robust design evaluation. Specifically, two different empirical models (model 1 and model 2) are developed and compared with one electrical model (model 3)

Given the complexity of the simulations, both models are based on the steady-state operations of BESS. This fact will affect the electrical model which has to be simplified accordingly. High dynamic responses of the BESS are in fact neglected in favour of faster simulation time.

The empirical models

In the empirical model, BESS is modelled as an ideal storage system (see Chapter 4). The main features are the SoC limits (SoC_{min} and SoC_{max}), charge (η_C) and discharge (η_D) efficiencies, minimum SoH (SoH_{min}) and capacity fade index cf (i.e. the loss of SoH per cycle as introduced in section 7.1). Moreover, the energy stored in the battery needs to be updated based on the amount previously stored ($E_{BESS}(k-1)$) as follows:

$$E_{BESS}(k) = \begin{cases} E_{BESS}(k-1) + \Delta E(k) * \eta_C , & \Delta E(k) > 0 \\ E_{BESS}(k-1) + \dfrac{\Delta E(k)}{\eta_D} , & \Delta E(k) < 0 \end{cases} \qquad (9.17)$$

At this point, the two proposed empirical models are differentiated as regards to the efficiency values:

- Model 1 assumes a fixed value of round-trip efficiency $\eta_{RT}= 95\%$ as claimed in literature and/or the manufacturers' data for similar studies. Symmetry in charge/discharge processes is used to derive η_C and η_D as per equation (8.14).
- Model 2 assumes a variable value of efficiency linked to the operating conditions during the specific time-step k. The reference trend is derived from the performance tests of Figure 7.5 where the efficiency is function of the registered C-rate[19].

Then, the new state of charge (SoC) is computed based on the previous value:

$$SoC(k) = SoC(k-1) \pm \frac{E_{BESS}(k)}{BESS_{size} * SoH(k-1)} \qquad (9.18)$$

Where SoH(k-1) represents the assumed aging state of the BESS during times step k (details about SoH computation are presented below).

LL can be updated as per equation (9.5). In detail:

$$LL(k) = LC_{ns}(k)\Big|_{(SoC < SoC_{min}) V \left(\frac{\Delta E}{\Delta t} \geq \frac{BESS_{size}}{EPR_{max}}\right)} \qquad (9.19)$$

The electrical model

Given the high accuracy demonstrated with the electrical model of Chapter 6, it is worthwhile to analyse the opportunity of using this modelling approach in energy planning analyses, especially to understand the discrepancies (if any) with the empirical models. However, the electrical model should be "adapted" for the sake of the purposes of the herein proposed methodology. Very long simulations (minute time-steps along the whole plant lifetime for several different LCs and scenarios) in fact make the use of the full electrical model developed in Chapter 6 unsuitable. However, proper simplifications can bring to a sustainable compromise between an acceptable simulation time and a higher accuracy.

Therefore, the electrical model (model C) proposed is based on two main assumptions

1. The analysis are carried out at the cell level. Power input from PV/load energy balance are scaled down in a way that the macroscopic effect at BESS level are preserved to

---

[19] C-rate is approximated by the E-rate. E-rate is defined as:

$$E - rate = \frac{\frac{\Delta E(k)}{\Delta t}}{BESS_{size}}$$
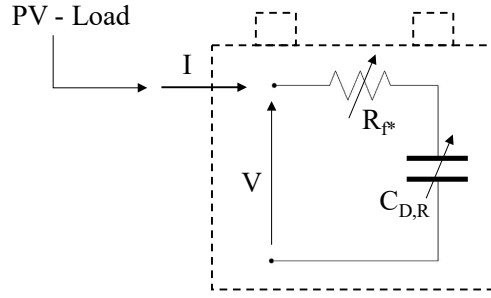
Figure 9.5 simplified electrical model adopted in the proposed methodology
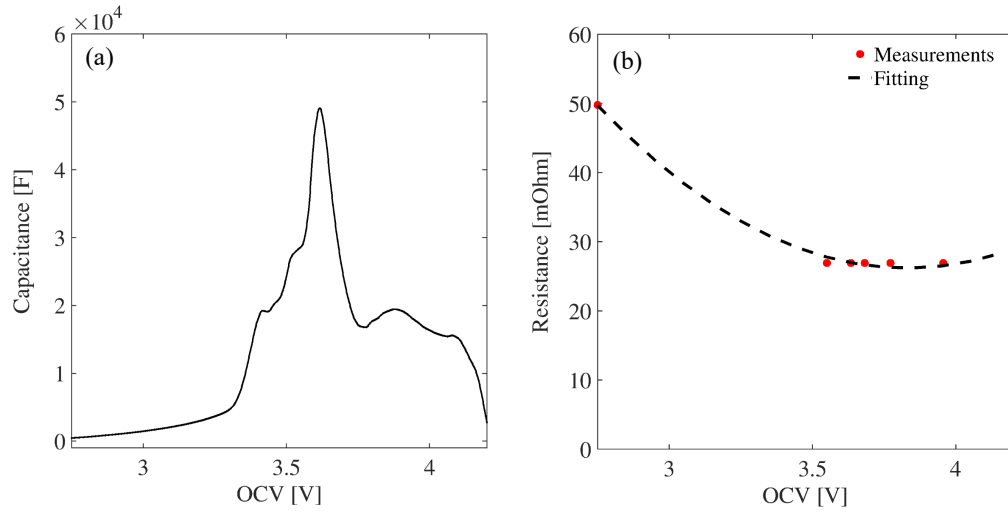
Figure 9.6 simplified R-C circuit assumptions: parameters $C_{D,R}$ (a) and R_{f*} (b) as function of the OCV (i.e. SoC)

the cell level.

2. The cell model is a substantial simplification of the full dynamic model presented in Figure 6.3 which is reduced to a two-elements model: the R-C series circuit of Figure 9.5. Specifically:

   – The resistance R_{f*} is used to describe the cell overpotential in regime conditions (i.e. power performances). It represents the equivalent resistance of the cell at a characteristic frequency $f*$ that depends on the typical input profile. Given the minute time-step ($\Delta t = 60s$), the BESS will never be subjected to solicitations faster than 60s in the simulations. The resistance is measured at the correspondent characteristic frequency (i.e. around 16 mHz) and mapped at the different SoCs. Figure 9.6-B shows the measurements of R_{f*} and the assumed quadratic fitting function[20] (see section 6.4) in fresh cell conditions:

$$R_{f*} = a_0{}^* + a_1{}^* V_{oc} + a_2{}^* V_{oc}{}^2 \tag{9.20}$$

   – The capacity $C_{D,R}$ represent the total capacity (i.e. energy performances) of the cell as detailed in section 6.2. The assumed IC curve is presented in Figure 9.6-A as

---

[20] With $[\,a_{2*},;\ a_{1*};\ a_{0*}\,] = [0.0201;\ -0.1543;\ 0.3217]$
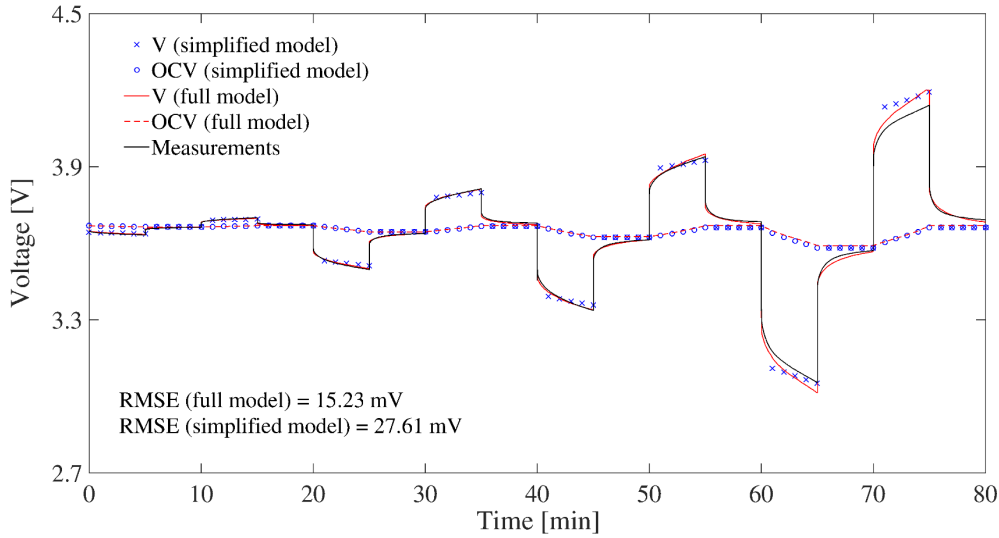
Figure 9.7 Simulated and measured voltage of the BOSTON POWER SWING5300™ cell when cycled with the slow *square current profile test* of section 6.4 (Figure 6.13). Four current steps (0.1C, 0.5C, 1C and 2C) of 5 minutes charge and discharge with a 5 minutes resting period at SoC =50%. Comparison between the full dynamic model of Chapter 6 and the simplified model of chapter 9

the average of the measured IC curve during sub-procedure D of the aging test of Chapter 7 (cell in fresh conditions).

Validation of the simplified model is presented in Figure 9.7 where it is compared with the full electrical model of Chapter 6 in reproducing cell response measured during the *square current profile* of section 6.4. As expected, a simplified model is unable to follow precisely the transitory subsequent to current variations. However, it can reproduce the steady-state behaviour of the terminal voltage and can accurately estimate OCV and therefore SoC. RMSE is 45% higher but acceptable in energy planning analyses like the one proposed in this chapter.

During simulation, a constant power is assumed to compute the current $I(k)$ that flows through the cell model:

$$I(k) = \frac{\frac{\Delta E(k)}{\Delta t}}{V(k) \cdot \frac{BESS_{size}}{E_{n,cell}}} \qquad (9.21)$$

Where the ratio at the denominator represent the number of equivalent cells inside the BESS and is used as the scaling factor to shift the calculation at cell level.

The open circuit voltage $V_{oc}(k)$ and $V(k)$ can be updated at instant k by accounting for the capacitance value $C_{D,R}$ and R_{f*} at the previous time-step.

$$V_{oc}(k) = V_{oc}(k-1) + \frac{I(k)}{C_{D,R}(k-1, V_{oc}(k-1))} \Delta t \qquad (9.22)$$

$$V(k) = V_{oc}(k) + R_{f*}(k-1, V_{oc}(k-1))I(k) \qquad (9.23)$$

SoC(k) indicator is directly derived from $V_{oc}(k)$ as detailed in Figure 6.11. Aging is accounted by $C_{D,R}$ and R_{f*} parameters: the SoH and SoR indicators are used to update both parameters during lifetime.

LL can be updated as per equation (9.5). In this case, BESS limitations are linked to the cell voltage limits rather than SoC limits:

$$LL(k) = LC_{ns}(k)\big|_{(V < V_{min})\, V\, \left(\frac{\Delta E}{\Delta t} \geq \frac{BESS_{size}}{EPR_{max}}\right)} \tag{9.24}$$

Lifetime modelling

As emerged in equations (9.18), (9.22) and (9.23) there exist dependencies on the SoH indicator. Aging phenomena are in fact taken into account in empirical and electrical models. Firstly, the cycles number registered during the time-step is computed as follows:

$$cy(k) = \frac{SoC(k) - SoC(k-1)}{2} \tag{9.25}$$

where *cy = 1* means that one full charge/discharge cycle has cycled through the BESS. SoH can be then updated:

$$SoH(k) = SoH(k-1) \pm cy(k) \cdot cf(k) \cdot \tag{9.26}$$

When *SoH(K) = SOH_{min}* the battery is assumed dead and replaced. *CF(y)* are updated as per equation (9.9) assuming replacement cost C_r (i.e. NPC estimation).

As regards to the capacity factor (*cf*), the three models are differentiated:

- Model 1 assumes constant *cf* which is based on the maximum number of cycles as claimed in literature (see equivalent full cycles to failure method in section 4.3) and/or the manufacturers' data for similar studies [132].

$$cf(k) = \frac{1 - SoH_{min}}{cy_{max}} \cdot \tag{9.27}$$

For instance, if *cy_{max}* = 5000 and *SoH_{min}* = 80%. *cf* will result in 0.004%/cycle.

- Model 2 and Model 3 assume a variable value of *cf* which is linked to the operating condition during the specific time-step *k*. *cf* is computed each time-step *k* by following the expression shown in Figure 7.8.

Once updated, the SoH indicator is used differently among models:

- Model 1 and Model 2: use SoH to update the BESS energetic content as shown in equation (9.18).
- Model 3: is based on the "hybrid approach" detailed in section 7.3. R and C parameters are updated each time-step accounting for capacity fade and power fade (i.e. resistance increase) phenomena. The IC curve of Figure 9.6-A is scaled proportionally to the SoH indicator (accepting the limitations discussed in Figure 7.10):

$$C_{D,R}(k) = C_{D,R} \cdot SoH(k) \tag{9.28}$$

While the resistance function of Figure 9.6-B is multiplied by the SoR indicator that accounts for the resistance increase at the time-step *k*:

Table 9.3 Main characteristics of the BESS models adopted in the proposed methodology

Model #	Model name	SoC estimation	SoH estimation
M1	Empirical(FIX)	– SoC limits – $\eta_{RT} = 95\%$	– $SoH_{min} = 80\%$ – cf = fix – cy_{max} = fix
M2	Empirical(VAR)	– SoC limits – η_{RT} = f(c-rate)	– $SoH_{min} = 80\%$ – cf = f(c-rate)
M3	Electrical	– Voltage limits – R_{f*} = f(SoC, SoR) – $C_{D,R}$ = f(SoC, SoH)	– cf = f(c-rate) – rf = f(c-rate)

$$R_{f*}(k) = R_{f*} \cdot SoR(k) \tag{9.29}$$

$$SoR(k) = SoR(k-1) \pm cy(k) \cdot rf(k) \cdot \tag{9.30}$$

Where *rf* is the resistance increasing factor that depends on the operating conditions during the specific time-step *k*. *rf* is computed each time-step by following the expression shown in Figure 7.9-B

Table 9.3 resumes the main assumptions of the three models adopted in the simulations.

9.4 Case study

The methodology of section 9.2 and the different BESS models of section 9.3 have been merged in the Poli.NRG tool and implemented in MATLAB®Simulink® (Figure 9.8). The methodology has been used to run different sets of simulations which are detailed in the following.
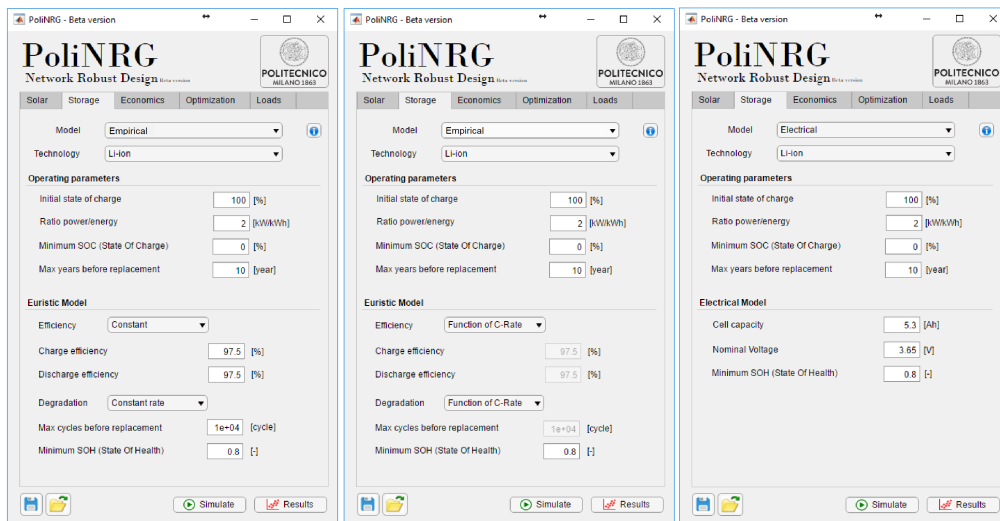
Figure 9.8 The Poli.NRG MATLAB® user interface - storage section. Settings are shown for the three BESS models adopted: M1 (left), M2 (centre) and M3 (right)
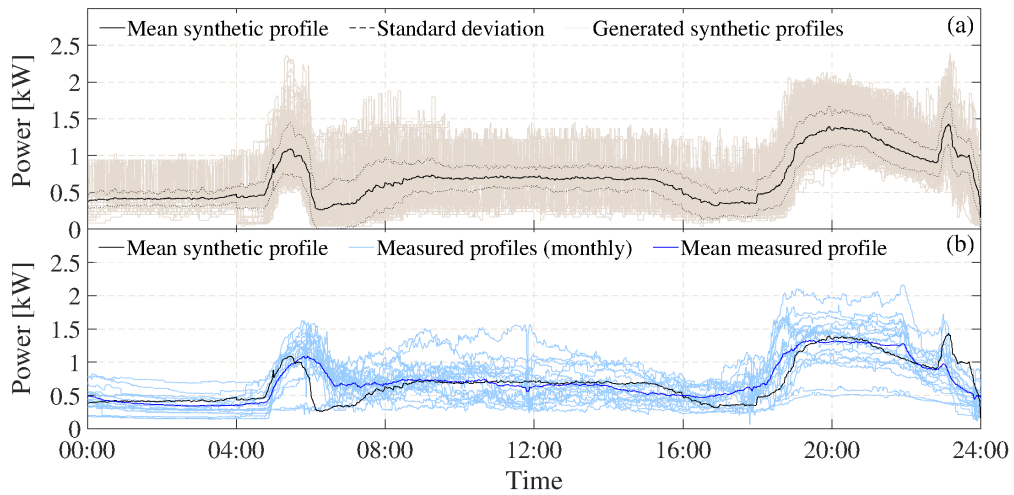
Figure 9.9 (a) Synthetic load profiles (grey), mean synthetic profile (solid-black) and standard deviation (dotted-black); (b) Comparison between the mean synthetic profile (black), measured monthly average profiles (light blue) and average measured profile (blue)

In the following, such procedures have been applied to design a "theoretical" new micro-grid capable of "optimally" feeding the Ngarenanyuki Secondary School which was involved in the *Energy4Growing* project (Annex A). The micro-grid is assumed to be based on PV generators coupled with BESS of lithium-ion technology.

Thanks to a specific survey, the electric needs of the Ngarenanyuki school have been collected. Data related to the number and the type of appliances in use, their nominal power, and some qualitative information about the users' behaviour with respect to each appliance are presented in Annex F.

On this basis, *LoadProGen* has been used to formulate different possible realistic load profiles LC_{is} to be used in the simulations. Figure 9.9-a depicts in grey the aggregation of all the N synthetic profiles, whilst it reports in solid and dotted black lines the average profile and the standard deviation around the average value respectively. The high variability in the collected data is preserved in the synthetic load curves. Figure 9.9-b compares the mean measured profile with the mean synthetic profile. Profiles are similar.

Figure 9.10 Daily irradiation values for Ngarenayuki (Tanzania) GPS coordinates [297]

Table 9.4 Parameters adopted in the simulations with Poli.NRG tool

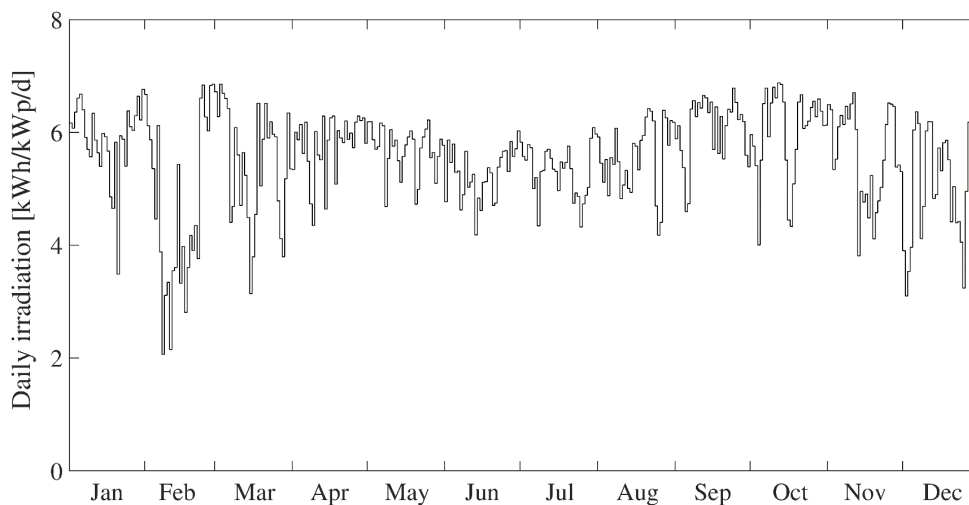| Parameter	Parameter name / note	Value
Economics		
Plant lifetime	LT	20 y
LLP target value	% of total load	5 %
PV modules cost	Monocrystalline	2500 €/kW
Battery cost (replacement)	Lithium-ion	Appendix D
Off-grid inverter cost	-	900 €/kW
Other investment costs	% on the main component costs	20 %
O&M cost	-	100 €/kWy
Discount rate	r	6 %
Components		
Balance of system efficiency	η_{BOS}	85 %
Inverter efficiency	η_{Inv}	90 %
BESS(M1-2-3) - Minimum SoH	SoH_{min}	80 %
BESS(M1-2-3) - Starting SoH	SoH_{start}	100%
BESS(M1-2-3) – Maximum lifetime	$LT_{BESS,max}$	10 y
BESS(M1-2-3) - Max Energy to Power ratio	EPR_{max}	0.5
BESS(M1-2) - Minimum SoC	SoC_{min}	0 %
BESS(M1-2) - Maximum SoC	SoC_{max}	100 %
BESS(M1-2) - starting SoC	SoC_{start}	100 %
BESS(M1) - Round-trip efficiency	η_{RT}	95 %
BESS(M1) - Maximum number of cycles	cy_{max}	Variable
BESS(M3) - Minimum Voltage	V_{min}	2.75 V
BESS(M3) - Minimum Voltage	V_{max}	4.2 V
BESS(M3) - starting OCV	OCV_{start}	4.2 V
BESS(M3) – starting SoR	SoR_{start}	100 %
Simulation settings (OpSim tool)		
Time step	Δt	60 s
Maximum number of Load profile	N	100
PV-BESS combinations	Z_{combs}	1000
Number of scenarios	S	6
Convergence criterion	j_{conv}	0.5 %
PV minimum size	PV_{min}	2 kW
PV maximum size	PV_{max}	6 kW
PV step size	PV_{step}	0.05 kW
PV scaling factor	W_{PV}	3
BESS minimum size	$BESS_{min}$	1 kWh
BESS maximum size	$BESS_{max}$	35 kWh
BESS step size	$BESS_{step}$	0.05 kWh
BESS scaling factor	w_{BESS}	2

Moreover, The mean synthetic profile is almost in the centre of the family of real measured profiles, meaning that the load for the case study is represented in an effective way.

Currently, the data collected in and on the field clearly depict how in a real-life scenario of DCs that there is not a single, clear, load profile, but loads change over time with respect to several factors. For these reasons, seasonal and intra-week variabilities have been neglected: no clear trends have been detected at this stage of the

Energy4Growing project. Thus, in agreement with the proposed methodology, different yearly load profiles have been generated by sampling from the synthetic profiles. Then each of the yearly load profile has been extended over the entire plant lifetime (20 years) according to six evolution scenarios. A linear increase of the yearly load profile with different increasing factors (from 10% to 50%) has been assumed. For instance, having an increasing factor of +10% means that at the end of the plant lifetime the load demand is forecasted to be 10% higher if compared to the first year of deployment.

As regards to the solar resource, approaches validated in [298] and available dataset published in [297] have been used to derive the profile for the simulations. Figure 9.9 reports the resulting daily irradiation profile for the Ngarenanyuki coordinates. The method employed is capable of taking into account the variability of the solar resource throughout the year. For instance, lower values of irradiation are expected in February and November, in correspondence to the rainy seasons.

Technical and economical parameters in the simulations are reported in Table 9.4. Cost information about PV modules, batteries, and off-grid inverters are the result of a survey among Tanzanian local suppliers, while O&M, other investment costs and modelling parameters (efficiencies mostly) have been estimated based on experience.

For each single lifetime profile and scenario LC_{is}, *OpSim* tool has been used to simulate all the possible configurations of PV-BESS. Specifically, the simulations were performed in MATLAB® by ranging the V array size from 0 to 6 kW ($w_{PV} = 3$) with a 50 W step and a BESS size from 0 to 35 kWh ($w_{BESS} = 2$) with a 50 Wh step. Then, the PV-BESS combination that results in having the minimum NPC while respecting a maximum LLP of 5% is identified as the optimum solution for the given LC_{ns}.

9.5 Simulations, results and discussion

Below, the results obtained by running different simulations through the Poli.NRG tool are presented. Specifically, the discussions will be focused on two different layers of analysis:

1. <u>Micro-grid simulation with different BESS models</u>. A detailed comparison between the different BESS models proposed in Table 9.3 is presented. Two are the modelling approaches compared: empirical (M1 and M2) and electrical (M3). As regards to M1, two different values for the maximum number of cycles (cy_{max}) are tested: (i) $cy_{max} = 10,000$ to reproduce the highest value claimed in literature for Li-ion technology (see Chapter 3) and (ii) $cy_{max} = 3,000$ which represent more reliable data which belongs to the Li-ion LNCO chemistry [107]. Simulations will demonstrate the high impact of the BESS modelling approach on SoC and SoH estimations.
2. <u>Micro-grid robust design</u>. The focus is on the micro-grid robust design as proposed in the novel procedure of section 9.2. Again, results will show how different BESS models will bring to different optimal plant configurations.
3. <u>Scenario-based design criteria for decision making</u>. The attention is moved to increase robustness of design solutions by accounting for load evolutions during plant lifetime, a fundamental factor in DCs. Simulations are repeated for several scenarios to create the *map of solutions*: a map for investment evaluations in the hands of the decision makers.

Micro-grid simulation with different BESS models

The first level of analysis does not deal with optimal design (i.e. PV-BESS sizes able to fulfil the load with the desired LLP at the minimum NPC) but in understanding how the assumed BESS modelling approaches of section 9.3 behave in reproducing micro-grid operations. Therefore, different configurations of the plant have been simulated in

Table 9.5 Hypotheses adopted to simulate different PV-BESS plant configurations with Poli.NRG tool

Hypothesis	BESS$_{size}$ [kWh]	PV$_{size}$ [kW]
Small plant	1	4
Medium plant	10	4
Big plant	100	4

order to compare the BESS models within the novel procedure for the robust design of off-grid systems. Table 9.5 shows the different hypotheses: (i) *hypothesis small* represents a small plant with a very small BESS and a very high probability to incur in high LoL; (ii) *hypothesis medium* represents a medium plant with a BESS of size comparable with the load and solar resources, very close to the optimal design; (iii) *hypothesis big* represents a big plant with an oversized BESS and a high probability of sustaining 100% of the load.

Figure 9.11 exemplifies the impact of the hypotheses of Table 9.5 on the simulations. The month of February is chosen as reference since it is characterized by high variability in the solar resources (Figure 9.10). Given the same PV profile and load profile for all the simulations, BESS behaves differently according to the correspondent hypothesis (i.e. configuration of the plant). The power to be delivered by the BESS is the same for the three simulated plants; however, the operating rate (E-rate) is the highest for the smallest BESS of *hypothesis small* (blue line) and lower for the larger BESS of *hypothesis medium* (red line) and *hypothesis big* (yellow line). Higher E-rates will clearly impact on the LoL and on the replacement costs making the hypothesis not afffordable from a techno-economic point of view. In the same way, a very big BESS (*hypothesis big*) will provide a very low LoL but at a very high cost (i.e. investment costs) that would make the configuration not convenient as well. This motivates the procedure proposed in section 9.2 that looks at the best configuration of the plant that satisfy a predefined level of LoL at the minimum NPC.

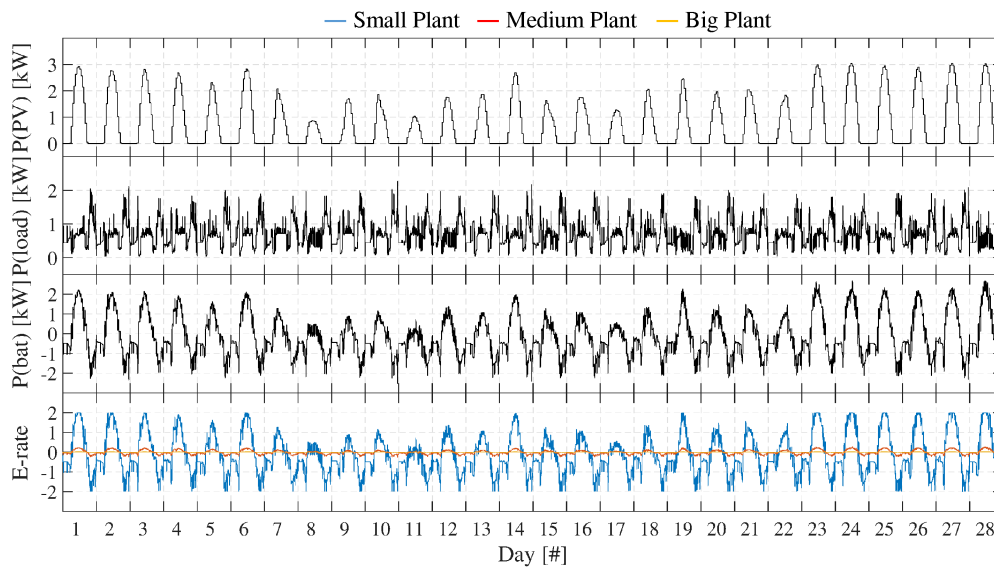Hypotheses of Table 9.5 will have different impacts according to the BESS modelling

Figure 9.11 Simulation results for the month of February of year 1 with empirical model M1: assumed photovoltaic and load power profiles; simulated BESS power profile; and operating rate derived for the hypotheses of Table 9.5.
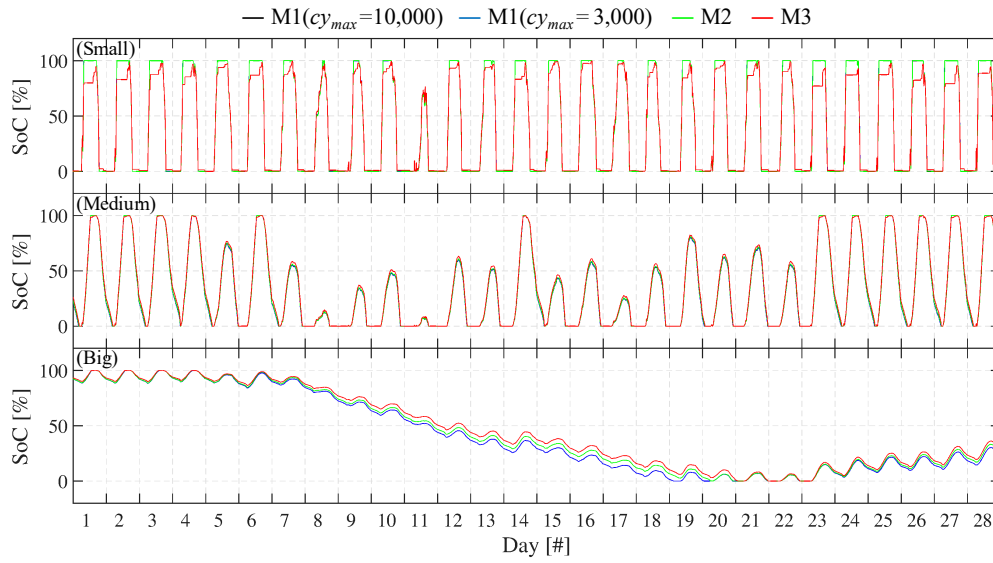
Figure 9.12 Simulation results for the month of February of year 1 with different BESS models: estimated SoC trends for the hypotheses of Table 9.5.

approach adopted. Figure 9.12 shows SoC trends for the four different models proposed (Table 9.3). The two empirical M1 (black and blue lines), which represent BESS with fixed efficiency and a fixed number of maximum cycles cy_{max}, are overlapped: differentiation will emerge due to aging and therefore after years. The empirical M2 (green line), which represents BESS with a variable efficiency and lifetime with the operating conditions, emerges in *hypothesis medium* and *hypothesis big*. It results that M1 overestimates the discharge profile: the assumed constant efficiency is probably too severe and it does not take into account the specific operating conditions. This is clearly a limitation of simplified models which use literature data and datasheet to set the parameters of the model. The differences between M1 and M2 do not emerge in *hypothesis small*. In this case, the simulated plant is undersized, consequently the BESS immediately saturates to its limits hiding the differences in SoC estimations. Even M2 cannot consider the high operating rates of *hypothesis small* in the SoC estimation. In general, this is a limitation of all empirical models which do not account for real technological limitations (i.e. voltage limits). Conversely, the electrical model M3 (red line) differs significantly from the empirical models. Charging phases stops at a low level of SoC due to exceeding voltage limits. The same happens in discharge phases, affecting the LoL estimation.

Figure 9.13 shows SoH trends along the plant lifetime. Sudden changes in the SoH indicator highlight replacements during the years. In this case, the two M1 models differentiate due to the different cy_{max}. Higher cy_{max} clearly means less replacements. However, empirical models, which relate to the SoH estimation only on the maximum number of cycles as per equation (9.27) without considering any cycling conditions, may end up in incorrect SoH estimations. This is clearly visible in case of *hypothesis small* (undersized BESS). The operating rate is so stressful (see E-rate in Figure 9.11) that it will certainly impact on BESS aging. It is almost impossible that BESS will last more than 10 years as suggested by M1 (black line), being replaced only because of reaching the maximum BESS lifetime $LT_{BESS,max}$. Therefore, empirical models totally rely on assumptions about BESS aggregated parameters (i.e: efficiency and maximum cycle numbers), which should be appropriate with respect to the final application. This is the case of the second assumption on M1 where the assumption of $cy_{max} = 3000$ brings about
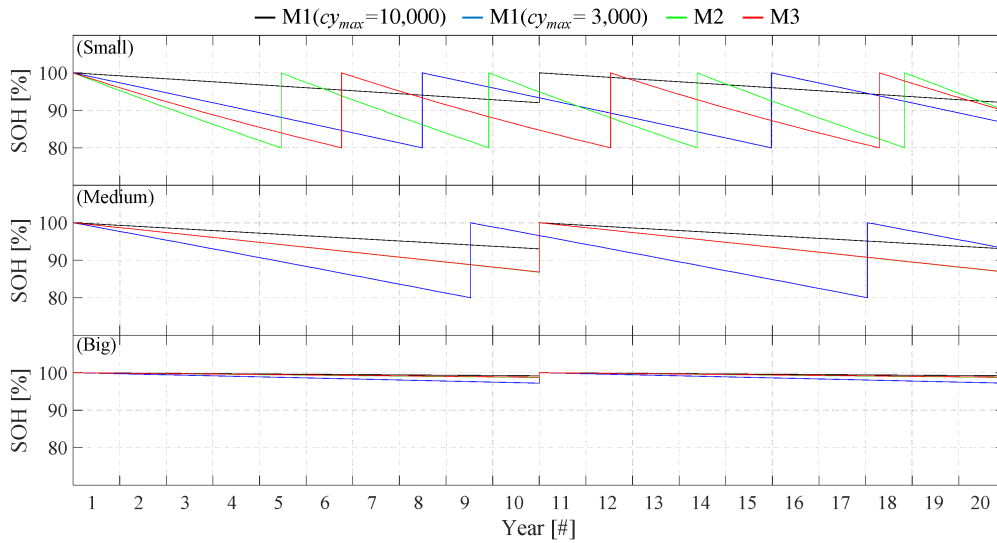
Figure 9.13 Simulation results along the plant lifetime (20 years) with different BESS models: estimated SoH trends for the hypotheses of Table 9.5.

more replacements as expected. The above problems are not present in the case of M2 and M3 because they take into account the cycling rate in the aging estimation. Apart from *hypothesis small*, these two models provide the same SoH estimation (red and green lines are overlapped in hypotheses M and B) because the function for the capacity fade is derived from the same set of measurements as detailed in section 9.3.

All the above findings, related to the SoC and SoH estimations, impact on the LoL estimations as shown in Table 9.6. In case of *hypothesis small*, lower differences are present between the models because, as already stated above, the operating conditions are so stressful that the BESS saturates very quickly in all the models. Different is the case of *hypothesis medium* and *hypothesis big*. M1 with cy_{max}=10000 results in a lower LoL if compared to M1 with cy_{max}=3000 and this is due to a higher capacity fade of the latter case: a lower capacity will in fact affect the LoL negatively. M3 results in the lowest values in all the three hypotheses. Given the higher accuracy provided by the electrical model, it results that empirical models tends to overestimate LoL. This fact can be explained by the totally different way used to model battery behaviours between empirical and electrical modelling approaches: the first one makes use of energy/power balances to compute SoC, while the second one uses electrical quantities (i.e. voltages/currents) to derive SoC. This clearly affects the charge/discharge paths that in the end result into different LoL indicators.

Focusing on the electrical model M3, Figure 9.14 shows the simulation results during the month of February of year 1. Equation (9.21) is used to compute the current (i.e. C-rate) and power profile at cell level. Given the nominal cell energy (appendix E), the power profile will never exceed the maximum energy to power ratio (EPR_{max}). The BESS behaviour is preserved also at cell level, as shown by the power profiles computed for the different hypotheses.

Table 9.6 Simulation results about LoL estimation with different BESS models

LoL [%]	M1 (cy_{max}=10000)	M1 (cy_{max}=3000)	M2	M3
Small plant	55.85	56.12	56.26	56.37
Medium plant	12.76	15.08	13.37	12.77
Big plant	1.51	1.52	0.44	0.28

In case of a very small plant the absorbed/delivered power is very high, while in *hypothesis medium* and *hypothesis big* they never approach the limit EPR_{max}. The cell voltage and OCV are then computed by equation (9.22) and equation (9.23). The latter is used to estimate the SoC. Figure 9.15 shows the trends of SoH (equation (9.26)), SoR (equation (9.30)) and LoL (equation (9.24)) along the plant lifetime. If SoH and LoL were already discussed in Figure 9.13 (red lines) and Table 9.6 (M3-column), SoR indicator belongs only to the electrical model. In both cases of undersized BESS and oversized BESS, a lower variation of SoR has been discovered if compared to *hypothesis medium*. This for two different reasons: small BESS means more frequent replacements due to a higher capacity fade (BESS is replaced before having the possibility of reaching a very high value of SoR), while big BESS means very low operating rates and a very small increase of internal resistance. In the case of *hypothesis medium* (BESS of size
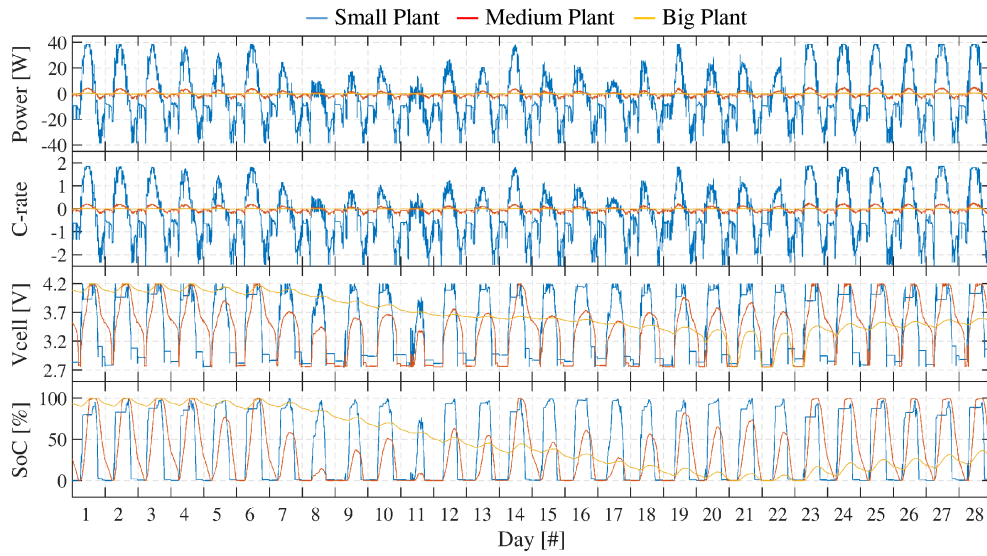

Figure 9.14 Simulation results for the month of February of year 1 with the electrical model M3: Power profile, C-rate profile, Voltage and estimated SoC for the hypotheses of Table 9.5
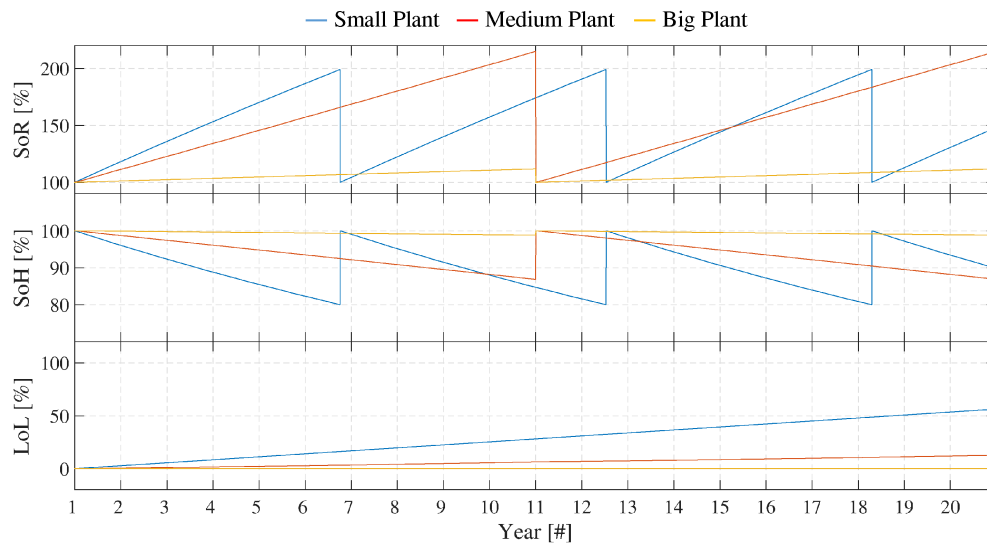
Figure 9.15 Simulation results along the plant lifetime (20 years) with the electrical model M3: estimated SoR, SoH and LoL trends for the hypotheses of Table 9.5

189
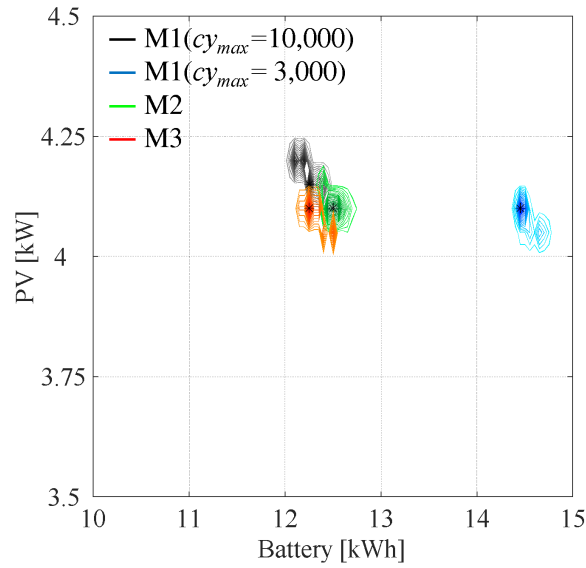
Figure 9.16 *area of solutions* obtained by running the proposed novel procedure (Poli.NRG) on the Tanzanian study case with different BESS models

Table 9.7 Robust design results obtained with different BESS models

BESS model	Simulation Time[21] [s/LC]	Simulated LCs [#]	Robust solution					
			f_{rbt}	PV_{rbt} [kW]	$BESS_{rbt}$ [kWh]	NPC [K€]	LCoE [€/kWh]	LLP [%]
M1 (10000)	640	32	6	4.15	12.25	29.9	0.453	5
M1 (3000)	640	31	10	4.10	14.45	31.2	0.472	5
M2	2180	96	22	4.10	12.50	29.8	0.452	5
M3	8900	60	12	4.10	12.25	29.7	0.449	5

comparable with the load, very similar to the optimal final solution) simulations suggest that BESS is expected to almost double its resistance before being replaced for reaching the maximum BESS lifetime.

Micro-grid robust design

The above simulations have been used to discuss the differences between the BESS models in estimating the operations of the plant. The novel procedure of section 9.2 has then been used to compute the micro-grid robust design that is to find the optimal plant configuration that satisfies a specific level of LLP at the minimum NPC over the entire plant lifetime. This is done by simulating several possible load profiles until the specific convergence criteria of equation (9.15) and equation (9.16). Figure 9.16 and Table 9.7 show the obtained results in terms of *area of solutions*. Each *area of solution* is related to a specific BESS modelling approach. In the case of M1, around 30 LCs are needed before reaching convergence, while M2 and M3 need more LCs: 96 and 60 respectively. The most frequent configuration within the simulated LCs indicates the most *robust solution* (PV_{rbt} ; $BESS_{rbt}$). f_{rbt} parameter indicates how many times the robust solution resulted in being the optimal solution for a specific LC. The PV optimal size is almost the same (4.10-4.15 kW) in all cases, being closely linked to the solar resources rather than the BESS models. The BESS optimal size is instead influenced by the modelling approach. Results say that BESS should range around 12.25-14.45 kWh with a maximum

---

[21] Intel® Core™ i7-4790 CPU @ 3.6GHz, RAM 16 GB.

variation of 18%. Empirical models of type M1 tend to oversize the plant, especially if wrong assumptions about cycling conditions (see M1 with cy_{max}=3000) are made. On the contrary empirical model of type M2 and the simplified electrical model M3 provide very similar results (i.e. the same PV size and the 2% of difference in between the BESS sizes). Given the technical findings, also economics are influenced by the adopted BESS model. NPC and LCoE are computed as the average value among the f_{rbt} simulated LCs that resulted in having the *robust solution* as the optimal one. Overall, NPC and LCoE for the robust plant configuration are around 30k€ and 0.45 €/kWh respectively.

In general, LLP and NPV estimations of model M3 are surely preferable because capacity fade and power fade are the results of capacitance and internal resistance variations: BESS dynamic and aging behaviours are linked to physical phenomena. But this comes at the price of a considerably higher simulation time: M3 is 14 times slower that M1 and 4 times slower that M2. Therefore, in planning tools like Poli.NRG, modified empirical models which account for capacity fade by using simplified analytical curves can represent a suitable compromise to obtain reliable results in a reasonable time.

Scenario-based design criteria for decision making

Finally, a characteristic feature of Poli.NRG is the possibility of carrying out the

Table 9.8 Robust design results over the six load evolution scenarios

Scenario	Description	Simulated LCs	Robust solution					
			f_{rbt}	PV_{rbt} [kW]	$BESS_{rbt}$ [kWh]	NPC [K€]	LCoE [€/kWh]	LLP [%]
S1	Stable	60	12	4.10	12.25	29.7	0.449	5
S2	Linear +10%	56	14	4.30	13.10	31.2	0.457	5
S3	Linear +20%	62	8	4.55	13.90	33.5	0.466	5
S4	Linear +30%	59	10	4.80	14.80	35.5	0.476	5
S5	Linear +40%	57	12	5.10	15.55	37.7	0.487	5
S6	Linear +50%	56	8	5.40	16.40	39.9	0.498	5

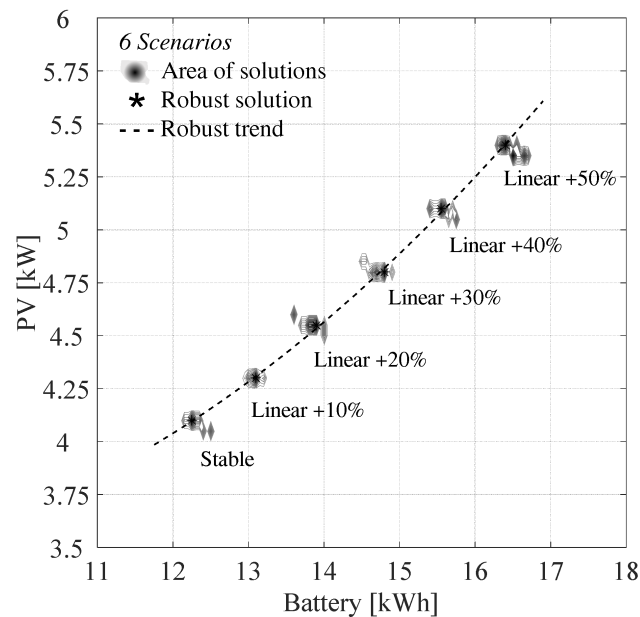
Figure 9.17 *area of solutions* obtained by running Poli.NRG with electrical model M3 for BESS on the Tanzanian study case with different load evolution scenarios

Table 9.9 Support table for decision makers

ΔL [%]	ΔNPC [%]	↑										
ΔPV [%]	ΔBESS [%]	S1		S2		S3		S4		S5		S6	
S1				-5.0	-5.1	-10.0	-13.5	-15.0	-20.8	-20.0	-26.9	-25.0	-33.9
				-4.9	-6.9	-11.0	-13.5	-17.1	-20.8	-24.4	-26.9	-31.7	-33.9
S2		+5.0	+5.1			-5.0	-7.4	-10.0	-13.0	-15.0	-18.7	-20.0	-25.2
		+4.9	+6.9			-5.8	-6.1	-11.6	-13.0	-18.6	-18.7	-25.6	-25.2
S3		+10.0	+13.5	+5.0	+7.4			-5.0	-6.0	-10.0	-11.9	-15.0	-18.0
		+11.0	+13.5	+5.8	+6.1			-5.5	-6.5	-12.1	-11.9	-18.7	-18.0
S4		+15.0	+20.8	+10.0	+13.0	+5.0	+6.0			-5.0	-6.2	-10.0	-10.8
		+17.1	+20.8	+11.6	+13.0	+5.5	+6.5			-6.3	-5.1	-12.5	-10.8
S5		+20.0	+26.9	+15.0	+18.7	+10.0	+11.9	+5.0	+6.2			-5.0	-5.8
		+24.4	+26.9	+18.6	+18.7	+12.1	+11.9	+6.3	+5.1			-5.9	-5.8
S6		+25.0	+33.9	+20.0	+25.2	+15.0	+18.0	+10.0	+10.8	+5.0	+5.8		
		+31.7	+33.9	+25.6	+25.2	+18.7	+18.0	+12.5	+10.8	+5.9	+5.5		

sensitivity of the robust design with different possible load evolution scenarios (a fundamental factor in DCs). Figure 9.17 shows the obtained results in terms of a *map of solutions,* composed of different *area of solutions*. In this case, each *area of solution* is related to a specific scenario of load evolution. It is recalled that having an increasing factor of +50% means that at the end of the plant lifetime the load demand is forecasted to be 50% higher if compared to the first year of deployment. Overall, the linear + 50% simulation will use a load profile 25% higher than the stable scenario. Table 9.8 shows the *robust designs* with respect to the six linear load evolution scenarios. As expected, the sizes of the components increase as the yearly load demand increasing factor rises. The NPC and LCoE rise as well because it is assumed to fulfill the same level of load during the plant lifetime (LLP fixed at 5%).

Currently, by supposing to have no growth in the energy needs (constant load scenario) the optimal microgrid design in the study case proposed would be PV = 4.1 kW, BESS = 12.25 kWh, while PV = 4.3 kW, BESS = 13.10 kWh in case of a 10% load increase during lifetime. Both the scenarios are robust, that is the dispersion of the optimal solutions around the solutions identified is very limited (Figure 9.17). Consequently, evaluating such results, the operator is properly driven in the decision-making process. Cross checking the solutions provided by Poli.NRG with the commercial products (PV and BESS capacity available) the operator will identify the option that could better fit with the study case.

Finally, in Table 9.9 a sensitivity analysis is carried out. The idea is to gather the information coming from Poli.NRG to give decision makers a comprehensive instrument to compare different action strategies. For instance, if the decision maker is not sure whether the load will increase by 30% (scenario S3) or 20% (scenario S2) along the plant lifetime, he/she can easily understand the different techno-economic impacts by comparing the two options in Table 6. He/she will conclude that passing through an S2 to an S3 is equivalent to increase the NPC, the size of PV and the size of BESS of about 6% while fulfilling 5% more load over the lifetime of the plant (with a fixed maximum LLP = 5%).

9.6 Summary

In this chapter, the final application of off-grid power systems for rural electrification

in Developing Countries (DCs) has been discussed.

After a brief contextualization about the bottom-up electrification paradigm and a short review about the off-grid systems design methodologies with specific attention on already available commercial software, a proper methodology has been proposed which is made up of four blocks separately facing the different design phases: (i) the data inputs gathering block provides a methodology to collect field data as regards to the weather conditions and load demand; (ii) the inputs processing block elaborates the inputs to obtain load and sources profiles over the entire lifetime of the plant; (iii) the system modelling and simulation block models the main components (i.e. BESS), simulates different off-grid system configurations and evaluates the related techno-economic performances; (iv) the output formulation block finds the most robust design for the context of analysis through specific optimization method. The analyses have been based on real data gathered within the framework of the *Energy4growing* project (Annex A). The methodology is proposed in the form of a computational tool in MATLAB® named Poli.NRG (POLItecnico di Milano –Network Robust design) and applied to size a PV+BESS microgrid system to supply power to a rural village in Tanzania.

When compared with the related literature, the hallmark of this methodology is the capability to incorporate the uncertainties inherent to rural electrification processes together with proper representation of BESS, which is recognized to be the crucial component of any off-grid systems. Load consumption uncertainties, load evolution scenarios, unpredictable energy sources and BESS modelling approaches have been determined as pivotal features to correctly evaluate final application performances and to address the robust design of off-grid systems. The *LoadProGen* tool allowed considering the uncertainties on a daily basis by creating a set of equi-probable daily load curves. The lifetime scenario generator allowed creating a set of lifetime load curves that include also the seasonal and year-by-year variations (i.e. different evolution scenarios). The operations of the systems (through the *OpSim* tool) have been simulated over the entire lifetime of the plant by using appropriate BESS models able to faithfully represent SoC and SoH indicators. The evaluation of the battery replacement costs, the Loss of Load Probability (LLP), the Net Present Cost (NPC) and the levelized cost of electricity are used as evaluation parameters to rank possible plant configurations. Several lifetime load profiles have been simulated by looking for the right plant configuration able to fulfill the desired LLP with the minimum NPC (i.e. heuristic optimization method). Each iteration highlights a point on a pre-defined searching space (i.e. PV and possible battery sizes) creating an area of solution instead of a single deterministic solution. The most robust solution has been computed as the most frequent of all the obtained optimum points inside a specific areas of solution. Finally, different load evolution scenarios are used to highlight different area of solution, which together create a map of solutions for energy planning purposes.

Several simulations on a 20 year basis (minute time-step) have been presented to discuss about: (i) the impact of different BESS models on the system energy design; (ii) the evaluation of the correct system design by accounting for different scenarios of load evolution. Results showed that different BESS models can affect the SoC and SoH estimations and consequently the LLP and NPC computations. Simplified empirical models, based on literature/manufacturers data might lead to oversized plant, especially if wrong assumptions about cycling conditions have been made. On the contrary, performances estimation made with simplified electrical model have been shown to be preferable because capacity fade and power fade are the results of capacitance and internal resistance variations: BESS dynamic and aging behaviours are linked to physical phenomena. However, results have highlighted that simulation time with electrical model increase by more than ten times. Therefore, in planning tools like Poli.NRG, modified

empirical models which account for capacity fade by using simplified analytical curves have been shown to represent a suitable solution to obtain reliable results in a reasonable time.

CHAPTER 10

Conclusions

This doctoral thesis is part of the research topic related to battery energy storage systems (BESS). BESS are becoming pivotal in the development of several and heterogeneous industrial sectors like energy, automotive, electronics, telecom etc. Data highlight that BESS installations (i.e Li-ion BESS) are increasing exponentially, while their specific cost is decreasing exponentially. The transition towards a renewable based energy sector, the rural electrification of Developing Countries and the rise of electric mobility are just some of the challenges of our today's society that are demanding more and more BESSs.

However, BESS performances cannot be assumed expandable from one technology to another and from one application to another (i.e. stationary, automotive, etc,). Energy/power densities, efficiencies, lifetime are application dependent and their right estimation affect the design criteria. Therefore, specific methods and models have to be used to tackle these issues. Analyses should start from a technological overview of available chemistries, define suitable modelling approaches to end up with a proper design criteria. Suggested models should be able to estimate SoC (State of Charge) and SoH (State of Health) indicators accepting different degrees of precision according to the specific application the model is used for.

In this context, this thesis has focused on proper models for BESS and appropriate design criteria for stationary applications. This theme has been specifically developed for lithium-ion battery technology and has been tested and validated in real life case studies.

The general result of the thesis has been to contribute expanding the knowledge about BESSs with particular attention on appropriate methods and models which are necessary to link the technological studies with the necessary economic analyses required in real life applications. Specific results have been: the development of a reference framework about technologies, performances and modelling of BESS; the proposal of innovative BESS models to represent dynamic and aging phenomena; the development of proper methodologies to analyse the techno-economic performances of BESS when deployed in stationary applications.

The work has been based on theoretical, numerical and experimental activities. A theoretical framework was needed to identify and formulate the correct BESS models according to the different available technologies. The experimental activities were fundamental to develop and tune the models. The numerical analyses, based on-field data were needed to test and validate the models on real applications.

Table 10.1 Selected areas of analysis about BESS within the PhD work

1	Analysis of the different technology from an application perspective
2	Analysis of the theoretical framework which is required to identify the main working characteristics
3	Analysis of typical representative models both from electric and energetic perspectives
4	Transfer of knowledge into suitable models
5	Analysis of proper design strategies/tools that embraces a correct quantitative representation of BESS performances
6	Analysis of the impact of proper modelling on the design phase and model selection

The thesis has been organized into three parts which dealt, through different chapters, with three levels of analysis. Specifically:

- The first part has offered the reference framework about BESS: from a comprehensive technology overview to an in-depth review of modelling approaches, through highlights about typical BESS performances in real applications. This is done by an intensive literature research coupled with experimental activities.

- The second part has represented the main element of originality of the thesis. Starting from theoretical fundamentals, a novel electrical model for lithium-ion cells based on experimental measurements has been presented, discussed and validated with real measurements. Lifetime modelling elements have been also proposed to create a wider background useful for application-oriented analyses, techno-economic analyses and investment evaluations.

- The third part has bridged the modelling phase with final applications. Specifically, the proposed model is compared with traditional or well-established literature approaches. Analyses have been carried out by analysing the specific application context, by proposing proper study approaches, by analysing the role of BESS modelling with respect to the applications, and by applying the methodology to specific case studies.
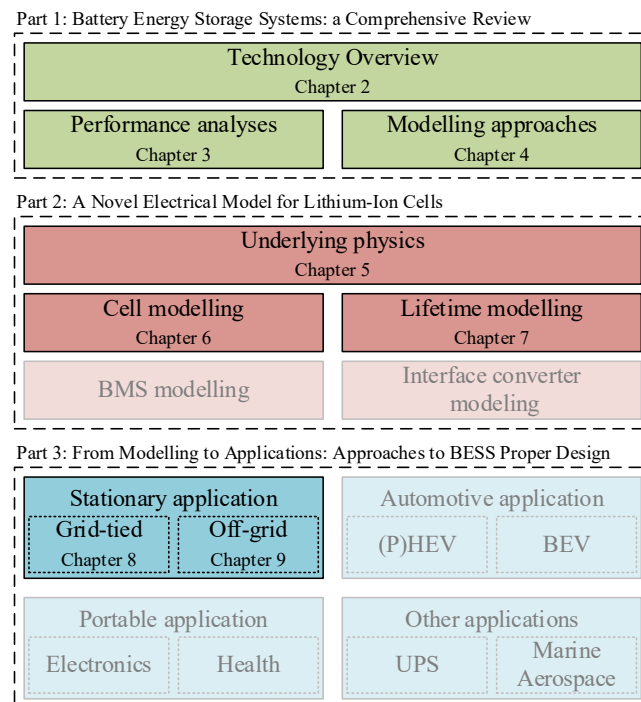

Figure 10.1 Summary of the thesis' contributions

All subjects have been elaborated by analysing some topics which were recognized as fundamental to tackle the main issues about BESS (Table 10.1). These topics have been identified by referring to the collaboration between the Politecnico di Milano and the CSEM-PV Center (Swiss Center for Electronics and Microtechnology) which allow intensive studies (theoretical and experimental) regarding dynamic behaviour and aging of Li-ion cells.

Figure 10.1 has shown a schematic structuring of these topics and has highlighted the specific contributions of the thesis. Part I constituted the framework of reference of the thesis and it was based on the review and analysis of the scientific literature. Part II constituted the modelling framework of the thesis that is based on experimental measurements coupled with theoretical studies. Part III constituted the design framework of the thesis that is focused on the final application and proper sizing process of BESS from a techno-economic point of view.

A brief summary of the thesis contributions is discussed below.

Part I Battery Energy Storage: a Comprehensive Review

Overview on Energy storage: from technologies to stationary applications. Chapter 2 has provided a comprehensive overview about Electrical Energy storage technologies. More attention has been dedicated to BESS with special focus on Li-ion chemistries. The different available cathode, anode and electrolyte materials have been presented by concentrating also on the expected performances, market share, producers and costs. Finally, the discussion has been contextualized in stationary applications. The typical features of storage technologies have been matched with the requirements of possible final applications. This has highlighted the feasibility of BESS in addressing the needs of today's electric power system scenario, in terms of expected performances and reliability. Given the high performances and the expected huge decrease in the specific cost, Li-ion technology is forecasted to be the most prominent option for renewable integration, frequency regulation, off-grid systems and peak-shaving.

Performance evaluation of lithium-ion cells. Chapter 3 has been dedicated to discuss about BESS performances. Experimental measurements have been presented about a technological comparison among three different Li-ion chemistries. Energy density, power density and efficiency are computed in different testing conditions (temperature, SoC, operating rate). The analyses have been carried out at cell level by following the IEC 62660-1 International standard coupled with novel testing procedures. The results highlighted the strong variabilities in the performances. Two novel procedures to overcome the discovered limitations of IEC 62660-1 have been also proposed: the Ragone test and the efficiency test. These testing procedures are demonstrated to be useful to system designers for a correct sizing as well as for the evaluation of the total cost of ownership of a BESS in the specific final applications. In general, this chapter has provided the reference of comparison for the development of a critical bibliographic review that aims at identifying the appropriate mathematical models capable of representing the dynamic behaviour and performances measured in the laboratory.

Review of approaches to battery modelling. Chapter 4 proposed a comprehensive literature review on battery modelling (mainly at cell level). The obtain result has been the creation of a framework of reference on which to rely in the modelling steps of part II of the thesis. The models have been grouped into four general approaches: electrochemical models, analytical (empirical) models, electrical models and stochastic models. Two main tasks have been identified for battery models: the estimation of the

operating conditions (i.e. SoC estimation) and the estimation of the lifetime (i.e. SoH estimation). Each modelling family/category has been discussed in all its features by detailing literature examples, typical equations, methodologies, available software/tool. *Electrochemical models* have been found to be the most accurate but characterized by a very high simulation time which make them unsuitable for techno/economic analyses. *Stochastic models* are found unreliable because they do not take into account the physical aspects behind battery operations at all. *Analytical models* have been described to be very simple being based on few equations and thus very suited for techno/economic analyses and energy planning studies; however, accuracy can represent an issue: Finally, *electrical models* are based on an equivalent electric circuit reproducing the responses at the external terminals. They can have different levels of complexity, being well suited for a wide range of applications: from design/energy analyses to real-time monitoring.

Overall, this chapter has highlighted the necessity to implement (part II of the thesis) and compare (part III of the thesis) different BESS models in order to understand the accuracy in reproducing the expected behaviour and performances (by referring to the experimental data of Chapter 3) with respect to the required computational time.

Part II A Novel Electrical Model for Lithium-Ion Cells

Physics of battery for impedance based modelling. Chapter 5 has provided the main theoretical pillars which are necessary for a proper electrical modelling process. The underlying physics about electrochemical cells functioning have been covered in depth. The main phenomena have been identified and discussed: electric and magnetic phenomena, the kinetic phenomena of the electrodes and diffusion phenomena. The main novelty is represented by the approach used to link electrochemical phenomena to the electrical modelling approach. The equivalent impedance representation is proposed for each phenomenon, which must be characterized by clear links in between the characterizing equations and the derived elements in the electrical model.

Novel electrical model for Lithium-ion cell. Chapter 6 presents a novel electrical model representative of the entire Li-ion technology. The model has been developed in the frequency domain by means of EIS measurements and it has been based on the theoretical framework presented in Chapter 5. The proposed model belongs to the family of passive electrical model and is capable of simulating the full dynamic response of lithium-ion batteries. The presented models is composed of 5 impedance blocks connected in series. Each block is derived from electrochemical equations which describe the dynamic processes of charge transfer and transport of mass. The SoC is estimated from the voltage of a nonlinear capacitance, thereby addressing the intercalation of ions into the electrode structure. In total, the model consists of an incremental capacitance look-up table and eight RC parameters. The complete model consists of an incremental capacitance look-up table and eight RC parameters. A procedure to estimate the parameters of the model has been presented and applied on a commercial lithium-ion cell (LNCO chemistry). Finally, validation of the model has been carried out in the time domain showing high accuracy in estimating the voltage at the device terminals, efficiency, power and energy density under different operating rates and SoCs. Specifically, different tests at 25 °C were carried out. The error in predicting the output voltage and the overall battery efficiency is less than 0.6% when the battery is cycled through SoCs between 20% and 80% and less than 2.2% when the SoC limits of 0% and 100% are used. The very high accuracy demonstrated by the proposed model is essential in assessing the technical and economic viability of the battery systems.

Elements on lifetime modelling. Chapter 7 investigated lifetime modelling of Li-ion cells. The topic of aging is discussed through experimental measurements. An innovative aging testing procedure, developed expressly to test Li-ion cells (LNCO chemistry) with different cycling conditions at ambient temperature, has been presented. Testing results gave evidence about the main aging effects: capacity fade, power fade and efficiency decrease. They are found to be highly dependent on the cycling rate. No clear influence has been found instead that relate the degradation with the DoD. The first obtained findings (at the moment of the thesis writing the aging tests were still ongoing) have been used to propose lifetime modelling approaches which have been discussed as regards to the experimental effort, the accuracy and the expected computational time. The proposed "Hybrid" approach is demonstrated to be a suitable compromise between empirical and electrical models. It can reach higher levels of accuracy if compared to empirical models, but with a lower computational burden if compared to electrical models. In general, this chapter contributed in creating a wider modelling background useful for application-oriented analyses, techno-economic analyses and investment evaluations. The modelling approaches of Figure 7.7 have been exploited in Part III of this thesis to deal with complex simulations.

Part III From Modelling to Applications: Approaches to BESS Proper Design

BESS for grid-tied applications: PCR service. Chapter 8 analysed the final application of grid-connected BESS for Primary Control Reserve (PCR). A proper methodology has been proposed which includes: specific control mechanism to change BESS working conditions with external signals; unconventional droop-control law that takes into account BESS characteristics; proper BESS models derived from the previous chapters. The proposed methodology is part of the approach for the optimum control of BESS operations. When compared with the related literature, this methodology aims at understanding how BESS features could be used to the advantage of the BESS owner. Thus, attention has been focused not only on the SoC control but also on the expected economic benefits for the BESS owner. The analyses have been based on real measurements taken at the Politecnico di Milano within the framework of the *IoT-StorageLab* (Annex B). The methodology has been proposed in the form of a computational tool in MATLAB®Simulink® named BESS4PCR and applied to the Italian context.

Simulation results showed that different BESS models highly affect the Loss of Regulation (LoR) estimation. Differences can reach up to 20%. It is shown how empirical models do not account for the influence of higher operating rates on BESS performances, while electrical models are more accurate. These differences are showed to also affect the BESS optimal design since they highly influence the NPV calculation. Investment evaluations have been carried out which consider revenue for PCR, investment costs (i.e. BESS cost), penalties due to LoR, replacement costs and residual value of BESS. If the electrical model is chosen as a reference, simulations showed that the optimal configuration is 1.4MW/1.4MWh with NPV slightly above 0 over a 10 years investment term. Finally, a detailed analysis of BESS operations using variable-droop control has been presented. This control strategy improves the BESS performances and profitability avoiding part of the penalties. LoR is shown to have reduced of 10 points, NPV to have more than double and Payback time to have almost halved.

Overall, grid-connected BESS have been shown to be a promising technology in providing ancillary services such as PCR to electric power system, especially if proper control strategies are adopted to enhance BESS performances. However, analysts or engineers must pay attention to the BESS model which is used to derive investment

evaluations. Electrical models are found to be a valid option in simulating the operation of a real BESS when the regulating framework (i.e. remuneration and penalty) is clearly defined. Empirical models represent a faster option in understanding the behaviour of the system but they can lead to undersize BESS solutions that will negatively affect the final performances.

BESS for off-grid applications: PV-BESS systems for rural electrification. Chapter 9 analysed the final application of off-grid power systems for rural electrification in Developing Countries (DCs). A novel sizing methodology has been proposed which is made up of four blocks which separately face the different design phases: (i) the data inputs gathering block provides a methodology to collect field data as regards weather conditions and load demand; (ii) the inputs processing block elaborates the inputs to obtain load and sources profiles over the entire lifetime of the plant; (iii) the system modelling and simulation block models the main components (i.e. BESS), simulates different off-grid system configurations and evaluates the related techno-economic performances; (iv) the output formulation block finds the most robust design for the targeted context through a specific optimization method. The analyses have been based on real data collected within the framework of the *Energy4growing* project (Annex A). The methodology has been proposed in the form of a computational tool in MATLAB® named Poli.NRG (POLItecnico di Milano –Network Robust design) and applied to size a PV+BESS microgrid system to supply power to a rural village of Tanzania.

The hallmark of this methodology is the capability of incorporating the uncertainties inherent to rural electrification processes together with a proper representation of BESS, which is recognized to be the crucial component of any off-grid system. The system operations have been simulated over the entire plant lifetime by using appropriate BESS models able to faithfully represent SoC and SoH indicators. The evaluation of the battery replacement costs, the Loss of Load Probability (LLP), the Net Present Cost (NPC) and the levelized cost of electricity are used as evaluation parameters to rank possible plant configurations. Several lifetime load profiles have been simulated by looking for the right plant configuration able to fulfill the desired LLP with the minimum NPC (i.e. heuristic optimization method). Each iteration highlights a point on a pre-defined searching space creating an area of solution instead of a single deterministic solution. The most robust solution has been computed as the most frequent of all the obtained optimum points inside a specific area of solution.

Several results showed that different BESS models highly affect the SoC and SoH estimations and thus LLP and NPC computations. Simplified empirical models, based on literature/manufacturers data might lead to oversized plant, especially if wrong assumptions about cycling conditions have been made. On the contrary, performances estimation made with simplified electrical model have been shown to be preferable because capacity fade and power fade are the results of capacitance and internal resistance variations: BESS dynamic and aging behaviours are linked to physical phenomena. However, results have highlighted that simulation time with electrical model increase by more than ten times. Therefore, in planning tools like Poli.NRG, modified empirical models which account for capacity fade by using simplified analytical curves have been shown to represent a suitable solution to obtain reliable results in a reasonable time.

Overall, this chapter has highlighted that attention is required when facing the design of off-grid power systems. Especially when dealing with the rural context of DCs, uncertainties on loads and resources need to be considered because a different set of inputs can lead to different optimum plant configurations. Moreover, analysts and decision makers must pay attention to the BESS model used to derive techno/economic

evaluations. Wrong modelling approaches can lead to a wrong performance estimation over the plant lifetime. For this reason, design software as Poli.NRG that provide robust design solutions embodying all the possible on-field set of inputs together with proper options for BESS, are strongly suggested.

Future works

There are several research directions on models and methodologies for the correct analysis and design of BESSs to explore extending the work presented in this thesis. In this section, some of them are discussed.

Thermal model of electrochemical cells: this thesis has presented an innovative dynamic model in Chapter 6, which has been developed at constant ambient temperatures (25°C) for time and resources reasons. Nevertheless, the effect of different ambient temperatures on the dynamic response of the cell has been briefly introduced in section 6.2 through experimental measurements (EIS). Further modeling efforts could be dedicated on this issue addressing the development of a thermal model of the electrochemical cells to be coupled with electrical models and aging models.

Comprehensive lifetime modelling: this thesis has introduced a first step about lifetime modelling in Chapter 7. All the analyses have been based on ongoing aging tests (at the moment of the thesis writing, hundreds of cycles have been completed: 400-800 depending on cycling conditions). Further improvements are needed as regards to: (i) the validation of the proposed results once all aging tests have been finished; (ii) the investigation of the DoD influence on aging since no clear relationship has been found so far. Moreover, the influence of the ambient temperature on the aging effects could be investigated with additional aging tests. Above all, intensive research activity is required to investigate the electrochemical phenomena behind aging effects and relate them with the modelling activity carried out in Chapter 6 (i.e. aging phenomena should be linked to changes in the impedance blocks of an electrical model).

Techno-economic optimization of grid-tied BESS for multi-services provision: this thesis has discussed the economic viability of BESS in providing PCR service in Chapter 8. The objective has been focused on loss of regulation minimization. The possible developments are oriented towards the study of multi-services mechanisms in which the battery is operated by exploiting several market opportunities at the same time. For instance, the BESS can keep providing PCR while doing arbitrage, or sustain off-grid systems while providing ancillary services to the same grid, etc..

Techno-economic optimization of complex off-grid systems: this thesis has discussed the proper design of PV-BESS based off-grid systems. However, off-grid systems can be more complex by aggregating several resources of different nature (e.g. mini-wind, micro-hydro, small diesel genset, etc.) to create bigger mini-grid. BESSs could be studied in providing balancing services to the grid to investigate the improvements in the reliability of self-sustained power systems.

Power electronics modelling integration: Overall, the analyses of part III have been centred on electrochemical batteries, considering power electronics well-established with respect to both industrial applications and mathematical modelling. However, power electronics and related BMS could impact on electrochemical cells performances. Modelling of these components can enhance the accuracy of the final results.

Appendix A

The project "Energy for Growing"

The project Energy4Growing (E4G) is an ongoing initiative that started in 2013 promoted by a research group at the Politecnico di Milano [299]. The main task of the project was the design and commissioning (the author has been actively involved in both activities) of an off-grid power system to supply electricity to the secondary school of Ngarenanyuki, a rural village in Northern Tanzania (Figure A-1). About 460 students attend the targeted school, 85% of them are resident in the institution facilities which include classrooms, offices, dormitories, library, kitchen, teachers' houses, etc.

At the time of starting the project, the local energy scenario was characterized by the following elements:

- The main power source of the school was a run-off-river Micro hydropower plant (MHP) based on a 3.2 kW Banki turbine (Figure A-2) coupled with 1-phase brushless synchronous generator (230 V, 50 Hz).
- The water flow to the turbine is diverted from a stream, which is managed by local farmers. Therefore, water availability is highly variable during the day and according to the season. For this reason several blackouts occur.
- The frequency regulation is based on a 4 kW dump load, which dissipates the excess power in the air.
- A 5 kW petrol generator was used when the MHP plant was off and only for important reasons (Figure A-2).
- The power supply was managed in the control room by means of a toggle switch that permits selecting the power source, while a group of breakers permits specific loads to be connected/disconnected manually.
- The number and type of the electric devices available in the school were determined by the limited generators and storage capacities. Moreover, the consumption patterns were deeply affected by the energy source availability (i.e. the water flow), which resulted in highly variable consumptions day-by-day and hour-by-hour (a typical feature of consumption patterns in rural areas).

This observation together with preliminary analyses on school power consumption habits suggested carrying out a monitoring of the system functioning in order to plan a

Figure A.1 NgareNanyuki Secondary School (TZ).

Figure A.2 Diesel generator and Banki turbine generator.

proper intervention. A meter was installed on site and energy consumption data as well as electric functioning parameters were monitored during the period from June to September 2014.

As shown by Figure A-3 (the Tukey boxplot of the metered load values throughout the whole day), the daily energy consumptions ranged from a few kWh to about 25kWh: this suggests a high variability of the water source availability on a daily basis. Every hour of the day the power loads ranged from 0W to values above 1.5kW.

In this framework, the E4G project has addressed the improvement of the power supply service of the school by increasing the generating capacity and by adopting an energy management system (EMS) capable of integrating different RES-E power sources together with BESS effectively and efficiently. Specifically, the author worked in the on-field deployment of a hybrid micro-grid in April 2015 that combined the power systems already available on-site with new installations (3kW of PV panels and 72 kWh of lead-acid batteries) by means of an interface converter (IC) with specific control units (Figure A-4).

Figure A-5 shows the architecture of the micro-grid that comprises a dc energy sources aggregation (Q1 board) and an *ac* double bus-bar system (Q2 board). In particular, Q1 is a *dc/ac* control board connecting PV panels and the lead-acid battery pack to the IC. The loads, the hydro turbine and petrol generator are connected to the *ac* double bus-bar board (i.e. Q2). Finally, an industrial PLC measures and controls the micro-grid, acting on the switchers of each line while calculating proper power set points
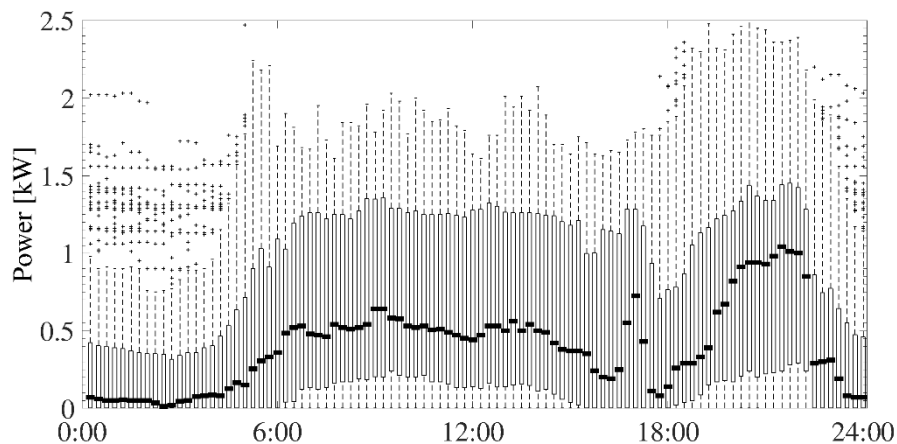
Figure A.3 Boxplot of the daily power consumption in NgareNanyuki (TZ) before E4G project intervention

Figure A.4 The new installed Interface Converter and the 3kW monocrystalline PV modules

for the IC.

Different operation modes have been implemented: manual mode, automatic mode, and grid-connected.

In the *manual mode*, the operator can manage the loads connection/disconnection and can select the power source. During this mode, the PLC controls Q1 to implement a grid forming operation.

In the *automatic mode,* the PLC measures voltage, current, frequency, and power and manages the system by means of four configurations:

1. Q1 on-grid – following the hydropower system. In this operation mode, the hydro generator manages voltage and frequency of the grid, while Q1 is controlled in the *following mode*. The control board of Q1 implements the MPPT algorithm to maximize the PV power. The PLC detects the dump-loads operating status and diverts the power (otherwise dissipated) to charge the battery pack.
2. Q1 off-grid – forming mode. In this operation mode, the PLC defines the IC voltage and frequency set-points, and it monitors battery SoC in order to properly manage its

Figure A.5 Hybrid Micro-grid configuration of the E4G project

discharge limits.
3. Hydropower in stand-alone mode. This operation mode is activated when the batteries SoC is too low, then the PLC manages the loads connection according to hydro production and different load priorities.
4. Double bus-bar mode. This configuration allows the hydropower and Q1 to work together, each one on a single bus-bar an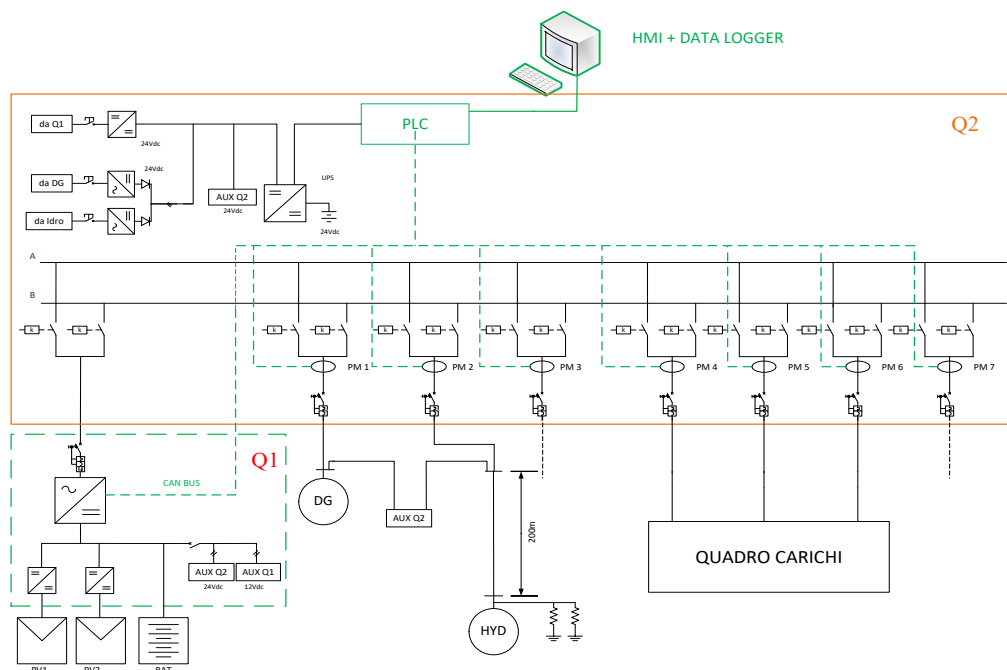d occurs in case of large power fluctuations (detected measuring both voltage and frequency). In this case and when the micro-grid is working in mode 1, the load lines are progressively switched to the second bus-bar which is managed by Q1 in forming mode.

Some considerations can be made about the integration of BESS in the micro-grid. In the original system (hydropower based), the dump loads kept the balance between generation and consumption (assuring stability at 50 Hz) to the detriment of energy dissipated into the air by the dump load. The new architecture can limit the dissipated energy. The PLC leaves only a small part of the hydropower to the dump load in order to carry out a fast regulation (i.e. guarantee stability control), but it takes as much energy as possible from the hydropower system to charge the battery. In other words, the battery pack is operated in order to absorb part of the power that was dissipated on the dump load thus increasing the overall system efficiency.

It is worth underlying how the micro-grid deployed by the E4G project requires several control actions (devoted to switching on/off the loads, the generators, to regulating the battery charge, etc.), consequently a synoptic control scheme has been developed (Figure A-4). This scheme is very different in comparison to other commercial solutions and it is not common for local technicians. Therefore, as part of the project activities, a 10 day on-site training programme was carried out in order to interact with local staff, to evaluate their needs and show how to manage the micro-grid via the control panel. Currently, local staff only has a primary education and no electric system skills, but after training they acquired all the capabilities required to properly manage the system, and they have been working quite independently so far.

At the moment of the thesis writing, two years after the micro-grid deployment, the E4G project is still ongoing. Actually, the project was developed to exploit Ngarenanyuki School as a research laboratory: micro-grid functioning parameters (voltage, current, frequency, etc.) are sampled each second, logged, saved and shared with the Politecnico di Milano ICT facilities thanks to a satellite connection. Such data are crucial for monitoring purposes to ensure the quality of supply, reliability, etc. but also for research purposes. Key elements under investigation are the BESS lifetime estimation, the analysis of consumption growth and the update of the system control logics in order to adapt the micro-grid to the new evolving scenarios that the school is facing (e.g. in 2016 the Tanzanian TSO extended the national grid to the areas of Ngarenanyuki).

Appendix B

The IoT StorageLab at the Politecnico di Milano

The IoT Lab of the Politecnico di Milano is devoted to the research on the Internet of Things concept. The Lab aims to create a suitable environment for the research, design, development and testing of IoT solutions, with specific reference to energy and power systems applications.

The main applicative scenarios for the solutions conceived within the laboratory are the smart home and the smart building environments, and the relevant paradigms of smart grid and smart cities. Actually, these scenarios are strongly characterized by the need to manage complex heterogeneous systems, including distributed sensors and controllers, generation units (typically from RES), EES, smart appliances, e-mobility, etc. In this scenario, ICT is widely exploited to interconnect all the elements included in the system and advanced user interfaces are required to exchange information with the end-user in an effective manner.

The IoT Lab focuses on the development of new strategies and logics to coordinate all the actors involved in such a novel scenario and on the design of the relevant hardware/software platforms. In more detail, the laboratory aims at providing a large-scale IoT system to collect information from the field and to transfer it to a control centre. The data are then exploited to effectively manage critical aspects of the smart home and smart building environments. To this purpose, a main task of the laboratory concerns the development of algorithms and strategies to define the best control actions needed to fully benefit from the opportunities provided by the new paradigm.

Four Departments of the Politecnico di Milano with specific expertise contribute to the laboratory: Dept. of Management, Economics and Industrial Engineering (DIG), Dept. of Electronics, Information and Bioengineering (DEIB), Dept. of Energy (DE) and Dept. of Design. The Lab is physically distributed in three different sites around Milan (Peschiera Borromeo, DEIB in Leonardo campus and DE in Bovisa campus), but all the
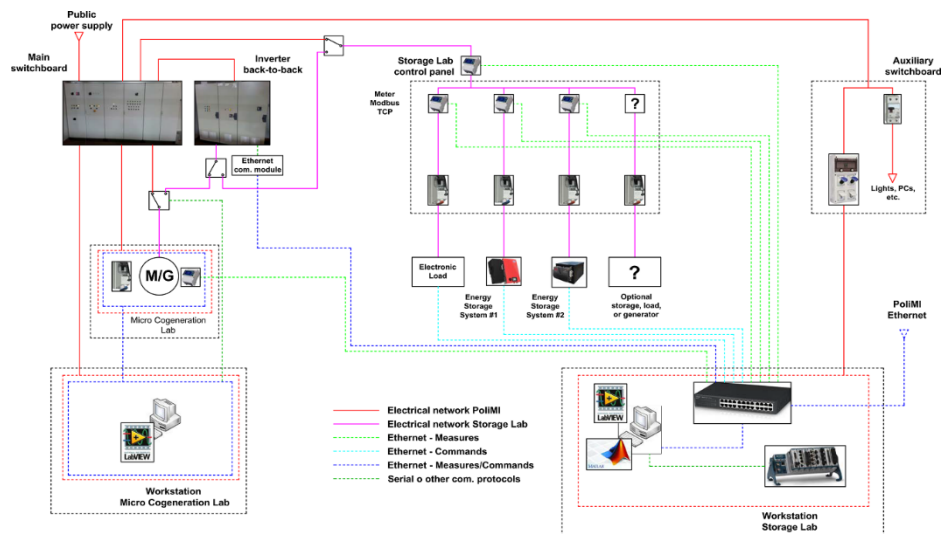

Figure B.1 Iot Storage Lab architecture in Bovisa Campus (Politecnico di Milano)

components and systems are conceived to operate in a coordinated way by communicating through the Web.

Focusing on the Bovisa site (Figure B.1), the IoT lab is particularly focused on the study of BESS. The IoT-Storage Lab is equipped with devices for the monitoring of energy consumption, sensors for the monitoring of environmental parameters (temperature, humidity and human presence), and the communication devices needed to share the data. More in detail, the core of the IoT-Storage Lab measurement system is an electric switchboard to which different electric loads, generators and ESS can be connected. The switchboard can operate islanded from the grid or supplied by different power sources (according to the specific scenario to be simulated):

- The external grid (i.e. power supply with standard electric parameters).
- A 100 kW back-to-back inverter, able to simulate the main grid with adjustable electrical parameters (voltage amplitude and frequency).

All data are collected in a National Instruments CompactRIO unit, which is able to: (i) elaborate the measurements collected in order to obtain performance indexes related to the BESS operation; (ii) compute control actions to be performed on the devices under test (e.g. for close loops control logics); (iii) share data and commands through the Cloud with the other sites of the IoT Lab, with the objective to implement distributed control strategies (e.g. to provide feedback regulations to the BESS installed in the Bovisa site of IoT Lab on the basis of the load and generation measured in other sites of the laboratory).

Apart from the research activities related to IoT concept, the IoT-Storage Lab will be focused on several aspects that involve battery systems such as:

- The performance measurements concerning different BESS technologies.
- The study of BESS performances during real-life operations. Different services/opportunities can be tested: the increase of self-consumption, the peak-shaving for grid relief; the ancillary service provision, etc.
- The testing of islanded or grid-connected modes of operation.
- The development of innovative control actions.

The author has been actively involved in the start-up of the IoT-Storage Lab with specific focus on the development of the LabVIEW platform which is currently used to acquire measurements and apply set-points to BESS devices.

Appendix C

Electrochemical Impedance Spectroscopy: a theoretical overview

Fundamentals of EIS began in the 1880s with the introduction of the concept of impedance in electrical engineering by Oliver Heaviside [197]. Warburg was the first extend the concept of impedance to electrochemical systems in the 19th century. Thanks to the work by Epelboin in the 1960s, EIS measurements become an analytical tool to investigate the corrosion mechanisms [300]. Thanks to the invention of the potentiostat and the first frequency analyser in the 1970s, it became possible to probe electrochemical systems at very low frequencies. Prior to that time, EIS measurements were limited to frequencies above 100Hz and mainly for the theoretical description of semiconductors and devices [301], [302].

EIS is a very powerful method mainly because it is a non-destructive technique to characterize the electrical properties of materials and their interfaces. EIS allows to measure impedance of a two terminal device (phase-shift and magnitude) without opening it but by measuring the voltage or current response at its terminals per effect of an applied current or voltage excitation. It may be used to investigate the mechanisms of diffusion of charge carriers in the bulk or at the interfaces of liquid and solid materials [122], [303]. The device is subjected to stimuli at different frequencies, each of them is able to excite a specific dynamic mechanism, so that the different phenomena are identified and evaluated.

There are three main types of electrical stimuli which are used for impedance spectroscopy, which consist in:

- Applying a voltage step through the device terminals and measuring the current response *i(t)*. the time varying resistance is evaluated as $V_{step}/i(t)$.
- Applying a voltage signal containing multiple frequencies (white noise) and measuring the resulting current. Then by using Fourier transform methods, it is possible to analyse the signals in the frequency domain and obtain the impedance over frequency.
- Measuring the voltage or current response of the system per effect of a single applied current or voltage. This is the most used technique since commercial systems of today measure automatically the impedance in the range of μHz to MHz.

In a linear system, the response to a sinusoidal input excitation at a given frequency is a sinusoidal output signal at the same frequency with different amplitude and phase. The impedance $Z(t)$ at the given frequency is defined as follow:

$$Z(t) = \frac{E_t(t)}{I_t(t)} = \frac{E_0 \cdot \sin(\omega t)}{I_0 \cdot \sin(\omega t + \varphi)} \tag{C.1}$$

In nonlinear systems, as electrochemical cells, the impedance can be defined by linearizing the system response for small perturbations around the equilibrium point [304] (Figure C.1), which is a fixed SoC at a stable temperature.
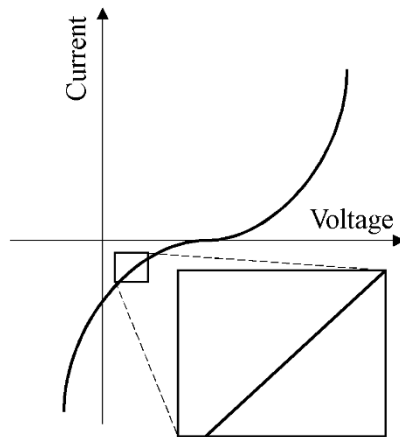
Figure C.1 Current versus Voltage Curve Showing Pseudo-linearity

The EIS spectrum is obtained by repeating measurements at different frequencies. While measuring the EIS spectrum, the device under test should remain in the same state. Impedance is in fact strongly affected by temperature and SoC variations. Consequently, EIS measurements cannot be performed while charging or discharging the battery, in this condition the quasi-linearity condition is not respected.

For instance, the Galvanostatic EIS (GEIS) measures the voltage response at the battery terminals per effect of a small sinusoidal current injection. The current excitation has to be small enough in order keep the voltage response in a quasi-linear region and with an amplitude large enough to be measured by the instrument. Today's EIS instruments are able to measure voltage signals of some tens of μV with high accuracy.

The time required for measuring an EIS spectrum depends on the number of points measured and on the selected frequency. More than one complete sinusoid is required for each impedance measurement (the number of complete sinusoids depends on the specific instrument and it is in the range of 1-5).

Results are studied by means of the so-called Nyquist diagrams (or Argand diagrams) and Bode diagram. Figure C.2-a shows a typical Nyquist plot of a lithium-ion cell in which the real and imaginary parts of the cell impedance are plotted for different
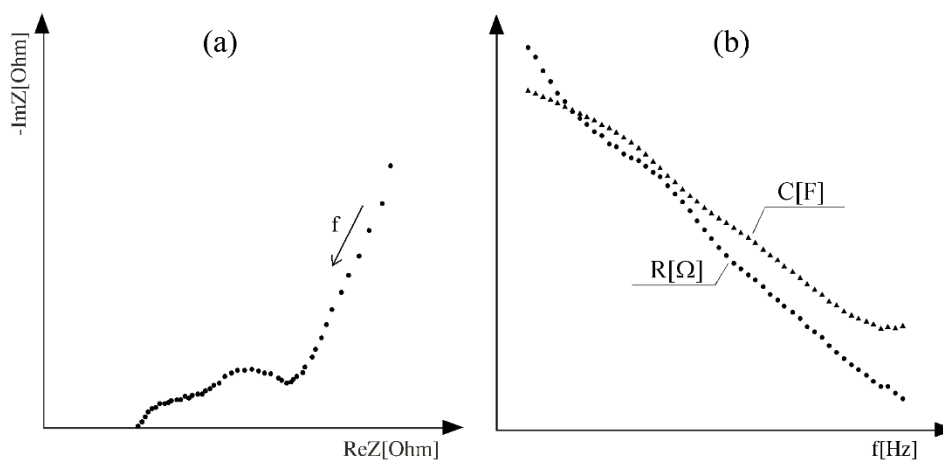
Figure C.2 Example of Nyquist plot (A) and Bode plot (B) for EIS representation.
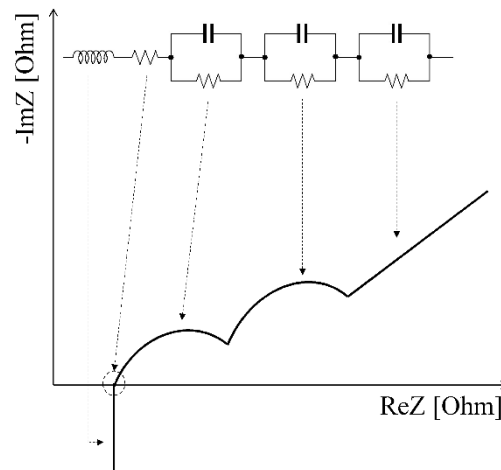
Figure C.3 Example of EIS interpretation for electrical modelling approaches

frequencies. The sign of imaginary parts is usually reverted since the behaviour of the battery is mainly capacitive. The points at the upper-right side of the diagram are measured at a very low frequency, while the highest frequencies are in the low-left side of the diagram. The plot crosses the axes $Im\{Z\}=0$ at the resonant frequency where the inductive reactance of the impedance equals the capacitive reactance. At higher frequencies, the device shows inductive behaviours, while capacitive ones at lower frequencies. The main limitation of a Nyquist plot is the impossibility to relate directly the impedance measured with the frequency. For this reason, the Bode plot of Figure C.2-b is also used, because it directly quantifies the resistive and capacitive behaviours at the different frequencies.

Modelling development is one of the most powerfull applications of EIS. The Nyquist plot is used to detect phenomena occurring in the battery and to estrapolate an equivalent electric circuit. Determination of the circuital paramenter can be found by fitting EIS curves at various SoC, temperature and aging conditions. Figure C.3 shows a typical interpretation and modelling of a Li-ion EIS [162], [305]. The frequency of each characteristic shapes can be related to a characteristic phenomenon happening inside the cell: (i) Inductive reactances of metallic elements in the cell and wires; (ii) ohmic resistance due to voltage drops at current collectors, electrolyte, active material and separators; (iii) impedance related to Solid Electrolyte Interface (SEI); (iv) charge transfer resistance of the electrodes in parallel with the double layer capacitance; (v) Diffusion processes inside and outside the electrodes

Appendix D

BESS cost assumptions

NPC estimations in Chapter 8 and Chapter 9 are based on BESS cost estimations. Projections on the BESS specific costs in the near future are needed to better evaluate the investment.

In this thesis, we assume a decreasing cost of BESS as per Figure D-1-A. The projection is based only on the future cost estimations derived from [1]. Specifically, the specific cost [€/kWh] in the specific year y is computed as follows:

$$c_{BESS}(y) \left[\frac{€}{kWh} \right] = 8.7\mathrm{E}^{53}\mathrm{e}^{-0.0586*y} \qquad \text{D-1}$$

Where y is the current year of installation (i.e. 2017). c_{BESS} is used to account for investment (*I*) and replacement costs (C_R) actualized to the year of cash flow.

Then, at the end of the investment, it is assumed that the BESS will still have some residual value (RV) computed as follows:

$$RV_{BESS}(y) = C_{BESS}(y_p) * \mathrm{DF} \qquad \text{D-2}$$

Where y_p is the year of BESS purchase and *DF* is the devaluation factor that accounts for the years of operations that the BESS has already faced. If the last replaced BESS has worked for only one year before the end of the investment evaluations, it should be evaluated with a higher residual value if compared with a BESS that is close to its maximum allowable lifetime (LT$_{BESS,max}$)

$$DF = \mathrm{e}^{\frac{\left(-y_{deployment} \right)}{2}} \qquad \text{D-3}$$

Where $y_{deployment}$ is the number of years the BESS is in operation.
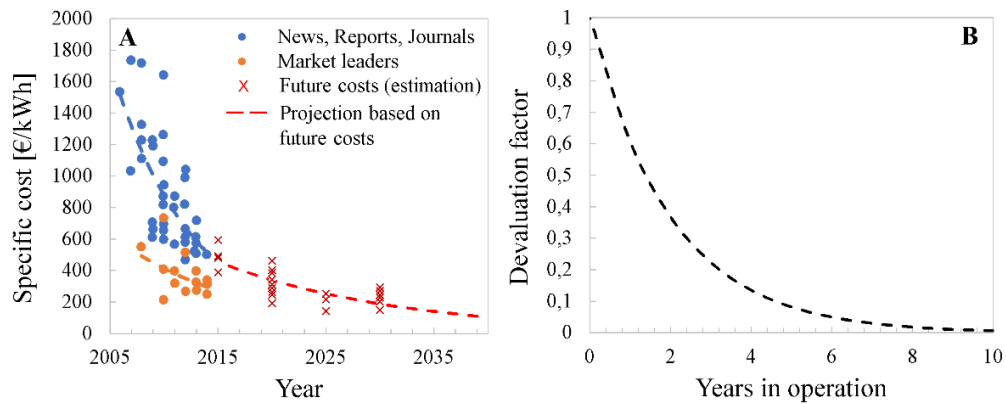
Figure D-1: (A) Projected Costs of Li-ion battery packs in automotive sector [1] and (B) devaluation factor for residual values computation.

Appendix E

Datasheets of the investigated Li-ion cells

This annex details the datasheets of the electrochemical cells which have been experimentally tested (LNCO, LFP, LTO in Chapter 3) and exploited for electrical modelling purposes (LNCO in Chapter 6 and Chapter 7).

Technology	LNCO
Brand	Boston Power SWING5300 [107]
Nominal capacity	5300 mAh
Nominal energy	19.345 Wh
Nominal voltage	3.65 V
Shape	prismatic
Cell dimension (L-H-W)	64.8-37.3-19.2 mm
Nominal cell weight	93.5 g
Energy density (gravimetric)	207 Wh/kg
Energy density (volumetric)	490 Wh/l
Nominal impedance	15.5 mΩ
Cycle life (DoD =100%, 0.5C)	>1000 cyles
Cycle life (DoD =90%, 0.5C)	>2000 cyles
Cycle life (DoD =80%, 0.5C)	>3000 cyles
Max continuous discharge rate (0-100% SoC)	13 A
Allowable 10s pulse capability (0-50% DoD)	1000 W/kg
Charging method – CC	3.7 A (0.7C) to 4.2 V
Charging method – CV	4.2 V to 50 mA
Max charge rate (continuous)	10.6 A
Operating temperature (charge)	-20°C - +60°C
Operating temperature (discharge)	-40°C - +70°C
Storage temperature	-40°C - +60°C

Technology	LFP
Brand	A123 ANR26650 [109]
Nominal capacity (nominal/minimum)	2.5 / 2.4 Ah
Nominal voltage	3.3 V
Shape	Cylindrical
Cell dimension	⌀ 26 x 65 mm
Nominal cell weight	76 g
Power density (gravimetric) 10s pulse	2600 W/kg
Power density (volumetric) 10s pulse	5800 W/l
Cycle life @ 10C discharge (DoD = 100%)	>1000
HPCC 10 s discharge pulse power 50% SoC	200 W
Internal impedance	6 mΩ
Recommended standard charge method	1C to 3.6 V CCCV, 45 min
Recommended fast charge method to 80% SoC	1C to 3.6 V CCCV, 12 min
Maximum continuous discharge	70 A
Maximum pulse discharge (10 s)	120 A
Operating temperatures	-30°C - +55°C
Storage temperature	-40°C - +60°C

Technology	LTO
Brand	GWL POWER LY-LTO-30Ah [110]
Nominal capacity (nominal/minimum)	30 / 27 Ah
Nominal voltage	2.4 V
Shape	Prismatic
Cell dimension (L-H-W)	235-135-29 mm
Nominal cell weight	> 1590 g
Max voltage per cell	2.80 V
Balancing voltage per cell	2.75 V
Discharge voltage per cell	2.75 V
Discharge voltage	1.85 V
Minimal voltage per cell	1.5 V
Operating voltages	1.85 – 2.75 V
Optimal discharge current	<30 A (1C)
Maximal discharge current	<450 A (15C)
Max peak discharge current	<600 A (20C, <10 s)
Optimal charge current	<30 A (1C)
Maximal charge current	<180 A (6C)
Internal resistance	< 1 mΩ
Cycle life (DoD =80%, 0.5C charge – 3C discharge)	>10000
Cycle life (DoD =80%, 0.5C charge – 1C discharge)	>20000
Cycle life (DoD =80%, 0.5C charge – 0.5C discharge)	>500000
Self-discharge rate	<3 % / month
Operating temperature (charge)	-15°C - +45°C
Operating temperature (discharge)	-25°C - +55°C
Temperature / Capacity (25°C)	100%
Temperature / Capacity (0°C)	>80%
Temperature / Capacity (-10°C)	>70%
Temperature / Capacity (-20°C)	>60%

Appendix F

Load data assumptions for the Ngarenanyuki study case

This annex details the data collected with interviews and audit in the Ngarenanyuki Secondary School (Arusha, Tanzania) in 2016 within the framework of the *Energy4growing* project (Appendix A). Most of the appliances hereinafter reported were either not working or resulted to being unavailable (i.e. desiderata) in the school.

Location	Appliance	Unit	Power [W]	Functioning hours per day	Usage
Building 2					
Office Headmaster	Laptop PC	1	40	from 08:00 to 19:00, sometimes 19:00-22:00	
Office HM Secretary	Desktop PC	1	400	from 08:00 to 16:00	continuously
Office HM Secretary	Laptop PC	1	40	from 08:00 to 16:00	continuously
Office Headmaster	Neon Light	1	40	5 days per week, from 08:00 to 19:00, sometimes 19:00-22:00	
Office HM Secretary	Neon Light	1	40	6 days per week, from 08:00 to 16:00	
Office HM Entrance	Neon Light	1	40	7 days per week, from 08:00 to 16:00	
Laboratory 1	Fluorescent Light	5	9	not common, from 19:00 to 23:00 before exams	continuously
Laboratory 2	Fluorescent Light	5	9	not common, from 19:00 to 23:00 before exams	continuously
Laboratory 3	Fluorescent Light	5	9	not common, from 19:00 to 23:00 before exams	continuously
Office HM Secretary	Photocopy Machine	1	1500	during examination period, from 08:00 to 16:00	
Office HM Secretary	Printer	1	150	from 08:00 to 16:00	continuously
Security Light	Neon Light	4	40		
Building 3					
Library Computer Room	Laptop PC	3	40	once a week, closed at night	
Library Book Room	Desktop PC	1	40	every two weeks, not at night	
Library Toilet	Fluorescent Light	7	9		
Library Study Room	Neon Light	9	40	19:00-23:00	continuously
Library Computer Room	Fluorescent Light	1	9	19:00-23:00	continuously
Library Book Room	Fluorescent Light	1	9	19:00-23:00	continuously
Library Study Room	Projector	1		once a week, closed at night	
Library Study Room	TV set	1	300	once a month	2 hours
Building 4					

Location	Appliance	Unit	Power [W]	Functioning hours per day	Usage
Offices Bursar	Laptop PC	1	80	from 06:00 to 21:00	continuously
Offices Science Teacher	Laptop PC	1	80	once a week, sometimes 19:00-23:00	2-3 hours
Offices Staff	Fluorescent Light	10	9	not common, sometimes 19:00-23:00	continuously
Offices Staff	Neon Security Light	2	40		
New Computer Room	TV set	1	250		
Building 5					
Classes	Fluorescent Light	8	9	from 19:00 to 23:00	continuously
Classes	Neon Security Light	1	40	from 19:00 to 05:00	continuously
Building 6					
Classes	Fluorescent Light	16	9	from 19:00 to 23:00	continuously
Classes	Neon Security Light	4	40	from 19:00 to 05:00	continuously
Building 7					
Office Second HM	Laptop PC	1	80		
Classes	Fluorescent Light	16	9	from 19:00 to 23:00	continuously
Office Second HM	Fluorescent Light	1	9	not common, sometimes 19:00-23:00	continuously
Academic Room	Fluorescent Light	1	9		
Common Room	Fluorescent Light	1	9		
Classes	Neon Security Light	2	40	from 19:00 to 05:00	continuously
Dormitory Girls					
Dormitory	Fluorescent Light	31	9	from 05:00 to 06:00, from 23:00 to 23:15	continuously
Common Room	Neon Light	2	40		
Offices		2			
Laundry	Fluorescent Light	2	9		
Showers	Fluorescent Light	2	9		
Toilets	Fluorescent Light	2	9		
Security Light	Fluorescent Light	4	9		
Dormitory Boys					
Dormitory	Fluorescent Light	12	9	from 05:00 to 06:00, from 23:00 to 23:15	continuously
Toilets	Fluorescent Light	3	9		
Security Light	Fluorescent Light	4	40	from 19:00 to 05:00	continuously
Kitchen					
	Fluorescent Light	6	9	from 04:00 to 06:00, from 19:00 to 23:00	
	Security light	2	40		
Canteen					
	Light	8	9		
	Fluorescent Light	1	9		
Garden					
	Water pump	1	700	every day, 05:00-09:00	continuously
	Egg incubator	1	40	all day	continuously
Shop					
	Fridge	1	500	all day	

Location	Appliance	Unit	Power [W]	Functioning hours per day	Usage
	Fluorescent Light	2	9	19:00-21:00	continuously
	Security light	3			
Residential					
	Fridge	1	80		
	Fluorescent Light	52	9		
	TV set	1	250		
	Security Light	17			
Rest house					
	Light	15			
	Neon Security Light	2	40		

References

[1]   Bloomberg New Energy Finance, "New Energy Outlook 2017," New York, 2017.

[2]   IEA, "Technology Roadmap: Energy storage," 2014.

[3]   IEC, "Electrical Energy Storage - White Paper," 2011.

[4]   UNFCCC. Conference of the Parties (COP), "Paris Climate Change Conference-November 2015, COP 21," *Adopt. Paris Agreement. Propos. by Pres.*, vol. 21932, no. December, p. 32, 2015.

[5]   Eurostat, "Gross electricity generation by fuel, EU-28, 1990-2014," 2014.

[6]   IEA, "World Energy Outlook 2016," *Int. Energy Agency Paris, Fr.*, p. 28, 2016.

[7]   ENTSO-E, "Network Code on Requirements for Grid Connection," 2012.

[8]   ENTSO-E, "Network Code on Load-Frequency Control and Reserves," 2013.

[9]   TERNA S.p.A., "Enclosure to the grid code A.70 - Technical Rules for the system requirements related to distributed generation," 2012.

[10]   TERNA S.p.A., "Enclosure to the grid code A.15 - Participation in the regulation of frequency and frequency/power," 2012.

[11]   EPRI, "Electric Energy Storage Technology Options: A White Paper Primer on Applications, Costs and Benefits," *Epri*, pp. 1–170, 2010.

[12]   T. J. Hammons, "Integrating renewable energy sources into European grids," *Int. J. Electr. Power Energy Syst.*, vol. 30, no. 8, pp. 462–475, Oct. 2008.

[13]   M. Singh, V. Khadkikar, A. Chandra, and R. K. Varma, "Grid Interconnection of Renewable Energy Sources at the Distribution Level With Power-Quality Improvement Features," *IEEE Trans. Power Deliv.*, vol. 26, no. 1, pp. 307–315, Jan. 2011.

[14]   P. Dubucq and G. Ackermann, "Frequency control in coupled energy systems with high penetration of renewable energies," in *2015 International Conference on Clean Electrical Power (ICCEP)*, 2015, pp. 326–332.

[15]   K. Moslehi and R. Kumar, "A Reliability Perspective of the Smart Grid," *IEEE Trans. Smart Grid*, vol. 1, no. 1, pp. 57–64, Jun. 2010.

[16]   J. a P. Lopes, N. Hatziargyriou, J. Mutale, P. Djapic, and N. Jenkins, "Integrating distributed generation into electric power systems: A review of drivers, challenges and opportunities," *Electr. Power Syst. Res.*, vol. 77, no. 9, pp. 1189–1203, 2007.

[17]   D. O. Akinyele and R. K. Rayudu, "Review of energy storage technologies for sustainable power networks," *Sustain. Energy Technol. Assessments*, vol. 8, pp. 74–91, 2014.

[18]   R. Yokoyama, Y. Hida, K. Koyanagi, and K. Iba, "The role of battery systems and expandable distribution networks for smarter grid," in *IEEE Power and Energy Society General Meeting*, 2011, pp. 3–4.

[19]   I. Hadjipaschalis, A. Poullikkas, and V. Efthimiou, "Overview of current and future energy storage technologies for electric power applications," *Renew. Sustain. Energy Rev.*, vol. 13, no. 6–7, pp. 1513–1522, 2009.

[20]   A. Gitis, M. Leuthold, and D. U. U. Sauer, *Applications and Markets for Grid-Connected Storage Systems*. Elsevier B.V., 2014.

[21]   Sandia, "Doe Global Energy Storage Database," *Database*, p. 1464 projects, 2016.

[22]   IEA, *World Energy Outlook 2014*. OECD Publishing, 2014.

[23]   E. Colombo, S. Bologna, and D. Masera, *Renewable Energy for Unleashing Sustainable Development*. Springer International Publishing, 2013.

[24]   K.-D. Merz, G. Crugnola, G. Bonduelle, R. Bruggeman, F. Linck, R. Linke, J. Cilia, H. Chris, and E. Marckx, "Battery Energy Storage for Rural Electrification Systems," 2013.

[25]   Alliance for Rural Electrification, "Using batteries to ensure clean, reliable and affordable universal electricity access," 2013.

[26]   Regional Academy on United Nations RAUN, "Sustainable Energy for All: Evaluation of battery storage technologies for sustainable and rural electrification in Sub-Saharan Africa," 2014.

[27]   "EV-Volumes - The Electric Vehicle World Sales Database," 2016. [Online]. Available: http://www.ev-volumes.com/. [Accessed: 04-Jul-2017].

[28]   IEA, "Global EV Outlook: Understanding the Electric Vehicle Landscape to 2020," 2013.

[29]   H. Chen, T. N. Cong, W. Yang, C. Tan, Y. Li, Y. Ding, H. Chen, T. N. Cong, T. N. Cong, W. Yang, W. Yang, C. Tan, C. Tan, Y. Li, Y. Li, Y. Ding, and Y. Ding, "Progress in electrical energy storage system: A critical review," *Prog. Nat. Sci.*, vol. 19, no. 3, pp. 291–312, 2009.

[30]   X. Luo, J. Wang, M. Dooner, and J. Clarke, "Overview of current development in electrical energy storage technologies and the application potential in power system operation," *Appl. Energy*, vol.

137, pp. 511–536, 2015.

[31] The Economist, "Energy Storage - Packing some power," *Econ.*, pp. 1–5, 2012.

[32] T. M. I. Mahlia, T. J. Saktisahdan, A. Jannifar, M. H. Hasan, and H. S. C. Matseelar, "A review of available methods and development on energy storage; technology update," *Renew. Sustain. Energy Rev.*, vol. 33, pp. 532–545, May 2014.

[33] M. Yekini Suberu, M. Wazir Mustafa, and N. Bashir, "Energy storage systems for renewable energy power sector integration and mitigation of intermittency," *Renew. Sustain. Energy Rev.*, vol. 35, pp. 499–514, Jul. 2014.

[34] H. Ibrahim, A. Ilinca, and J. Perron, "Energy storage systems-Characteristics and comparisons," *Renew. Sustain. Energy Rev.*, vol. 12, no. 5, pp. 1221–1250, 2008.

[35] M. Aneke and M. Wang, "Energy storage technologies and real life applications – A state of the art review," *Appl. Energy*, vol. 179, pp. 350–377, 2016.

[36] G. Huff, A. B. Currier, B. C. Kaun, D. M. Rastler, S. B. Chen, D. T. Bradshaw, and W. D. Gauntlett, "DOE/EPRI 2013 electricity storage handbook in collaboration with NRECA," 2013.

[37] M. Raju and S. Kumar Khaitan, "Modeling and simulation of compressed air storage in caverns: A case study of the Huntorf plant," *Appl. Energy*, vol. 89, no. 1, pp. 474–481, Jan. 2012.

[38] R. Madlener and J. Latz, "Economics of centralized and decentralized compressed air energy storage for enhanced grid integration of wind power," *Appl. Energy*, vol. 101, pp. 299–309, Jan. 2013.

[39] T. Kousksou, P. Bruel, A. Jamil, T. El Rhafiki, and Y. Zeraouli, "Energy storage: Applications and challenges," *Solar Energy Materials and Solar Cells*, vol. 120, no. PART A. pp. 59–80, Jan-2014.

[40] M. E. Amiryar and K. R. Pullen, "A Review of Flywheel Energy Storage System Technologies and Their Applications," *Appl. Sci.*, vol. 7, p. 286, 2017.

[41] G. Fuchs, B. Lunz, M. Leuthold, and D. U. Sauer, *Overview of Nonelectrochemical Storage Technologies*. Elsevier B.V., 2014.

[42] F. Díaz-González, A. Sumper, O. Gomis-Bellmunt, and R. Villafáfila-Robles, "A review of energy storage technologies for wind power applications," *Renew. Sustain. Energy Rev.*, vol. 16, no. 4, pp. 2154–2171, May 2012.

[43] M. H. Ali, Bin Wu, and R. A. Dougal, "An Overview of SMES Applications in Power and Energy Systems," *IEEE Trans. Sustain. Energy*, vol. 1, no. 1, pp. 38–47, Apr. 2010.

[44] CLEFS CEA, "Magnets and magnetic materials - Superconducting magnets for fusion," 2007.

[45] Schoenung Susan M., "Characteristics and Technologies for Long-vs. Short-Term Energy Storage. A study by DOE Energy Storage Systems Program," 2001.

[46] M. Beaudin, H. Zareipour, A. Schellenberglabe, and W. Rosehart, "Energy storage for mitigating the variability of renewable electricity sources: An updated review," *Energy Sustain. Dev.*, vol. 14, no. 4, pp. 302–314, Dec. 2010.

[47] J. Radcliffe, "The future role for energy storage in the UK Main Report," 2011.

[48] A. Sharma, V. V. Tyagi, C. R. Chen, and D. Buddhi, "Review on thermal energy storage with phase change materials and applications," *Renew. Sustain. Energy Rev.*, vol. 13, no. 2, pp. 318–345, Feb. 2009.

[49] M. F. Demirbas, "Thermal Energy Storage and Phase Change Materials: An Overview," *Energy Sources, Part B Econ. Planning, Policy*, vol. 1, no. 1, pp. 85–95, Jan. 2006.

[50] J. Eyer, J. Iannucci, and P. C. Butler, "Estimating Electricity Storage Power Rating and Discharge Duration for Utility Transmission and Distribution Deferral. A Study for the DOE Energy Storage Program," 2005.

[51] R. F. Nguyen, T., Savinell, "Flow batteries," *Electrochem. Soc. Interface*, vol. 19, no. 3, pp. 54–56, 2010.

[52] L. K. Gonzalez Adolfo, Ó Gallachóir Brian, McKeogh Eamon, "Study of Electricity Storage Technologies and Their Potential to Address Wind Energy Intermittency in Ireland," 2004.

[53] P. Leung, X. Li, C. Ponce de León, L. Berlouis, C. T. J. Low, F. C. Walsh, F. C. Walsh, G. S. Wei, G.-G. Xia, Z. Yang, J. Liu, and Z. G. Yang, "Progress in redox flow batteries, remaining challenges and their applications in energy storage," *RSC Adv.*, vol. 2, no. 27, p. 10125, Oct. 2012.

[54] T. K. A. Brekken, A. Yokochi, A. von Jouanne, Z. Z. Yen, H. M. Hapke, and D. A. Halamay, "Optimal Energy Storage Sizing and Control for Wind Power Applications," *IEEE Trans. Sustain. Energy*, vol. 2, no. 1, pp. 69–77, Jan. 2010.

[55] J. Arai, K. Iba, T. Funabashi, Y. Nakanishi, K. Koyanagi, and R. Yokoyama, "Power electronics and its applications to renewable energy in Japan," *IEEE Circuits Syst. Mag.*, vol. 8, no. 3, pp. 52–66, 2008.

[56] M. Osiak, H. Geaney, E. Armstrong, and C. O' Dwyer, "Structuring materials for lithium-ion batteries: advancements in nanomaterial structure, composition, and defined assembly on cell performance," *J. Mater. Chem. A*, vol. 2, no. 25, pp. 9433–9460, 2014.

[57] J. Warner, *The handbook of Lithium-ion battery pack design. Chemistry, components, types and*

terminonology. 2015.

[58] J. Kondoh, I. Ishii, H. Yamaguchi, A. Murata, K. Otani, K. Sakuta, N. Higuchi, S. Sekine, and M. Kamimoto, "Electrical energy storage systems for energy networks," *Energy Convers. Manag.*, vol. 41, no. 17, pp. 1863–1874, Nov. 2000.

[59] EastPenn, "A closer analysis of the UltraBattery," 2013.

[60] K. C. Divya and J. Østergaard, "Battery energy storage technology for power systems-An overview," *Electr. Power Syst. Res.*, vol. 79, no. 4, pp. 511–520, 2009.

[61] DTI, "Review of electrical energy storage technologies and systems and of their potential for the UK," pp. 1–34, 2004.

[62] V. G. Lacerda, A. B. Mageste, I. J. B. Santos, L. H. M. da Silva, and M. do C. H. da Silva, "Separation of Cd and Ni from Ni–Cd batteries by an environmentally safe methodology employing aqueous two-phase systems," *J. Power Sources*, vol. 193, no. 2, pp. 908–913, Sep. 2009.

[63] D. Linden and T. B. Reddy, *Handbook of batteries*, 3rd ed. McGraw-Hill Professional, 2001.

[64] M. A. Fetcenko, S. R. Ovshinsky, B. Reichman, K. Young, C. Fierro, J. Koch, A. Zallen, W. Mays, and T. Ouchi, "Recent advances in NiMH battery technology," *J. Power Sources*, vol. 165, no. 2, pp. 544–551, Mar. 2007.

[65] W. H. Zhu, Y. Zhu, Z. Davis, and B. J. Tatarchuk, "Energy efficiency and capacity retention of Ni-MH batteries for storage applications," *Appl. Energy*, vol. 106, pp. 307–313, Jun. 2013.

[66] "EPRI-DOE Handbook of Energy Storage for Transmission and Distribution Applications," Palo Alto, CA; Washington, DC, 2003.

[67] A. Bito, "Overview of the sodium-sulfur battery for the IEEE stationary battery committee," in *IEEE Power Engineering Society General Meeting, 2005*, pp. 2346–2349.

[68] C.-H. Dustmann, "Advances in ZEBRA batteries," *J. Power Sources*, vol. 127, no. 1–2, pp. 85–92, Mar. 2004.

[69] J. M. Tarascon and M. Armand, "Issues and challenges facing rechargeable lithium batteries," *Nature*, vol. 414, no. 6861, pp. 359–67, 2001.

[70] M. S. Whittingham, "Electrical Energy Storage and Intercalation Chemistry," *Science (80-.).*, vol. 192, no. 4244, pp. 1126–1127, 1976.

[71] K. Mizushima, P. C. Jones, P. J. Wiseman, and J. B. Goodenough, "LixCoO2 (0<x≤1): A new cathode material for batteries of high energy density," *Solid State Ionics*, vol. 3–4, no. C, pp. 171–174, Aug. 1981.

[72] D. Deng, "Li-ion batteries: basics, progress, and challenges," *Energy Sci. Eng.*, vol. 3, no. 5, pp. 385–418, 2015.

[73] G. Pistoia, *Lithium-Ion Batteries: Advances and Applications*. Elsevier, 2014.

[74] Y. Mekonnen, A. Sundararajan, and A. I. Sarwat, "A review of cathode and anode materials for lithium-ion batteries," *SoutheastCon 2016*, no. 1541108, pp. 1–6, 2016.

[75] J. Garche, C. K. Dyer, P. T. Moseley, Z. Ogumi, D. A. J. Rand, and B. Scrosati, "Encyclopedia of electrochemical power sources," *Elsevier Sci.*, 2009.

[76] X. Chen, W. Shen, T. T. Vo, Z. Cao, and A. Kapoor, "An overview of lithium-ion batteries for electric vehicles," in *2012 10th International Power & Energy Conference (IPEC)*, 2012, pp. 230–235.

[77] C. Pillot, "The Rechargeable Battery Market and Main Trends 2016-2025," in *International Battery Seminar & Exhibit*, 2017.

[78] T. H. Kim, J. S. Park, S. K. Chang, S. Choi, J. H. Ryu, and H. K. Song, "The current move of lithium ion batteries towards the next phase," *Adv. Energy Mater.*, vol. 2, no. 7, pp. 860–872, Jul. 2012.

[79] N. Nitta, F. Wu, J. T. Lee, and G. Yushin, "Li-ion battery materials: Present and future," *Mater. Today*, vol. 18, no. 5, pp. 252–264, 2015.

[80] J. Wang, Y. K. Chen-Wiegart, and J. Wang, "In Situ Three-Dimensional Synchrotron X-Ray Nanotomography of the (De)lithiation Processes in Tin Anodes," *Angew. Chemie Int. Ed.*, vol. 53, no. 17, pp. 4460–4464, Apr. 2014.

[81] I. A. Courtney and J. R. Dahn, "Electrochemical and In Situ X-Ray Diffraction Studies of the Reaction of Lithium with Tin Oxide Composites," *J. Electrochem. Soc.*, vol. 144, no. 6, p. 2045, Jun. 1997.

[82] J. Wang, P. Liu, J. Hicks-Garner, E. Sherman, S. Soukiazian, M. Verbrugge, H. Tataria, J. Musser, and P. Finamore, "Cycle-life model for graphite-LiFePO4 cells," *J. Power Sources*, vol. 196, no. 8, pp. 3942–3948, 2011.

[83] B. Scrosati and J. Garche, "Lithium batteries: Status, prospects and future," *J. Power Sources*, vol. 195, no. 9, pp. 2419–2430, 2010.

[84] The Boston Consulting Group, "Batteries for Electric Cars: challenges, opportunities, and outlook to 2020," 2010.

[85] IRENA, "Battery Storage for Renewables: Market Status and Technology Outlook," 2015.

[86] A.-I. Stan, M. Swierczynski, D.-I. Stroe, R. Teodorescu, and S. J. Andreasen, "Lithium ion battery

chemistries from renewable energy storage to automotive and back-up power applications — An overview," *2014 Int. Conf. Optim. Electr. Electron. Equip.*, pp. 713–720, 2014.

[87]   T.-F. Yi, L.-J. Jiang, J. Shu, C.-B. Yue, R.-S. Zhu, and H.-B. Qiao, "Recent development and application of Li4Ti5O12 as anode material of lithium ion battery," *J. Phys. Chem. Solids*, vol. 71, no. 9, pp. 1236–1242, Sep. 2010.

[88]   P. G. Bruce, B. Scrosati, and J.-M. Tarascon, "Nanomaterials for Rechargeable Lithium Batteries," *Angew. Chemie Int. Ed.*, vol. 47, no. 16, pp. 2930–2946, Apr. 2008.

[89]   L. A.-W. Ellingsen, C. R. Hung, G. Majeau-Bettez, B. Singh, Z. Chen, M. S. Whittingham, and A. H. Stromman, "Nanotechnology for environmentally sustainable electromobility," *Nat Nano*, vol. 11, no. 12, pp. 1039–1051, Dec. 2016.

[90]   T. Horiba, "Lithium-ion battery systems," *Proc. IEEE*, vol. 102, no. 6, pp. 1–12, 2014.

[91]   J. Christensen, P. Albertus, R. S. Sanchez-Carrera, T. Lohmann, B. Kozinsky, R. Liedtke, J. Ahmed, and A. Kojic, "A Critical Review of Li⁄Air Batteries," *J. Electrochem. Soc.*, vol. 159, no. 2, p. R1, 2012.

[92]   Cadex Electronics Inc., "Battery University." [Online]. Available: /batteryuniversity.com/. [Accessed: 26-Nov-2016].

[93]   U.S. Department of Energy, "Energy Storage: Program Planning Document," 2011.

[94]   T. Diaz de la Rubia, F. Klein, B. Shaffer, N. Kim, and G. Lovric, "Energy storage: Tracking the technologies that will transform the power sector," *Deloitte*, pp. 1–21, 2015.

[95]   B. Zakeri and S. Syri, "Electrical energy storage systems: A comparative life cycle cost analysis," *Renew. Sustain. Energy Rev.*, vol. 42, pp. 569–596, 2015.

[96]   K.-P. Kairies, "Battery storage technology improvements and cost reductions to 2030: A Deep Dive," *Int. Renew. Energy Agency Work.*, 2017.

[97]   TERNA S.p.A., "Grid Code: Chapter 4- Dispatching Regulations," 2012.

[98]   N. Omar, P. Van den Bossche, G. Mulder, M. Daowd, J. M. Timmermans, J. Van Mierlo, and S. Pauwels, "Assessment of performance of lithium iron phosphate oxide, nickel manganese cobalt oxide and nickel cobalt aluminum oxide based cells for using in plug-in battery electric vehicle applications," *2011 IEEE Veh. Power Propuls. Conf.*, pp. 1–7, 2011.

[99]   IEC-62660-1, "Secondary lithium-ion cells for the propulsion of electric road vehicles – Part 1: Performance testing," 2010.

[100]   A. Burke and M. Miller, "The UC Davis Emerging Lithium Battery Test Project," 2009.

[101]   FreedomCAR Program Electrochemical Energy Storage Team, "FreedomCAR Battery Test Manual For Power-Assist Hybrid Electric Vehicles," 2003.

[102]   R. Lazzari, E. Micolano, M. Conte, and F. Vellucci, "Procedura di prova RSE-ENEA per batterie litio-ioni," 2013.

[103]   D. Gallo, C. Landi, M. Luiso, A. Rosano, M. Landi, and V. Paciello, "Testing protocols for battery characterization," *Conf. Rec. - IEEE Instrum. Meas. Technol. Conf.*, pp. 374–379, 2014.

[104]   S. Alessandrini, E. Rizzuto, and Z. Del Prete, "Characterizing different types of lithium ion cells with an automated measurement system," *J. Energy Storage*, vol. 7, pp. 244–251, 2016.

[105]   USCAR, "USABC Electric Vehicle Battery Test Procedures Manual." [Online]. Available: http://www.uscar.org. [Accessed: 03-Mar-2017].

[106]   N. Omar, M. Daowd, O. Hegazy, G. Mulder, J.-M. Timmermans, T. Coosemans, P. Van den Bossche, and J. Van Mierlo, "Standardization Work for BEV and HEV Applications: Critical Appraisal of Recent Traction Battery Documents," *Energies*, vol. 5, no. 12, pp. 138–156, Jan. 2012.

[107]   Boston Power, "Datasheet - Swing 5300," 2013. [Online]. Available: www.boston-power.com/products. [Accessed: 25-Jan-2017].

[108]   Boston Power, "Datasheet: Sonata 5300 and Swing 5300 Material Safety," 2013.

[109]   Datasheet, "A123 - ANR26650." [Online]. Available: http://www.a123systems.com/. [Accessed: 25-Jan-2017].

[110]   Datasheet, "GWL POWER - LY-LTO-20AH." [Online]. Available: https://www.ev-power.eu/. [Accessed: 25-Jan-2017].

[111]   F. Leng, C. M. Tan, M. Pecht, G. B. Less, and A. M. Sastry, "Effect of Temperature on the Aging rate of Li Ion Battery Operating above Room Temperature," *Sci. Reports, Nat.*, vol. 5, p. 12967, Aug. 2015.

[112]   B. Lin and W. Wu, "Economic viability of battery energy storage and grid strategy: A special case of China electricity market," *Energy*, vol. 124, pp. 423–434, 2017.

[113]   F. Wankmüller, P. R. Thimmapuram, K. G. Gallagher, and A. Botterud, "Impact of battery degradation on energy arbitrage revenue of grid-level energy storage," *J. Energy Storage*, vol. 10, pp. 56–66, 2017.

[114]   M. R. Jongerden and B. R. Haverkort, "Which battery model to use?," *IET Softw.*, vol. 3, no. 6, p. 445, 2009.

[115]   N. El Ghossein, J. P. Salameh, N. Karami, M. El Hassan, and M. B. Najjar, "Survey on electrical

References

modeling methods applied on different battery types," *2015 3rd Int. Conf. Technol. Adv. Electr. Electron. Comput. Eng. TAEECE 2015*, pp. 39–44, 2015.

[116] V. Rao, G. Singhal, A. Kumar, and N. Navet, "Battery model for embedded systems," *VLSI Des. 2005. 18th Int. Conf.*, pp. 105–110, 2005.

[117] D. W. Dees, V. S. Battaglia, and A. Bélanger, "Electrochemical modeling of lithium polymer batteries," *J. Power Sources*, vol. 110, no. 2, pp. 310–320, 2002.

[118] National Renewable Energy Laboratory (NREL), "HOMER - Hybrid Renewable and Distributed Generation System Design Software," 2010. [Online]. Available: homerenergy.com/. [Accessed: 10-Feb-2016].

[119] L. Tao, J. Ma, Y. Cheng, A. Noktehdan, J. Chong, and C. Lu, "A review of stochastic battery models and health management," *Renew. Sustain. Energy Rev.*, vol. 80, pp. 716–732, Dec. 2017.

[120] C. Chiasserini and R. R. Rao, "Pulsed Battery Discharge in Communication Devices," in *MobiCom '99 Proceedings of the 5th annual ACM/IEEE international conference on Mobile computing and networking*, 1999, pp. 88–95.

[121] M. Winter and R. J. Brodd, "What are batteries, fuel cells, and supercapacitors?," *Chem. Rev.*, vol. 104, no. 10, pp. 4245–4269, 2004.

[122] E. Barsoukov and J. R. Macdonald, *Impedance Spectroscopy Theory, Experiment, and Applications*, 2nd ed. Wiley-Interscience, 2005.

[123] M. Doyle, T. . Fuller, and J. Newman, "Modeling of Galvanostatic Charge and Discharge of the Lithium/Polymer/Insertion Cell," *J. Hydrol.*, vol. 139, no. 1, pp. 79–96, 1992.

[124] C. Lin and A. Tang, "Simplification and Efficient Simulation of Electrochemical Model for Li-ion Battery in EVs," *Energy Procedia*, vol. 104, pp. 68–73, 2016.

[125] V. Ramadesigan, P. W. C. Northrop, S. De, S. Santhanagopalan, R. D. Braatz, and V. R. Subramanian, "Modeling and Simulation of Lithium-Ion Batteries from a Systems Engineering Perspective," *J. Electrochem. Soc.*, vol. 159, no. 3, pp. R31–R45, 2012.

[126] P. Albertus and J. Newman, "Introduction to Dualfoil 5.0," 2007.

[127] COMSOL Inc., "COMSOL Multiphysics® Modeling Software," 2017. [Online]. Available: comsol.com/. [Accessed: 26-Aug-2017].

[128] L. Cai and R. E. White, "Mathematical modeling of a lithium ion battery with thermal effects in COMSOL Inc. Multiphysics (MP) software," *J. Power Sources*, vol. 196, no. 14, pp. 5985–5989, 2011.

[129] PDE Solutions, "FlexPDE finite element model builder for Partial Differential Equations," 2013. [Online]. Available: http://www.pdesolutions.com/.

[130] L. R. Petzold, "A description of Dassl: A differential / algebraic system solver," in *10th IMACS World Congress*, 1982.

[131] D. Rekioua and E. Matagne, *Optimization of Photovoltaic Power Systems Modelization, Simulation and Control*. Springer, 2014.

[132] R. Dufo-López, J. M. Lujano-Rojas, and J. L. Bernal-Agustín, "Comparison of different lead-acid battery lifetime prediction models for use in simulation of stand-alone photovoltaic systems," *Appl. Energy*, vol. 115, pp. 242–253, Feb. 2014.

[133] D. U. Sauer and H. Wenzl, "Comparison of different approaches for lifetime prediction of electrochemical systems—Using lead-acid batteries as example," *J. Power Sources*, vol. 176, no. 2, pp. 534–546, Feb. 2008.

[134] N. Etherden and M. H. J. Bollen, "Dimensioning of energy storage for increased integration of wind power," *IEEE Trans. Sustain. Energy*, vol. 4, no. 3, pp. 546–553, 2013.

[135] M. Pedram and Q. Wu, "Battery-powered digital CMOS design," *Proc. -Design, Autom. Test Eur. DATE*, vol. 10, no. 5, pp. 72–76, 1999.

[136] A. A. H. Hussein and I. Batarseh, "An overview of generic battery models," *IEEE Power Energy Soc. Gen. Meet.*, no. 4, pp. 4–9, 2011.

[137] J. B. Copetti, E. Lorenzo, and F. Chenlo, "A general battery model for PV system simulation," *Prog. Photovoltaics Res. Appl.*, vol. 1, no. 4, pp. 283–292, 1993.

[138] O. Tremblay, L.-A. Dessaint, and A.-I. Dekkiche, "A Generic Battery Model for the Dynamic Simulation of Hybrid Electric Vehicles," in *2007 IEEE Vehicle Power and Propulsion Conference*, 2007, no. V, pp. 284–289.

[139] J. F. Manwell and J. G. McGowan, "Lead acid battery storage model for hybrid energy systems," *Sol. Energy*, vol. 50, no. 5, pp. 399–405, 1993.

[140] D. Rakhmatov, S. Vrudhula, and D. A. Wallach, "A model for battery lifetime analysis for organizing applications on a pocket computer," *IEEE Trans. Very Large Scale Integr. Syst.*, vol. 11, no. 6, pp. 1019–1030, 2003.

[141] R. Rao, S. Vrudhula, and N. Chang, "Battery optimization vs energy optimization: Which to choose and when?," in *IEEE/ACM International Conference on Computer-Aided Design, Digest of Technical Papers, ICCAD*, 2005, pp. 438–444.

[142] C.-F. Chiasserini and R. R. Rao, "Energy efficient battery management," *IEEE J. Sel. Areas Commun.*, vol. 19, no. 7, pp. 1235–1245, 2001.

[143] J. Kalawoun, P. Pamphile, G. Celeux, B. Krystyna, and M. Montaru, "Estimation of the Battery State of Charge: a Switching Markov State-Space Model," in *Signal Processing Conference (EUSIPCO), 2015 23rd European*, 2015, pp. 1950–1954.

[144] A. Fotouhi, D. J. Auger, K. Propp, S. Longo, and M. Wild, "A review on electric vehicle battery modelling: From Lithium-ion toward Lithium-Sulphur," *Renew. Sustain. Energy Rev.*, vol. 56, pp. 1008–1021, 2016.

[145] S. M. Mousavi G. and M. Nikdel, "Various battery models for various simulation studies and applications," *Renew. Sustain. Energy Rev.*, vol. 32, pp. 477–485, 2014.

[146] M. Einhorn, F. V. Conte, C. Kral, and J. Fleig, "Comparison, selection, and parameterization of electrical battery models for automotive applications," *IEEE Trans. Power Electron.*, vol. 28, no. 3, pp. 1429–1437, 2013.

[147] K. Sun and Q. Shu, "Overview of the types of battery models," *Proc. 30th Chinese Control Conf.*, pp. 3644–3648, 2011.

[148] T. Hu and H. Jung, "Simple algorithms for determining parameters of circuit models for charging/discharging batteries," *J. Power Sources*, vol. 233, pp. 14–22, 2013.

[149] S. Barcellona, "A novel lithium ion battery model: A step towards the electrochemical storage systems unification," in *Clean Electrical Power (ICCEP), 2017 6th International Conference on*, 2017.

[150] Y. Gao, J. Jiang, C. Zhang, W. Zhang, Z. Ma, and Y. Jiang, "Lithium-ion battery aging mechanisms and life model under different charging stresses," *J. Power Sources*, vol. 356, pp. 103–114, 2017.

[151] J. Gomez, R. Nelson, E. E. Kalu, M. H. Weatherspoon, and J. P. Zheng, "Equivalent circuit model parameters of a high-power Li-ion battery: Thermal and state of charge effects," *J. Power Sources*, vol. 196, no. 10, pp. 4826–4831, 2011.

[152] N. Devillers, M.-C. Péra, S. Jemei, F. Gustin, and D. Bienaimé, "Complementary characterization methods for Lithium-ion Polymer secondary battery modeling," *Electr. Power Energy Syst.*, vol. 67, pp. 168–178, 2014.

[153] E. Karden, "Using low-frequency impedance spectroscopy for characterization, monitoring, and modeling of industrial batteries," RWTH Aachen University, 2001.

[154] J. Kalawoun, K. Biletska, F. Suard, and M. Montaru, "From a novel classification of the battery state of charge estimators toward a conception of an ideal one," *J. Power Sources*, vol. 279, pp. 694–706, 2015.

[155] G. Piłatowicz, A. Marongiu, J. Drillkens, P. Sinhuber, and D. U. Sauer, "A critical overview of definitions and determination techniques of the internal resistance using lithium-ion, lead-acid, nickel metal-hydride batteries and electrochemical double-layer capacitors as examples," *J. Power Sources*, vol. 296, pp. 365–376, 2015.

[156] V. H. Johnson, A. A. Pesaran, and T. Sack, "Temperature-Dependent Battery Models for High-Power Lithium-Ion Batteries," in *17th Annual Electric Vehicle Symposium*, 2000.

[157] L. Gao, S. Liu, R. A. Dougal, and S. Member, "Dynamic Lithium-Ion Battery Model for System Simulation," vol. 25, no. 3, pp. 495–505, 2002.

[158] H. He, R. Xiong, and J. Fan, "Evaluation of lithium-ion battery equivalent circuit models for state of charge estimation by an experimental approach," *Energies*, vol. 4, no. 4, pp. 582–598, 2011.

[159] J. Lee, J. Lee, O. Nam, J. Kim, B. H. Cho, H.-S. Yun, S.-S. Choi, K. Kim, J. H. Kim, and S. Jun, "Modeling and Real Time Estimation of Lumped Equivalent Circuit Model of a Lithium Ion Battery," in *12th International Power Electronics and Motion Control Conference*, 2006, pp. 1536–1540.

[160] E. Samadani, S. Farhad, W. Scott, M. Mastali, L. E. Gimenez, M. Fowler, and R. A. Fraser, "Empirical modeling of lithium-ion batteries based on electrochemical impedance spectroscopy tests," *Electrochim. Acta*, vol. 160, pp. 169–177, 2015.

[161] M. Dubarry, C. Truchot, and B. Y. Liaw, "Cell degradation in commercial LiFePO4 cells with high-power and high-energy designs," *J. Power Sources*, vol. 258, pp. 408–419, 2014.

[162] D. Andre, M. Meiler, K. Steiner, C. Wimmer, T. Soczka-guth, and D. U. Sauer, "Characterization of high-power lithium-ion batteries by electrochemical impedance spectroscopy . I . Experimental investigation," *J. Power Sources*, vol. 196, no. 12, pp. 5334–5341, 2011.

[163] L. C. Stevanatto, V. J. Brusamarello, and S. Tairov, "Parameter identification and analysis of uncertainties in measurements of lead-acid batteries," *IEEE Trans. Instrum. Meas.*, vol. 63, no. 4, pp. 761–768, 2014.

[164] S. E. Li, B. Wang, H. Peng, and X. Hu, "An electrochemistry-based impedance model for lithium-ion batteries," *J. Power Sources*, vol. 258, pp. 9–18, 2014.

[165] J. Vetter, P. Novák, M. R. R. Wagner, C. Veit, K.-C. C. Möller, J. O. O. Besenhard, M. Winter, M. Wohlfahrt-Mehrens, C. Vogler, and A. Hammouche, "Ageing mechanisms in lithium-ion batteries,"

J. Power Sources, vol. 147, no. 1–2, pp. 269–281, Sep. 2005.

[166] S. Erol and M. E. Orazem, "The influence of anomalous diffusion on the impedance response of LiCoO2/C batteries," *J. Power Sources*, vol. 293, pp. 57–64, 2015.

[167] S. Buller, M. Thele, R. W. De Doncker, and E. Karden, "Impedance-Based Simulation Models of Supercapacitors and Lithium-ion Batteries for Power Electronic Applications," *IEEE Ind. Appl. Mag.*, vol. 11, no. 2, pp. 742–747, 2005.

[168] D. Andre, M. Meiler, K. Steiner, H. Walz, T. Soczka-guth, D. U. Sauer, C. Wimmer, T. Soczka-guth, and D. U. Sauer, "Characterization of high-power lithium-ion batteries by electrochemical impedance spectroscopy. II: Modelling," *J. Power Sources*, vol. 196, no. 12, pp. 5349–5356, 2011.

[169] M. Urbain, M. Hinaje, S. Raël, B. Davat, and P. Desprez, "Energetical modeling of lithium-ion batteries including electrode porosity effects," *IEEE Trans. Energy Convers.*, vol. 25, no. 3, pp. 862–872, 2010.

[170] A. Barrè, B. Deguilhem, S. Grolleau, M. Gèrard, F. Suard, and D. Riu, "A review on lithium-ion battery ageing mechanisms and estimations for automotive applications," *J. Power Sources*, vol. 241, pp. 680–689, 2013.

[171] V. Marano, S. Onori, Y. Guezennec, G. Rizzoni, and N. Madella, "Lithium-ion batteries life estimation for plug-in hybrid electric vehicles," in *IEEE Vehicle Power and Propulsion Conference*, 2009, pp. 536–543.

[172] M. Ebner, F. Marone, M. Stampanoni, and V. Wood, "Visualization and Quantification of Electrochemical and Mechanical Degradation in Li Ion Batteries," *Science (80-.).*, vol. 342, no. 6159, pp. 716–720, 2013.

[173] S. Tippmann, D. Walper, L. Balboa, B. Spier, and W. G. Bessler, "Low-temperature charging of lithium-ion cells part I: Electrochemical modeling and experimental investigation of degradation behavior," *J. Power Sources*, vol. 252, pp. 305–316, 2014.

[174] M. Broussely, S. Herreyre, P. Biensan, P. Kasztejna, K. Nechev, and R. J. Staniewicz, "Aging mechanism in Li ion cells and calendar life predictions," *J. Power Sources*, vol. 97–98, pp. 13–21, 2001.

[175] A. P. Schmidt, M. Bitzer, Á. W. Imre, and L. Guzzella, "Model-based distinction and quantification of capacity loss and rate capability fade in Li-ion batteries," *J. Power Sources*, vol. 195, no. 22, pp. 7634–7638, 2010.

[176] P. Ramadass, B. Haran, P. M. Gomadam, R. White, and B. N. Popov, "Development of First Principles Capacity Fade Model for Li-Ion Cells," *J. Electrochem. Soc.*, vol. 151, no. 2, p. A196, 2004.

[177] N. Omar, M. A. Monem, Y. Firouz, J. Salminen, J. Smekens, O. Hegazy, H. Gaulous, G. Mulder, P. Van den Bossche, T. Coosemans, and others, "Lithium iron phosphate based battery–Assessment of the aging parameters and development of cycle life model," *Appl. Energy*, vol. 113, pp. 1575–1585, 2014.

[178] E. V. Thomas, H. L. Case, D. H. Doughty, R. G. Jungst, G. Nagasubramanian, and E. P. Roth, "Accelerated power degradation of Li-ion cells," *J. Power Sources*, vol. 124, no. 1, pp. 254–260, 2003.

[179] M. Swierczynski, D. I. Stroe, A. I. Stan, R. Teodorescu, and S. K. K??r, "Lifetime Estimation of the Nanophosphate LiFePO<inf>4</inf>/C Battery Chemistry Used in Fully Electric Vehicles," *IEEE Trans. Ind. Appl.*, vol. 51, no. 4, pp. 3453–3461, 2015.

[180] J. Purewal, J. Wang, J. Graetz, S. Soukiazian, H. Tataria, and M. W. Verbrugge, "Degradation of lithium ion batteries employing graphite negatives and nickel-cobalt-manganese oxide + spinel manganese oxide positives: Part 2, chemical-mechanical degradation model," *J. Power Sources*, vol. 272, pp. 1154–1161, 2014.

[181] C. Guenther, B. Schott, W. Hennings, P. Waldowski, and M. A. Danzer, "Model-based investigation of electric vehicle battery aging by means of vehicle-to-grid scenario simulations," *J. Power Sources*, vol. 239, pp. 604–610, 2013.

[182] B. Xu, A. Oudalov, A. Ulbig, G. Andersson, and D. Kirschen, "Modeling of Lithium-Ion Battery Degradation for Cell Life Assessment," *IEEE Trans. Smart Grid*, vol. 3053, 2016.

[183] J. Schiffer, D. U. Sauer, H. Bindner, T. Cronin, and R. Kaiser, "Model prediction for ranking lead-acid batteries according to expected lifetime in renewable energy systems and autonomous power-supply systems," *J. Power Sources*, vol. 168, pp. 66–78, 2007.

[184] N. Michelusi, L. Badia, R. Carli, L. Corradini, and M. Zorzi, "Energy management policies for harvesting-based wireless sensor devices with battery degradation," *IEEE Trans. Commun.*, vol. 61, no. 12, pp. 4934–4947, 2013.

[185] D. I. Stroe, M. Swierczynski, S. K. Kar, and R. Teodorescu, "A comprehensive study on the degradation of lithium-ion batteries during calendar ageing: The internal resistance increase," in *Energy Conversion Congress and Exposition (ECCE)*, 2016.

[186] S. S. Zhang, K. Xu, and T. R. Jow, "EIS study on the formation of solid electrolyte interface in Li-

ion battery," *Electrochim. Acta*, vol. 51, no. 8–9, pp. 1636–1640, 2006.

[187] M. Dubarry and B. Y. Liaw, "Identify capacity fading mechanism in a commercial LiFePO4 cell," *J. Power Sources*, vol. 194, no. 1, pp. 541–549, 2009.

[188] M. Dubarry, B. Y. Liaw, M. S. Chen, S. S. Chyan, K. C. Han, W. T. Sie, and S. H. Wu, "Identifying battery aging mechanisms in large format Li ion cells," *J. Power Sources*, vol. 196, no. 7, pp. 3420–3425, 2011.

[189] R. Wright, C. Motloch, and J. Belt, "Calendar-and cycle-life studies of advanced technology development program generation 1 lithium-ion batteries," *J. power*, vol. 110, pp. 445–470, 2002.

[190] I. Bloom, B. W. Cole, J. J. Sohn, S. A. Jones, E. G. Polzin, V. S. Battaglia, G. L. Henriksen, C. Motloch, R. Richardson, T. Unkelhaeuser, D. Ingersoll, and H. L. Case, "An accelerated calendar and cycle life study of Li-ion cells," *J. Power Sources*, vol. 101, no. 2, pp. 238–247, 2001.

[191] B. Y. Liaw, R. G. Jungst, G. Nagasubramanian, H. L. Case, and D. H. Doughty, "Modeling capacity fade in lithium-ion cells," *J. Power Sources*, vol. 140, no. 1, pp. 157–161, 2005.

[192] M. Einhorn, V. F. Conte, C. Kral, J. Fleig, and R. Permann, "Parameterization of an electrical battery model for dynamic system simulation in electric vehicles," in *Vehicle Power and Propulsion Conference (VPPC)*, 2010.

[193] A. Eddahech, O. Briat, E. Woirgard, and J. M. Vinassa, "Remaining useful life prediction of lithium batteries in calendar ageing for automotive applications," *Microelectron. Reliab.*, vol. 52, no. 9–10, pp. 2438–2442, 2012.

[194] S. Cheng, B. Li, Z. Yuan, F. Zhang, and J. Liu, "Development of a lifetime prediction model for lithium thionyl chloride batteries based on an accelerated degradation test," *Microelectron. Reliab.*, vol. 65, pp. 274–279, 2016.

[195] J. Lai, S. Levy, and M. F. Rose, "High Energy Density Double-Layer Capacitors for Energy Storage Applications," *IEEE AS Mag.*, pp. 14–19, 1992.

[196] J. Song and M. Z. Bazant, "Effects of Nanoparticle Geometry and Size Distribution on Diffusion Impedance of Battery Electrodes," *J. Electrochem. Soc.*, vol. 160, no. 1, pp. A15–A24, 2013.

[197] D. D. Macdonald, "Reflections on the history of electrochemical impedance spectroscopy," *Electrochim. Acta*, vol. 51, pp. 1376–1388, 2006.

[198] N. Kularatna, "Dynamics and modeling of rechargeable batteries: What electrochemists' work tells the electronic engineers," *IEEE Power Electron. Mag.*, vol. 1, no. 4, pp. 23–33, 2014.

[199] M. Park, X. Zhang, M. Chung, G. B. Less, and A. M. Sastry, "A review of conduction phenomena in Li-ion batteries," *J. Power Sources*, vol. 195, no. 24, pp. 7904–7929, Dec. 2010.

[200] A. Jossen, "Fundamentals of battery dynamics," *J. Power Sources*, vol. 154, pp. 530–538, 2006.

[201] P. Verma, P. Maire, and P. Novák, "A review of the features and analyses of the solid electrolyte interphase in Li-ion batteries," *Electrochim. Acta*, vol. 55, no. 22, pp. 6332–6341, Sep. 2010.

[202] J. Kim and S. Pyun, "Comparison of transmissive permeable and reflective impermeable interfaces between electrode and electrolyte," *J Solid State Electrochem*, vol. 15, pp. 2447–2452, 2011.

[203] A. Lasia, *Electrochemical Impedance Spectroscopy and its Applications*, vol. 29, no. 3_4. 2014.

[204] P. Mauracher and E. Karden, "Dynamic modelling of lead/acid batteries using impedance spectroscopy for parameter identification," *J. Power Sources*, vol. 67, no. 1–2, pp. 69–84, 1997.

[205] C. Ho, "Application of A-C Techniques to the Study of Lithium Diffusion in Tungsten Trioxide Thin Films," *J. Electrochem. Soc.*, vol. 127, no. 2, p. 343, 1980.

[206] M. A. Tankari, G. Lefebvre, K. Bellache, M. B. Camara, and B. Dakyo, "Supercapacitor Lifetime Estimation Based on Rainflow Cycle Counting Method," in *Vehicle Power and Propulsion Conference (VPPC)*, 2015, pp. 1–6.

[207] M. B. Pinson and M. Z. Bazant, "Theory of SEI Formation in Rechargeable Batteries: Capacity Fade, Accelerated Aging and Lifetime Prediction," *J. Electrochem. Soc.*, vol. 160, no. 2, pp. A243–A250, 2013.

[208] A. Eddahech, O. Briat, and J. M. Vinassa, "Performance comparison of four lithium-ion battery technologies under calendar aging," *Energy*, vol. 84, pp. 542–550, 2015.

[209] M. Delfanti, D. Falabretti, M. Merlo, and G. Monfredini, "Distributed generation integration in the electric grid: energy storage system for frequency control," *J. Appl. Math.*, pp. 1–13, 2014.

[210] L. Lo Schiavo, M. Delfanti, E. Fumagalli, and V. Olivieri, "Changing the regulation for regulating the change: Innovation-driven regulatory developments for smart grids, smart metering and e-mobility in Italy," *Energy Policy*, vol. 57, pp. 506–517, 2013.

[211] Italian Electrical Committee (CEI), "Technical standard CEI 0-16 - Reference technical rules for the connection of active and passive consumers to the HV and MV electrical networks of distribution Company," 2014.

[212] Italian Electrical Committee (CEI), "Technical standard CEI 0-21 - Reference technical rules for the connection of active and passive users to the LV electrical Utilities," 2014.

[213] M. Delfanti, D. Falabretti, M. Merlo, G. Monfredini, S. Nassuato, C. Rosati, and G. Marchegiani, "Storage application for ancillary service support to the main grid," *CIRED Work.*, no. 0390, pp.

11–12, 2014.

[214] EU Commission, "Communication from the commission to the European parliament, the council, the European economic and social committee, the committee of the regions and the European investment bank – Clean Energy for All Europeans," *EU Winter Packag.*, 2016.

[215] Autorità per l'Energia Elettrica il Gas e il Sistema Idrico (AEEGSI), "DCO 298/2016/R/eel: Prima fase della riforma del mercato per il servizio di dispacciamento: apertura alla domanda, alle fonti rinnovabili non programmabili e alla generazione distribuita," 2016.

[216] P. Mercier, R. Cherkaoui, A. Oudalov, S. Member, and A. Oudalov, "Optimizing a Battery Energy Storage System for Frequency Control Application in an Isolated Power System," *IEEE Trans. Power Syst.*, vol. 24, no. 3, pp. 1469–1477, 2009.

[217] A. Zeh, M. Müller, M. Naumann, H. C. Hesse, A. Jossen, and R. Witzmann, "Fundamentals of Using Battery Energy Storage Systems to Provide Primary Control Reserves in Germany," *Batteries*, vol. 2, no. 29, pp. 1–21, 2016.

[218] J. Schmutz, "Primary Frequency Control Provided By Battery," ETH, 2013.

[219] Autorità per l'Energia Elettrica il Gas e il Sistema Idrico (AEEGSI), "231/2013/R/EEL: Trattamento economico dell'energia erogata dalle unità di produzione per la regolazione primaria di frequenza (Remuneration of power units for primary frequency regulation)," 2013.

[220] TERNA S.p.A., "Nota informativa: Avvio del meccanismo di remunerazione della regolazione primaria di frequenza (Starting of the remuneration mechanism for primary frequency regulation)," 2014.

[221] German TSO, "Anforderungen an die Speicherkapazität bei Batterien für die Primärregelleistung," p. 9, 2015.

[222] National Grid, "Enhanced Frequency Control Capability (EFCC)," 2015.

[223] K. Smethurst, S. Williams, and V. Walsh, "Testing guidance for providers of enhanced frequency response balancing service," 2017.

[224] ENTSO-E, "Public consultation on 'FCR cooperation' potential market design evolutions," 2017.

[225] "Internet platform for tendering control reserve." [Online]. Available: https://www.regelleistung.net/ext/static/prl?lang=en. [Accessed: 26-Sep-2017].

[226] B. Schwark, "A journey towards Pan-European ancillary services," in *Symposium on European Grid Service Markets*, 2017, pp. 1–40.

[227] T. Thien, H. Axelsen, M. Merten, H. Axelsen, S. Zurmùhlen, and M. Leuthold, "Planning of Grid-Scale Battery Energy Storage Systems: Lessons Learned from a 5 MW Hybrid Battery Storage Project in Germany," *Battcon - Int. Station. Batter. Conf. 2015*, no. 03, p. 10, 2015.

[228] T. S. Borsche, A. Ulbig, and G. G. Andersson, "Impact of frequency control reserve provision by storage systems on power system operation," *IFAC Proc. Vol.*, vol. 19, pp. 4038–4043, 2014.

[229] T. Košický, M. Kolcun, and Ľ. Be, "Influence of State of Charge Level on Frequency Control Reserve Provision by Energy Storage Systems," vol. 4, no. 2, pp. 36–41, 2015.

[230] A. Oudalov, D. Chartouni, and C. Ohler, "Optimizing a battery energy storage system for primary frequency control," *Power Syst. IEEE*, vol. 22, no. 3, pp. 1259–1266, 2007.

[231] O. Mégel, J. L. Mathieu, and G. Andersson, "Maximizing the potential of energy storage to provide fast frequency control," in *4th IEEE/PES Innovative Smart Grid Technologies Europe (ISGT Europe)* , 2013.

[232] T. Borsche, A. Ulbig, M. Koller, and G. Andersson, "Power and energy capacity requirements of storages providing frequency control reserves," in *IEEE Power and Energy Society General Meeting*, 2013.

[233] M. Arnold and G. Andersson, "Model Predictive Control of Energy Storage including Uncertain Forecasts," in *17th Power Systems Computation Conference*, 2011, pp. 1–7.

[234] A. Ulbig, M. D. Galus, S. Chatzivasileiadis, and G. Andersson, "General Frequency Control with Aggregated Control Reserve Capacity from Time-Varying Sources: The Case of PHEVs," in *IREP Symposium – Bulk Power System Dynamics and Control – VIII (IREP),* , 2010.

[235] M. Khalid and A. V. Savkin, "An optimal operation of wind energy storage system for frequency control based on model predictive control," *Renew. Energy*, vol. 48, pp. 127–132, Dec. 2012.

[236] H.-J. Kunisch, K. G. Kramer, and H. Dominik, "Battery Energy Storage Another Option for Load-Frequency-Control and Instantaneous Reserve," *IEEE Transactions on Energy Conversion*, vol. EC-1, no. 3. pp. 41–46, 1986.

[237] M. Koller, T. Borsche, A. Ulbig, and G. Andersson, "Review of grid applications with the Zurich 1MW battery energy storage system," *Electr. Power Syst. Res.*, vol. 120, pp. 128–135, Mar. 2015.

[238] M. Benini, S. Canevese, E. Ciapessoni, D. Cirio, M. Gallanti, A. Gatti, and A. Pitto, "Il servizio di regolazione primaria tramite batteria: valutazioni tecnico-economiche (The primary frequency regulation using batteries: techno-economical evaluations)," *Energ. Elettr.*, vol. 91, no. 5, p. 9, Sep. 2015.

[239] B. Lian, A. Sims, D. Yu, C. Wang, and R. Dunn, "Optimizing LiFePO4 Battery Energy Storage

Systems for Frequency Response in the UK System," *IEEE Trans. Sustain. Energy*, vol. 8, no. 1, pp. 385–394, 2017.

[240] P. C. Kjær and R. Lærke, "Experience with primary reserve supplied from energy storage system," in *17th European Conference on Power Electronics and Applications (EPE-ECCE Europe)*, 2015.

[241] M. Dubarry, A. Devie, K. Stein, M. Tun, M. Matsuura, and R. Rocheleau, "Battery Energy Storage System battery durability and reliability under electric utility grid operations: Analysis of 3 years of real usage," *J. Power Sources*, vol. 338, pp. 65–73, 2017.

[242] J. Fleer, S. Zurmühlen, J. Badeda, P. Stenzel, J. Hake, and D. U. Sauer, "Model-based economic assessment of stationary battery systems providing primary control reserve," in *10th International Renewable Energy Storage Conference – IRES* , 2016.

[243] S. Mandelli, M. Molinas, E. Park, M. Leonardi, E. Colombo, and M. Merlo, "The Role of Storage in Emerging Country Scenarios," *Energy Procedia*, vol. 73, pp. 112–123, 2015.

[244] N. U. Blum, R. Sryantoro Wakeling, and T. S. Schmidt, "Rural electrification through village grids - Assessing the cost competitiveness of isolated renewable energy technologies in Indonesia," *Renew. Sustain. Energy Rev.*, vol. 22, pp. 482–496, 2013.

[245] M. Lee, D. Soto, and V. Modi, "Cost versus reliability sizing strategy for isolated photovoltaic micro-grids in the developing world," *Renew. Energy*, vol. 69, pp. 16–24, 2014.

[246] H. Ahlborg and L. Hammar, "Drivers and barriers to rural electrification in Tanzania and Mozambique – grid extension, off - grid and renewable energy sources," *Renew. Energy*, vol. 61, pp. 117–124, 2012.

[247] M. Welsch, M. Bazilian, M. Howells, D. Divan, D. Elzinga, G. Strbac, L. Jones, A. Keane, D. Gielen, V. S. K. S. K. M. Balijepalli, A. Brew-Hammond, and K. Yumkella, "Smart and Just Grids for sub-Saharan Africa: Exploring options," *Renew. Sustain. Energy Rev.*, vol. 20, pp. 336–352, Apr. 2013.

[248] J. C. Rojas-Zerpa and J. M. Yusta, "Methodologies, technologies and applications for electric supply planning in rural remote areas," *Energy Sustain. Dev.*, vol. 20, no. 1, pp. 66–76, Jun. 2014.

[249] S. C. Bhattacharyya, "Review of Alternative Methodologies for Analysing Off-Grid Electricity Supply," *SSRN Electron. J.*, vol. 16, no. 1, pp. 677–694, Aug. 2011.

[250] D. P. Kaundinya, P. Balachandra, and N. H. Ravindranath, "Grid-connected versus stand-alone energy systems for decentralized power-A review of literature," *Renewable and Sustainable Energy Reviews*, vol. 13, no. 8. pp. 2041–2050, 2009.

[251] S. Szabó, K. Bódis, T. Huld, and M. Moner-Girona, "Sustainable energy planning: Leapfrogging the energy poverty gap in Africa," *Renewable and Sustainable Energy Reviews*, vol. 28. pp. 500–509, 2013.

[252] S. Mandelli, J. Barbieri, R. Mereu, and E. Colombo, "Off-grid systems for rural electrification in developing countries: Definitions, classification and a comprehensive literature review," *Renew. Sustain. Energy Rev.*, vol. 58, pp. 1621–1646, 2016.

[253] energypedia, "PicoPV Database," 2011. .

[254] S. Murni, J. Whale, T. Urmee, J. K. Davis, and D. Harries, "Learning from experience: A survey of existing micro-hydropower projects in Ba'Kelalan, Malaysia," *Renew. Energy*, vol. 60, pp. 88–97, Dec. 2013.

[255] O. S. Ohunakin, S. J. Ojolo, and O. O. Ajayi, "Small hydropower (SHP) development in Nigeria: An assessment," *Renew. Sustain. Energy Rev.*, vol. 15, no. 4, pp. 2006–2013, May 2011.

[256] C. S. Kaunda, "Energy situation, potential and application status of small-scale hydropower systems in Malawi," *Renew. Sustain. Energy Rev.*, vol. 26, pp. 1–19, Oct. 2013.

[257] L. Mishnaevsky, P. Freere, R. Sinha, P. Acharya, R. Shrestha, and P. Manandhar, "Small wind turbines with timber blades for developing countries: Materials choice, development, installation and experiences," *Renew. Energy*, vol. 36, no. 8, pp. 2128–2138, Aug. 2011.

[258] H. Borhanazad, S. Mekhilef, R. Saidur, and G. Boroumandjazi, "Potential application of renewable energy for rural electrification in Malaysia," *Renew. Energy*, vol. 59, pp. 210–219, Nov. 2013.

[259] L. Mariam, M. Basu, and M. F. Conlon, "A Review of Existing Microgrid Architectures," *J. Eng.*, vol. 2013, pp. 1–8, 2013.

[260] T. Khatib, A. Mohamed, and K. Sopian, "A review of photovoltaic systems size optimization techniques," *Renew. Sustain. Energy Rev.*, vol. 22, pp. 454–465, Jun. 2013.

[261] T. Khatib, I. A. Ibrahim, and A. Mohamed, "A review on sizing methodologies of photovoltaic array and storage battery in a standalone photovoltaic system," *Energy Conversion and Management*, vol. 120. pp. 430–448, 2016.

[262] M. M. H. Bhuiyan and M. Ali Asgar, "Sizing of a stand-alone photovoltaic power system at Dhaka," *Renew. Energy*, vol. 28, no. 6, pp. 929–938, 2003.

[263] S. Kebaili and H. Benalla, "Optimal Sizing of Stand Alone Photovoltaic Systems: a Review," *J. Electr. Eng.*, vol. 14, no. 4, pp. 1–11, 2014.

[264] A. N. Celik, "Effect of different load profiles on the loss-of-load probability of stand-alone

	photovoltaic systems," *Renew. Energy*, vol. 32, no. 12, pp. 2096–2115, Oct. 2007.
[265]	A. Bouabdallah, J. C. Olivier, S. Bourguet, M. Machmoum, and E. Schaeffer, "Safe sizing methodology applied to a standalone photovoltaic system," *Renew. Energy*, vol. 80, pp. 266–274, 2015.
[266]	T. Khatib, A. Mohamed, K. Sopian, and M. Mahmoud, "A new approach for optimal sizing of standalone photovoltaic systems," *Int. J. Photoenergy*, vol. 2012, pp. 1–7, 2012.
[267]	N. D. Nordin and H. Abdul Rahman, "A novel optimization method for designing stand alone photovoltaic system," *Renew. Energy*, vol. 89, pp. 706–715, 2016.
[268]	J. Chen, J. Chen, C. Gong, and X. Deng, "Energy management and power control for a stand-alone wind energy conversion system," *IECON 2012 - 38th Annu. Conf. IEEE Ind. Electron. Soc.*, pp. 989–994, 2012.
[269]	Rekioua Djamila, "Optimization of a photovoltaic pumping system in Bejaia (Algeria) climate," *J. Electr. Eng.*, vol. 15, no. 2, 2015.
[270]	S. Sinha and S. S. Chandel, "Review of software tools for hybrid renewable energy systems," *Renew. Sustain. Energy Rev.*, vol. 32, pp. 192–205, Apr. 2014.
[271]	CANMET, "RETScreen International Home," 2016. [Online]. Available: nrcan.gc.ca/energy/software-tools/7465. [Accessed: 05-Aug-2017].
[272]	Thermal Energy System Specialists LLC, "TRNSYS - Transient System Simulation Tool," 2012. [Online]. Available: trnsys.com/. [Accessed: 10-Feb-2016].
[273]	University of Zaragoza, "Software iHOGA - improved Hybrid Optimization by Genetic Algorithms," 2013. .
[274]	Wind Energy Center - University of Massachusetts, "Hybrid2 Software," 2014. [Online]. Available: umass.edu/windenergy/research/topics/tools/software/hybrid2. [Accessed: 08-Feb-2016].
[275]	National Renewable Energy Laboratory (NREL), "System Advisor Model Report," 2014. [Online]. Available: sam.nrel.gov. [Accessed: 26-Apr-2017].
[276]	PVSyst S.A., "PVSyst photovoltaic sofware," 2016. [Online]. Available: pvsyst.com/en/. [Accessed: 26-Apr-2017].
[277]	L. Parshall, D. Pillai, S. Mohan, A. Sanoh, and V. Modi, "National electricity planning in settings with low pre-existing grid coverage: Development of a spatial model and case study of Kenya," *Energy Policy*, vol. 37, no. 6, pp. 2395–2410, 2009.
[278]	IRENA, "Global Atlas for Renewable Energy 2015: A World of Renewables," 2015. [Online]. Available: irena.masdar.ac.ae/gallery/#gallery. [Accessed: 05-Aug-2017].
[279]	NASA, "Surface meteorology and Solar Energy: A renewable energy resource website," 2010. [Online]. Available: eosweb.larc.nasa.gov/sse/. [Accessed: 05-Aug-2017].
[280]	UE JRC's Directorate, "PVGIS," 2010. [Online]. Available: re.jrc.ec.europa.eu/pvgis/. [Accessed: 07-Aug-2017].
[281]	S. Mandelli, M. Merlo, and E. Colombo, "Novel procedure to formulate load profiles for off-grid rural areas," *Energy Sustain. Dev.*, vol. 31, pp. 130–142, Apr. 2016.
[282]	A. Al-Karaghouli and L. L. Kazmerski, "Optimization and life-cycle cost of health clinic PV system for a rural area in southern Iraq using HOMER software," *Sol. Energy*, vol. 84, no. 4, pp. 710–714, 2010.
[283]	G. Bekele and G. Tadesse, "Feasibility study of small Hydro/PV/Wind hybrid system for off-grid rural electrification in Ethiopia," *Appl. Energy*, vol. 97, pp. 5–15, Sep. 2012.
[284]	S. Szabó, K. Bódis, T. Huld, and M. Moner-Girona, "Energy solutions in rural Africa: mapping electrification costs of distributed solar and diesel generation versus grid extension," *Environ. Res. Lett.*, vol. 6, no. 3, pp. 1–9, 2011.
[285]	M. Zeyringer, S. Pachauri, E. Schmid, J. Schmidt, E. Worrell, and U. B. Morawetz, "Analyzing grid extension and stand-alone photovoltaic systems for the cost-effective electrification of Kenya," *Energy Sustain. Dev.*, vol. 25, pp. 75–86, 2015.
[286]	W. X. Shen, "Optimally sizing of solar array and battery in a standalone photovoltaic system in Malaysia," *Renew. Energy*, vol. 34, no. 1, pp. 348–352, Jan. 2009.
[287]	J. K. Kaldellis, "Optimum technoeconomic energy autonomous photovoltaic solution for remote consumers throughout Greece," *Energy Convers. Manag.*, vol. 45, no. 17, pp. 2745–2760, Oct. 2004.
[288]	A. Q. Jakhrani, A.-K. Othman, A. R. H. Rigit, S. R. Samo, and S. A. Kamboh, "A novel analytical model for optimal sizing of standalone photovoltaic systems," *Energy*, vol. 46, no. 1, pp. 675–682, Oct. 2012.
[289]	P. Tsalides and A. Thanailakis, "Loss-of-load probability and related parameters in optimum computer-aided design of stand-alone photovoltaic systems," *Sol. Cells*, vol. 18, no. 2, pp. 115–127, Aug. 1986.
[290]	F. A. Farret and M. G. Simões, "Micropower System Modeling with Homer," in *Integration of Alternative Sources of Energy*, Wiley-IEEE Press, 2006, pp. 379 – 418.

[291] IEA, *Projected Costs of Generating Electricity*, vol. 118 Suppl, no. 7. Paris Cedex: OECD Publishing, 2010.

[292] T. D. Couture and C. Becker-Birck, "Energy policy design for low and middle income countries: From best practices to 'Next' practices," in *In Colombo E., Bologna S., Masera D, Renewable Energy for Unleashing Sustainable Development.*, Springer, Cham, 2013, pp. 239–251.

[293] H. Yang, L. Lu, and W. Zhou, "A novel optimization sizing model for hybrid solar-wind power generation system," *Sol. Energy*, vol. 81, no. 1, pp. 76–84, Jan. 2007.

[294] S. Diaf, D. Diaf, M. Belhamel, M. Haddadi, and A. Louche, "A methodology for optimal sizing of autonomous hybrid PV/wind system," *Energy Policy*, vol. 35, no. 11, pp. 5708–5718, Nov. 2007.

[295] J. L. Bernal-Agustìn and R. Dufo-Lòpez, "Simulation and optimization of stand-alone hybrid renewable energy systems," *Renewable and Sustainable Energy Reviews*, vol. 13, no. 8. pp. 2111–2118, Oct-2009.

[296] E. Atashpaz-Gargari and C. Lucas, "Imperialist competitive algorithm: An algorithm for optimization inspired by imperialistic competition," in *2007 IEEE Congress on Evolutionary Computation*, 2007, pp. 4661–4667.

[297] S. Pfenninger and I. Staffell, "Renewables.ninja." [Online]. Available: renewables.ninja/. [Accessed: 16-Aug-2017].

[298] S. Pfenninger and I. Staffell, "Long-term patterns of European PV output using 30 years of validated hourly reanalysis and satellite data," *Energy*, vol. 114, pp. 1251–1265, 2016.

[299] Politecnico di Milano - E4G research team, "Energy4Growing Project," 2014. [Online]. Available: it.it.facebook.com/energy4growing2014. [Accessed: 05-Aug-2017].

[300] D. D. Macdonald, "A Brief History of Electrochemical Impedance Spectroscopy," *Electrochem. Soc. Proc.*, vol. 13, 2002.

[301] J. E. B. Randles, "Kinetics of rapide electrode applications," *Discuss. Faraday Soc.*, vol. 34, no. 4, pp. 355–358, 1947.

[302] J. R. Macdonald, "Theory of ac space-charge polarization effects in photoconductors, semiconductors, and electrolytes," *Phys. Rev.*, vol. 92, no. 1, pp. 4–17, 1953.

[303] Q.-C. Zhuang, X.-Y. Qiu, and S.-D. Xu, "Diagnosis of Electrochemical Impedance Spectroscopy in Lithium-Ion Batteries," *Lithium Ion Batter. – New Dev.*, pp. 189–226, Feb. 2012.

[304] N. A. Hampson, S. Karunathilaka, and R. Leek, "Impedance of Electrical Storage-Cells," *J. Appl. Electrochem.*, vol. 10, no. 1, pp. 3–11, 1980.

[305] S. Yoon, I. Hwang, C. Wee, H. Shin, and K. Hyun, "Power capability analysis in lithium ion batteries using electrochemical impedance spectroscopy," vol. 655, pp. 32–38, 2011.